Desert Winds: Monitoring Wind-Related Surface Processes in Arizona, New Mexico, and California

USGS
science for a changing world

Desert Winds: Monitoring Wind-Related Surface Processes in Arizona, New Mexico, and California

By Carol S. Breed *and* Marith C. Reheis, *Editors*

U.S. DEPARTMENT OF THE INTERIOR
BRUCE BABBITT, Secretary

U.S. GEOLOGICAL SURVEY
Charles G. Groat, Director

PREFACE

The Desert Winds Project was established in 1979 to obtain high-resolution meteorological data and related surface geological and vegetation data for natural (that is, uncultivated) desert sites where wind is or has been a major erosive or depositional force. The vulnerability of undisturbed arid and semiarid lands to erosion by wind has been difficult to establish due to the general absence of data from deserts on climatological parameters, especially wind speed and direction. The objectives of the project were twofold: (1) to provide detailed field measurements needed to carry out quantitative studies of wind as an agent of surface geologic change and (2) to establish a baseline for defining the normal range of climatic conditions that can be expected to occur on a decadal time scale in areas considered representative of the major American deserts. The long-term goal for acquiring and analyzing Desert Winds Project data is to use them to help recognize climate change, as distinct from normal variations, and to address problems of land resource degradation by wind, whether resulting from climatic variation (aridification) or human activities (desertification) or both.

Throughout a period of 12 years, five instrumented field sites were established in Arizona, New Mexico, and California in areas that represent the five major desert regions of the North American Desert. (1) The Gold Spring Geomet (geological and meteorological) station, at the eastern edge of the Great Basin Desert in northeastern Arizona, was the first constructed in 1979; it lies on the Moenkopi Plateau within the Navajo Indian Reservation. This site is continental steppe and receives moisture both from Pacific-derived winter storms and from the summer Arizona monsoon from the south. (2) The Desert Wells site in west-central Arizona represents the lower Sonoran Desert life zone and was constructed in 1981. This site primarily receives moisture during the summer monsoon season. The area around this site is subject to intense dust storms that regularly disrupt traffic on nearby State and Interstate highways. (3) The Yuma Geomet station in southwestern Arizona, established in 1982, represents the Lower Colorado Valley subdivision of the Sonoran Desert, the most arid part of North America and one of the most active in terms of sand movement. The Yuma area is a transitional zone between the wetter parts of the Sonoran Desert to the east, which are under the influence of the summer monsoon, and the Mojave Desert to the west, which mainly receives moisture in the winter. (4) The Jornada site was established in 1986 to represent the northern part of the Chihuahuan Desert in south-central New Mexico. This site is the least arid of the five Geomet stations; it receives moisture mainly during the summer monsoon and also during winter storms. The Geomet station is located in the Jornada Experimental Range, a study site established by the U.S. Department of Agriculture more than 50 years ago in recognition of the ongoing desertification of the area; the desert grassland of this area has been progressively invaded and replaced by mesquite duneland, which is useless for grazing. (5) The last Geomet site, Owens Lake, was constructed in 1992 on a playa in the northern edge of the Mojave Desert in east-central California. This region is in the rain shadow of the Sierra Nevada and receives moisture mostly in the winter and spring. It was in operation for only 6 years, but provided highly valuable information on the conditions that control the extremely large dust storms that originate from the artificially desiccated bed of Owens Lake; this lake bed is presently the single largest source of fine dust in North America.

The eight chapters in this volume describe the settings (chap. A) and operation (chap. H) of the five Geomet stations maintained by the Desert Winds Project and summarize eolian-related research conducted to date at and around these stations. This research includes: studies of the sand-moving effectiveness of winds during storms at Gold Spring, Yuma, and Jornada (chap. B); wind erosion susceptibility of different ground-surface types at Desert Wells (chap. C); occurrences of dust storms at Yuma related to meteorological conditions (chap. D); the effectiveness of different types of vegetation that mediate wind erosion (chap. E); the usefulness of satellite (Landsat) remote sensing to detect climatic variations related to vegetation changes (chap. F); and a study of the amount and composition of dust deposited regionally in southern Nevada and California compared to that near the major dust source of Owens Lake (chap. G). These studies fulfill some of the research goals envisioned in the original plan of the Desert Winds Project, but there are many other potential scientific uses of the sites and their data.

The Desert Winds Project ended in 1997 after 18 years of operation, but data collection continues at four of the sites (Owens Lake site was dismantled in 1997). The operation of the stations and the collection, storage, and public release of the data will continue for an indefinite period of time by the Desert Research Institute (DRI), Reno, Nev., under the terms of a Memorandum of Understanding between DRI and the U.S. Geological Survey (USGS). We hope that this arrangement will permit further research and exploration by other scientists and public agencies utilizing the priceless data collected at the Geomet stations.

ACKNOWLEDGMENTS

CONTENTS

[Letters designate chapters]

Monitoring Surface Changes in Desert Areas

By Carol S. Breed

DESERT WINDS: MONITORING WIND-RELATED SURFACE PROCESSES IN
ARIZONA, NEW MEXICO, AND CALIFORNIA

Carol S. Breed and Marith C. Reheis, *Editors*

U.S. GEOLOGICAL SURVEY PROFESSIONAL PAPER 1598–A

CONTENTS

FIGURES

TABLES

Monitoring Surface Changes in Desert Areas

By Carol S. Breed[1]

INTRODUCTION

Arid and semiarid climates prevail over most of western North America, in a zone that covers about 2,000,000 km^2 from southern Canada to central Mexico (MacMahon, 1979). This "North American Desert" is subdivided by degree of aridity and temperature and by seasonality of precipitation (fig. 1; Meigs, 1953). Some researchers define the deserts by differences in vegetation and animal inhabitants, others by topography (barriers to precipitation). The boundaries of the deserts thus vary and are somewhat arbitrary, as are different authors' definitions of aridity. Unlike the true deserts of Africa and Asia, however, where no rain may fall for 12 consecutive months or more, all the North American deserts have definite rainy seasons that differ among the subdivisions.

The Sonoran, Mojave, and Chihuahuan subdivisions of the North American Desert (fig. 1) are subtropical, warm-temperate deserts lying at elevations mostly lower than 1,000 m above sea level, whereas the Great Basin is a higher latitude, cold-temperate desert lying at elevations more than 1,000 m above sea level in the rain shadow of the Sierra Nevada. The areas selected for study by the Desert Winds Project (McCauley and others, 1984, and fig. 1) form a rough climatic transect from the Chihuahuan Desert, which receives most of its precipitation from summer convective storms (Arizona summer monsoon of Bryson and Lowry, 1955), westward to the Sonoran Desert, which receives rainfall biseasonally both from the summer monsoon and from winter Pacific frontal storms, to the Mojave Desert and Great Basin, where winter storms predominate and summer rainfall is sparse. The areas also represent a wide range of aridity and temperature.

About 5 percent of the North American deserts are extremely arid, receiving less than 100 mm annual precipitation (MacMahon, 1979); about half the rest are arid (less than about 200 mm precipitation) or semiarid (less than about 400 mm precipitation). As a consequence, most of the region

west of long 100°W., within the United States (fig. 2), receives too little precipitation to support agriculture without irrigation, as recognized more than a century ago by Powell (1879). The desert grasslands and scrublands typical of the U.S. deserts are therefore used primarily as rangeland and for irrigated farming. Some contain urban centers, such as Las Vegas, Albuquerque, Tucson, and Phoenix; typically, these desert cities depend on pumped ground water or on imported surface water from distant perennial sources, such as the Colorado River.

Not only is most of the Western United States dry (fig. 1), it is surfaced largely with fine-grained sediment in alluvial and valley floor deposits. Some has been reworked by wind and redistributed in sand dunes, sand sheets, and dust blankets during the Quaternary (fig. 2). Much of the eolian (wind-blown) material has since been fixed in place by soil development and vegetation, but many sandy areas remain chronically vulnerable to reactivation—they are preconditioned to blow with the wind, given a return to greater aridity or removal of native vegetation or other disturbance of the natural surface. Where such conditions prevail, wind erosion can be a major agent of surface change. Pimentel and others (1976) estimate (conservatively) that wind erosion removes as much as about 1 billion metric tons of sediment and soil each year from farm fields in the United States. Less well known is the vulnerability of dry or disturbed rangeland to wind erosion. Wind erosion of rangeland is a global problem, exacerbated by population growth in the semiarid lands that border many of the world's core deserts. A result of population pressure is desertification: the degradation and loss of biological productivity, which may be due to climate change or human activity or both. Desertification has been likened to a skin disease that breaks out in vulnerable areas subject to stress (United Nations, *in* Sheridan, 1981). Parts of the U.S. deserts, including two sites examined by the Desert Winds Project (Gold Spring, Arizona, and Jornada, New Mexico) are in extremely desertified rangeland (Dregne, 1986).

Windblown sand not only destroys soils and vegetation, but its impact (by bouncing in saltation) on dry, fine-grained surfaces also generates dust palls, as described by Gillette (1986). Airborne dust may affect the global radiation budget, possibly even having feedback effects on climate (Idso and

[1]U.S. Geological Survey (retired), 189 Wilson Canyon Rd., Sedona, AZ 86336.
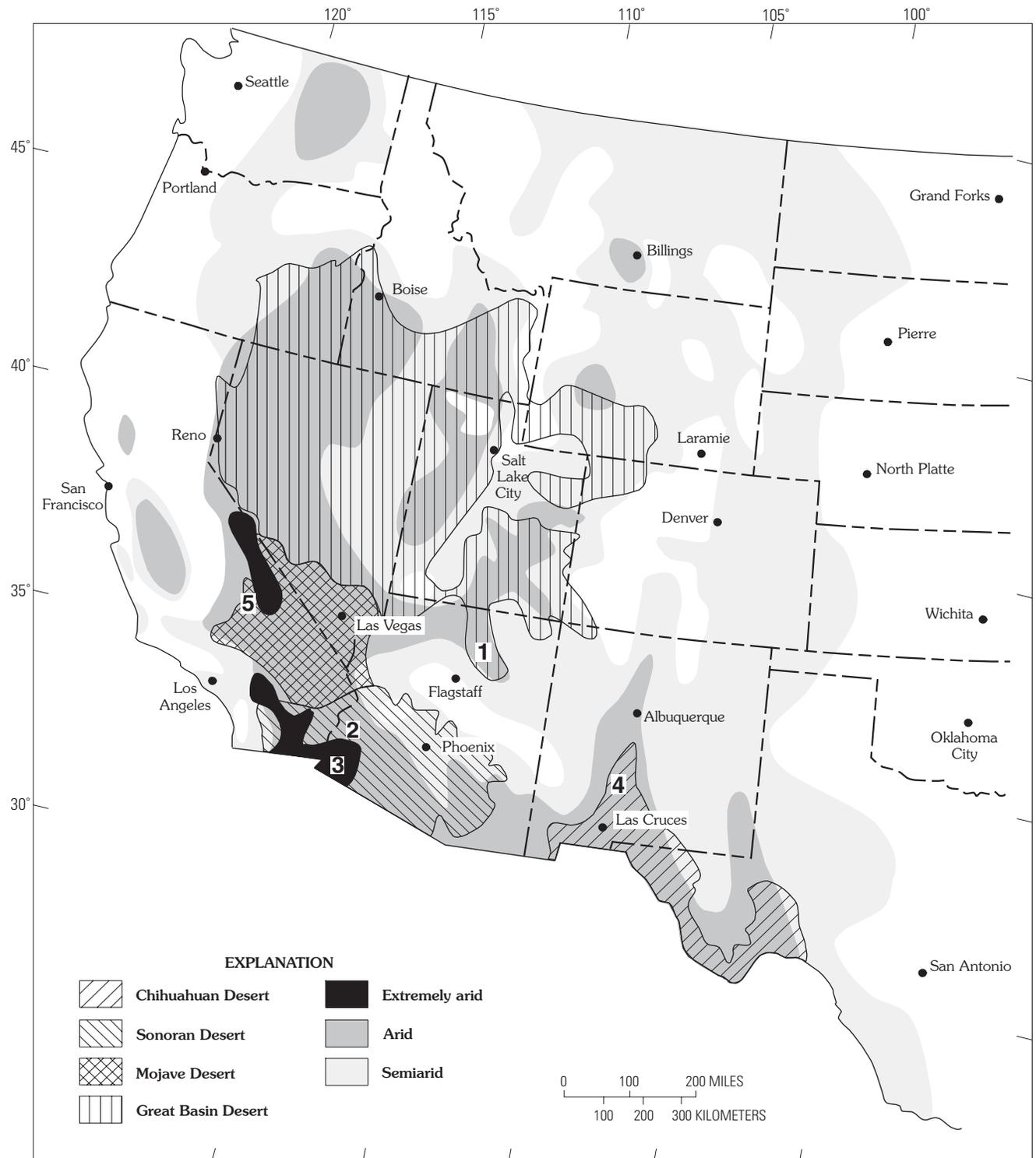
Figure 1. United States portion of the North American Desert: range of aridity (from Meigs, 1953; MacMahon, 1979) and major subdivisions (from Sheridan, 1981, and others). Numbers refer to locations of Geomet sites: 1, Gold Spring; 2, Desert Wells; 3, Yuma; 4, Jornada; 5, Owens Lake.

Brazel, 1978; Idso, 1981). Wind erosion produces almost immediate signals of environmental changes in the form of deflating surfaces, dust emission, and migrating sand dunes, and wind-eroded materials provide evidence of past episodes of aridity in the paleoclimatic records of dunes and of dust infiltrated into ice, lake and marine sediments, and soils. The recognition of widespread eolian components in marine sediments, in glacial ice, and in soils worldwide (Yaalon and
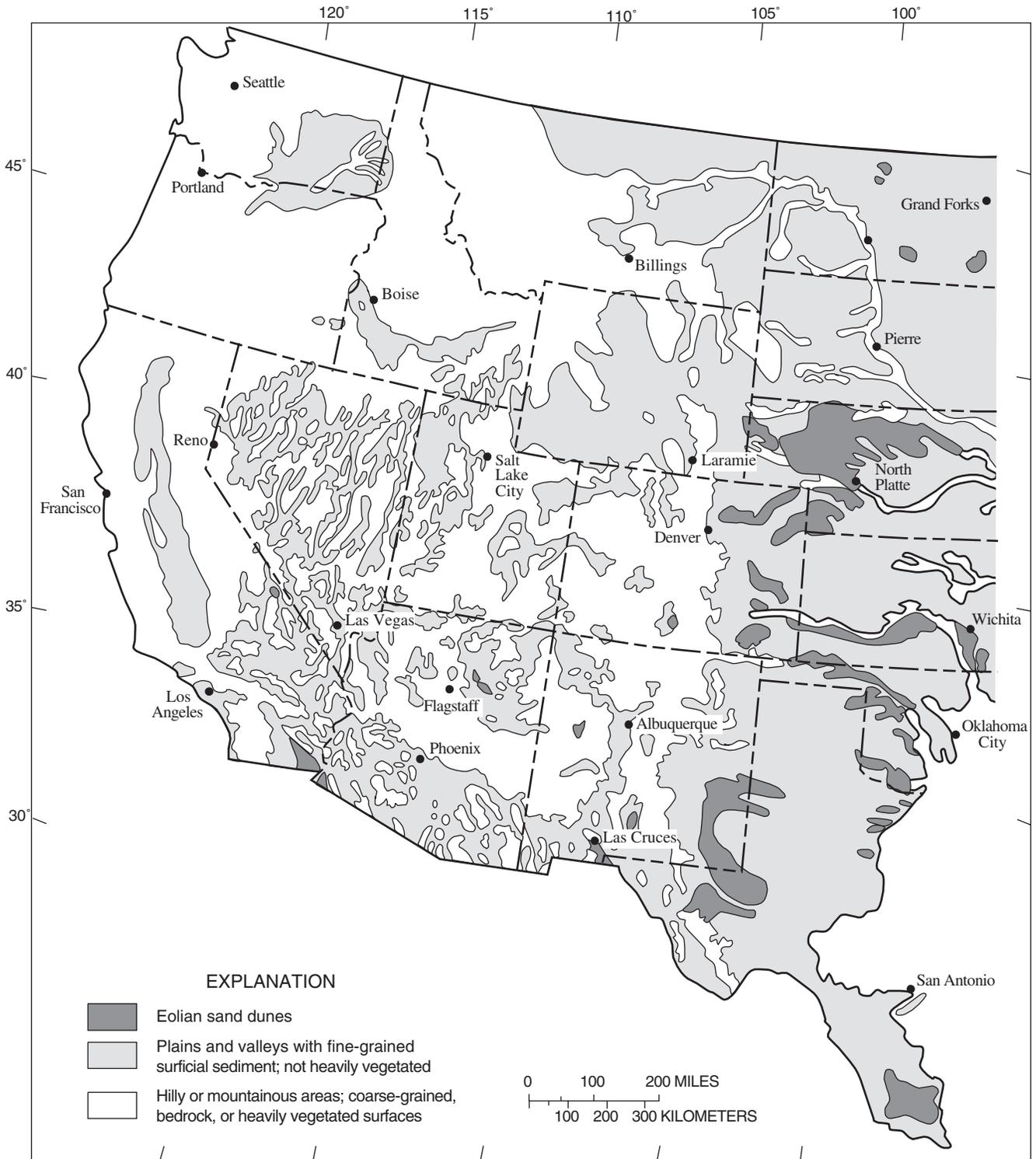
Figure 2. General distribution of fine-grained surficial sediment of eolian and mixed (eolian-alluvial-colluvial) origin in the Western United States (adapted from Hunt, 1986).

Ganor, 1975; Thompson and Mosely-Thompson, 1981; Janacek and Rea, 1983, and many others) coincided with the perception, based on satellite tracking of dust storms, that wind is capable of transcontinental and even global transport (Jackson and others, 1973; Gillette, 1981; Péwé, 1981).

The absence of hard data on wind erosion (outside of cultivated areas) was brought home by the eolian events that followed severe droughts in 1975 and 1976 in North Africa and in the Western United States. In 1977 both regions were subjected to unusually destructive wind storms accompanied

by blowing dust on a continental scale (McCauley and others, 1981; Wilshire and others, 1981). Because wind was long thought to be only a minor agent for the erosion, transport, and deposition of sediment, particularly in the United States, the long-range transport of an estimated 1,000,000 metric tons of sediment from the Texas-New Mexico-Colorado region to the Atlantic Ocean during a single windstorm (Windom and Chamberlain, 1978) came as a surprise to many investigators. At about the same time, Earth-orbiting satellites such as Landsat provided the global database necessary for mapping large-scale eolian sand bodies in deserts (Breed and others, 1979), and the Mariner 9 and Viking missions revealed evidence of extensive wind-erosion features on the planet Mars (McCauley, 1973; Carr, 1981). These events sparked new interest in desert surface processes and awareness of the need to reassess the effectiveness of wind as a geologic agent capable of expressing and reinforcing global change.

THE DESERT WINDS PROJECT

BACKGROUND AND PURPOSE

The erosional effectiveness of wind is known to vary rapidly with changes in land-surface climatology (precipitation, wind speed and direction, soil moisture, vegetation) and with human activity (farming, grazing, construction, war). But, despite years of study of erosion and sediment transport by running water, only recently have many geologists begun to define the basic geologic and climatic controls on wind erosion under natural conditions typical of rangeland (for example, outside of farm fields). Some studies that helped to define rates of erosion, transportation, and deposition of airborne sediment, past and present, were collected in a volume on desert dust by Péwé (1981); the first regional information on modern rates of dust deposition in the American Southwest is reported by Reheis and Kihl (1995). More such quantitative data are needed for inclusion in global climate models, for forecasting adverse effects of wind erosion on vulnerable land surfaces, for detecting and assessing variations in eolian activity that may be early warning signals of climate change, and for calibrating paleoclimatic reconstructions.

The Desert Winds Project represents a limited attempt to address this problem. The acquisition of quantitative data on wind erosion under actual field conditions, in real time, has until recently been very difficult. Reliable equipment, capable of surviving long-term monitoring in the abrasive environments where eolian processes are most active, has not been readily available. Most early geologic studies of wind erosion necessarily relied on brief field observations supplemented by analyses of proxy data, such as sedimentary structures in sand dunes (McKee, 1957, 1966) and wind

tunnel experiments such as those by D. Gillette and his colleagues (Gillette, 1978; Gillette and others, 1980, 1982) and by Musick and others (1996). These efforts led to better understanding of the physics of wind erosion, but rates of sediment transport by wind on natural (uncultivated) desert surfaces, typically characterized by uneven topography, variable precipitation and temperature, and different types of vegetation and surface sediment, have rarely been investigated except for short intervals that do not adequately represent the natural climatic variability of such areas.

Long-term field-modeling of wind erosion at desert sites became practical with the advent, in the late 1970's, of automated equipment (data-collection platforms, DCP's) that allow remote monitoring of surface geological and meteorological ("Geomet") conditions round-the-clock in localities that are widely separated and difficult to access. Automated sensors on these platforms could be uniformly designed and calibrated to permit comparison of measurements among sites. Previous researchers have lamented the general absence of data on climatological parameters in deserts, especially on wind speed and direction, which are generally measured only at airports located on the margins of desert areas (Landsberg, 1986, and many others). The conceptual basis for establishing a network of automated Geomet stations on natural sites representative of the major U.S. deserts and brief descriptions of the early project work were presented by McCauley and others (1984). Later upgrades of the DCP's, which included the deployment of electronic sand-flux sensors (SENSIT's), are described by Tigges and others (chap. H, this volume). The SENSIT's (Stockton and Gillette, 1990) are particularly important to studies of wind erosion as a geologic process because these experimental piezoelectric devices are able to detect and record automatically the movement of sand in saltation (bouncing along the surface) during windstorms and are able to relay these signals to the DCP's while the other sensors measure wind speed and direction, precipitation, and other climatological conditions. Helm and Breed (chap. B, this volume) report preliminary results of field measurement of the movement of sand by wind under monitored climatic conditions, using data from SENSIT's deployed at the Geomet stations.

SCOPE OF THE PROJECT

FIELD SITES

Field sites for the Desert Winds Project (table 1) were chosen to represent terrains typical of the major subdivisions of the North American Desert in the Western United States. Beginning in 1979, in the following order, sites for Geomet studies were selected in the Great Basin, Sonoran, Chihuahuan, and Mojave Deserts. Terrain types at the Geomet sites include high plateau, piedmont

Table 1. Field sites of the Desert Winds Project.

[Climate data from Geomet station records. See Helm and Breed, chap. B, this volume for detailed Geomet data and analysis for Gold Spring, Yuma, and Jornada sites. m.s.l., mean sea level; temp., temperature; max., maximum; min., minimum; precip., precipitation; leaders (--) indicate no data]

Location and date of start of operations	Desert	Geomorphic setting	Latitude/ longitude	Elevation (m above m.s.l.)	Mean annual temp. (max. temp./ min. temp.)	Mean annual precip. (max. precip./ min. precip.)	Period of record summarized for this report
GOLD SPRING GEOMET STATION							
Northeast Arizona 10/27/1979	Great Basin	Plateau	35°46′42″N./ 111°3′21″W.	1,667	12°C (38.2°C, 1989/ −25.3°C, 1982)	142.5 mm (186.2 mm, 1988/ 87.4 mm, 1991)	1980–1992
DESERT WELLS GEOMET STATION							
West-central Arizona 1/1/1981	Sonoran	Dry wash (axial valley)	33°42′8″N./ 113°48′40″W.	344	21°C (--/ --)	128 mm (--/ --)	1982–1992
YUMA GEOMET STATION							
Southwest Arizona 2/1/1982	Sonoran	Site 1: alluvial fan	32°27′30″N./ 114°23′25″W.	135	21.4°C (46.9°C, 1985/ −2.9°C, 1983)	128.3 mm (--/ --)	1982–1987
		Site 2: fluvial terrace	32°31′50″N./ 114°30′45″W.	82.3	23.2°C (51°C, 1990/ −7°C, 1990)	51.9 mm (103.6 mm, 1992/ 21.8 mm, 1989)	1989–1992
JORNADA GEOMET STATION							
South-central New Mexico 9/18/1986	Chihuahuan	Alluvial plain	32°34′45″N./ 106°46′35″W.	1,323	15.3°C (44°C, 1989/ −20°C, 1987)	233 mm (254.2 mm, 1992/ 197.9 mm, 1989)	1987–1992
OWENS LAKE GEOMET STATION							
East-central California 5/19/1992	Mojave	Playa	36°21′20″N./ 117°56′35″W.	1,187.2	-- (43°C, 1992/ −17°C, 1992)	125 mm (--/ --)	1992

slope, lowland basin, and playa. Selection of specific localities was influenced by the need to assure security for the arrays of electronic equipment deployed at each station and to allow access for maintenance and for field studies, including repeat photography, of the surficial geology and vegetation. Brief general descriptions of each site follow. These descriptions include the geographic, climatic, and geologic setting of each site (including a site map where appropriate), surface characteristics, and station histories. Detailed descriptions of the geometeorological data are given by Helm and Breed (chap. B, this volume). The research conducted in and around each site and reported in this volume is discussed in a later section.

GOLD SPRING

The Great Basin Desert (fig. 1) is the largest of the North American deserts; it consists of many internally drained basins that extend southward from eastern Washington and Oregon and southern Idaho across most of Utah and Nevada (where the Great Basin meets the northern Mojave Desert) into Arizona. Because the Desert Winds Project was initially designed to operate entirely within Arizona, the Gold Spring locality (fig. 3) was selected to represent that small part of the Great Basin Desert that extends into northeastern Arizona. The Geomet station (fig. 4A) sits on the surface of the Moenkopi Plateau on the Navajo Indian Reservation.
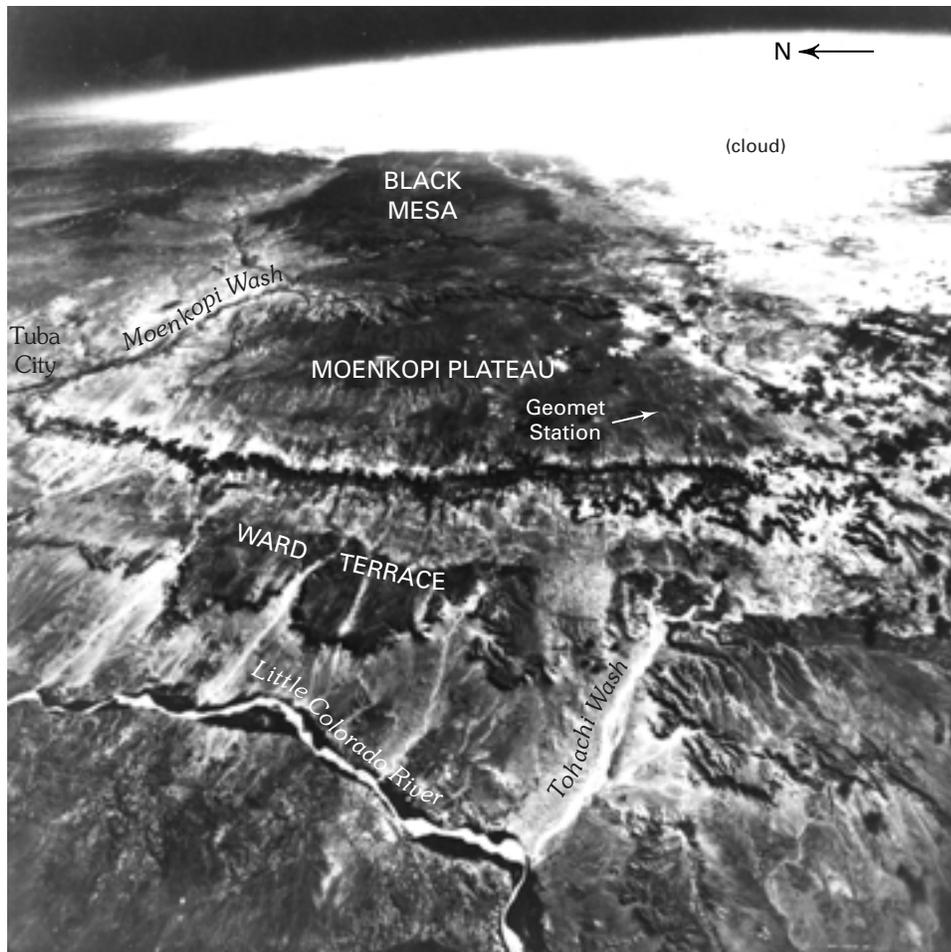
Figure 3.   High-altitude (U-2) photograph showing setting of Gold Spring Geomet site.

The geologic setting of the Gold Spring station (fig. 3) is representative of much of the plateau and canyon country in the southern part of the Colorado Plateau physiographic province. The Moenkopi Plateau is underlain by sedimentary rocks (mostly sandstones) of Mesozoic age that dip very gently (1° to 2°) to the northeast (Billingsley, 1987a). The Geomet site lies 2 km northeast of 158-m-high cliffs that mark the edge of the Moenkopi Plateau and that topographically separate the upland from the badlands east of the Little Colorado River (fig. 3). Total relief from the top of the plateau to the river flood plain is about 300 m. The cliff edge has been intricately dissected by episodic (seasonal) fluvial runoff and sapping into many reentrants. One of the most prominent reentrants is occupied by Gold Spring. Wind erosion has modified the reentrants to U-shaped amphitheaters in which parts of the exposed bedrock have been streamlined into yardangs (Breed and others, 1984).

The surface of the Moenkopi Plateau is a sand plain (fig. 4B) developed on an unconsolidated eolian sand sheet that is crossed by subparallel sand ridges (linear dunes), which extend northeastward from the cliff edge. Ages of the dunes range from Pleistocene or older to late Holocene (Breed and

Breed, 1979; Breed and others, 1984; Billingsley, 1987a, 1987b; Stokes and Breed, 1993), suggesting that the area has undergone repeated eolian transport and reworking of sand deposits throughout the Quaternary. Deposition of the linear dunes on the Moenkopi Plateau originated when sand grains blown northeastward from the Little Colorado River valley reached that elevation (via saltation up climbing dunes (sand ramps): Breed and Breed, 1979; Billingsley, 1987b). The sand ramps have since been eroded from the cliff head, and the upwind ends of the dunes have been stripped from the edge of the plateau by deflation. In the absence of climbing dunes, windblown sand can no longer reach the top of the Moenkopi Plateau, but the sand already there is subject to episodic eolian reworking and redeposition.

The Geomet station is on a slight rise on the sand plain in an interdune corridor (fig. 4B). Local topographic relief within the 2.9 km^2 (1 mi^2) area mapped in detail around the Gold Spring station (fig. 5) is less than 3 m. A geologic map encompassing five 7^1/$_2$-minute quadrangles in the vicinity of the Gold Spring station shows details of the dunes and other surficial units in relation to the regional geology (Billingsley, 1987a).

Figure 4. *A*, Ground-level photograph of Gold Spring Geomet station. *B*, Low-altitude aerial photograph of Gold Spring area showing linear dunes and desertscrub vegetation on sand plain. Arrow points to Geomet station.

The average (modal) grain size of the surficial sediment at the station is 0.104 mm (very fine sand). The sand sheet is partly mantled by a lag gravel of angular chert fragments as large as about 3 cm in diameter, let down or washed in by erosion from local bedrock outcrops. The soils developed in the eolian sand cover of this area are fine-grained sandy loams. A trench in the sand sheet in an interdune corridor near the Geomet station showed 1.1 m of eolian sand bearing a soil with a weak argillic horizon and a stage-II calcic horizon, underlain by gravelly alluvium (B. Musick, University of New Mexico, written commun., 1993).

Vegetation at the Gold Spring site is typical Great Basin plains grassland, surrounded on the rest of the Moenkopi Plateau by Great Basin desertscrub (Hendricks, 1985). The vegetation community in the interdune corridor near the Geomet station is dominated by broom snakeweed and galleta, a bush grass that grows as individual tufts; nearby dune crests are dominated by Mormon tea and by sandhill muhly, a grass that grows in mats. Most other vegetation around the Geomet station consists of yucca, black grama, and needle-and-thread grass (B. Musick, University of New Mexico, written commun., 1993).

Figure 5. Detailed map of surficial geology of Gold Spring Geomet site (G. Billingsley, written commun., 1981).

Table 2. Seasons of the year, as defined by a sampling of researchers in the American West.

Researchers	Fall	Winter	Spring	Summer
Helm and Breed; Baudat and Breed; Musick (this volume)	October 1 ------	January 31	February 1– May 31	June 1– September 30
Murray (1959)	September 16– November 30	December 1– March 31	April 1– June 30	July 1– September 15
Changery (1983); Bryson and Hare (1974); Reitan (1974)	September 1– November 30	December 1– February 28	March 1– May 31	June 1– August 31
Tang and Reiter (1984)	September 1– October 31	November 1– March 31	April 1– May 31	June 1– August 31
Brazel and Nickling (1987)		November 1– April 30		June 1– September 30
Betancourt (1988);	September 1–	November 1–	May 1–	July 1–

The Gold Spring area is arid steppe (Hendricks, 1985), hot in summer and cold in winter (table 1), and is used only for grazing cattle, horses, and sheep. Winter snows arrive with large-scale frontal storms that move in from the northern Pacific Ocean, typically accompanied by strong winds. Because no special equipment is installed to measure snowfall, the precipitation gauge at Gold Spring probably underestimates the winter moisture. Summer rains arrive in July with the Arizona summer monsoon (Bryson and Lowry 1955; Hales, 1974). Occasionally, in late summer or early fall, the area receives rain from incursions of tropical moisture driven by hurricanes off the west coast of Mexico; these downpours produce flashy runoff and alluviation in the normally dry washes in northeastern Arizona (Hereford, 1989). Rain that falls on the sandy surface of the Moenkopi Plateau is quickly absorbed and produces little runoff there except into clay pans in deflation hollows in the sand cover. Between the biseasonal snows and rains, spring and fall seasons are dry. (Table 2 defines the seasons used in this volume and compares this definition with those of other authors.)

The first Geomet station installed at Gold Spring was a basic type (Tigges and others, chap. H, this volume), equipped with a data collection platform (DCP) with automated sensors to record and transmit observations of a small set of near-surface phenomena: average and peak-gust wind speeds, wind direction, precipitation, relative humidity, barometric pressure, air temperature, and soil temperature.

The Gold Spring site was retrofitted to "superstation" status in 1990, when it was provided with additional sensors, including a SENSIT (detailed information on the station equipment and operation is provided by Tigges and others, chap. H, this volume). The Geomet station (fig. 4A) now consists of a free-standing tower that supports a solar power system, a data-collection platform with a radio transmitter, and 19 sensors that sample 22 land surface climatology parameters. Geometeorological (but not sand flux) data acquired from 1979 to 1992 are available on CD-ROM and on the Internet at http://wwwflag.wr.usgs.gov and http://geochange.er.usgs.gov/pub/deserts/OFR_95-78 (Helm and others, 1995).

Field studies at and around the Gold Spring site have focused mainly on the history of the nearby dunes and climatic implications (Breed and Breed, 1979; Breed and others, 1984; Billingsley, 1987b; Stokes and Breed, 1993). Based on plant cover characteristics, B. Musick (University of New Mexico, written commun., 1993) estimates a threshold friction velocity of 82 cm/s—that is, he predicts a higher susceptibility to wind erosion for sand on the crests of the linear dunes at Gold Spring than for sediment in the interdune corridors and at the Geomet station, which he estimates have threshold friction velocities of 108 cm/s and 113 cm/s, respectively. Most of the linear dunes on the Moenkopi Plateau are presently inactive, but at least one that has lost much of its vegetation cover is active, developing and changing

slipface orientations with seasonal changes of wind direction (Breed and others, 1984). Several pulses of dune sand reactivation on the plateau have been dated by the optically stimulated luminescence method; the ages (approximately 400, 2,000–3,000, and 4,700 years ago) suggest that the dunes have episodically been more active during the late Holocene than at present (Stokes and Breed, 1993). Preliminary analyses of the experimental sand-flux data from the Gold Spring Geomet site are presented by Helm and Breed (chap. B, this volume).

DESERT WELLS

The Sonoran Desert (fig. 1) is the most varied part of the North American Desert. The Desert Wells station was intended to represent the semiarid Arizona Upland subdivision of the Sonoran Desert, where the vegetation includes subtrees (very large shrubs with single bases: MacMahon, 1979) such as paloverde, and cacti such as saguaro (Van Devender, 1990). Instead, for security reasons, the Geomet station was placed at a lower elevation on the bajada west of Vicksburg (fig. 6), where the vegetation is desertscrub typical of the Lower Sonoran life zone (Lower Colorado Valley subdivision) and the climate is arid warm temperate (table 1).

The Desert Wells site (fig. 6) is about 160 km west of Phoenix in west-central Arizona (fig. 1). The Geomet station (fig. 7A) lies in an axial valley on bare, limy hardpan (calcrete) exposed in the floor of the usually dry Bouse Wash and is surrounded by abandoned farmland and rangeland. Bouse Wash runs between broad alluvial fans that mantle the piedmont slopes of low mountain ranges (fig. 7B). The distal ends of the fans and the central part of the basin are surfaced with sediment of late Pleistocene to Holocene age, which include grussy sand, silt, clay, and local gravel, reworked from the dissected piedmonts (Demsey, 1988). To the north and west of the station are low barchanoid (transverse) dunes without slipfaces and sand drifts (patches of mobile sand sheet) (figs. 7C, 8). The distribution of these features is shown on a detailed surficial map (fig. 8). Vegetation is sparse and consists mostly of creosotebush, bursage, mesquite, and occasional bunch grasses that are concentrated on the eolian sand deposits (both drifts and dunes).

Loose sand on the hardpan surface of the Geomet site at Desert Wells is mostly medium size, poorly sorted, angular, and highly abrasive. It is replenished episodically by occasional runoff across the site (fig. 7D). Soils on the eolian sediments are minimally developed sandy loams. The nearby routes of U.S. 60 and Interstate 10 (fig. 6) are subject to notorious dust storms generated by wind erosion of the barren surfaces in this area.

Geometeorological data at Desert Wells were recorded intermittently in 1981 and then continuously from January 1982. A basic array of sensors regularly samples, records, and transmits data on eight near-surface climatological

parameters (Tigges and others, chap. H, this volume). This station was not of as much interest to the scientists at Fort Belvoir, who provided much of the instrumentation and related research for this project, as was the station at Yuma (also in the Sonoran Desert), and therefore the Desert Wells station was not upgraded to superstation status until relatively late in its operational history (Tigges and others, chap. H, this volume). Early attempts to collect airborne sediment during windstorms resulted in destruction of PVC-pipe catchers by the abrasive sand in saltation and indicated that the electronic sand-flux sensors deployed at ground level at the other Geomet sites would likely not survive at Desert Wells. For this reason, no SENSIT was deployed there before 1995. Although no detailed experiments were carried out by USGS researchers, S. Wolfe (now at the Geological Survey of Canada), obtained detailed field measurements of sediment transport using a dense array of anemometers deployed temporarily at nearby field sites on five different types of desert surfaces. A detailed description of results of his experiments is presented by Wolfe and Helm (chap. C, this volume). Geometeorological data, including sand-flux data, acquired from 1981 to 1986 are available on CD-ROM (Helm and others, 1998) and are available on the Internet at http://geochange.er.usgs.gov.

YUMA

A Geomet site in the Yuma desert (fig. 9) was selected to represent the Lower Colorado Valley subdivision of the Sonoran Desert (fig. 1), the most arid part of North America (Henning and Flohn, 1977; Cole, 1986; Hall and others, 1988).

The Yuma desert occupies the southernmost part of a broad topographic and structural basin along the border of the United States with Mexico (fig. 9). The Yuma desert is bounded on the west by the irrigated Yuma Valley of the Lower Colorado River and on the north by the irrigated South Gila Valley. Farther west, in California and Mexico, lies a rift valley (the Salton Trough) that contains the Algodones Dunes and, off the map (fig. 9) to the south, the delta of the modern Colorado River where it empties into the head of the Gulf of California. Diagonally across the Yuma desert (and nearly across the Geomet site) lies the Algodones fault zone, which is the eastern edge of the rift valley (Olmsted and others, 1973; Aiken and others, 1980). To the east lie the piedmont slopes and alluvial fans of the Gila Mountains. These mountains consist of Precambrian crystalline rocks that are mostly granitic but include other plutonic, volcanic, and metamorphic rocks (Wilson, 1933; Olmsted and others, 1973).

Most of southwestern Arizona has been structurally stable since the Pliocene (Morrison, 1985), allowing backwearing of the northwest-trending mountains formed by normal faulting during the Tertiary and filling of the

Figure 6. Part of Landsat thematic mapper image showing setting of the Desert Wells Geomet station (Landsat TM image 40142-17384, 5 December 1982).

downdropped structural basins between them with thousands of meters of Tertiary sediments. This consolidated basin fill is overlain by Pleistocene alluvium deposited by the ancestral Colorado and Gila Rivers and by Holocene alluvium of the modern rivers and washes (Eberly and Stanley, 1978; Johnson and Miller, 1980; Peirce, 1984). The basin beneath the Fortuna Plain (fig. 9) may contain as much as 5,000 m of Tertiary basin fill (Olmsted and others, 1973); the ancestral Colorado River sediments are as thick as 330 m about 20 km south of Yuma (Johnson and

Miller, 1980). As a result of erosion of the mountains and deposition in the basins, the topography of southwestern Arizona now consists of only about 10 percent mountains and 90 percent plains (Bull, 1984).

The Yuma desert Geomet station (location 2 on fig. 9; fig. 10) is on Upper Mesa about 1 km east of the very gentle slope of Yuma Mesa, a Colorado River terrace of middle Pleistocene age (Morrison, 1983). An unconsolidated sand sheet about 1 m thick covers the surface around the Geomet station (fig. 10). Only minimal soil is developed
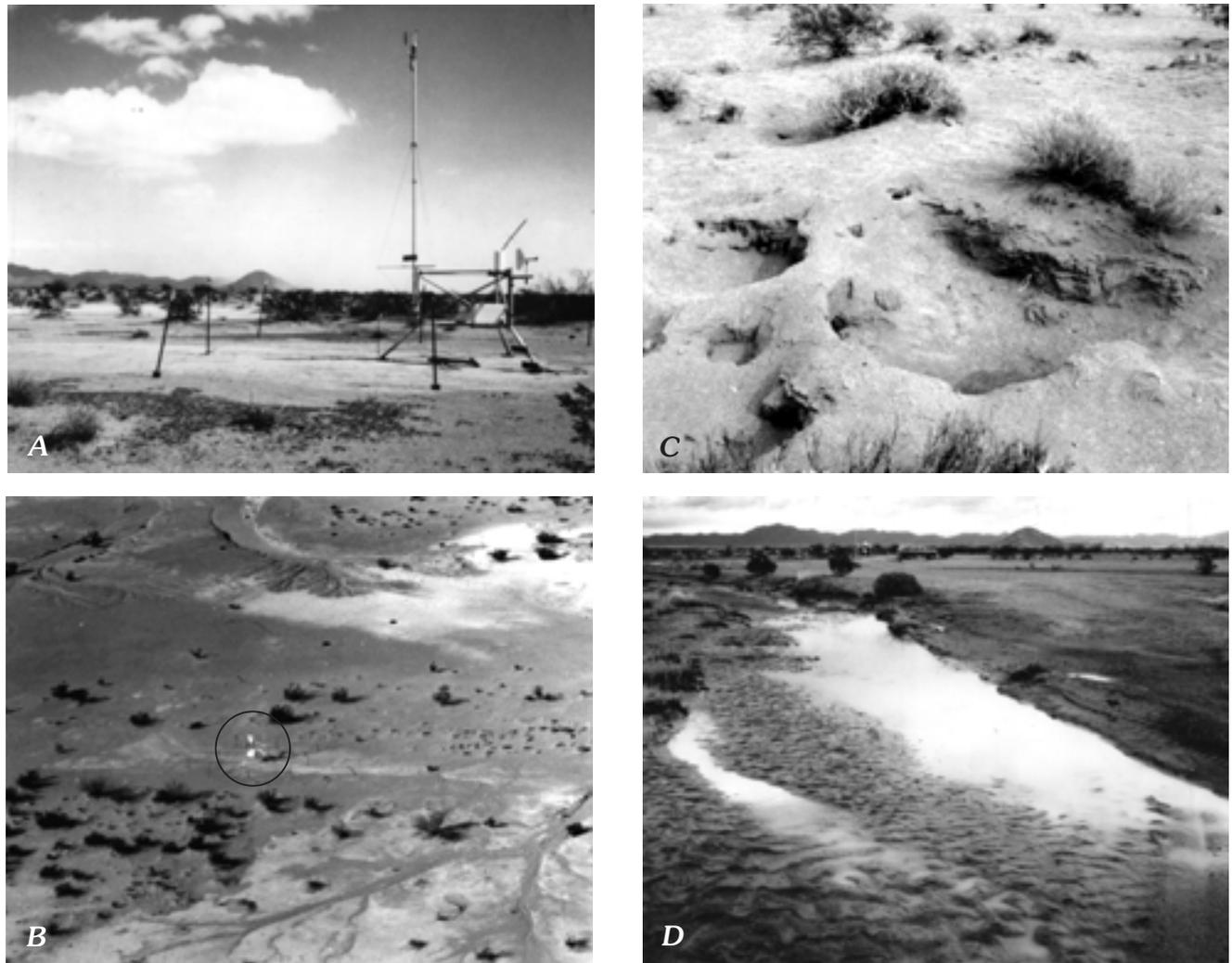
Figure 7. Characteristics of Desert Wells Geomet site. *A*, Ground view of Geomet station; *B*, Low-altitude aerial photograph showing Geomet site on alluvial plain of Bouse Wash (station is circled); *C*, surface of dunes at Geomet site; *D*, rare runoff in channel at Geomet station, January 19, 1988.

on the sand sheet, but beneath it, a stage III to IV calcic soil horizon (Gile and others, 1965) a meter or more thick has developed in the gravelly alluvium that forms the surface in much of the Yuma desert and underlies the eolian cover sands. Lag gravel covers much of the surface of the Fortuna Plain in the eastern part of the desert, and well-developed desert pavements have formed on the alluvial fan surfaces there and on Gila Mesa (fig. 9). The granitic grus that covers much of Upper Mesa and the Fortuna Plain is light toned on the satellite image (fig. 9), but the desert pavement and lag gravel derived from other rock types are typically darkened by heavy coatings of desert varnish. Morrison (1983) assigns a Pleistocene age to the alluvial fans. At present, runoff from the modern washes rarely, if ever, reaches as far west as Yuma Mesa, and the dominant agent of surface change in the central, southern, and western parts of the Yuma desert is wind.

Because of the uniformity of the surface at this locality, unlike the Gold Spring and Desert Wells sites, no detailed surficial map was made. Because the station is in a restricted (military) area, no low-altitude aerial photographs could be obtained. Repeat ground photography (fig. 10*B* in Helm and Breed, chap. B, this volume, and fig. 7 in MacKinnon and others, 1990) shows that the loose sand is frequently mobilized by wind and rearranged into ripples and small lee dunes behind bushes. Many patches of mobile eolian sand are at the Geomet site and farther south and east on Yuma Mesa as well as on Upper Mesa and the Fortuna Plain (fig. 9). The largest accumulation of active dunes is in the Fortuna Dunes along the border with Mexico. These dunes may supply sand to the northern and western parts of the Gran Desierto sand sea of northern Sonora, as suggested by Blount and Lancaster (1990).

Figure 8.   Detailed map of surficial geology of Desert Wells Geomet site (G. Billingsley, written commun., 1981).
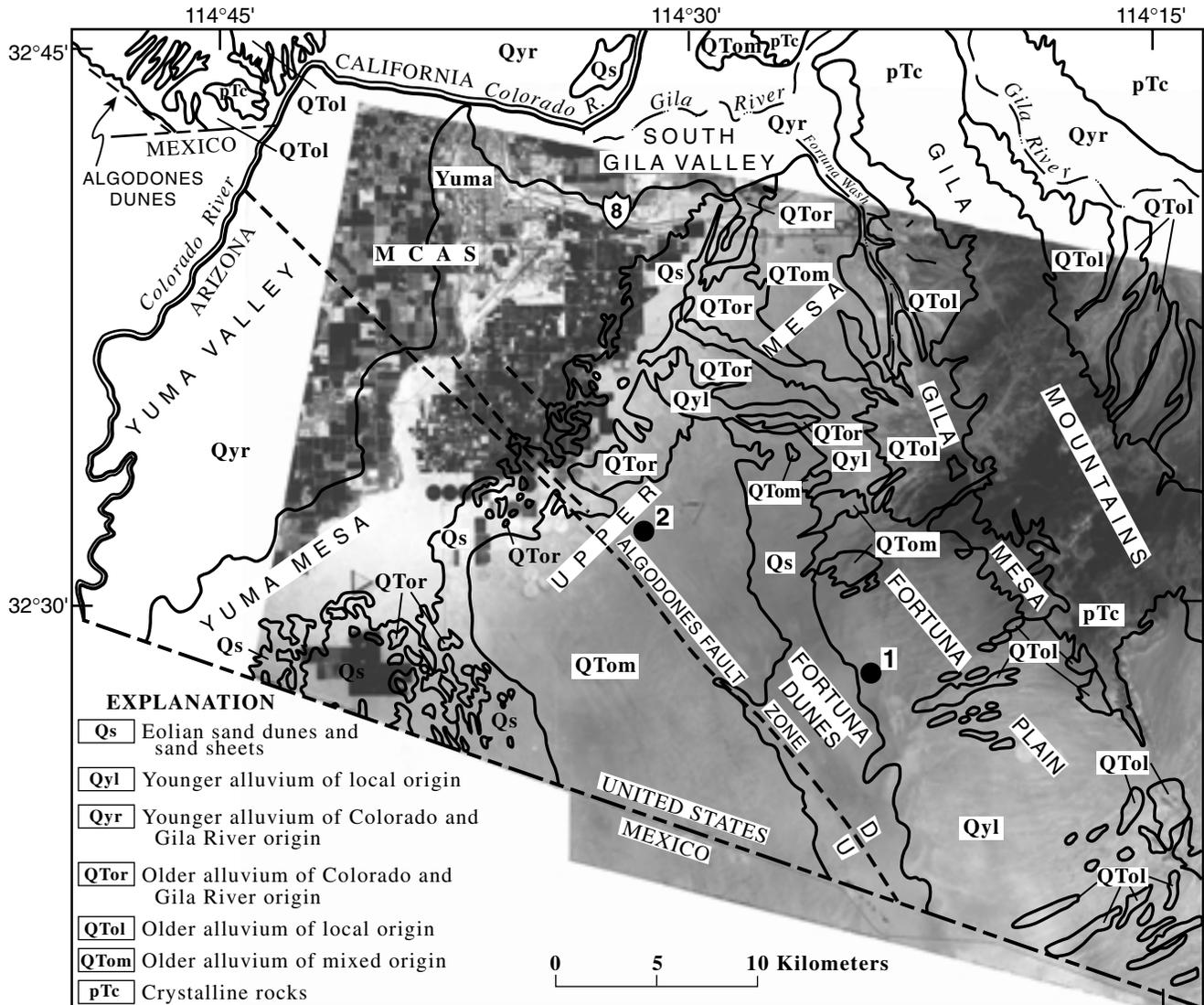
Figure 9. Annotated Système Probatoire d'Observation de la Terre (SPOT) image of the Yuma desert and vicinity showing locations of sites 1 and 2 (●) for the Geomet station (SPOT panchromatic image, 27 June 1988). Geology from Olmsted and others (1973).

Ninety-four samples of airborne sediment collected in field dust catchers (Fryrear and others, 1991; Tigges and others, chap. H, this volume) at the Geomet site were petrographically analyzed by P. Luttrell (Tallpines Environmental Consulting, Flagstaff, Ariz., written commun., 1990). The sediment ranges in grain size from silt to very coarse sand; grains are typically subrounded and moderately sorted. Compositionally, most grains are quartz (95 percent); other components include feldspar (>1 percent), fragments of igneous rock, both plutonic and volcanic (<5 percent), and traces of accessory minerals that include phlogopite, most likely derived from metamorphic rocks of the Gila Mountains. Luttrell (Tallpines Environmental Consulting, Flagstaff, Ariz., written commun., 1990) points out that the composition of the sediment presently being transported on Yuma Mesa is very different from that of

sediment in the Algodones Dunes, a 75-km-long field of actively migrating bodies of eolian sand (Smith, 1978; Sweet and others, 1988) that lies upwind to the northwest in the Salton Trough (fig. 9). As reported by Merriam (1964), the Algodones Dunes contain foraminifera shells derived from sources (the Mancos Shale of Cretaceous age) far upstream in the Upper Colorado River Basin; presumably the shells and other components that suggest a Colorado River origin were blown by wind from river deposits to the Algodones Dunes. Recent work by Muhs and others (1995) indicates that the sand in the Algodones Dunes came from ancient lake sediment derived from the Colorado River. In contrast, the eolian sand in the Yuma Mesa area is probably derived locally from Holocene alluvium washed down from the Gila Mountains by ephemeral drainages.
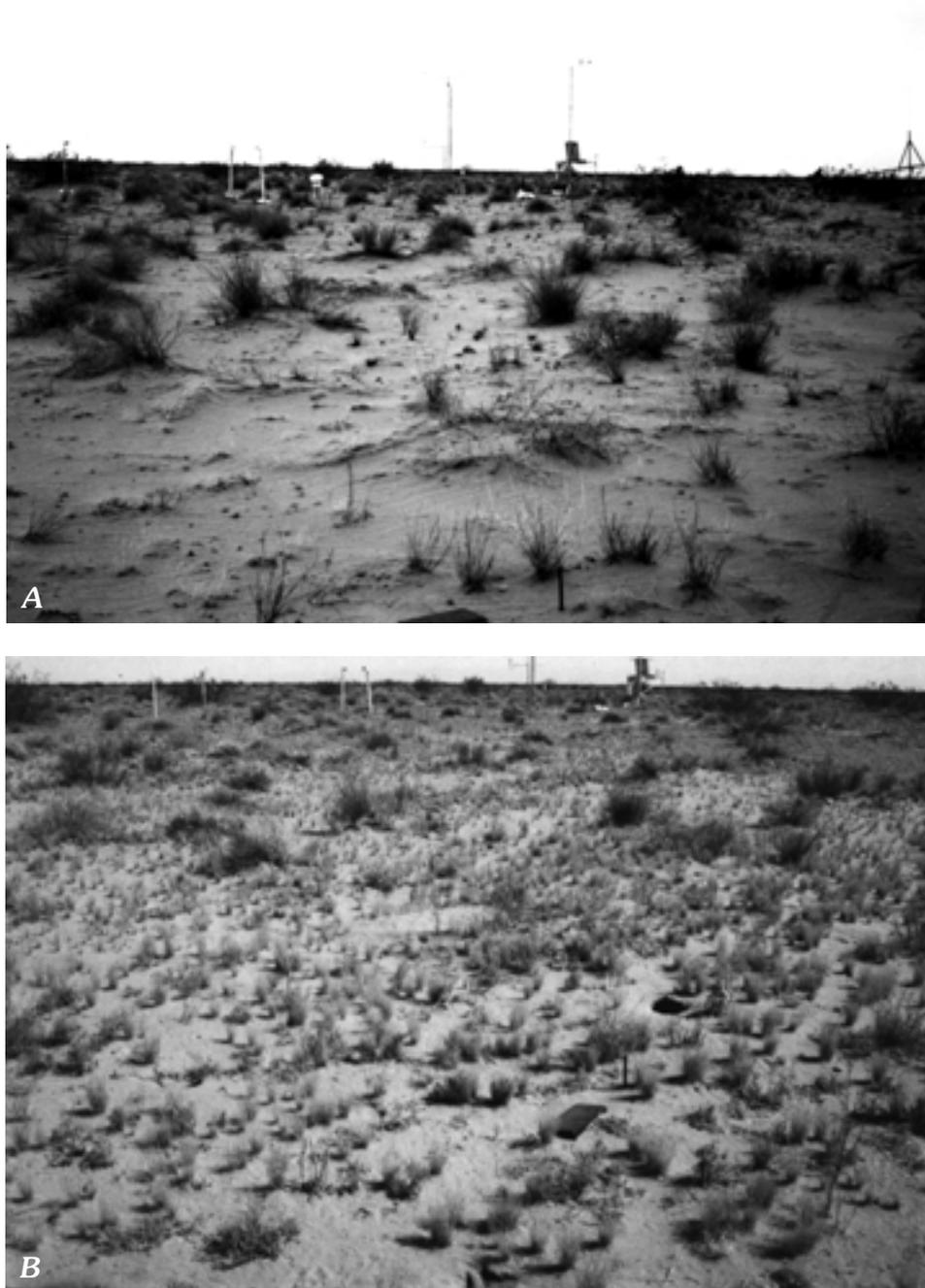
Figure 10. Yuma Geomet station. *A*, Sand sheet with ripples and lee dunes; *B*, same view after rain, with newly grown annual plants, eolian features obliterated.

The perennial vegetation at the Yuma site is very sparse, subtropical xeric scrub (fig. 10*A*). To the east on Upper Mesa are stands of ocotillo and mesquite, and other trees inhabit the dry washes. Vegetation in the Lower Colorado River Valley has undergone marked changes associated with changes in temperature and precipitation regimes during the Holocene; the modern subtropical vegetation community was established only about 4,000 years ago (Van Devender, 1990). At the Geomet station, perennial vegetation is mostly creosote-bush and white bursage with big galleta grass, but annual plants also appear after rain (fig. 10*B*). Musick (chap. D, this volume) reports on the observed changes in vegetation along transects at the present Geomet site near Yuma Mesa. Vegetation growth is strongly dependent on the antecedent (previous year's) rainfall and thereby mediates the strong association of antecedent rainfall with the production of dust, by wind erosion, as reported for southern Arizona by Brazel and others (1986) and by Brazel and Nickling (1986, 1987).

The Yuma desert is hot as well as extremely arid (thermic arid: Hendricks, 1985). It lies entirely within the 75 mm precipitation isohyet of the U.S. Weather Bureau Map of Normal Annual Precipitation (U.S. Weather Bureau, 1960). Using the Budyko aridity index (a ratio of radiational energy to the energy required for evaporation of the mean annual precipitation: Henning and Flohn, 1977; Fitzpatrick, 1979), the Salton Trough, including the Yuma desert, is assigned a value of 10. This value means that the average annual precipitation (table 1) must be multiplied by 10 in order for collected runoff to occur (that is, streamflow in usually dry washes) (by comparison, Death Valley has a value of 7 and the Western Desert of Egypt a value of 200). The Yuma area "probably has been a core North American desert for much of the Quaternary" (Cole, 1986).

At present, the Yuma area represents a transitional climatic zone between the wetter parts of the Sonoran Desert to the east and the Mojave Desert to the west. In the desert to the east, most precipitation comes in thunderstorms of the summer monsoon from the south and east; in areas to the west, most moisture comes from frontal storms in winter, from the north and west. Occasionally, in late summer or early fall, moist tropical air is driven into the Yuma area by hurricanes off the west coast of Mexico; these storms bring rare soaking rains. Late spring (April–June) is generally dry.

A major difference is apparent between mean annual precipitation values (table 1) recorded at site 1, on the Fortuna Plain, and at site 2, near Yuma Mesa (fig. 9). This difference probably reflects the influence of unusually heavy rainfall during the El Niño years 1983 and 1984 (Keen, 1987), when site 1 received more than 200 mm of annual rainfall. It also reflects the well-known spatial variability of rainfall in the Sonoran Desert (Ezcurra and Rodrigues, 1986).

The move from site 1 to site 2 was required by military authorities. The Yuma desert is used as a missile and gunnery training range by the U.S. Air Force and is managed by the Marine Corps Air Station at Yuma. In 1988, changes in the bombing and strafing patterns of military aircraft flying over the original Geomet site on the Fortuna Plain made it necessary to move the station to a safer site near Yuma Mesa, about 13 km to the west-northwest (site 2 on fig. 9). Although the surface characteristics of the two sites differ (the surface at the first site is an alluvial plain with a lag of pea gravel; the surface at the second site is about 1-m-thick eolian sand sheet on a fluvial terrace), the surficial geologic units at both sites are classified in a highly general way and in the same category by Morrison (1983) as "alluvium of early to middle Pleistocene [age], with some overlying eolian sand of middle Pleistocene to Holocene age, on gently sloping Pliocene to middle Pleistocene mesa and piedmont surfaces, with soil development that ranges from nil to strong."

Following the move to a safer site, a SENSIT was installed at the Geomet site near Yuma Mesa in May 1988, as the station was upgraded to superstation status (described by

Tigges and others, chap. H, this volume). Several different research efforts were carried out in and around the station. Helm (1991) and Helm and Breed (chap. B, this volume) report preliminary results of Yuma sand-flux studies using SENSIT and climatic data. Musick (chap. D, this volume) compares the sheltering effect of the sparser vegetation at Yuma with that at Jornada. Baudat and Breed (chap. E, this volume) report results of efforts to identify types of windstorms associated with blowing sand and the presence of dust in the Yuma area, using Geomet data in concert with synoptic weather data and observations of visibility and cloud cover by military observers at the Marine Corps Air Station at Yuma. Crowley and Bowers (chap. F, this volume) report variations in surface properties indicated by changes on retrospective Landsat multispectral (MSS) images between 1980 and 1988, including the years 1982–1986 when the Geomet station was at its original location on the Fortuna Plain (site 1 on fig. 9).

JORNADA

The Jornada Geomet site (fig. 11) was selected to represent the northern part of the Chihuahuan Desert in south-central New Mexico (fig. 1). The Jornada Geomet station (fig. 12) is on the U.S. Department of Agriculture/Agricultural Research Service (USDA/ARS) Jornada Experimental Range (JER), about 37 km northeast of Las Cruces, N. Mex. The station lies on the sandy surface of a plain bounded on the east by the Organ and San Andres Mountains and on the west by the Doña Ana Mountains and Robledo Hills. Farther to the west is the valley of the Rio Grande River, entrenched 100 m below the elevation of the Jornada Del Muerto Plain.

The geologic setting of the Jornada area (summarized by Hawley and others, 1969; Hawley and Kottlowski, 1969) is a north-trending, aggraded basin of internal drainage whose surface forms the Jornada Del Muerto Plain. The Jornada Basin is one of a series of linked, en echelon structural basins formed within the Rio Grande rift by block faulting during the middle Tertiary. In the Jornada area, the basin is filled to a depth of about 300 m with consolidated basin fill (clay, sand, and gravel) deposited as alluvial fan and fluvial sediments of the Santa Fe Group of Miocene to middle Pleistocene age. The uppermost unit of the Santa Fe Group is the Camp Rice Formation, which consists mostly of fluvial sediments deposited by the ancestral Rio Grande prior to about 0.6 Ma. After 0.6 Ma, the modern river cut into the basin fill in several successive stages that produced a sequence of geomorphic surfaces (Ruhe, 1967), which step up topographically from the Rio Grande Valley to the piedmont slopes of the bounding mountains. The entrenchment left the surface of the Jornada del Muerto as a closed basin of internal drainage, high above the present river valley and not graded to the modern Rio Grande.

Figure 11. False-color Landsat thematic mapper image (principal components of bands 1, 4, 7) merged with SPOT panchromatic image data showing location of Jornada Geomet site (x) on sand plain of the Jornada del Muerto. Eolian veneer, shown in pink, crosses several mapped units. Compare with extent of stippled units identified as eolian on geologic map (Seager and others, 1987). (Landsat TM image 50193-17092, 10 September 1984). JER, Jornada Experimental Range.

Much of the bolson plain is overlain by unconsolidated Organ alluvium of Holocene age, a unit that includes occasional lacustrine and eolian deposits and is "seldom more than 4.5 m thick" (Hawley and others, 1969). The specially processed Landsat thematic mapper image (fig. 11) suggests a much broader pattern of eolian deposition than is shown on the conventional geologic map (Seager and others, 1987). On the Landsat image, false colors represent the spectral reflectance of the upper few microns of the land surface, such that, although a surface material may be only millimeters thick, its composition may dominate the spectral response. The distribution of surface materials shown as bright pink in figure 11 corresponds only partly to the distribution of eolian deposits shown on the map. It is much more extensive and continuous, suggesting that the image may illustrate blanketing of the desert surface by a thin veneer of eolian dust. Such a phenomenon has been recognized in the Safsaf area of the Egyptian Sahara, where

Figure 12.   Ground-level photograph of Jornada Geomet station.

similar Landsat color patterns (fig. 9 in Davis and others, 1993) are interpreted as the spectral signature of hematite-rich, fine-grained particles (eolian dust) on the desert surface. At Jornada, as in other desert areas, windblown dust may infiltrate loose, permeable sediment on the surface and contribute to the development of soil. The potential addition of various components to soils by windblown dust has been described by Gile and others (1965), Yaalon and Ganor (1975), Colman (1982), McFadden and Weldon (1987), Reheis and others (1995), and many others.

Because of the uniformity of the surface at this locality, as at Yuma, no detailed surficial geologic map was made of the Geomet site. The surface at the Geomet site consists of sandy loam developed in a Holocene sand sheet about 0.5 m thick. At several localities the Holocene sand cover has been deflated, exposing calcrete (stage IV of Gile, 1967) that developed in the underlying Pleistocene basin fill. The soils of this agricultural region have been well mapped, but soils around the Geomet station are not so well studied as those several kilometers to the south, which were examined in detail by the Desert Project of the U.S. Soil Conservation Service from 1957 to 1972 (Gile and others, 1981).

The northern Chihuahuan Desert is mesic, warm, and semiarid (table 1); it is the least arid of the areas included in the Desert Winds Project. Precipitation comes mostly from the Arizona summer monsoon in July, August, and September, but also from winter moisture from Pacific frontal storms.

The Jornada area has been a focus of desert studies related to rangeland management for more than half a

century, and recently it has been identified (Dregne, 1986) as one of the four most desertified places in the United States (the Gold Spring area in northeastern Arizona, described above, is another). The concern at the Jornada Experimental Range rises from the observations, by many biologists and ecologists, that the desert grassland of southern New Mexico has been progressively invaded and replaced by mesquite duneland, which is useless for grazing and therefore has a much reduced economic value (Buffington and Herbel, 1965).

Present-day vegetation on the Jornada Experimental Range is a mosaic of desert grasslands (fig. 13*A*) dominated by black grama, and desert dunelands dominated by mesquite (Musick, chap. D, this volume). Each mesquite bush typically accumulates windblown sand around its base, forming a coppice dune. In areas to the northeast of the Geomet site, coppice dunes reach heights of 2 to 3 m above the surface of the sand plain, forming an irregular, hummocky topography (fig. 13*B*). The Geomet station (fig. 12) lies in the ecotone where mesquite has progressively displaced grassland. One of the vegetation transects on which changes have been monitored by USDA-ARS scientists since 1935 traverses the area north of the station (Hennessy and others, 1983). Gibbens and others (1983) report that the frequency of black grama grass on that transect dropped from 27.2 percent (relatively abundant) in 1935 to half that in 1950, then dropped to 0.9 percent in 1955, and to zero in 1980. As mesquite replaces grass, coppice dunes develop and produce a hummocky topography in place of flat grass-lands. The change in topography is exacerbated by wind

Figure 13. Changes in surface characteristics exacerbated by wind erosion are illustrated by differences in topography and vegetation from an upwind area (*A*) to the downwind area (*B*). Localities shown in *A* and *B* also indicated on figure 11. *A*, Grassland at Jornada; *B*, Dunelands at Jornada.

erosion with distance downwind across the Jornada plain (fig. 13).

The Jornada station was deployed in cooperation with the U.S. Army Topographic Engineering Center, Fort Belvoir, Va., which provided many of the sensors necessary for their remote monitoring of ground surface changes associated with the Geomet-monitored climatic conditions (Krusinger, 1988). Because of the long history of monitored vegetational changes at the Jornada Experimental Station, the Desert Winds Project studies at Jornada have focused largely on identifying vegetation characteristics that influence the erosivity of measured winds. A report by
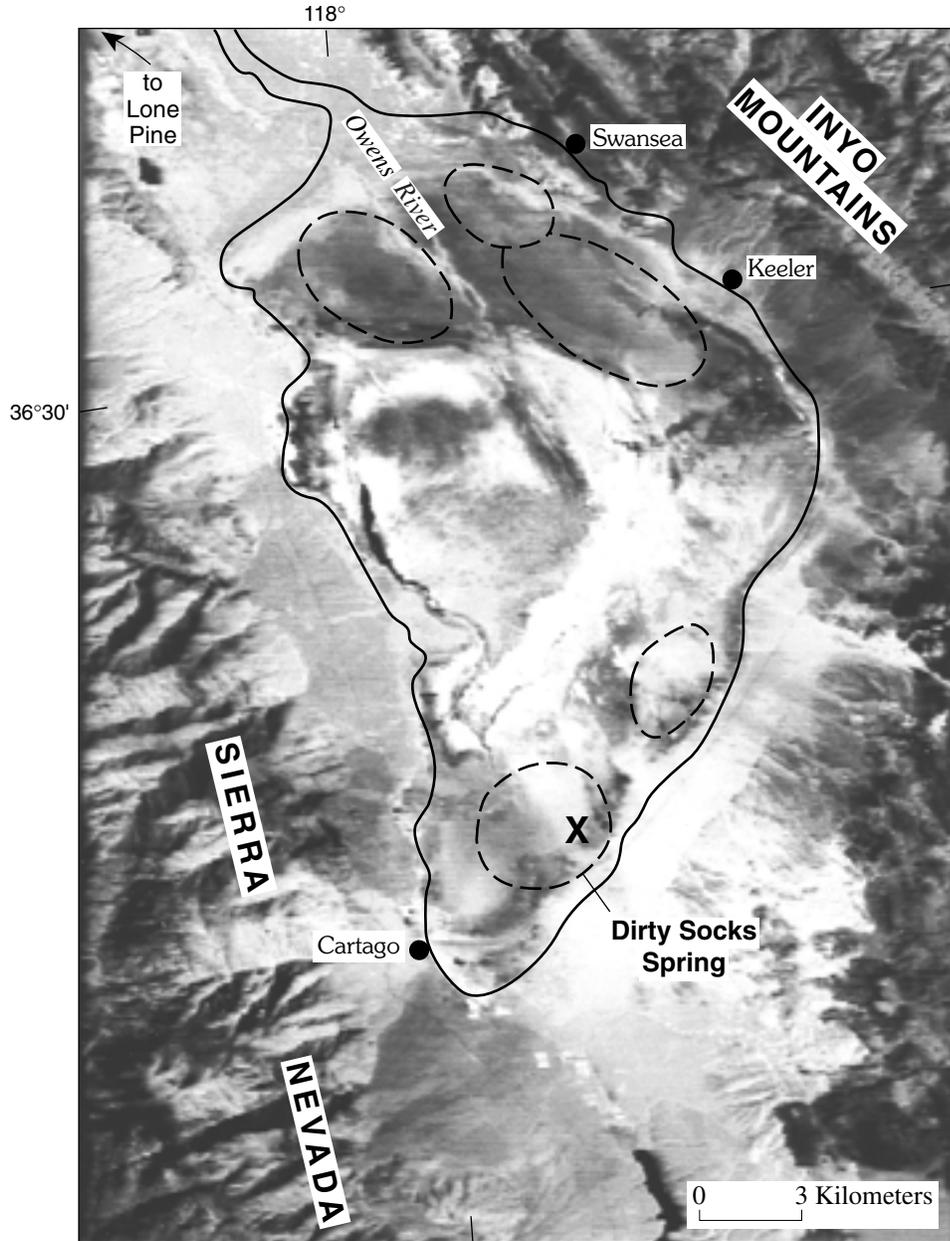
Figure 14.   Annotated Landsat multispectral image of Owens Lake showing location of Geomet site (x). Dashed lines indicate dust-producing areas (Cahill and others, 1994). (Landsat MSS image 1396-18001-7, 22 August 1973).

Musick (chap. D, this volume) is one of several on the subject of vegetation cover at Jornada and its influence on wind erosion (Musick and Gillette, 1990; Musick and others, 1995, 1996, 1998).

OWENS LAKE

The Mojave Desert (fig. 1), which lies mostly in southern California, is transitional in climate, topography, and vegetation between the Sonoran Desert to the south and east, and the Great Basin Desert to the north and east. Owens Valley, Panamint Valley, and Death Valley of east-central California are included in the Mojave Desert because the desertscrub vegetation in those valleys is more closely allied to that of the southern California region than to that of the Great Basin Desert in Nevada and Utah (Bailey, 1995). The Owens (dry) Lake Geomet site (fig. 14) was selected to represent one type of terrain—playas—common in the Mojave Desert, although the site is at the northwesternmost limit of the Mojave, and Owens Lake is dry primarily because its water has been exported

Figure 15. Ground-level photograph of Owens (dry) Lake Geomet station.

to Los Angeles. The Owens Lake site replaced the original Mojave playa site at Red Lake, Ariz., which was vandalized shortly after a Geomet station was deployed there. The Owens Lake Geomet station (fig. 15) is deployed on the dry lake bed about 2.5 km north of Dirty Socks Spring (fig. 14). The site is accessible only when the lake bed around the station is dry, by a single raised roadway of packed salt and gravel guarded by locked gates.

Owens Lake occupies the southern part of the Owens Valley, a narrow (30 km wide) structural basin between the Sierra Nevada, which rise to more than 4,000 m elevation to the west, and the White and Inyo Mountains, which rise to more than 3,000 m elevation to the east. The complex graben that underlies Owens Valley marks the western boundary of the Basin and Range physiographic province and is part of an active tectonic zone marked by recent volcanism and earthquakes (Bierman and others, 1991). The valley is partly filled with alluvial, lacustrine, and colluvial sediment and volcanic deposits of Tertiary and Quaternary age.

Owens Lake is an artificial rather than a naturally occurring playa, for its desiccation was accelerated by diversion of water from the Owens River system to urban use via the Los Angeles Aqueduct, beginning in 1912. Prior to diversion, Owens Lake was about 10 m deep and covered 270 km^2. During Quaternary pluvial periods (times of increased effective moisture), Owens Lake was one of a chain of lakes that, during times of maximum runoff, extended from Mono Lake (which still holds water) downstream as far as Lake Manly in Death Valley (Smith, 1984).

Because the Owens Valley lies in the rain shadow of the Sierra Nevada range, it is an arid area where precipitation (table 1) falls mostly in winter and spring. The lake surface is commonly sticky and impassable after rainstorms. No vegetation grows on the lakebed, but the margins of the lake, which are perennially wetted by springs and local runoff, support saltgrass and saltbush scrub (Cahill and others, 1994, table XVb). Because vegetation is absent around the Geomet station, no vegetation transects were established for this site.

For more than half a century since diversion of its water, Owens (dry) Lake has been a notorious source of noxious dust, probably the most prolific source of very fine, health-threatening aerosolic dust particles in the United States (Reinking and others, 1975; Cahill and others, 1996). So pervasive is the unusually fine dust blown from the lakebed that it is known locally (for a community east of the lake) as "Keeler fog" (Cahill and others, 1996). Because production of dust is the most important consequence of wind erosion at this locality, the primary role of the Geomet station at Owens Lake is to obtain field data on the local climatic conditions that control the generation of dust from the surface of the lake bed and to provide long-term data relevant to studies reported by Reheis (chap. G, this volume) of the transportation and deposition of dust in soils at localities downwind. Based on satellite tracking, dust generated from Owens Lake is reported to travel more than 250 km downwind to the south, rising to heights of more than 1,300 m above the ground and covering nearly 10,000 km^2 (Reinking and others, 1975). On the other hand, Reheis (1997, and chap. G, this volume) reports that the input of Owens Lake dust to soils to the south diminishes beyond about 50 km distance downwind.

The lakebed surface of crusted salt, silt, and clay is impacted by sand grains blown from dunes near Dirty Socks Spring (fig. 14) and from another dune field near Swansea during windstorms from the north, west, and south (Cahill and others, 1996). The mechanism by which saltating

(bouncing) sand grains generate dust from vulnerable surfaces is described by Gillette (1981, 1986).

At Owens Lake, the Geomet station became fully operational in May 1992, with a full set of superstation sensors supplied by the National Oceanic and Atmospheric Administration (NOAA, Air Resources Laboratory, Boulder, Colo.) and by the U.S. Army Topographic Engineering Center, Fort Belvoir, Va. (equipment and operations are described by Tigges and others, chap. H, this volume). The generation of dust under Geomet-monitored conditions of wind speed, wind direction, and precipitation has been recorded by an array of three additional SENSIT's emplaced north of the Geomet station by Gillette and others (1997) to supplement the data on sand flux from the SENSIT at the Geomet station. Additional meteorological information for their study was contributed from instruments located in towns around the lakeshore, but the erosivity of wind, recorded on site by the Geomet station, commonly differed significantly from that of winds recorded outside the lakebed. Cahill and others (1996) conclude that "on-lakebed studies are essential for quantitative prediction of dust events."

RESEARCH ASSOCIATED WITH GEOMET SITES

Research is conducted in or around the Geomet sites by geologists, biologists, physicists, and other scientists, several of whom work independently of, but in collaboration with, the Desert Winds Project of the U.S. Geological Survey. These independent studies fill some gaps in the research program envisioned in the original project plan, but not all potential scientific uses of the sites and their geometeorological data have been realized. Many shortages and changes in personnel and modifications in the technology for remote monitoring have occurred since 1979, with consequent changes in project research priorities. In addition, periods of record vary with the length of time that Geomet stations were operational (3 times longer at Gold Spring, for example, than at Owens Lake). Inevitably, unequal attention was given to various research goals among the sites. For example, vegetation monitoring and repeat photography were carried out more consistently at some sites, such as Yuma and Jornada, than at others, whereas surficial geologic mapping was done only at Gold Spring and Desert Wells, where diverse surface materials and topography warranted the effort. Researchers with specific scientific objectives tend to concentrate their efforts at one site or another that has attributes most applicable to a particular research problem (for example, the problems of dust generation and transport is addressed mainly by scientists at the Owens Lake site). Research that compares and contrasts the effects of measured winds on ground surfaces at more than one desert site, a primary goal of the project, has been limited to the efforts of Helm and Breed (chap. B, this volume) and of Musick (chap. D, this volume).

In chapter B of this volume, Helm and Breed report the sand-moving effectiveness of winds recorded during particular storms associated with different seasons at Gold Spring, Yuma, and Jornada in 1991 and 1992. Though preliminary, their analysis represents an attempt to characterize the vulnerability of natural surfaces to wind erosion under climatic conditions monitored over a relatively long period of record. Results of a similar but short-term study of the movement of sand by measured winds at field sites around the Desert Wells Geomet site are reported by Wolfe and Helm in chapter C of this volume. Their results indicate that the vegetation cover at most of the sites, including rangeland, abandoned farmland, and desert scrubland, is not sufficient to protect these surfaces from erosion by strong winds.

In chapter E of this volume, Baudat and Breed report on the occurrences of dust observed at Yuma Marine Corps Air Station in association with particular types of storms (shown on daily U.S. Weather Service maps), during periods when sand-moving winds were recorded at the Yuma desert Geomet site. Their analysis, built on the work of Nickling and Brazel (1984), Brazel and others (1986), and of Brazel and Nickling (1986, 1987), suggests that blowing dust occurs year-round in Yuma in a fairly predictable pattern associated with several different types of weather patterns. Large interannual variations in the frequency of dust-producing events at Yuma are, as recognized earlier, related to antecedent precipitation. In particular, changes in the frequency of sand-flux events may mark the duration of effects of El Niño on vegetation, and thereby on surface vulnerability to wind erosion.

A key aspect of the capacity of wind erosion to modify land surfaces is the sheltering effect of vegetation. Vegetation acts as roughness elements that mediate the erosivity of wind, as described by Gillette and Stockton (1989) and Musick and Gillette (1990). In chapter D of this volume, Musick reports the results of his studies of vegetation changes at Yuma and Jornada in 1988 and 1987, respectively, to 1992. Although limited to these two sites, his observations reported in this volume and in related papers (cited above) are significant because they represent plant/wind interactions in both the most arid (Yuma) and least arid (Jornada) parts of the North American Desert (figs. 1, 2). Key goals of Musick's work have been to identify threshold values for amounts of vegetation cover that can protect natural surfaces from wind erosion under given sets of climatic conditions and to identify the structural characteristics of plants that influence wind erosivity. Recently, he has shown that airborne synthetic aperture radar (AIRSAR) of the Jornada site can be used to discriminate woody shrubs, such as the invasive mesquite, from grasslands by remote sensing (Musick and others, 1998), thus demonstrating a new technique for monitoring vegetation change.

Vegetation also serves as a proxy indicator for historic changes in land surfaces related to climate variations. In chapter F of this volume, Crowley and Bowers relate surface (primarily vegetation) changes observed on Landsat images of the Yuma desert to variations in rainfall. This effort was only minimally successful because an insufficient number of Landsat scenes were available for analysis (that is, the twice-yearly observations of surface characteristics were too widely spaced over the time period) and because the rainfall data were from a point source (the Geomet station) in a region where rainfall is notorious for its spatial variability. In general, the usefulness of retrospective satellite imaging for long-term monitoring of surface changes in desert areas depends on the availability of satellite data obtained with sufficient frequency to track changes, as well as the availability of detailed climatic data from a closely spaced network of ground stations. Both requirements entail expensive investments not likely to be applied to U.S. desert regions where land values are low.

A second, less conventional type of remote sensing of land surface changes depends on data from automated instruments mounted on ground stations. Various remote sensors that record incoming and outgoing (reflected or emitted) solar energy in the visible to infrared parts of the spectrum (described by Tigges and others, chap. H, this volume) were placed at the Geomet sites at Yuma, Jornada, and Gold Spring. These instruments were provided by the U.S. Army Topographic Engineering Center (TEC) at Fort Belvoir, Va., which operates a station similar to the USGS Geomet stations but in a humid environment. Since 1986, TEC has joined in the operations, maintenance, and refurbishing of Geomet stations by the Desert Winds Project in order to obtain data for comparison between their humid site (Virginia) and the USGS' extremely arid (Yuma), arid (Gold Spring), and semiarid (Jornada) sites, and at Owens Lake. They use the radiation data to study changes in the radiometric temperatures of surface features, including vegetation, under specific climatic conditions recorded by other Geomet sensors. Recognizing climate-related changes in the background temperatures in different environments is critical to solving problems of target detection, camouflage, cover and concealment, and other aspects of military operations. A sample of the data from these sensors is provided by Tigges and others (chap. H, this volume), and a preliminary technical report has been published (Krusinger, 1988).

The generation of dust from the Owens (dry) Lake Geomet site and the transport of dust to soils in downwind areas are described by Reheis (1997) and in chapter G of this volume. In 1991, she placed seven dust traps at localities in and near Owens Lake, including one on the lakebed near the Geomet station (fig. 15) north of Dirty Socks Spring. Three dust traps are placed southward along a 50-km transect in southern Owens Valley, two are north of the lake (one on each side of the valley), and another is on a slope of the White Mountains high above the valley. Reheis (1997 and

chap. G, this volume) reports that 3 years of data show "abnormally high" rates of dust deposition downwind from Owens Lake, which are "one to two orders of magnitude greater than regional average rates," with the highest rates in winter. Her documentation of the input of windblown dust into desert soils is a significant contribution to a growing body of evidence that many components of desert soils are supplied mostly by the incorporation of windblown dust (Yaalon and Ganor, 1975; Gile and others, 1981; Chadwick and Davis, 1990; Slate and others, 1991; Reheis and others, 1995).

Chapter H of this volume, by Tigges and others, describes the operations and maintenance of the Geomet stations and the various automated sensors deployed there.

The Desert Winds Project has brought new understanding of the climatic variability from desert to desert and within each area over relatively short periods of time. Helm and Breed (chap. B, this volume) show that the percent duration of effective (sand-moving) winds varies with the type and seasonality of storms (summer thunderstorms, fall/winter frontal storms) from site to site. Dramatic changes in land surface sediments and vegetation have been observed (figs. 10A, 10B, 13A, 13B; Helm and Breed, chap. B, this volume, fig. 3; Musick, chap. D, this volume, fig. 3) in relation to climatic conditions that have varied from drought to the unusually heavy rainfalls associated with El Niño events. The extreme variability of climatic conditions represented by the Geomet records is significant because the repeated changes from dry to wet and back again makes such transitional areas particularly vulnerable to wind erosion, as surfaces respond to changing climate with attempts by geologic processes to restore equilibrium.

SUMMARY AND CONCLUSIONS

The Desert Winds Project has produced a database of climatic records for desert sites that represent the major subdivisions of the North American Desert. Periods of record range from 18 years (Gold Spring station) to 5 years (Owens Lake station). Unlike records from most ordinary weather stations, the Geomet records include measurements of wind speeds and directions obtained as frequently as 10 times per hour, and measurements of solar energy reflected and emitted from selected desert surfaces. These data, as well as the records of other parameters (precipitation, humidity, barometric pressure, soil temperature, sand flux, and so on: Tigges and others, chap. H, this volume) are being prepared for release on CD-ROM, as have some of the data for the Gold Spring station (Helm and others, 1995) and the data for the Desert Wells station (Helm and others, 1998).

The addition of experimental sand-flux sensors (Tigges and others, chap. H, this volume) to the array of automated Geomet instruments has made feasible the remote detection of eolian sand transport under known conditions of wind

speeds and durations, of rainfall, air and soil temperatures, and other parameters over much longer periods of time than previously possible. Parts of the records for stations at Yuma, Gold Spring, and Jornada have been analyzed by Helm and Breed (chap. B, this volume), and similar records for Owens Lake have been analyzed by Gillette and others (1997).

Shortcomings of the Desert Wind Project are related to the uneven applications of research efforts at the various Geomet sites, largely due to changes in research goals, resources, and priorities. Early efforts were concentrated at Gold Spring, which is most accessible from project headquarters in Flagstaff, Ariz., and at Yuma and Jornada, where P. Helm, B. Musick, and U.S. Army Topographic Engineering Center scientists applied most of their efforts. Studies at Desert Wells were carried out mainly by S. Wolfe, while studies at Owens Lake began much later in the project and have been carried out primarily by M. Reheis along with D. Gillette and his associates. As a result, original goals such as systematic monitoring of changes in vegetation and surface sediment distribution (dunes, sand sheets, gravel spreads, and so on) by measurements along permanent transects and by repeat photography at camera stations established at each site (for example, as mapped on figs. 5 and 8) have been met only unevenly.

Despite these shortcomings, the Desert Winds Project has managed to obtain an unparalled database for climate variation and associated wind erosion in type localities in the North American Desert. This database provides baseline information for detecting future changes related to human activity and (or) climate variation. The baseline data on climatic variability are critical to future interpretations of climate change.

REFERENCES CITED

Aiken, C.L., Wetterauer, R.H., and de la Fuente, M.F., 1980, A merging of aeromagnetic data sets in southwest Arizona and northwest Mexico and analysis of the results, *in* Jenney, J.P., and Stone, Claudia, eds., Studies in Western Arizona: Arizona Geological Society Digest, v. 12, p. 31–43.

Bailey, R.G., 1995, Descriptions of the ecoregions of the United States: U.S. Department of Agriculture Forest Service Miscellaneous Publication 1391, 108 p., scale 1:17,000,000.

Betancourt, J.L., 1988, El Niño/Southern Oscillation (ENSO) and climate of the southwestern United States: Paleoecology Workshop, February 15–17, Boston, National Oceanic and Atmospheric Administration and National Science Foundation, p. 55–79.

Bierman, Paul, Gillespie, Alan, Whipple, Kelin, and Clark, Douglas, 1991, Quaternary geomorphology and geochronology of Owens Valley, California: Geological Society of America Field Trip, *in* Walawender, M.J., and Hanan, B.B., eds., Geological Excursions in Southern California and Mexico: Guidebook, 1991 Annual Meeting, Geological Society of America, San Diego, Calif., October 21–24, p. 199–222.

Billingsley, G.H., 1987a, Geologic map of the southwestern Moenkopi Plateau and southern Ward Terrace, Coconino County, Arizona: U.S. Geological Survey Miscellaneous Investigations Series Map I-1793, scale 1:31,680.

———1987b, Geology of the southwestern Moenkopi Plateau and southern Ward Terrace, Arizona: U.S. Geological Survey Bulletin 1672, 18 p.

Blount, Grady, and Lancaster, Nicholas, 1990, Development of the Gran Desierto sand sea, northwestern Mexico: Geology, v. 18, p. 724–728.

Brazel, A.J., and Nickling, W.G., 1986, The relationship of weather types to dust storm generation in Arizona (1965–1980): Journal of Climatology, v. 6, p. 255–275.

———1987, Dust storms and their relation to moisture in the Sonoran-Mojave Desert region of the Southwestern United States: Journal of Envrionmental Management, v. 24, p. 279–291.

Brazel, A.J., Nickling, W.G., and Lee, Jeffrey, 1986, Effect of antecedent moisture conditions on dust storm generation in Arizona, *in* Nickling, W.G., Aeolian Geomorphology: Boston, Allen and Unwin, p. 261–271.

Breed, C.S., and Breed, W.J., 1979, Dunes and other windforms of Central Australia (and a comparison with linear dunes on the Moenkopi Plateau, Arizona), *in* El-Baz, F., and Warner, D.M., eds.: U.S. National Aeronautics and Space Administration Special Paper SP-412, p. 319–358.

Breed, C.S., Fryberger, S.G., Andrews, Sarah, McCauley, Camilla, Lennartz, Frances, Gebel, Dana, and Horstman, Kevin, 1979, Regional studies of sand seas, using Landsat (ERTS) imagery, *in* McKee, E.D., ed., A Study of Global Sand Seas: U.S. Geological Survey Professional Paper 1052, p. 305–397.

Breed, C.S., McCauley, J.F., Breed, W.J., McCauley, C.K., and Cotera, A.S., Jr., 1984, Eolian (wind-formed) landscapes, *in* Smiley, T.L., Nations, J.D., Péwé, T.L., and Schafer, J.P., eds., Landscapes of Arizona: New York, University Press, p. 359–413.

Bryson, R.A., and Hare, F.K., eds., 1974, World survey of climatology, v. 11, Climates of North America: New York, Elsevier, p. 193–335.

Bryson, R.A., and Lowry, W.P., 1955, Synoptic climatology of the Arizona summer precipitation singularity: Bulletin of the American Meteorological Society, v. 36, p. 329–339.

Buffington, L.C., and Herbel, C.H., 1965, Vegetational changes on a semidesert grassland range from 1858 to 1963: Ecological Monographs, v. 35, p. 139–164.

Bull, W.B., 1984, Alluvial fans and pediments of southern Arizona, *in* Smiley, T.L., Nations, J.D., Péwé, T.L., and Schafer, J.P., eds., Landscapes of Arizona—The Geological Story: New York, University Press, p. 229–252.

Cahill, T.A., Gill, T.E., Reid, J.S., Gearhart, E.A., and Gillette, D.A., 1996, Saltating particles, playa crusts, and dust aerosols from Owens (dry) Lake, California: Earth Surface Processes and Landforms, v. 21, p. 621–639.

Cahill, T.A., Gillette, D.A., Gill, T.E., Gearhart, E.A., Reid, J.S., and Yau, M-L, 1994, A collaborative Owens Lake aerosol study: Draft final report, 4/14/94, Contract A-132-05, Research Division, California Air Resources Board, Sacramento, Calif., 142 p.

Carr, M.H., 1981, The Surface of Mars: New Haven, Yale University Press, 232 p.

Chadwick, O.A., and Davis, J.O., 1990, Soil-forming intervals caused by eolian sediment pulses in the Lahontan basin, northwestern Nevada: Geology, v. 18, p. 243–246.

Changery, M.J., 1983, A dust climatology of the Western United States: National Climatic Data Center NUREG/CR 3211, RB: National Oceanic and Atmospheric Administration, Asheville, N.C., 40 p.

Cole, K.L., 1986, The Lower Colorado River Valley: A Pleistocene desert: Quaternary Research, v. 25, p. 392–400.

Colman, S.M., 1982, Clay mineralogy of weathering rinds and possible implications concerning the source of clay minerals in soils: Geology, v. 10, p. 370–375.

Davis, P.A., Breed, C.S., McCauley, J.F., and Schaber, G.G., 1993, Surficial geology of the Safsaf region, south-central Egypt, derived from remote sensing and field data: Remote Sensing of Environments, v. 46, p. 183–203.

Demsey, K.A., 1988, Quaternary geologic map of the Salome 30×60 minute quadrangle, west-central Arizona, 1:1,000,000: U.S. Geological Survey COGEOMAP Program, no. 14-08-001-A0378.

Dregne, H.E., 1986, Desertification of arid lands, *in* El-Baz, F., and Hassan, M.H.A., eds., Physics of Desertification: Boston, Martinus Nijhoff Publishers, p. 4–34.

Durrenberger, R.W., 1976, Climatic regions of Arizona: Arizona Resources Information Systems Cooperative Publication no. 8, Office of Arizona State Climatologist, Tempe, Arizona State University, 25 p.

Eberly, L.D., and Stanley, T.B., Jr., 1978, Cenozoic stratigraphy and geologic history of southwestern Arizona: Geological Society of America Bulletin, v. 89, p. 921–940.

Ezcurra, Exequiel, and Rodrigues, Valdemar, 1986, Rainfall patterns in the Gran Desierto, Sonora, Mexico: Journal of Arid Environments, v. 10, p. 13–28.

Fitzpatrick, E.A., 1979, Radiation, *in* Goodall, D.W., Perry, R.A., and Howes, K.M.W., eds., International Biological Programme, Arid-Land Ecosystems: Structure, Functioning, and Management, London, Cambridge University Press, v. 1, p. 347–370.

Fryrear, D.W., Stout, I.G., Hagen, L.J., and Vories, E.D., 1991, Wind erosion: Field measurement and analysis: Transactions of the American Society of Agricultural Engineers, v. 34, no. 1, p. 155–160.

Gibbens, R.P., Tromble, J.M., Hennessy, J.C., and Cardenas, M., 1983, Soil movement in mesquite dunelands and former grasslands of southern New Mexico from 1983 to 1980: Journal of Range Management, v. 36, p. 145–148.

Gile, L.H., 1967, Soils of an ancient basin floor near Las Cruces, New Mexico: Soil Science, v. 103, no. 4, p. 265–276.

Gile, L.H., Hawley, J.W., and Grossman, R.B., 1981, Soils and geomorphology in the Basin and Range area of Southern New Mexico—Guidebook to the Desert Project: New Mexico Bureau of Mines and Mineral Resources Memoir 39, 222 p.

Gile, L.H., Peterson, F.F., and Grossman, R.B., 1965, The K horizon—A master soil horizon of carbonate accumulation: Soil Science, v. 99, no. 2, p. 74–82.

Gillette, D.A., 1978, A wind tunnel simulation of the erosion of soil: Effect of soil texture, sand blasting, wind speed, and soil consolidation on dust production: Atmospheric Environment, v. 12, p. 1735–1743.

————1981, Production of dust that may be carried great distances, *in* Péwé, T.L., ed., Desert Dust: Origin, Characteristics and Effect on Man: Geological Society of America Special Paper 186, p. 11–26.

————1986, Production of dust, *in* El-Baz, F., and Hassan, M.H.A., eds., Physics of Desertification: Boston, Martinus Nijhoff Publishers, p. 251–260.

Gillette, D.A., Adams, J., Endo, A., Smith, D., and Kihl, R., 1980, Threshold velocities for input of soil particles into the air by desert soils: Journal of Geophysical Research, v. 85, p. 5621–5630.

Gillette, D.A., Adams, J., Muhs, D., and Kihl, R., 1982, Threshold friction velocities and rupture moduli for crusted desert soils for the input of soil particles into the air: Journal of Geophysical Research, v. 87, p. 9003–9015.

Gillette, D.A., Fryrear, D.W., Xiao, J.B., Stockton, P.H., Ono, D., Helm, P.J., Gill, T.E., and Ley, T., 1997, Large-scale variability of wind erosion mass flux rates at Owens Lake, Part I: Vertical profiles of horizontal mass fluxes of wind-eroded particles with diameter greater than 50 μm: Journal of Geophysical Research, v. 102, no. D22, p. 25977–25987.

Gillette, D.A., and Stockton, P.H., 1989, The effect of nonerodible particles on wind erosion of erodible surfaces: Journal of Geophysical Research, v. 94D, p. 12885–12893.

Hales, J.E., 1974, Southwestern United States summer monsoon source—Gulf of Mexico or Pacific Ocean: Journal of Applied Meteorology, v. 13, p. 331–342.

Hall, W.E., Van Devender, T.R., and Olson, C.A., 1988, Late Quaternary arthropod remains from Sonoran Desert packrat middens, southwestern Arizona and northwestern Sonora: Quaternary Research, v. 29, p. 277–293.

Hawley, J.W., and Kottlowski, F.E., 1969, Quaternary geology of the south-central New Mexico border region, *in* Kottlowski, F.E., and Le Mone, D.V., eds., Border Stratigraphy Symposium: New Mexico Bureau of Mines and Mineral Resources Circular 104, p. 89–115.

Hawley, J.W., Kottlowski, F.E., Seager, W.R., King, W.E., Strain, W.S., and Le Mone, D.V., 1969, The Santa Fe Group in the south-central New Mexico border region, *in* Kottlowski, F.E., and Le Mone, D.V., eds.; Border Stratigraphy Symposium: New Mexico Bureau of Mines and Mineral Resources Circular 104, p. 52–74.

Helm, P.J., 1991, Measurement of sand movement and associated parameters for storms in the Sonoran Desert [abs.]: American Geophysical Union 1991 Fall Meeting, Abstract H21B-3, p. 161.

Helm, P.J., Breed, C.S., Tigges, Richard, and Creighton, Shawn, 1998, Geometeorological data collected by USGS Desert Winds Project at Desert Wells, Sonoran Desert, central-west Arizona, 1981–1996: U.S. Geological Survey Open-File Report 98-361, CD-ROM.

Helm, P.J., Breed, C.S., Tigges, Richard, and Garcia, P.A., 1995, Geometeorological data collected by the USGS Desert Winds Project at Gold Spring, Great Basin Desert, northeastern Arizona, 1979–1992: U.S. Geological Survey Open-File Report 95-78, CD-ROM [with Sun/Unix Display Software by P.N. Schweitzer].

Hendricks, D.M., 1985, Arizona soils: College of Agriculture, Tucson, University of Arizona, 244 p.

Hennessy, J.T., Gibbens, R.P., Tromble, J.M., and Cardenas, M., 1983, Vegetation changes from 1935 to 1980 in mesquite dunelands and former grasslands of southern New Mexico: Journal Range Management, v. 36, no. 3, p. 370–374.

Henning, D., and Flohn, H., 1977, Climate aridity index map, *in* Proceedings of United Nations Conference on Desertification, United Nations Environmental Programme, Nairobi, Kenya: United Nations document A/CONF. 74/31.

Hereford, Richard, 1989, Variation of warm-season rainfall frequency in the southern Colorado Plateau and its effect on runoff and alluvial-channel morphology: A preliminary analysis: U.S. Geological Survey Open-File Report 89-330, 36 p.

Hunt, C., 1986, Surficial Deposits of the United States: New York, Van Nostrand Reinhold Co., 188 p.

Idso, S.B., 1981, Climatic change: The role of atmospheric dust, *in* Péwé, T.L., ed., Desert Dust: Origin, Characteristics, and Effect on Man: Geological Society of America Special Paper 186, p. 207–222.

Idso, S.B., and Brazel, A.J., 1978, Atmospheric dust: Climatological consequences: Science, v. 201, p. 378–379.

Jackson, M.L., Gillette, D.A., Danielsen, E.F., Blifford, I.H., Bryson, R.A., and Syers, J.K., 1973, Global dustfall during the Quaternary as related to environments: Soil Science, v. 116, p. 135–145.

Janecek, T.R., and Rea, D.K., 1983, Eolian deposition in the northeast Pacific Ocean: Cenozoic history of atmospheric circulation: Geological Society of America Bulletin, v. 94, p. 730–738.

Johnson, Carl, and Miller, Daryl, 1980, Late Cenozoic alluvial history of the lower Colorado River, *in* Fife, D.L., and Brown, A.R., eds., Geology and Mineral Wealth of the California Desert: Santa Ana, Calif., South Coast Geological Society, p. 441–446.

Keen, R.A., 1987, El Niño: Skywatch, the Western Weather Guide: Golden, Colo., Fulcrum Inc., p. 110–116.

Krusinger, A.E., 1988, An empirical surface temperature model: U.S. Army Corps of Engineers, Engineer Topographic Laboratories Publications ETL-0503, Fort Belvoir, Va., 126 p.

Landsberg, H.E., 1986, Potentialities and limitations of conventional climatological data for desertification monitoring and control: Climatic Change, v. 9, p. 123–128.

MacKinnon, D.J., Elder, D.F., Helm, P.J., Tuesink, M.F., and Nist, C.A., 1990, A method of evaluating effects of antecedent precipitation on duststorms and its application to Yuma, Arizona, 1981–1988: Climatic Change, v. 17, nos. 2–3, p. 331–360.

MacMahon, J.A., 1979, North American deserts: Their floral and faunal components, *in* Goodall, D.W., and Perry, R.A., eds., Arid-Land Ecosystems: Structure, Functioning, and Management, v.1: International Biological Program, Cambridge University Press, p. 21–82.

McCauley, J.F., 1973, Mariner 9 evidence for wind erosion in the equatorial and mid-latitude regions of Mars: Journal of Geophysical Research, v. 78, p. 4123–4137.

McCauley, J.F., Breed, C.S., Grolier, M.J., and MacKinnon, D.J., 1981, The U.S. dust storm of February 1977, *in* Péwé, T.L., ed., Desert Dust: Origin, Characteristics, and Effect on Man: Geological Society of America Special Paper 186, p. 123–147.

McCauley, J.F., Breed, C.S., Helm, P.J., Billingsley, G.H., MacKinnon, D.J., Grolier, M.J., and McCauley, C.K., 1984, Remote monitoring of processes that shape desert surfaces: The Desert Winds Project: U.S. Geological Survey Bulletin 1634, 19 p.

McFadden, L.D., and Weldon, R.J. II, 1987, Rates and processes of soil development on Quaternary terraces in Cajon Pass, California: Geological Society of America Bulletin, v. 98, p. 280–293.

McKee, E.D., 1957, Primary structures in some Recent sediments: American Association of Petroleum Geologists Bulletin, v. 41, p. 1704–1747.

———1966, Structures of dunes at White Sands National Monument, New Mexico (and a comparison with structures of dunes from other selected areas): Sedimentology, v. 7, no. 1, p. 3–69.

Meigs, Peveril, 1953, World distribution of arid and semi-arid homoclimates, *in* Reviews of Research on Arid Zone Hydrology: Paris, Arid Zone Programme-1, United Nations Educational, Scientific, and Cultural Organization, p. 203-209.

Merriam, R., 1964, Source of sand dunes of southeastern California and northwestern Sonora, Mexico: Geological Society of America Bulletin, v. 80, p. 531–534.

Morrison, R.B., 1983, Map of late Pliocene and Quaternary geology, El Centro quadrangle: State of Arizona, Bureau of Geology and Mineral Technology Open-File Report 84-2, scale 1:250,000, with 5 p. text.

———1985, Pliocene/Quaternary geology, geomorphology, and tectonics of Arizona, *in* Weide, D.L., ed., Soils and Quaternary Geology of the Southwestern United States: Geological Society of America Special Paper 203, p. 123–146.

Muhs, D.R., Bush, C.A., Cowherd, S.D., and Mahan, Shannon, 1995, Geomorphic and geochemical evidence for the source of sand in the Algodones Dunes, Colorado Desert, southeastern California, *in* Tchackerian, V.P., ed., Desert Aeolian Processes: New York, Chapman and Hall, p. 38–74.

Murray, A.V., 1959, An analysis of changes in Sonoran Desert vegetation for the years 1928–1957: Tucson, University of Arizona, M.S. thesis, 146 p.

Musick, H.B., and Gillette, D.A., 1990, Field evaluation of relationships between a vegetation structural parameter and sheltering against wind erosion: Land Degradation and Rehabilitation, v. 2, p. 87–94.

Musick, H.B., Schaber, G.G., and Breed, C.S., 1995, Use of AIRSAR to identify woody shrub invasion and other indicators of desertification in the Jornada LTER: Summaries of the Fifth Annual JPL Airborne Earth Science Workshop, January 23–26, 1995, Jet Propulsion Laboratory Publication 95-1, v. 3, p. 31–34.

———1998, AIRSAR studies of woody shrub density in semiarid rangeland: Jornada del Muerto, New Mexico: Remote Sensing of Environment, v. 66, p. 29-40.

Musick, H.B., Trujillo, S.M., and Truman, C.R., 1996, Wind-tunnel modeling of the influence of vegetation structure on saltation threshold: Earth Surface Processes and Landforms, v. 21, p. 589–605.

Nickling, W.G., and Brazel, A.J., 1984, Temporal and spatial characteristics of Arizona dust storms: Journal of Climatology, v. 8, p. 1–16.

Olmsted, F.H., Loeltz, O.J., and Irelan, Burdge, 1973, Geohydrology of the Yuma area, Arizona and California: U.S. Geological Survey Professional Paper 486-H, 227 p., scale 1:125,000.

Péwé, T.L., ed., 1981, Desert dust: origin, characteristics, and effect on man: Geological Society of America Special Paper 186, 303 p.

Peirce, H.W., 1984, Some late Cenozoic basins and basin deposits of southern and western Arizona, *in* Smiley, T.L., Nations, J.D., Péwé, T.L., and Schafer, J.P., eds., Landscapes of Arizona—The Geological Story: New York, University Press, p. 207–227.

Pimentel, David, Terhune, E.C., Dyson-Hudson, Rada, Rochereau, Stephen, Samis, Robert, Smith, E.A., Denman, Daniel, Refschneider, David, and Shepard, Michael, 1976, Land degradation: Effects on food and energy resources: Science, v. 194, p. 151–152.

Powell, J.W., 1879, Report on the lands of the arid regions of the United States: Washington, D.C., Government Publications Office, 195 p.

Reheis, M.C., 1997, Dust deposition downwind of Owens (dry) Lake, 1991–1994: Preliminary findings: Journal of Geophysical Research, v. 102, no. D22, p. 25999–26008.

Reheis, M.C., Goodmacher, J.C., Harden, J.W., McFadden, L.D., Rochwell, T.K., Shroba, R.R., Sowers, J.M., and Taylor, E.M., 1995, Quaternary soils and dust deposition in southern Nevada and California: Geological Society of America Bulletin, v. 107, p. 1003–1022.

Reheis, M.C., and Kihl, Rolf, 1995, Dust deposition in southern Nevada and California, 1984–1989: Relations to climate, source area, and source lithology: Journal of Geophysical Research, v. 100, no. D5, p. 8893–8918.

Reinking, R.F., Mathews, L.A., and St.-Armand, Pierre, 1975, Dust storms due to the desiccation of Owens Lake: Proceedings of the International Conference on Environmental Sensing and Assessment, Session 37, v. 2, Paper 37-4, Las Vegas, Nevada, p. 1–9.

Reitan, C.H., 1974, Frequencies of cyclones and cyclogenesis for North America, 1951–1970: Monthly Weather Review, v. 102, p. 861–868.

Ruhe, R.V., 1967, Geomorphic surfaces and surficial deposits in Southern New Mexico: Socorro, New Mexico State Bureau of Mines and Mineral Resources, Memoir 18, 65 p.

Seager, W.R., Hawley, J.W., Kottlowski, F.E., and Kelley, S.A., 1987, Geology of east half of Las Cruces and northeast El Paso 1°×2° sheets, New Mexico: New Mexico Bureau of Mines and Mineral Resources Geologic Map 57, sheet 1, 1:125,000.

Sheridan, David, 1981, Desertification of the United States: Council on Environmental Quality, Washington, D.C., United States Government Printing Office, 142 p.

Slate, J.L., Bull, W.B., Ku. T.-L., Shafiqullah, M. Lynch, D.J., and Huang, Y.-P., 1991, Soil-carbonate genesis in the Pinacate volcanic field, northwestern Sonora, Mexico: Quaternary Research, v. 35, p. 400–416.

Smith, G.I., 1984, Paleohydrologic regimes in the southwestern Great Basin, 0–3.2 m.y. ago, compared with other long records of "global" climate: Quaternary Research, v. 22, p. 1–17.

Smith, R.S.U., 1978, Guide to selected features of aeolian geomorphology in the Algodones dune chain, Imperial County, California, *in* Greeley, Ronald, Womer, M.B., Papson, R.P., and Spudis, P.D., eds., Aeolian Features of Southern California: A Comparative Planetary Geology Guidebook: National Aeronautics and Space Administration, Washington, D.C., U.S. Government Printing Office no. 033-000-00706-0, p. 74–98.

U.S. Weather Bureau, 1960, Normal annual precipitation in inches, 1931–1960, State of Arizona: U.S. Department of Commerce, map WR1210A.

Stockton, P.H., and Gillette, D.A., 1990, Field measurement of the sheltering effect of vegetation on erodible land surfaces: Land Degradation and Rehabilitation, v. 2, p. 77–85.

Stokes, Stephen, and Breed, C.S., 1993, A chronostratigraphic reevaluation of the Tusayan Dunes, Moenkopi Plateau and southern Ward Terrace, northeastern Arizona, *in* Pye, K., ed., 1993, The Dynamics and Environmental Context of Aeolian Sedimentary Systems: Geological Society [London] Special Publication no. 72, p. 75–90.

Sweet, M.L., Nielson, Jamie, Havholm, K., and Farrellyk, John, 1988, Algodones dune field of southeastern California: Case history of a migrating modern dune field: Sedimentology, v. 35, p. 939–952.

Tang, Maocang, and Reiter, E.R., 1984, Plateau monsoons of the Northern Hemisphere: A comparison between North America and Tibet: Monthly Weather Review, v. 112, p. 617–637.

Thompson, L.G., and Mosley-Thompson, E., 1981, Microparticle concentration variations linked with climatic change: Evidence from polar ice cores: Science, v. 212, p. 812–815.

Van Devender, T.R., 1990, Late Quaternary vegetation and climate of the Sonoran Desert; United States and Mexico, *in* Betancourt, J.L., Van Devender, T.R., and Martin, P.S., eds., Packrat Middens: The Last 40,000 Years of Biotic Change: Tucson, University of Arizona Press, p. 134–165.

Wilshire, H.G., Nakata, J.K., and Hallett, Bernard, 1981, Field observations of the December 1977 wind storm, San Joaquin Valley, California, *in* Péwé, T.L., ed., Desert Dust: Origin, Characteristics, and Effect on Man: Geological Society of America Special Paper 186, p. 233–251.

Wilson, E.D., 1933, Geology and mineral deposits of southern Yuma County, Arizona: Arizona Bureau of Mines, Geological Series 7, Bulletin 134, 236 p.

Windom, H.L., and Chamberlain, F.G., 1978, Dust storm transport of sediments to the North Atlantic Ocean: Journal of Sedimentary Petrology, v. 48, no. 2, p. 385–388.

Yaalon, D.H., and Ganor, E., 1975, The influence of dust on soils during the Quaternary: Soil Science, v. 116, p. 146–155.

Instrumented Field Studies of
Sediment Transport by Wind

By Paula J. Helm *and* Carol S. Breed

DESERT WINDS: MONITORING WIND-RELATED SURFACE PROCESSES IN
ARIZONA, NEW MEXICO, AND CALIFORNIA

Carol S. Breed and Marith C. Reheis, *Editors*

U.S. GEOLOGICAL SURVEY PROFESSIONAL PAPER 1598–B

CONTENTS

FIGURES

TABLES

Instrumented Field Studies of
Sediment Transport by Wind

By Paula J. Helm[1] *and* Carol S. Breed [2]

ABSTRACT

Long-term data from automated instruments and field measurements at three geometeorological (Geomet) stations (Gold Spring and Yuma in Arizona, and Jornada in New Mexico) provide a new basis on which to assess sediment transport for natural desert areas. The susceptibility of each instrumented site to sediment transport is characterized by its surface grain size, threshold wind speed, drift potential, precipitation frequency, and vegetation cover (lateral cover). The first four parameters define the potential for sand movement, whereas actual (monitored) eolian activity additionally corresponds to vegetation cover. The potential for sediment transport is moderately high at the Gold Spring site and low at the Yuma and Jornada sites; yet, for the period of record, Yuma was the most active sand-moving site, whereas Jornada and Gold Spring showed less activity, possibly due to denser vegetation cover at these two sites.

Relations of measured wind speeds and directions, measured amounts of short-term antecedent precipitation, and movement of sand in saltation (detected by sand-flux sensors) for seasonal storms at each site indicate the complex nature of weather and land surface response. Storm sandroses based on Geomet data illustrate the relative amount of wind energy, effective wind direction, and resultant net potential sand movement and direction associated with each recorded storm. These empirical examples document the effects of different types of storms on sand movement on natural surfaces. Spring sand-moving storms had frontal storm characteristics: strong initial winds that taper off as the storm dies down, constant wind directions, and long durations. These storms only produced sand movement in the initial phase. Summer storms were classic thunderstorms with swift, powerful downdrafts and turbulent wind speeds and directions. Sand moved throughout the duration of these thunderstorms, except when rain fell. The fall/winter storms were frontal storms associated with upper-level, low-pressure troughs. These storms had a pulsating character with wind speeds that rose above and dropped below threshold wind speed, some quite dramatically, throughout their duration. The pulsating character of the winds of low-pressure-trough storms produced intermittent sand movement throughout the duration of these storms.

Precipitation occurred within 10 days before all but one sand-moving storm, confirming the minor effect of short-term antecedent precipitation on the vulnerability of these sites to sediment transport. The consequence of long-term antecedent precipitation (rainfall during previous seasons) is reflected in the inhibiting effect of vegetation cover on sediment transport during subsequent seasons.

INTRODUCTION

Field data on the land surface and near-surface atmospheric conditions at five desert sites have been acquired by automated instruments deployed at geometeorological (Geomet) stations (Breed, chap. A, this volume; Tigges and others, chap. H, this volume). At all but one of these sites (Desert Wells, near Vicksburg, Ariz.), an automated sand-flux sensor (SENSIT: Stockton and Gillette, 1990) was added to the sensor array, and this experimental instrument has provided field data on the actual (as opposed to potential) movement of sand by the Geomet-recorded winds under monitored conditions of precipitation and vegetation cover. This paper reports the methodology, the baseline geometeorology, and preliminary observations of experimental field measurements of the movement of sediment by wind on natural arid and semiarid surfaces. Geometeorologic characterization and preliminary sand-moving storm observations are reported for the Gold Spring and Yuma sites (Arizona) and for the Jornada site (New Mexico). The geometeorologic characterization for the Desert Wells site (Arizona) is reported by Wolfe and Helm (chap. C, this volume); data are as yet insufficient for analysis of the Owens Lake (California) site.

[1]U.S. Geological Survey, Building 3, 2255 North Gemini Dr., Flagstaff, AZ 86001.

[2]U.S. Geological Survey (retired), 189 Wilson Canyon Rd., Sedona, AZ 86336.

SEDIMENT TRANSPORT PARAMETERS

INSTRUMENTATION

On each Geomet wind tower (described in detail by Tigges and others, chap. H, this volume), an anemometer at a height of 6.1 m measures wind speeds that are averaged every 6 minutes. A wind vane at the top of each data collection platform (DCP) tower (also 6.1 m high) records wind directions simultaneously with the wind-speed measurements. A tipping bucket rain gauge sits on a small platform on each DCP tower at a height of 2 m. The cumulative precipitation is logged every 12 minutes. The air-temperature sensor (a thermistor) is encased in a radiation shield and is mounted 1.2 m above the ground surface. Instantaneous air-temperature readings are recorded every 12 minutes.

Measured wind speeds and directions and measured amounts and frequencies of precipitation used with the record of sand-flux events detected by the SENSIT (described below and by Tigges and others, chap. H, this volume) provide the essential support for our field-based studies of sediment transport on natural surfaces. The SENSIT is an automated sand-flux sensor (Stockton and Gillette, 1990) that contains a piezoelectric crystal, which records the impacts of saltating sand grains as electronic pulses. These pulses signal the onset and record the duration of saltation (wind-driven bouncing of sand). Because the SENSIT is an experimental instrument that has been developed over more than 5 years of project work, different models produced by manufacturer's redesign of the instrument have been deployed at the Geomet sites; as a consequence, comparisons of the SENSIT records from site to site must compensate for these sensor differences, particularly in heights above the ground. At both the Gold Spring and the Jornada sites, the crystal height is 5.5 cm; but the crystal height at the Yuma site is 15 cm. The Yuma SENSIT is the oldest model still in use and has not been replaced with the newer, shorter model because of the need to maintain continuity of the long and substantial data set recorded with the 15-cm-high SENSIT. As a consequence, in order to be recorded by the SENSIT, sand grains at the Yuma site must saltate to more than twice the height of the sand grains that saltate at the Gold Spring or Jornada site.

METHODS

Using field measurements and Geomet data, the sediment transport parameters that characterize each desert site are surface grain size, threshold wind speed (Bagnold, 1941), drift potential (Fryberger and Dean, 1979), precipitation frequency, and vegetation cover (Musick, chap. D, this

volume). In this paper, threshold wind speed (V_t) is defined as the horizontal wind speed, measured at 6.1 m, required to initiate saltation on a flat, dry, unvegetated surface of mixed grain size. The equations of Bagnold (1941, p.101) are chosen for calculations because they contain only one variable, surface grain size, which is easily measured. The fluid threshold gradient or threshold friction velocity (V_{*t}), which represents the minimum drag on the predominant surface grain size at which air can begin to move grains by direct fluid pressure, varies as the square root of the grain size, as follows:

$$V_{*}t = A\sqrt{\frac{\sigma - \rho}{\rho}gd} \qquad (1)$$

where

A is a constant based on fluid medium (for air, A=0.1),
σ is the density of quartz (2.65 g/cm^2),
ρ is the density of air (1.22×10^{-3} g/cm^3),
g is the acceleration of gravity (980.665 cm/s^2), and
d is the predominant (modal) grain-size diameter, in centimeters, for each site.

The surface grain size (d), the singular key variable, is determined by sampling surficial sediment at each site. Mean grain size is used in wind tunnel studies (Bagnold, 1941; Zingg, 1953; Belly, 1964), but empirical evidence led Bagnold (1941) to suggest that the mode is a better statistical expression for natural, mixed-grain surfaces. Continuing research (Gillette and others, 1980) indicates that mode, rather than mean, controls the value of the threshold friction velocity (V_{*t}) in natural areas, although the complex surfaces of natural areas are likely to produce a range of threshold friction velocities (Chepil, 1945; Nickling, 1988; Fryrear and others, 1991) rather than a constant value. For example, a minimum V_{*t} would move the smaller grains on the surface whereas progressively higher V_{*t} would be needed for each larger grain size in the mix. In this report, a first-order threshold friction velocity value is calculated using the modal grain size for each site.

To determine the modal grain-size diameter, the area around the SENSIT is sampled by running a flat piece of cardboard along the surface at a depth of 2 cm. In the laboratory, a standard 500 grams derived from this bulk sample is sieved and weighed to obtain amounts of sediment in each grain-size category (Folk, 1964). The mode is the grain-size category containing the greatest weight (largest amount) of the sample material. Where the sample weights are bimodal or multimodal, a mean value between or among modes is selected.

The threshold friction velocity value (V_{*t}), based on the modal grain size at each site, is then used to calculate the horizontal threshold wind speed (V_t), at the anemometer height (z) of 6.1 m above the surface, using the Bagnold logarithmic wind profile equation:

$$V_t\,(z) = \, 5.75\,V_{*t}\, \log\frac{z}{z_0} \qquad\qquad (2)$$

where

$V_t(z)$ is the threshold wind speed measured at 6.1 m height,

V_{*t} is the fluid threshold gradient (threshold friction velocity),

$z = 6.1$ m, and

z_0 is the roughness height ($d/30$), based on predominant (modal) grain-size diameter.

Threshold wind speed (V_t) then becomes the comparison standard for each site that defines the wind speed needed to move the predominant grain size if the site were flat, unvegetated, and completely dry.

The measure of the effective (potential sand-moving) winds summed for recorded winds from all directions at a given location is the drift potential (Fryberger and Dean, 1979). In Fryberger and Dean's approach, all wind speeds greater than the established threshold wind speed for a standard grain size of quartz sand (0.25 mm) are considered sand-moving winds, and surfaces of sediment transport are assumed to be of uniform grain size, dry, and bare. Fryberger and Dean modified the Lettau-Lettau (1978) equation, an updated version of the Bagnold sand-flux equation, in order to use the frequency of the occurrence of winds in speed groups recorded hourly by standard World Meteorological Organization (WMO) weather stations. Fryberger and Dean's method allowed them to characterize most sand deserts of the world in terms of their potential sand movement by wind and to compare them on a global scale using standard numerical values (vector units or VU). Sandroses (fig. 1) are the graphical representation of the wind energy from each of the 16 wind-direction categories plus the resultant amount and direction of potential sand drift. The Fryberger and Dean sandroses, therefore, represent the potential amount and upwind direction of the wind force as well as the resultant net potential amount and downwind direction of the sand movement over the period of record.

For this project, each Geomet site sandrose is evaluated, and drift potential at each site in VU is calculated using the sum of the arms of the sandrose. The Geomet sandroses are constructed using the mean frequency of measured wind speeds above the site-specific threshold wind speed over the period of Geomet record. The drift potential value is then used to categorize the type of wind environment, as compared to other world desert sites, and to quantify the potential vulnerability of each site to the wind. Each site sandrose describes the overall directional power and variability of the wind and the potential net effect of the wind activity on the surface material. For comparison with the actual effectiveness of wind during storms that produce SENSIT-recorded

sand movement, storm sandroses are also derived (see figs. 4B–12B).

A measure of precipitation, when evaluated as a sediment transport parameter, needs to define the effectiveness of rainfall to decrease sand movement by stabilizing the surface through crusting or vegetation growth. Although mean annual rainfall or normal annual rainfall is the usual method of characterizing precipitation at any location, a frequency distribution of precipitation amounts may be a more meaningful description of the effect rainfall has on the surface and the vegetation. Given a mean annual rainfall of 150 mm, a desert in which most of the total yearly amount occurs during a 2-month period will differ in character from a desert in which the same amount is distributed equally in all months. Two frequency distributions of precipitation for each site are graphed: monthly (fig. 2) and daily (see fig. 14). Each graph of precipitation frequency shows, for the period of record at each site, the mean number of months or days per year having a total rainfall within each precipitation range. The monthly precipitation frequency is useful for evaluation of the general character of a site (Chepil, 1958), whereas the daily precipitation frequency gives a more detailed view of the relations between rainfall and individual seasonal storms. The calculations of precipitation frequencies are based on recorded field data from each site.

Vegetation cover is represented by numerical values that describe relative amounts of the surface covered by plants versus bare ground; these values are derived from periodic measurements, using vegetation transects, of plant frequency, size, and shape at the Geomet sites (Musick, chap. D, this volume). Lateral cover (L_c: Marshall, 1971) is a measure of the ratio of frontal silhouette area to the ground area occupied by the plants. Musick and Gillette's (1990) analysis of changes in L_c at the Yuma and Jornada Geomet sites confirms that protection of natural surfaces against sand movement by wind increases with increased value of lateral cover. The lateral cover values for the sites thus provide a rough index of vulnerability of each site to eolian activity.

CHARACTERISTICS OF THE GEOMET SITES

GOLD SPRING, ARIZONA

The Gold Spring Geomet site is in the high, seasonally cool Great Basin Desert, at an altitude of 1,667 m. The station is on shallow subsurface bedrock (mostly sandstone) mantled with an eolian sand sheet, in an interdune corridor between two linear dunes. The land is historically a part of the Navajo/Hopi Indian Joint Use Area, and a Navajo family living nearby grazes cattle, some sheep, and horses. Vegetation consists almost entirely of grasses and bushes; the four
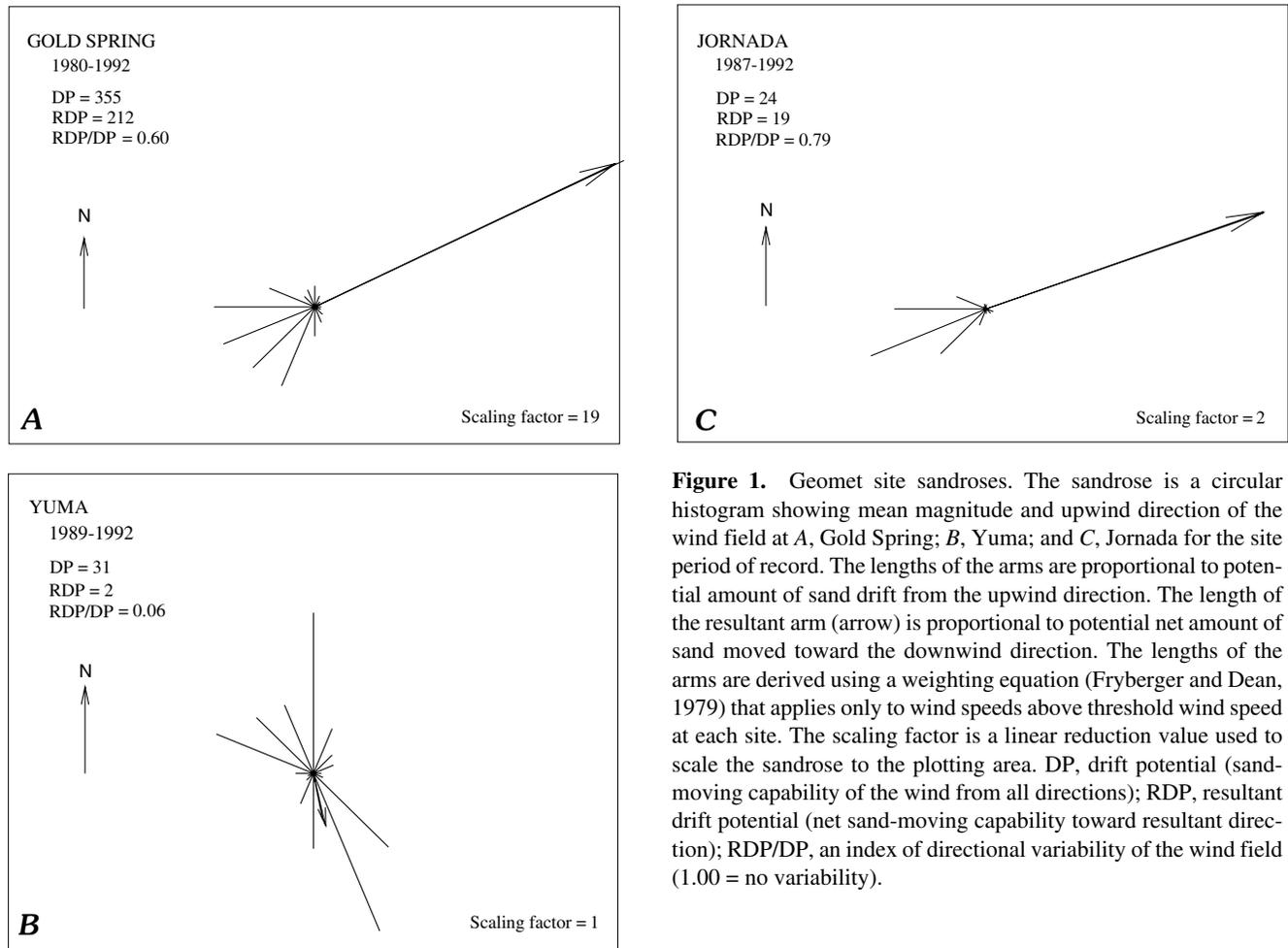
Figure 1. Geomet site sandroses. The sandrose is a circular histogram showing mean magnitude and upwind direction of the wind field at *A*, Gold Spring; *B*, Yuma; and *C*, Jornada for the site period of record. The lengths of the arms are proportional to potential amount of sand drift from the upwind direction. The length of the resultant arm (arrow) is proportional to potential net amount of sand moved toward the downwind direction. The lengths of the arms are derived using a weighting equation (Fryberger and Dean, 1979) that applies only to wind speeds above threshold wind speed at each site. The scaling factor is a linear reduction value used to scale the sandrose to the plotting area. DP, drift potential (sand-moving capability of the wind from all directions); RDP, resultant drift potential (net sand-moving capability toward resultant direction); RDP/DP, an index of directional variability of the wind field (1.00 = no variability).

major species are broom snakeweed, galleta, yucca, and needle-and-thread grass (H.B. Musick, University of New Mexico, written commun., 1992). Black grama is also present in lesser quantities and is heavily grazed. The Geomet site is fenced with barbed wire to protect the equipment from livestock.

The Gold Spring Geomet station began operations in October 1979, and the Gold Spring data available for this study cover a 13-year period, 1980–1992, which is a significant record for the establishment of long-term means (table 1) and other geometeorological calculations. The mean annual wind speed is 3.7 m/s, and the drift potential evaluated for the site is 355 VU. This VU value places the site in the upper range of the intermediate wind-energy environment of deserts worldwide as defined by Fryberger and Dean (1979). The Geomet site sandrose (fig. 1) indicates that the resultant drift direction is to the east-northeast, which shows the effect of strong prevailing southwesterly winds. The mean annual precipitation is 143 mm, and the monthly precipitation frequency (fig. 2) indicates that, during 8 months of an average year, the site receives a precipitation total of less than 13 mm; whereas during 1 month (usually July or

August), it receives a rainfall amount greater than 38.3 mm, and during 1 month (usually June), it receives no precipitation at all.

The modal surface grain diameter of 0.104 mm (very fine sand) yields a threshold wind speed of 5.3 m/s (11.9 mph). This small modal grain size forces the threshold friction velocity, and thus the threshold wind speed, close to the minimum of the Bagnold threshold curve (Bagnold, 1941, p. 88). Smaller and larger grain sizes require higher threshold wind speeds to begin saltation. The lateral cover value of the vegetation in 1991 was 0.41 (H.B. Musick, University of New Mexico, written commun., 1992).

The Gold Spring site has powerful winds, fine surface grain sizes, and a very low threshold wind-speed value, all of which produce a great potential for sand movement. Rains come mostly in small increments—a pattern common to all the arid and semiarid Geomet sites—which minimizes the effect of the total yearly precipitation on the surface and the vegetation. A few soaking rains do occur, and this site receives snow that sometimes remains on the ground for days. Gold Spring presently has a relatively high value for lateral cover, which suggests that the vegetation density and

GOLD SPRING
1980 - 1992

A

YUMA
1989 - 1992

B

JORNADA
1987 - 1992

C
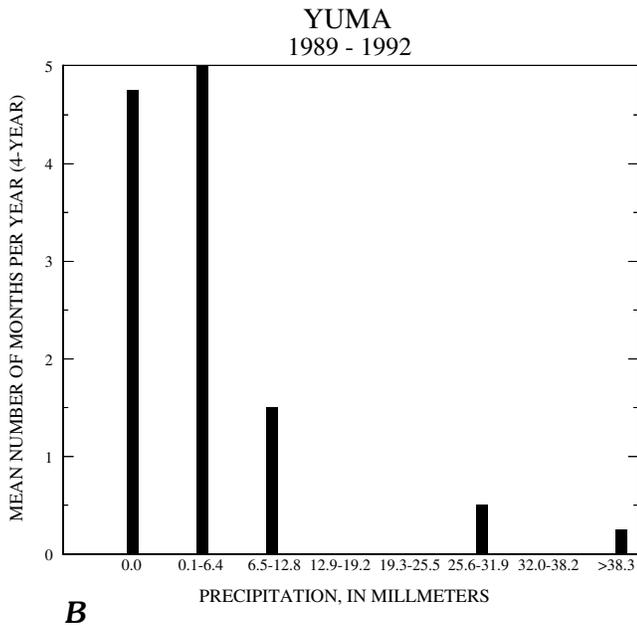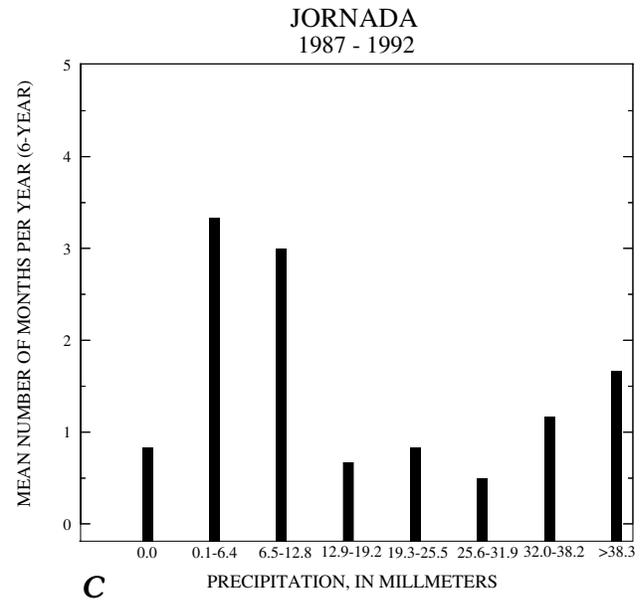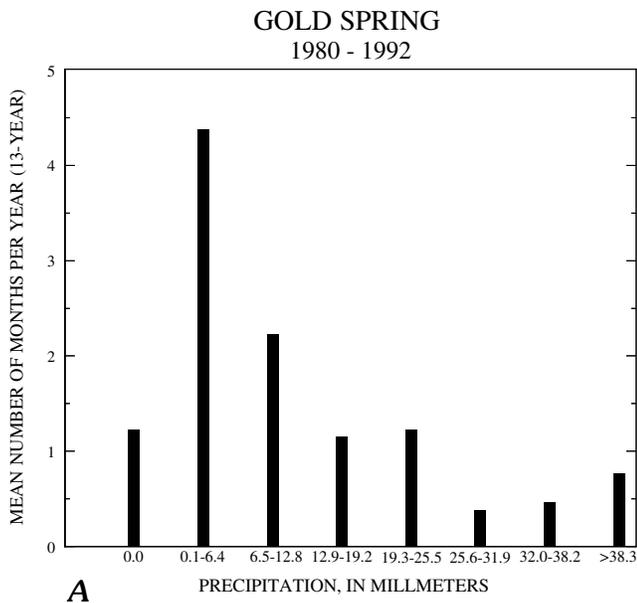
Figure 2. Monthly precipitation frequency distributions showing mean number of months per year with total rainfall in each precipitation range for the period of record at *A*, Gold Spring; *B*, Yuma; and *C*, Jornada.

spacing characteristics provide some protection of the ground surface from sand movement.

YUMA, ARIZONA

Although a basic Geomet station has recorded conditions in the Yuma desert since June 1981, the equipment was moved to a new site, 9.5 miles west-northwest from the first locality, and upgraded to a superstation, including installation of a SENSIT sand-flux sensor (Tigges and others, chap. H, this volume) in May 1988. The two Yuma sites, although both within the lower Colorado River valley section of the Sonoran Desert, have different meteorological and surface characteristics. Because the equipment

at the new site includes the sand-flux sensor, which is essential to detect and record actual saltation events, the geometeorological descriptions in this paper are based on data from the new site only. This Yuma Geomet site is at 75 m altitude in the lower Sonoran Desert, the most arid region of the United States (Henning and Flohn, 1977). The Geomet station is located on a sand sheet on a virtually flat, intermontane plain, known locally as the Yuma desert, south and east of the Colorado River (Breed, chap. A, this volume). Access is restricted, as the site is on part of the aerial gunnery range of the Barry M. Goldwater Air Force Range (administered by the U.S. Marine Corps Air Station in Yuma). The vegetation at the Geomet site is sparse; the three major species are white bursage, big galleta, and creosotebush (Musick and Gillette, 1990; Musick, chap. D, this volume). An annual

Table 1. Mean, minimum, and maximum meteorological parameters at the Geomet sites.

Site Period of record	Gold Spring 1980–1992	Yuma 1989–1992	Jornada 1987–1992
Temperature			
Mean annual	12.0°C	23.2°C	15.3°C
Maximum (year)	38.2°C (1989)	51.0°C (1990)	44.0°C (1989)
Minimum (year)	–25.3°C (1982)	–7.0°C (1990)	–20.0°C (1987)
Precipitation			
Mean annual	142.5 mm	51.9 mm	233.1 mm
Maximum annual (year)	186.2 mm (1983)	103.6 mm (1992)	265.2 mm (1992)
Minimum annual (year)	87.4 mm (1991)	21.8 mm (1989)	197.9 mm (1989)
Wind speed			
Mean annual	3.7 m/s	2.9 m/s	2.7 m/s
Maximum peak gust (year)	30.4 m/s (1984)	27.9 m/s (1989)	29.8 m/s (1991)

grass (schismus barbatus) grows abundantly when fall/winter rains are heavy. The Yuma Geomet site is not fenced because no livestock graze in the area.

Although the superstation was erected in May 1988, problems with the power system throughout the summer severely reduced the data set for that year, such that the period of record for calculation of annual means starts in 1989. This short period of record (4 years) reduces the significance of the site long-term means, but monitoring at this site continues and is expected to improve the values. The 4-year means for precipitation, air temperature, and wind speed for the Yuma site are listed in table 1. Mean annual air temperature of 23.2°C and mean annual precipitation of 52 mm demonstrate the aridity of the region.

The threshold wind speed (at a height of 6.1 m), based on a predominant (modal) surface grain size of 0.280 mm (medium sand), is 8.2 m/s (18.3 mph). The drift potential for the Yuma site is 31 VU, a low wind-energy environment compared to deserts worldwide (Fryberger and Dean, 1979). The resultant drift direction (fig. 1) is to the south-southeast, but the site sandrose shows diametrically opposed modes (northwest and southeast quadrants) that neutralize the magnitude of the resultant (net) potential sand drift and produce a reversing yearly resultant drift direction. The Yuma site rarely has significant, saturating rains (fig. 2). For 11 months a year, on average, rain falls in monthly amounts less than 13 mm; for 5 of those 11 months, no rain falls at all. The vegetation cover at Yuma is generally sparse but highly variable from year to year, corresponding closely to a wide range of fall/winter precipitation totals. The lateral cover value in 1988 was 0.24, and in 1990, 0.14. By 1992, the value returned to 0.23 (Musick, chap. D, this volume).

Although the Yuma Geomet site has a low drift potential and a relatively high threshold wind speed, the aridity of the area allows considerable sand-moving activity. When vegetation cover, especially grasses, is sparse, each wind storm having speeds above threshold can move surface sediment for an extended period of time, and the winds that come from opposing directions, depending on the season, move the sand back and forth over the sand sheet. Yuma has extreme fluctuations in amount of total yearly precipitation (Ezcurra and Rodrigues, 1986), which produce variable seasonal vegetation growth. During the 11-year period of observations at both Yuma Geomet sites, the desert surface has fluctuated twice between sparsely vegetated sand sheet with leafless creosotebush and grassland with fully leafed shrubs (fig. 3). Some of the surface changes evident on Landsat images are documented by Crowley and Bowers (chap. F, this volume). Such temporal shifts of climatic and land-surface characteristics give the Yuma site a highly variable potential for eolian activity.

JORNADA, NEW MEXICO

The Jornada Geomet site, on the Jornada Experimental Range north of Las Cruces, N. Mex., is located on a virtually flat, intermontane valley floor in the northern Chihuahuan Desert at an altitude of 1,323 m. The vegetation is presently abundant and varied; the three major species are mesquite, snakeweed, and dropseed (Musick and Gillette, 1990; Musick, chap. D, this volume). The U.S. Department of Agriculture–Agricultural Research Service (USDA-ARS) uses the range to experiment with different grazing methods, mainly for cattle but also for sheep and other animals. The Geomet site at Jornada is not grazed as often as the site at Gold Spring, but even limited grazing requires that the equipment be fenced.

The Jornada Geomet station has operated since September 1986; a 6-year (1987–1992) period of record provides
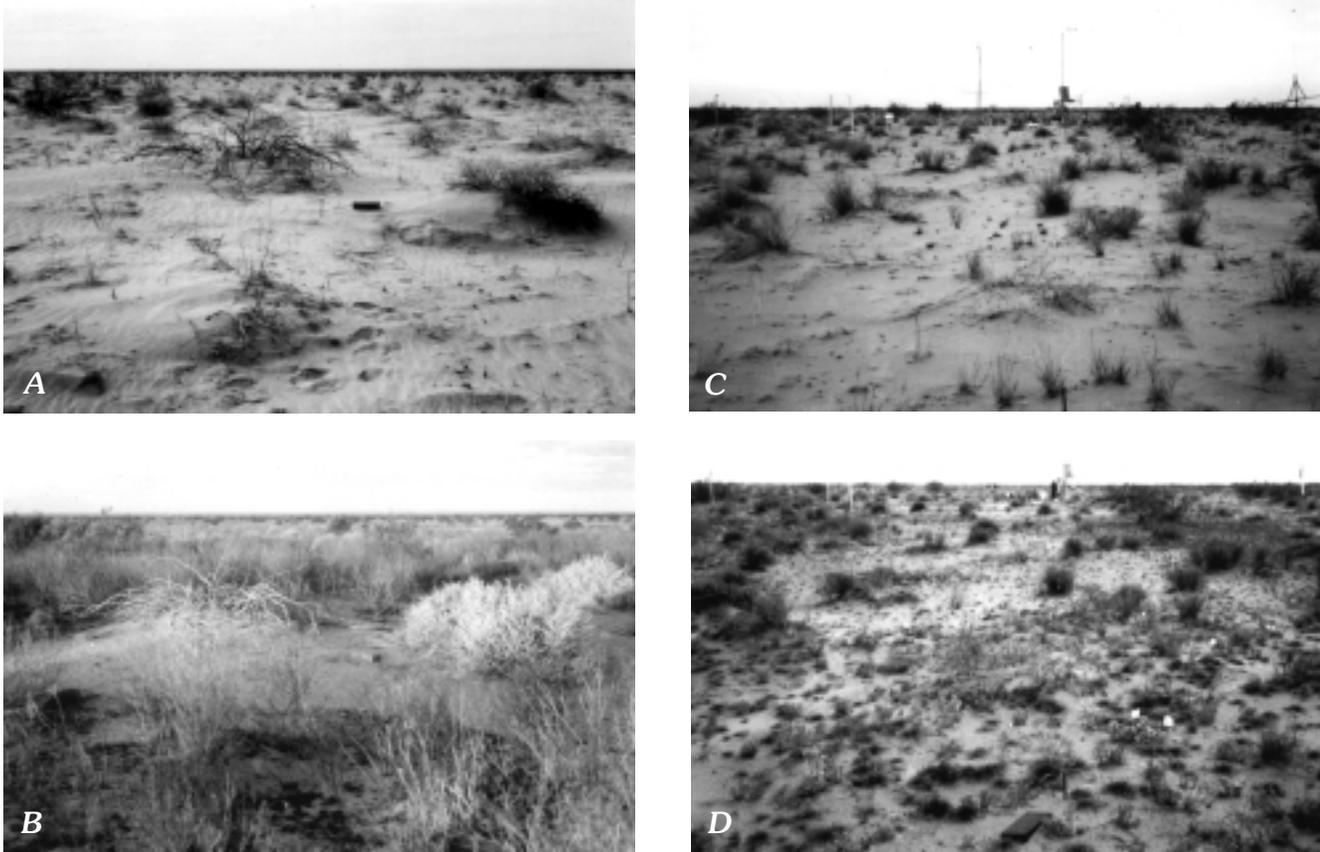
Figure 3. Vegetation changes at the Yuma Geomet sites as shown by repeat photography. *A*, Original site (1982) after drought; *B*, original site (1984) after 2 years of heavy rains during El Niño years; *C*, present site (1991) after drought; *D*, present site (1992) during an El Niño year.

data for the means (table 1) calculated for this site. The 6-year mean annual precipitation of 233 mm presently provides sufficient moisture for vegetation growth. The monthly precipitation frequency (fig. 2) shows that, for an average year, only 7 months have precipitation amounts less than 13 mm; precipitation is absent during 1 of these 7 months (typically June). However, during 1 month a year, more than 32 mm of rain falls, and for almost 2 months a year, on average, precipitation amounts are greater than 38 mm. Snow falls occasionally at Jornada, but it melts quickly.

The drift potential calculated for the Jornada site is 24 VU, indicating a low wind-energy environment compared with deserts worldwide (Fryberger and Dean, 1979). The site sandrose (fig. 1) displays a strong west to southwest wind directional regime, and, therefore, the resultant drift direction is to the east-northeast. The predominant (modal) surface grain size at Jornada is 0.351 mm (medium sand) from which a threshold velocity (at 6.1 m height) of 9.0 m/s (20.1 mph) is calculated. The lateral cover in 1992 was 0.42 (Musick, chap. D, this volume).

The high frequency of present-day precipitation at Jornada, with amounts greater than 13 mm during 5 months of the year, encourages significant plant growth, which in turn discourages sand movement. The low wind-energy environment and the high threshold wind speed (based on a relatively large surface modal grain size) also limit the potential for eolian activity. Historically, however, this area has experienced severe wind erosion that has produced large coppice dunes less than a mile from the Geomet site (Breed, chap. A, this volume). Therefore, the Jornada site may demonstrate a temporal variability of surface vulnerability to sediment transport, where each phase lasts a decade or more.

FIELD-BASED ANALYSIS OF SEDIMENT TRANSPORT

METHODS

In order to study the relations of recorded winds to actual sand movement, storms accompanied by winds that moved sand during each season at each of three Geomet sites (Gold Spring, Yuma, and Jornada) were selected for preliminary analysis. The criteria for selecting the sample storms
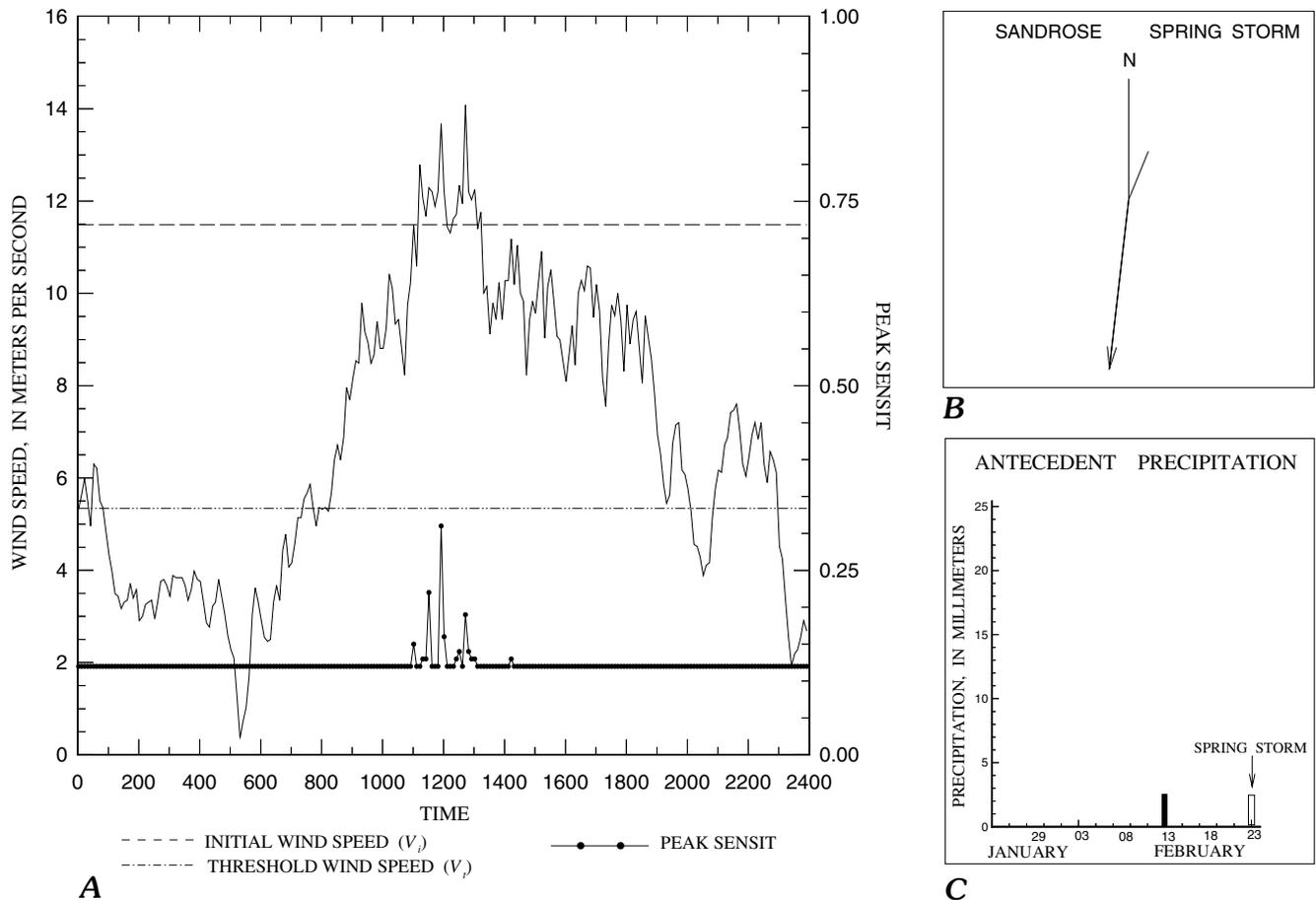
Figure 4. Spring storm data at Gold Spring for February 23, 1992. *A*, Seasonal storm with 6-minute average wind speeds measured at a height of 6.1 m and corresponding 6-minute peak SENSIT value (sand-movement indicator) for a 24-hour period. Initial wind speed (V_i) is the 6-minute average wind speed recorded with the first SENSIT-recorded sand movement; threshold wind speed (V_t) is the calculated (Bagnold, 1941) threshold wind speed at 6.1 m for a flat, bare, dry surface consisting of modal grain-size surface sand for each Geomet site. *B*, Storm sandrose indicates potential amount (length of arms) and upwind direction of sand movement produced by storm winds above V_t. Resultant (arrow) arm shows net potential amount of sand movement toward downwind direction. *C*, Antecedent precipitation shows rainfall totals for each day in the 30-day period before the seasonal storm.

are threefold: the site, the season, and the detected movement of sand. For this paper, three seasons are defined based on synoptic storm types of the southwestern deserts (Brazel and Nickling, 1986) and the effect of seasonal precipitation on vegetation growth (Crosswhite and Crosswhite, 1982; Bowers, 1987). The spring season, February through May, corresponds to the probable occurrence of large frontal storm systems that roll across the Southwest, some of which, in late spring, are occasionally associated with upper-level, low-pressure troughs. The summer, June through September, corresponds to convective activity that produces thunderstorms. The fall/winter season corresponds to the revival of frontal activity, which usually is associated with upper-level or cut-off, low-pressure troughs. The fall/winter season also is the time when precipitation (rain or snow) provides the stimulus or lack of stimulus for plant germination, which produces spring growth (Musick, chap. D, this volume). The spring

vegetation growth is an indicator of biomass, the main inhibitor of sand movement, for an area (Brazel and others, 1986; Lougeay and others, 1987; MacKinnon and others, 1990).

For each storm chosen, the full day of 6-minute average wind speeds, measured at a height of 6.1 m, and the corresponding peak electric pulse from the SENSIT recorded in the 6-minute period are graphed on the same time axis (figs. 4A–12A). The pulse from the SENSIT is not fully calibrated and, therefore, is an undefined quantity, aside from its crucial role of providing automatic signals that detect the onset, and mark the duration, of saltation under Geomet-measured wind conditions. The pulses are known to be related to the impact of sand grains and to have both mass and velocity components, such that the magnitude of the pulse does not solely reflect the amount of sand moved; to some unknown extent, it also reflects the strength of the wind. The SENSIT values on the graph of each storm, then, represent times when sand

Table 2. Summary information on selected seasonal storms at each Geomet site.

[Storm duration, amount of time the wind speed was above the site threshold wind speed. (Times when wind speeds drop below threshold during a storm, as in the fluctuating storms, are not included in the storm duration total.) Sand movement duration, amount of time of SENSIT-recorded sand movement. Percent time, percent of storm duration during which sand moved. V_t, threshold wind speed for the site. V_i, initial sand-moving wind speed of the storm. Mean (sd), mean and standard deviation of winds that produced sand movement. Storm direction, dominant wind direction associated with wind speeds above site threshold wind speed. Storm type, synoptic storm type based on Brazel and Nickling (1986). Sand-moving wind speeds $< V_t$, number of wind speed values associated with SENSIT-recorded sand movement that were less than the site threshold wind speed. Rain (direction), direction of the wind when rain began to fall]

| Geomet site | Storm duration | Sand movement | | V_t | V_i | Mean of sand-moving | Storm direction | Storm type | Sand-moving wind speeds | Miscellaneous |
| | | Duration | Percent | | | | | | | |
Season (mo/yr)	(hours)	(hours)	time	(m/s)	(m/s)	winds (sd)			$< V_t$	
Gold Spring										
Spring (2/92)	15.2	1.3	8.6	5.3	11.5	12.3 (0.81)	N	Post-front	0	
Summer (8/92)	1.1	0.5	45.5	5.3	5.2	9.8 (2.68)	ENE	T-storm	1	
Fall/winter (11/91)	11.8	1.0	8.5	5.3	12.6	13.0 (1.06)	WSW	Pre-front	0	Cut-off low-pressure trough.
Yuma										
Spring (3/91)	4.7	2.5	53.2	8.2	7.9	11.1 (1.33)	NW	Post-front	1	
Summer (9/91)	0.7	0.4	57.1	8.2	8.2	12.1 (2.88)	E	T-storm	0	Rain (ENE).
Fall/winter (10/91)	4.0	3.5	87.5	8.2	8.7	9.0 (0.82)	NNW	Post-front	6	Low-pressure trough.
Jornada										
Spring (4/92)										
A	6.1	1.9	31.1	9.0	8.8	10.9 (0.87)	WSW/W	Pre-front	1	
B	1.2	1.1	91.7	9.0	11.3	10.7 (1.58)	N	Front	1	
Total	7.3	3.0	41.1	9.0	8.8	10.8 (1.16)	WSW/W	Front	2	Rain (NNW).
Summer (8/92)	0.6	0.4	66.7	9.0	8.3	11.7 (2.54)	NE	T-storm	1	Rain (E).
Fall/winter (11/91)	10.1	4.2	41.6	9.0	7.4	10.1 (1.36)	SSW	Front	6	Low-pressure trough.

is moving but does not represent the amount moved. Also, only one SENSIT is connected to the data collection platform at each Geomet site; therefore, the spatial variability of saltation at the SENSIT area and of saltation at other areas around the Geomet station is unknown. This preliminary analysis is based on the temporal information of sand movement and associated wind speeds, wind directions, and precipitation.

The storm sandroses (figs. 4B–12B) are evaluated using actual Geomet-measured wind data above threshold wind speed for each site to show the relative amount of wind energy, wind direction, and resultant net potential sand movement and direction in a given storm. The antecedent precipitation graphs (figs. 4C–12C) show the amount of daily precipitation received at the Geomet site during the 30-day period preceding each storm.

As a companion to the storm graphs, table 2 lists basic information about each storm, such as duration, wind speeds and directions associated with the storm, and storm type.

Initial wind speed (V_i) is the recorded 6-minute average wind speed at which sand actually began to move for each storm, whereas threshold wind speed (V_t) is the calculated standard wind speed at which sand should begin to saltate under ideal conditions of a dry, bare, and flat surface. Storm direction in table 2 is the wind direction defined by each storm sandrose (figs. 4B–12B) and represents the prevailing direction from which the storm winds above threshold blew. Rain accompanying the storm, if any, is recorded in the "miscellaneous" column (table 2).

STORMS AT GOLD SPRING

A spring storm on February 23, 1992 (fig. 4A), was a post-frontal storm with strong winds out of the north. The storm duration of 15.2 hours was the longest of all the storms presented and thus produced the greatest drift potential, as shown in the length of the arms of the storm sandrose. At
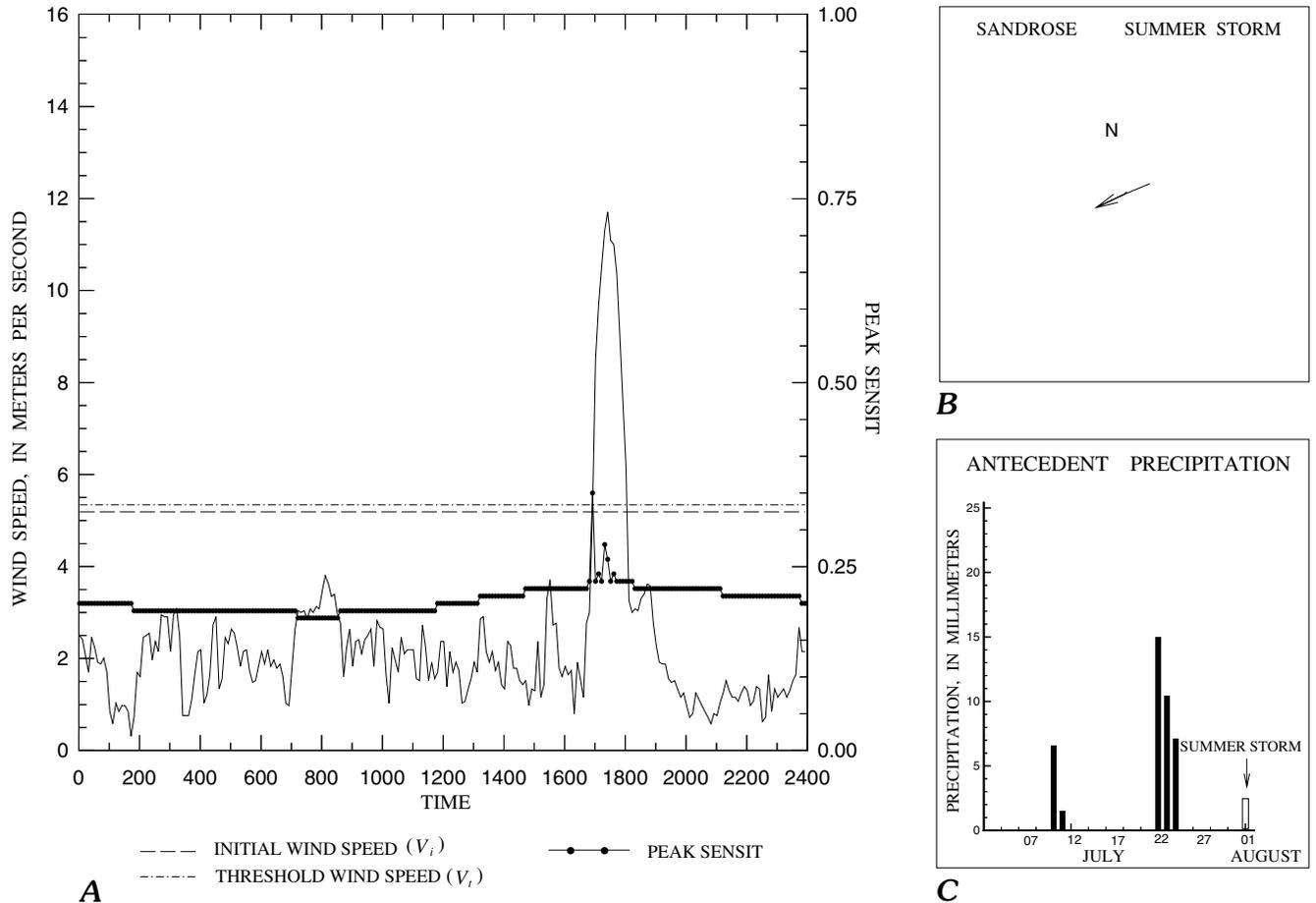
Figure 5.   Summer storm data at Gold Spring for August 1, 1992. See figure 4 caption for explanation.

Gold Spring, with a low threshold wind speed (5.3 m/s) and relatively high wind energy, most storms tend to be of long duration and tend to have large potential for sand movement. Most of the energy in the spring storm was produced by wind speeds greater than threshold (V_t) but less than the initial wind speed (V_i) of 11.5 m/s. The mean wind speed associated with sand movement was 12.3 m/s, with little variation about the mean (0.81), a pattern that indicates constant, strong winds. As the wind speeds tapered off from the initial wind speed, sand movement stopped, although the wind speeds remained well above threshold for hours. The northerly direction of the storm (fig. 4B) is in contrast to the site sandrose (fig. 1), which shows the long-term directions of potentially effective winds and has a very small northerly component.

A summer storm on August 1, 1992 (fig. 5A), showed a pattern typical of the three thunderstorms presented: low initial wind speeds compared to subsequent high speeds; high effectiveness, with sand movement during most, if not all, of the duration of the storm; variable wind directions; and rainfall at the end of the storm. The initial wind speed of this thunderstorm was 5.2 m/s; the average of all wind

speeds that produced sand movement was 9.8 m/s, almost twice the initial wind speed. Sand moved for 46 percent of the storm's duration, but then abruptly stopped without apparent reason; no measurable rain (greater than 0.25 mm) fell that might have caused cessation. The variable wind directions were from the north, northeast, and east-north-east, with east-northeast being the major direction of the storm (fig. 5B). East-northeast is not a dominant direction of potential sand-moving winds at Gold Spring, as indicated by the site sandrose.

A fall/winter storm of November 17, 1991 (fig. 6A), displayed a series of winds pulsating above and below the site threshold. This pre-frontal storm was associated with an upper-level, cut-off low-pressure trough. The duration of this storm—that is, the amount of time the wind was above threshold, even if not continuous—was 11.8 hours; again, this storm was long and had most wind speeds between threshold and initial wind speed, and had sand movement associated mostly with winds above initial wind speed. The winds in this storm, however, had a different character than the spring storm. The major winds and the sand movement in the spring storm occurred at the beginning of the storm, when
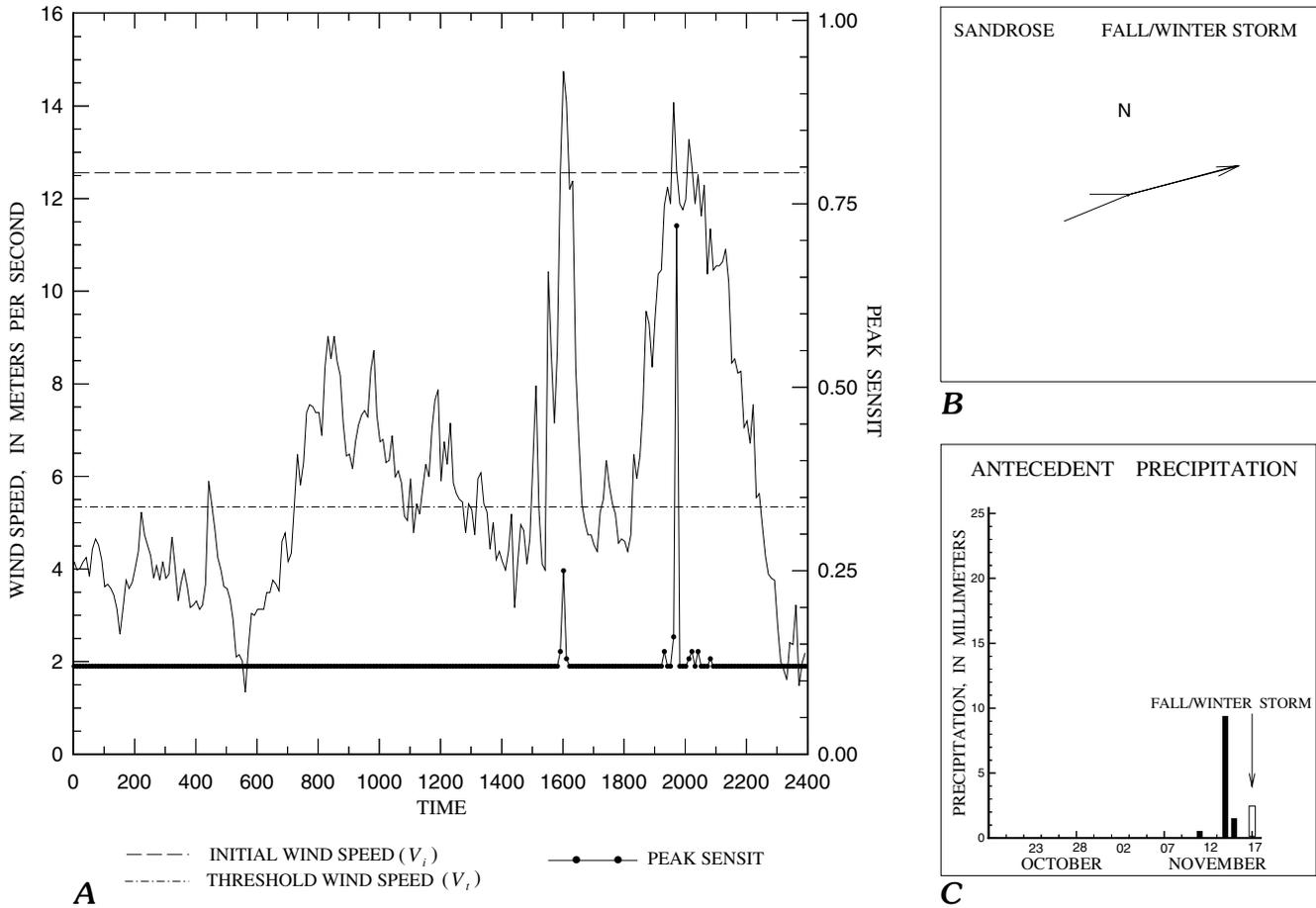
Figure 6. Fall/winter storm data at Gold Spring for November 17, 1991. See figure 4 caption for explanation.

wind speeds were above the initial wind speed, whereas the fall/winter storm showed pulses of wind above initial wind speed throughout the storm. The net result of the pulsating winds in the fall/winter storm was that the last pulse moved the sand with lesser winds than the first pulse. The high initial wind speed (12.6 m/s) and the mean value of sand-moving winds (13.0 m/s) defined a very powerful storm. The directions of the storm were from the west and west-southwest (fig. 6B), which correspond to the prevailing directions of potentially effective winds at the site as shown in the site sandrose.

STORMS AT YUMA

A spring storm on March 11, 1991 (fig. 7A), was a post-frontal storm similar to the spring storm at Gold Spring but shorter in duration (4.7 hours). The initial wind speed (V_i) associated with the storm (7.9 m/s) and threshold wind speed (V_t) for the site (8.2 m/s) agreed closely in value. Sand movement was greatest at the beginning and then ceased, although the decreasing winds remained above

initial wind speed and threshold for slightly more than 1 hour. Sand movement began with a low initial wind speed of 7.9 m/s, but the average of the wind speeds producing sand movement was significantly higher, at 11.1 m/s. The direction of the storm was from the northwest (fig. 7B), a dominant direction of storms in this area, as shown in the site sandrose (fig. 2).

A summer storm on September 2, 1991 (fig. 8A), demonstrated the sand-moving activity produced by a haboob (Idso and others, 1972; McCauley and others, 1984, fig. 13). A large pulse of sand movement occurred but was terminated abruptly by the ensuing rain, which totaled only 1.78 mm. Sand moved during the entire time that the wind was above initial wind speed, except when the rain fell. The initial wind speed (V_i) was 8.2 m/s, whereas the average speed of the sand-moving winds was 12.1 m/s, the highest average wind speed of the three storms described for Yuma. At the beginning of the storm, the winds were from the southeast, then from the east-southeast, and finally from the east. The wind direction during the 18-minute rainy phase was from the east-northeast, which shows a directional progression of the thunderstorm cell, in this instance from south to north.
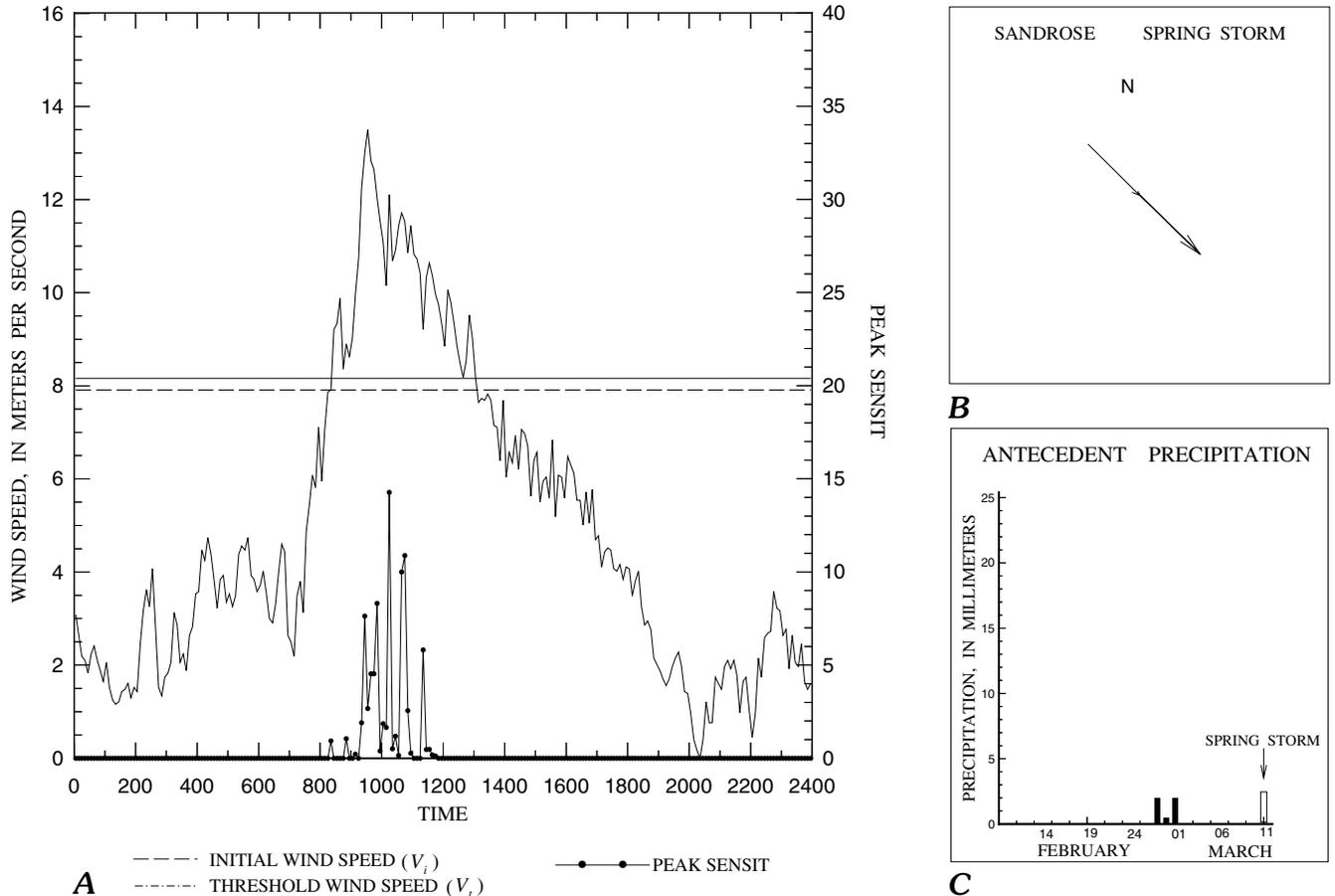
Figure 7. Spring storm data at Yuma for March 11, 1991. See figure 4 caption for explanation.

The dominant direction of the storm winds was from the east (fig. 8*B*), a common direction for thunderstorms in this area (Brazel and Nickling, 1986).

A fall/winter storm on October 30, 1991 (fig. 9*A*), was a post-frontal storm associated with an upper-level, low-pressure trough. This storm was characterized by pulses of winds that produced sand movement 88 percent of the storm time. Sand moved throughout each pulse above threshold wind speed, including the final, somewhat weaker, pulse of the series. The initial wind speed (V_i) of 8.7 m/s was in the same range as other initial wind speeds at Yuma, but the mean of sand-moving winds, a low 9.0 m/s, signaled relatively weak storm winds. This fall/winter storm was very effective at moving sand with inferior winds. The storm winds oscillated between north and north-northwest, two directions defined by the Yuma sandrose as dominant for the site.

STORMS AT JORNADA

A spring storm on April 18, 1992 (fig. 10*A*), showed a complex pattern. The pre-frontal first phase (A, table 2) produced bidirectional winds from the west-southwest and west (fig. 10*B*), two of the dominant directions of potentially effective winds for the Jornada site (fig. 1). Wind speeds then dropped below threshold for 78 minutes, only to rise again much stronger than before as the full force of the front was felt at the site. The frontal phase (B, table 2) brought north and north-northwest winds (insignificant potentially effective directions for the site). This highly efficient second phase of the storm lasted 1.2 hours and produced sand movement 92 percent (1.1 hours) of that time. The winds dropped again, and the rain arrived 1 hour later. For one 6-minute period while rain fell, the wind speed jumped above threshold. At the end of this storm, 4.57 mm of rain had fallen. The initial wind speed of the storm (V_i) and its first phase was 8.8 m/s, matching the threshold wind speed (V_t) for the site (9.0 m/s). The second-phase initial wind speed was 11.3 m/s, well above the initial wind speed associated with the first phase and threshold wind speed, but the averages of sand-moving winds for both phases were virtually equivalent (10.9 m/s and 10.7 m/s, respectively).

A summer storm of August 19, 1992 (fig. 11*A*), was an evening (20:32 m.s.t.) thunderstorm. The initial wind speed
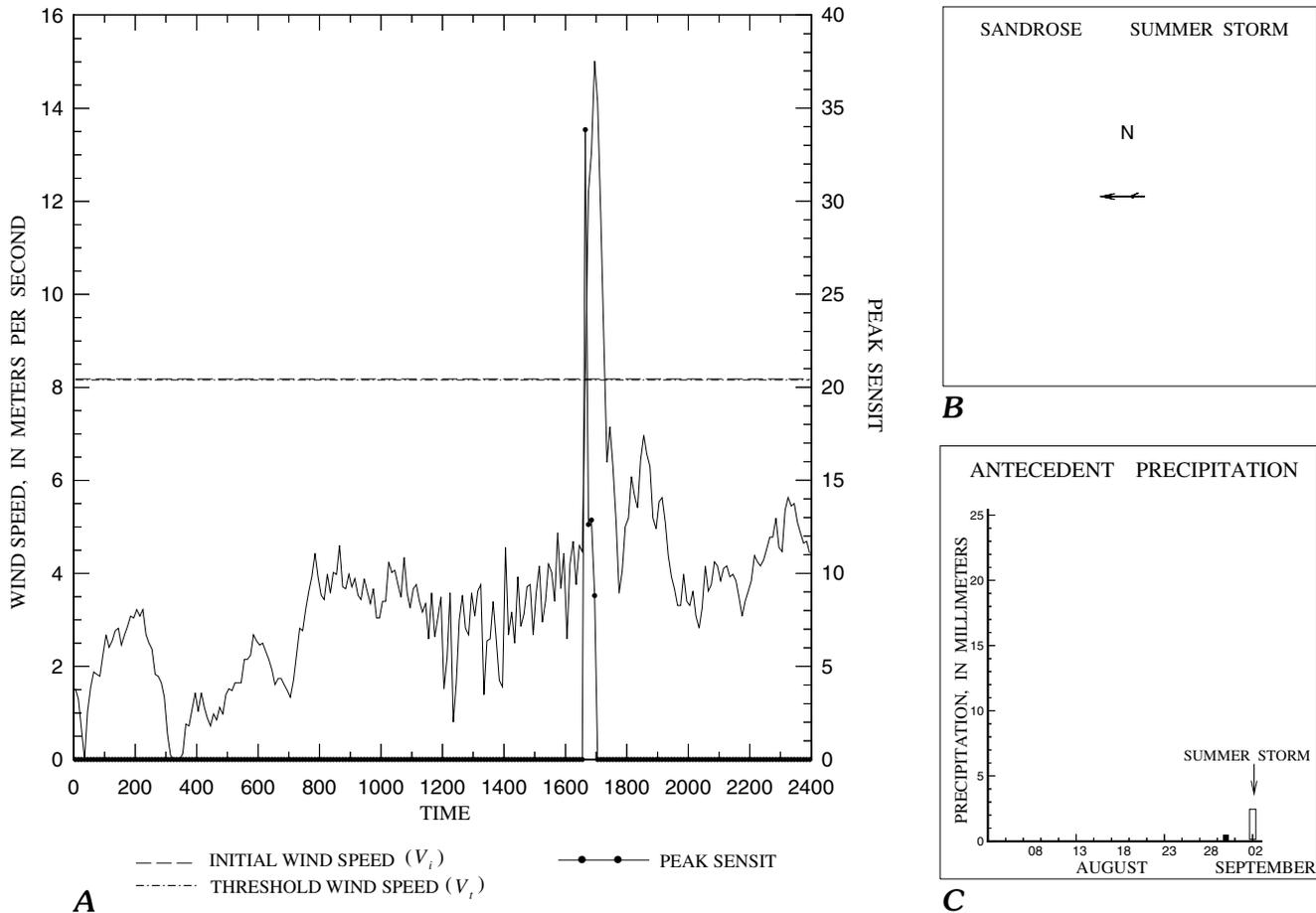
Figure 8.   Summer storm data at Yuma for September 2, 1991. See figure 4 caption for explanation.

(V_i) associated with the onset of saltation was 8.3 m/s, whereas the high subsequent winds averaged 11.7 m/s. Sand moved throughout the storm until rain fell. The multidirectional nature (fig. 11B) of this thunderstorm began with winds and initial sand movement from the east-northeast; the winds shifted, blowing from the northeast for 18 minutes; then the rain arrived and the wind direction returned to east. Rain continued until 01:00 m.s.t. and total precipitation was 4.32 mm. The northeasterly wind direction of this storm is not a dominant direction for this site, based on the site sandrose.

A fall/winter storm on November 28–29, 1991 (fig. 12A), started at 15:20 m.s.t. and continued in a pulsating manner throughout the night until 14:08 m.s.t. the next afternoon. The storm front associated with an upper-level low produced a pre-frontal first day and post-frontal second day, with most sand movement taking place in the pre-frontal stage. The winds on the first day were from the south-southwest and southwest, and the winds on the second day shifted to west-southwest and west (fig. 12B). All these directions, except south-southwest (the direction of the first-phase and more powerful winds) are major directions of the site sandrose. The sand moved at the beginning and end of the

storm in a manner comparable to that of the other storms that showed this fluctuating pattern. The low initial wind speed of 7.4 m/s was similar to the V_i during the other two Jornada storms, all of which had initial wind speeds below threshold for the site. The average of sand-moving winds, 10.1 m/s, was consistent with the mean effective winds of other Jornada storms.

EFFECTS OF PRECIPITATION

ROLE OF SHORT-TERM ANTECEDENT PRECIPITATION

Studies of the role of soil moisture in wind erosion generally rely on measurements of antecedent precipitation, a meteorological parameter that is much more readily available than continuous field measurements of soil moisture, which are rarely taken and are notoriously unreliable for desert soils (Baker, 1990). To develop a climatic erosivity factor that quantifies the effects of soil moisture in
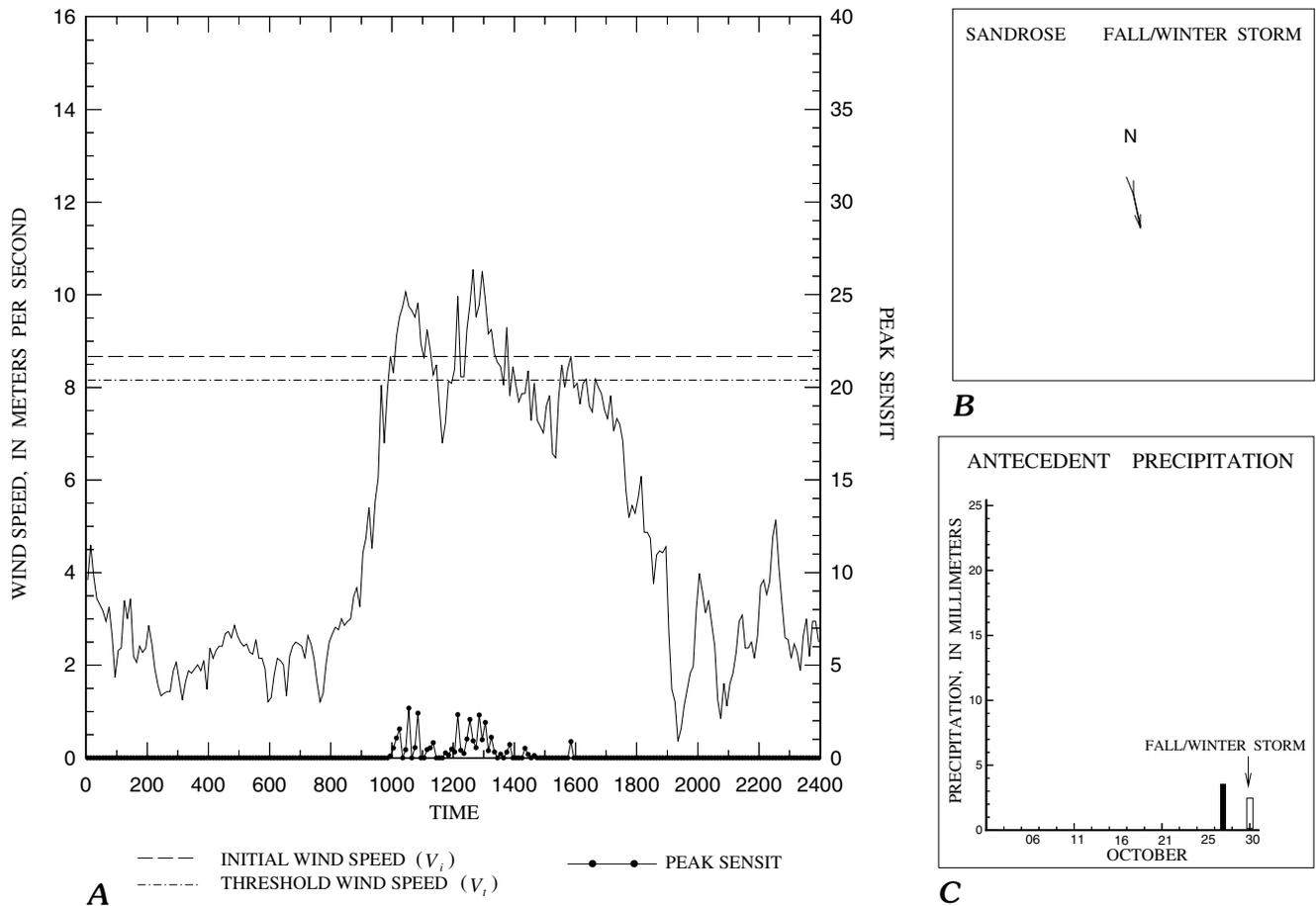
Figure 9.   Fall/winter storm data at Yuma for October 30, 1991. See figure 4 caption for explanation.

their predictions of wind erosion on farm fields of the subhumid American Midwest, U.S. Department of Agriculture researchers (Chepil and others, 1962) used the Thornthwaite (1931) PE ratio, a dryness index based on monthly precipitation (P) and evaporation (E) amounts. In the Chepil climatic equation, however, P/E ratios are not valid for monthly rainfall amounts less than 13 mm—a common occurrence in arid and semiarid regions (fig. 2). Skidmore (1986) and the Food and Agriculture Organization (1979) modified the equation by eliminating the soil moisture influence for conditions when monthly precipitation is less than 13 mm, thus substantiating that wind speed alone dominates the climatic erosivity factor for most months in arid and semiarid regions.

The sand surfaces of arid and semiarid lands dry quickly after rain, especially if the wind is blowing. Studies that have attempted to relate short-term antecedent precipitation to frequencies of dust storms in southern Arizona (Brazel and others, 1986; MacKinnon and others, 1990) indicate that short-term antecedent rainfall (less than a season's accumulation) most likely does not hinder the generation of dust storms, which are phenomena initiated by saltation of sand. An empirical example of a Yuma storm

shows that a storm that started with rain can end with sand blowing (fig. 13), although the wetted surface probably required a higher initial wind speed (11 m/s) to begin saltation than the initial wind speed (8 m/s) of the Yuma spring storm 10 days later, when the subsurface was drier.

The main mechanism by which short-term antecedent precipitation may affect movement of surface material is crusting, particularly in areas where soils contain significant amounts of clay (Chepil, 1958; Gillette and others, 1980, 1982; Zobeck, 1991). Such crusts must first be broken down in order for surface grains to be available for saltation. Sandy surfaces at the three Geomet sites discussed in this report have so little clay content (less than 2 percent) that surface-stabilizing crusts do not form, or, as at Gold Spring, they are very weak.

Short-term antecedent precipitation is plotted for the illustrated sandstorms at the three Geomet sites (figs. 4C–12C). In four cases, rain fell within 5 days before the storm, and in eight cases, rain fell within 10 days before the storm. Only the fall/winter sand-moving storm at Jornada was preceded by a dry period of more than 10 days. For those four storms with antecedent precipitation within 5 days, daily rainfall amounts were less than 13 mm, the
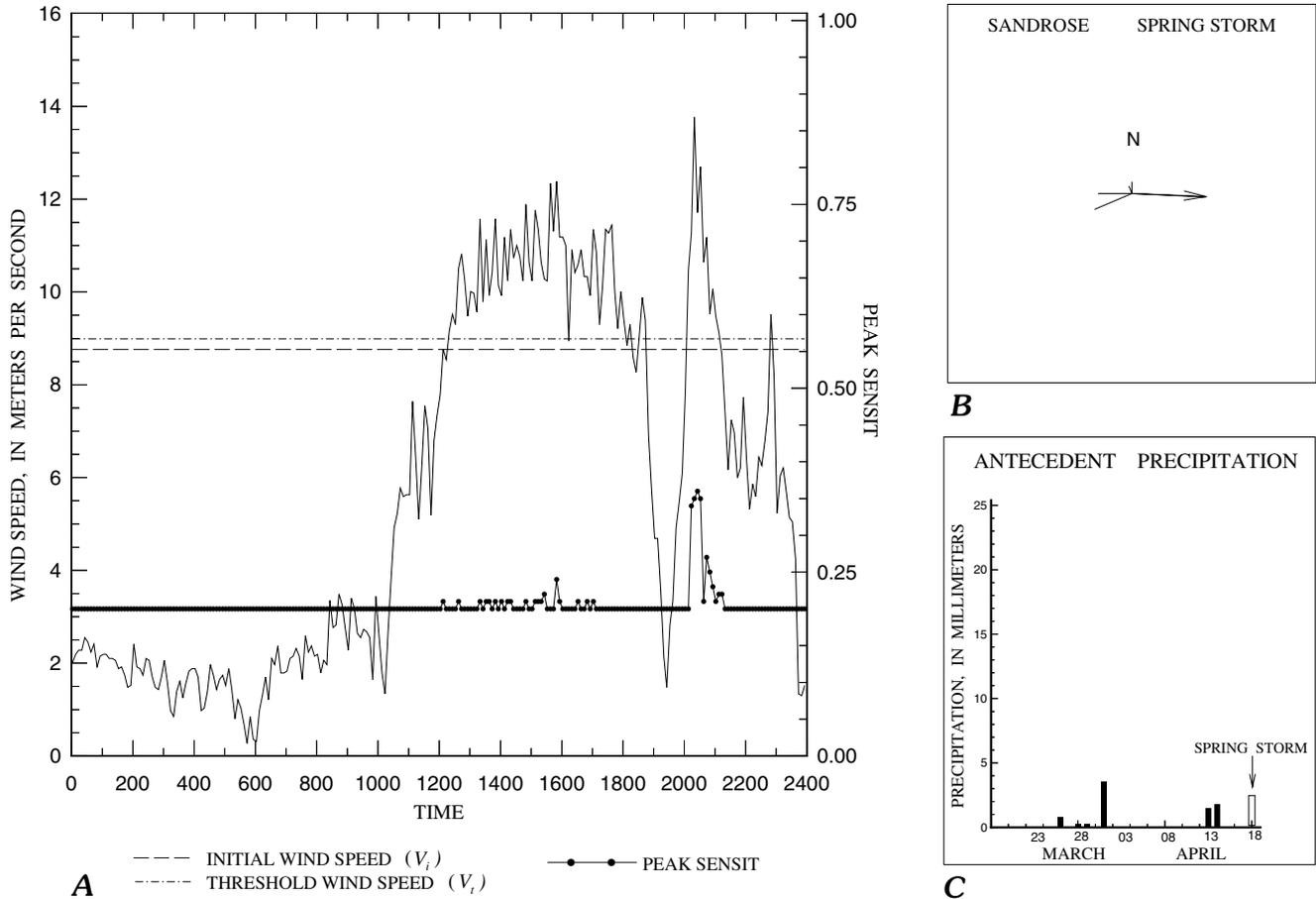
Figure 10.   Spring storm data at Jornada for April 18, 1992. See figure 4 caption for explanation.

precipitation range within which most daily desert rains occur, as shown in the daily precipitation frequency graphs for each site (fig. 14). In the Gold Spring fall/winter storm, a 2-day precipitation total of 10.9 mm fell within 1 day of the sandstorm, and the Yuma fall/winter storm was preceded by 3.6 mm of rain within 2 days. Both of these storms, with fluctuating wind patterns, produced sand movement throughout the storms. Sand movement activity increased as the Gold Spring storm progressed, possibly showing the drying effect of the wind on the surface; the Yuma storm was a powerful sand-mover with relatively weak winds. These storms provide empirical examples of the limits of short-term antecedent precipitation as an inhibitor of saltation on sandy surfaces.

ROLE OF LONG-TERM ANTECEDENT PRECIPITATION

A more important role for eolian processes can be ascribed to soil moisture provided by long-term antecedent precipitation, rainfall that occurred in previous seasons (Brazel and others, 1986; MacKinnon and others, 1990). Fall/winter moisture, in particular, appears to be crucial for estab-

lishing the germination and growth of spring vegetation (Musick, chap. D, this volume). At the Yuma Geomet site, for example, precipitation totals were meager (less than 13 mm) for the fall/winter seasons of 1988 through 1990, which resulted in a decrease of lateral cover from 0.24 to 0.14. Then during the fall/winter of 1991, 22 mm of rain fell, which produced an abundant growth that returned the lateral cover value to 0.23 in the spring of 1992. The spring vegetation, especially the grass schismus, effectively stopped the movement of sand. No storms at Yuma in 1992 were chosen for preliminary analysis because no significant sand movement occurred during the entire year. Thus, the effects of precipitation during a prior season on present conditions for saltation are closely related to the types and amounts of vegetation cover that flourished or dwindled in response to the previous season's contribution to soil moisture.

DISCUSSION

The graphical analyses of the seasonal storms at each Geomet site show the influence of synoptic weather systems on the vegetated land surface and the corresponding response of the sediments on these desert surfaces to
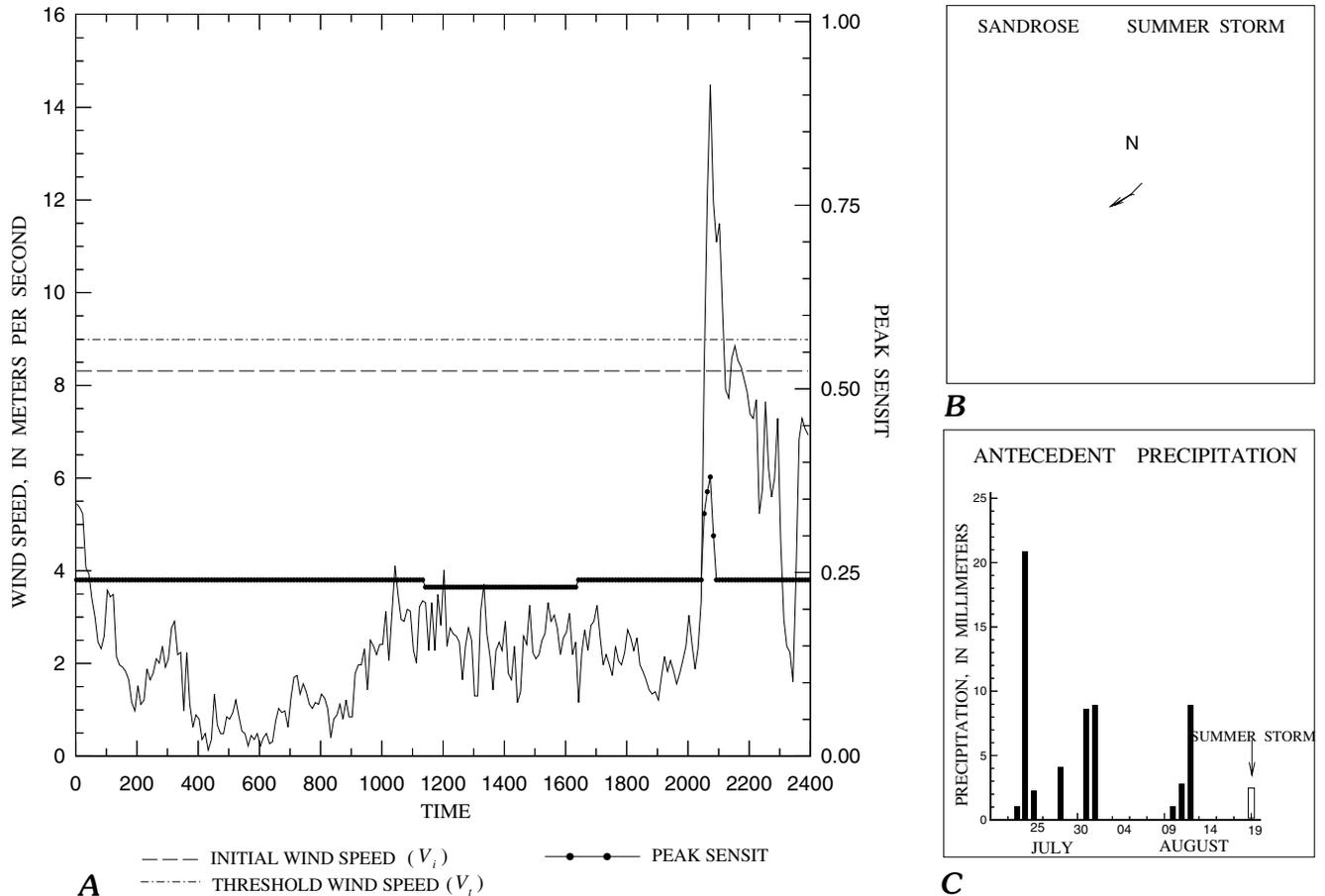
Figure 11. Summer storm data at Jornada for August 19, 1992. See figure 4 caption for explanation.

meteorological forces. The spring storms (figs. 4*A*, 7*A*, 10*A*) show frontal storm characteristics: strong initial winds that tapered off as the storm died down, constant westerly wind directions ranging from the south to the north (Brazel and Nickling, 1986), and long durations, with winds above threshold for hours. Because of long durations and relatively high wind speeds, these spring frontal storms, both pre-frontal and post-frontal, have the potential to move large amounts of sand, especially later in the spring if the initial burst of spring vegetation growth has died back. Yet, during all three spring storms (Gold Spring, Yuma, and the first phase of Jornada (fig. 10*A*)), the sand movement ceased before the winds dropped below the site threshold (V_t), and in two of the storms, Yuma and Jornada, the sand movement ceased before the winds dropped below the initial wind speeds (V_i) for each storm. Wind tunnel studies (Bagnold, 1941) and research on unvegetated agricultural fields (D.W. Fryrear, USDA-ARS, oral commun., 1993) show that, once sand begins to saltate, the movement can be sustained by lower wind speeds. None of the three spring storms showed this phenomenon; in fact, these storms showed the opposite behavior, with sand movement ceasing with high as well as with decreasing wind speeds. The threshold wind speed (V_t), as a defined standard wind speed needed to initiate saltation

if the site surface were bare and dry, should be lower than the initial wind speed (V_i), the wind speed that initiated saltation on a vegetated surface (Musick and Gillette, 1990). However, only at Gold Spring, a highly vegetated site (L_c=0.41), was the initial wind speed higher than the threshold. The Yuma site was poorly vegetated (L_c=0.14) during the spring storm because of recent drought conditions, which provides a possible explanation for the low initial wind speed; but the Jornada site, with high lateral cover (L_c=0.42), also had a low initial wind speed for the first phase of the spring storm.

Furthermore, the Jornada spring storm (fig. 10*A*), which was similar to an unusually severe, dust-producing 1977 storm in the Clovis, N. Mex., area (McCauley and others, 1981, fig. 11) can be considered as two storms: the first phase provided the most wind energy and the second phase produced a short-term, dramatic assault on the surface from a different wind direction. Sand moved during most of the pre-frontal first phase of the storm, and the wind direction of this phase was from the west and west-southwest. Because most of the wind energy was produced by this phase, the resultant (net) potential sand-moving winds, as defined by the storm sandrose (fig. 10*B*), were from the west (moving sand toward the east). Later, the front itself moved through the area, and thereby produced the second-phase activity, with associated
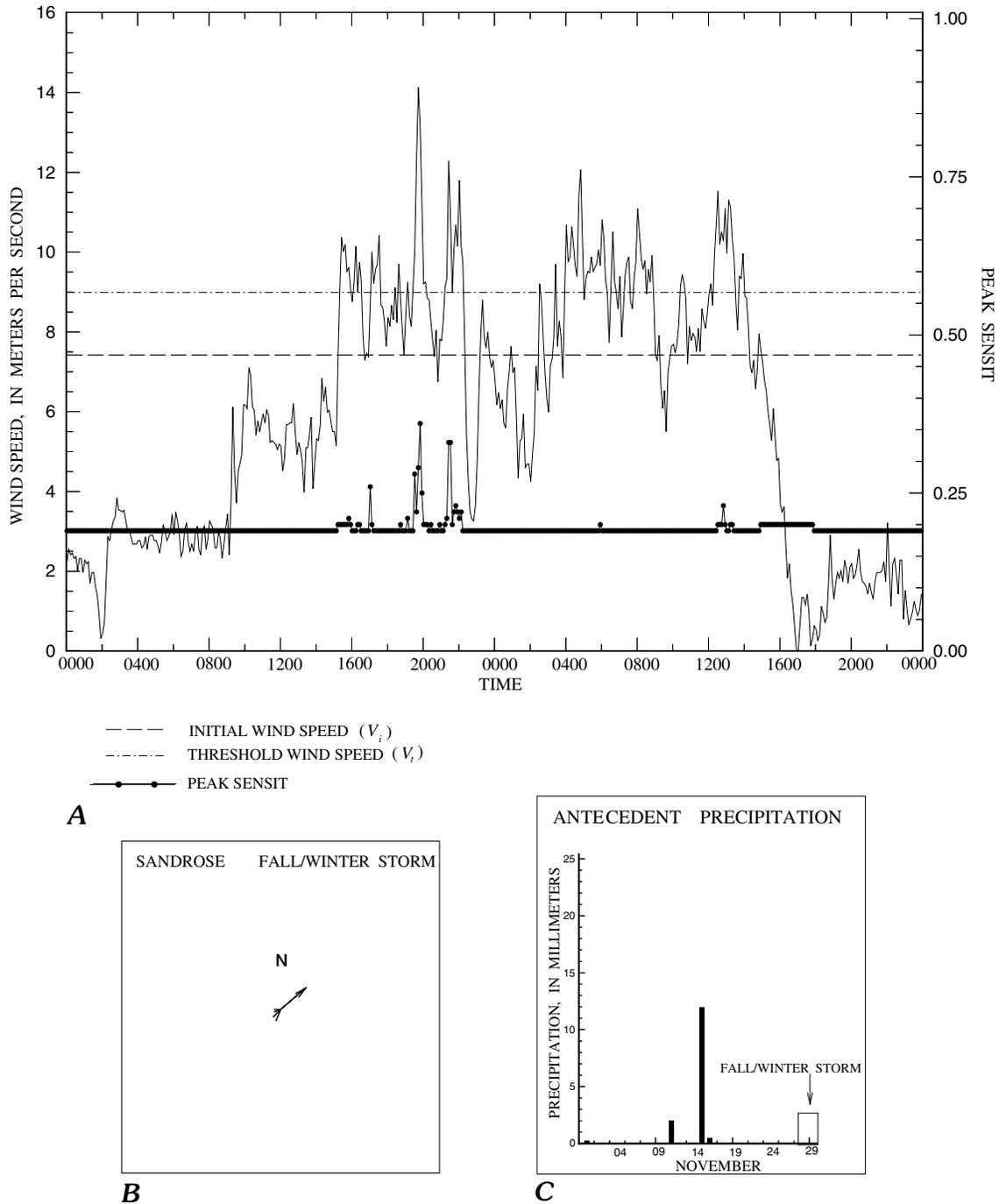
Figure 12. Fall/winter storm data at Jornada for November 28–29, 1991. See figure 4 caption for explanation.

sand-moving winds from the north. The amount of sand moved separately by each phase of the storm is unknown; but each phase was effective at moving sand, and the storm sandrose may not adequately show the actual sand-moving influence of the north winds on the net sand flow. Frontal storms are a relatively simple, synoptic storm type; however, the graphs of the frontal storms at each site suggest that the interaction among the wind, vegetation, and sand surface was more complex.

The summer storms described above have the classic signatures of thunderstorms—swift, powerful downdrafts and turbulent wind speeds and directions. These storms are of short duration, generally less than 1 hour (Brazel and Nickling, 1986), but because of their power, they produce sand movement. Two of the storms, at Yuma and Jornada (figs. 8A, 11A), produced rain, and those same two storms also produced sand movement each time the wind speed rose above threshold until the rain finally stopped the movement.
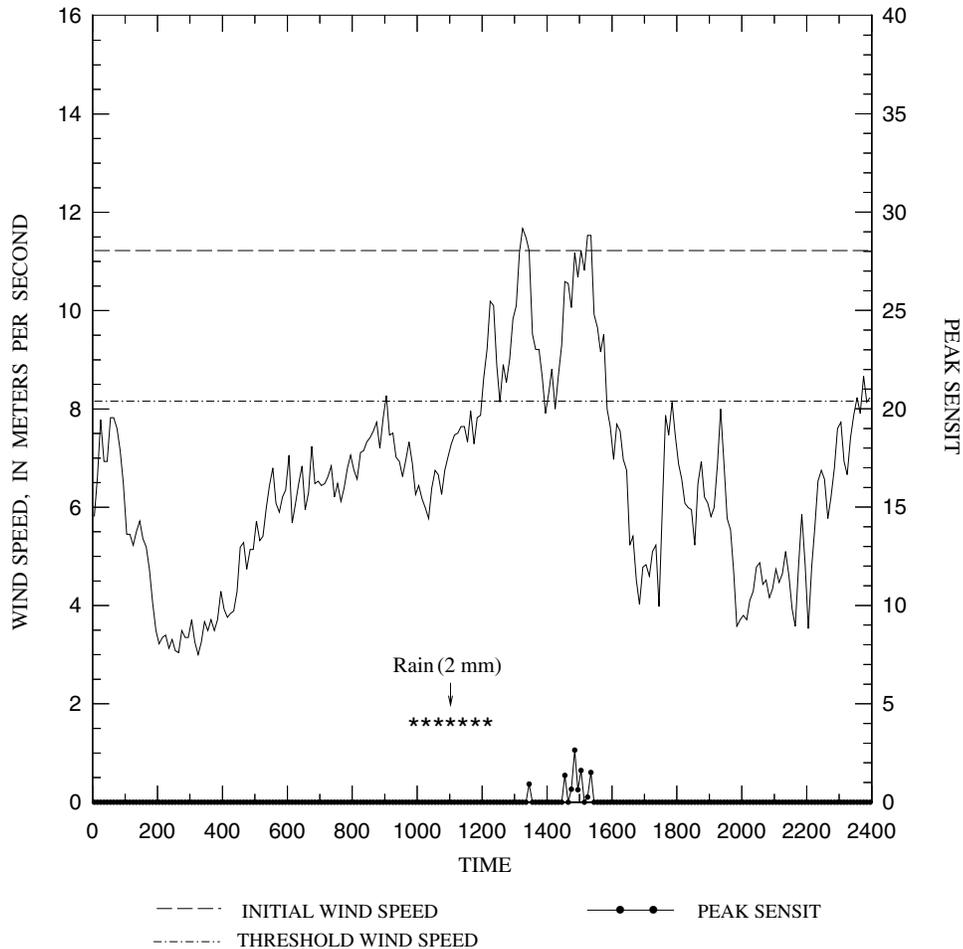
Figure 13. A spring storm at Yuma (March 1, 1991) showing a 2-mm rainfall at the beginning of the storm and sand moving, as recorded by the SENSIT, 1 hour later.

Wind directions during these two storms were multidirectional, with the Yuma storm demonstrating the progression of the thunderstorm cell through the Geomet site and the Jornada storm showing turbulent directions that continually shifted throughout the storm. The Gold Spring storm (fig. 5A) was less powerful than the other two with no rain, a more constant direction, and less time of SENSIT-recorded sand movement. Sand movement there stopped while storm winds continued at speeds above both threshold and initial wind speed of the storm. For all three summer storms, the initial wind speed was the same as the threshold wind speed despite the presence or absence of vegetation at each   site.

The fall/winter storms had a pulsating character, with wind speeds that rose above and dropped below initial wind speed, some quite dramatically, throughout their duration. In all of these storms, the wind direction also pulsated between two adjacent directions. These fall/winter pulsating storms were frontal storms associated with upper-level, low-

pressure troughs—one of which, at Gold Spring (fig. 6A), was a cut-off low. Such pulsating winds might produce more sand movement than winds from a constant direction by episodically shifting in speed and direction throughout the storm. For example, at Yuma (fig. 9A) sand moved 88 percent of the time in the fall/winter storm compared with 53 percent of the time in the spring storm (table 2), although the fall/winter storm had only half the wind energy (as shown in the storm sandroses) of the spring storm; because of the drought conditions during that year, vegetation cover was constant throughout both seasons. The pulsating character of the storms also may help explain sand movement associated with wind speeds less than threshold during the two storms at Yuma and Jornada (table 2). The fluctuating wind speeds and directions may destabilize the surface enough to expose grains to the wind field that could be easily moved by lower wind speeds.

In the Southwest, spring is generally considered the windy season, because the large frontal storms that move through the region at this time of year produce so much wind

GOLD SPRING
1980 - 1992

JORNADA
1987 - 1992
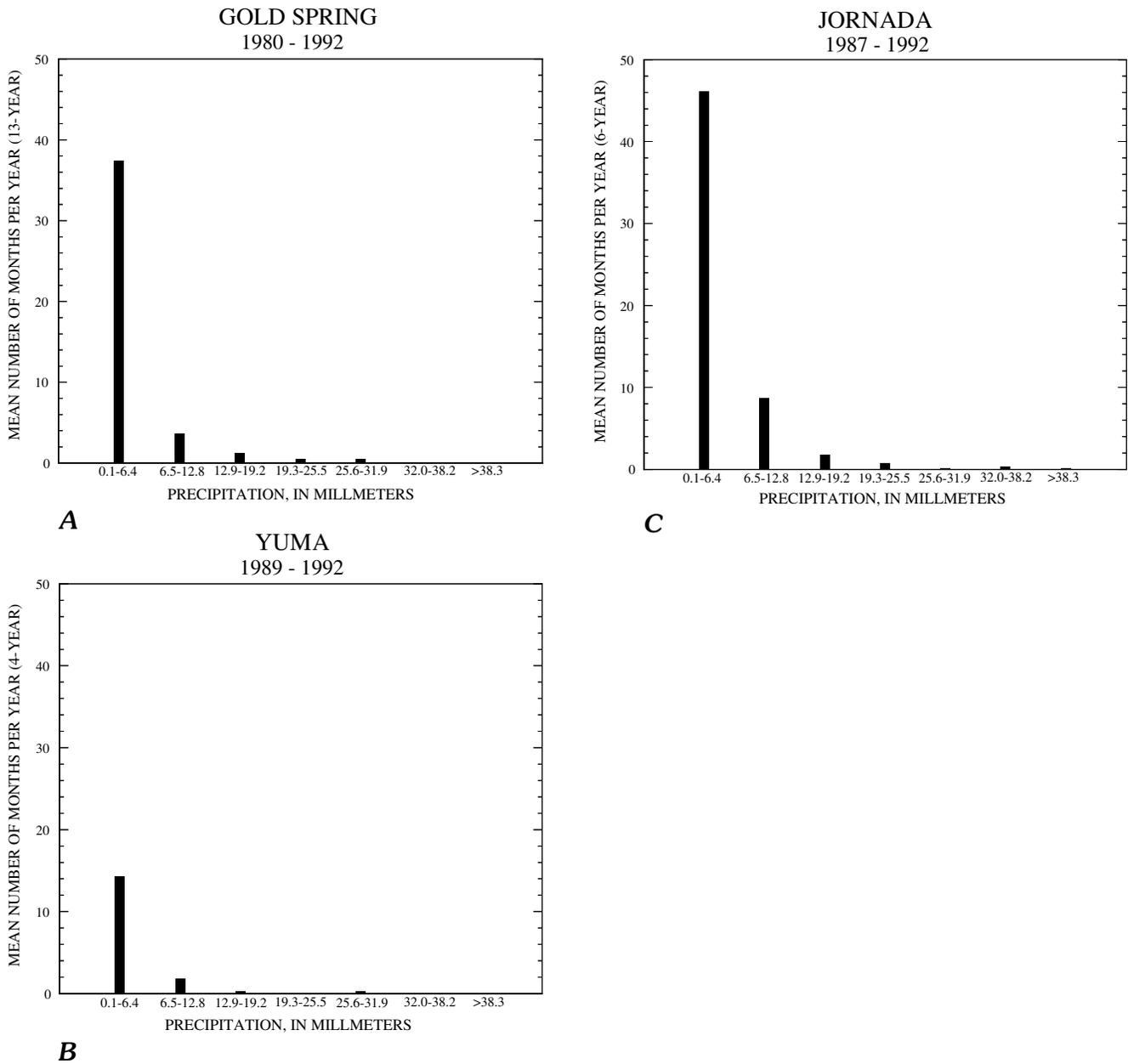
YUMA
1989 - 1992

Figure 14. Daily precipitation frequency distributions showing mean number of days per year with total rainfall in each precipitation range for the period of record at *A*, Gold Spring; *B*, Yuma; and *C*, Jornada.

energy. The summer generally is considered the dust season, because the thunderstorms associated with the Arizona monsoon produce haboobs that move great quantities of dust, particularly in the Phoenix area (Brazel and Nickling, 1986). Fall/winter storms have not received as much attention as the other two seasonal storm types, and yet examples of substantial sand movement by winds associated with upper-level lows in the fall/winter season at the Geomet sites suggest that the effect of these low-pressure troughs on the land surface may be greater than previously recognized.

SUMMARY

The three Geomet sites (Gold Spring, Yuma, and Jornada) in the arid and semiarid deserts of the Southwest United States have different eolian characteristics. The interactions among the land surface, synoptic wind regime, vegetation, and precipitation patterns create unique environments for potential sediment transport. The movement of sediment in these desert areas produces dust storms, erosion and deposition of soils, and destruction of

vegetation. The storms described in this paper demonstrate the variety of wind regimes and surface responses that are observed by monitoring actual sand-moving events in natural areas. Key data provided by automated sensors include wind speed, wind direction, precipitation, and sediment transport, which is recorded concurrently with wind speed by the SENSIT. The threshold wind speed (V_t), calculated using the surface grain size, and the local wind field define the potential for sand movement, which differs from the actual eolian transport at each site. The synoptic storm types produce distinctive surface wind regimes that seem to have characteristic effects on the land surface. Short-term antecedent precipitation (rainfall received during the present season) has a limited effect on surface stabilization, whereas long-term antecedent precipitation (rainfall received during a previous season) affects the surface vulnerability to sediment transport by supporting or thwarting vegetation growth in the following season.

Yet, relations between vegetation cover and the onset of saltation remain uncertain. More study of SENSIT-recorded sandstorms, complete calibration of the SENSIT such that amounts of material moved can also be measured, employment of multiple SENSIT instruments to better define spatial variability, and analysis of potential sand-moving storms that do not produce saltation are needed to provide greater understanding of the natural (actual) relations among atmospheric conditions, vegetation cover, and the land surface response.

REFERENCES CITED

Bagnold, R.A., 1941, The physics of blown sand and desert dunes: London, Chapman and Hall, 265 p.

Baker, J.M., 1990, Measurement of soil water content, *in* Becker, Francois, ed., Remote Sensing Reviews: Instrumentation for Studying Vegetation Canopies for Remote Sensing in Optical and Thermal Infrared Regions: Reading, Berkshire, UK, Harwood Academic Publishers, 360 p.

Belly, Pierre-Yves, 1964, Sand movement by wind, *with* Addendum 2, by Kadib, Abdel-Latif: U.S. Army Corps of Engineers, Coastal Engineering Research Center Technical Memorandum 1, 85 p.

Bowers, M.A., 1987, Precipitation and the relative abundances of desert winter annuals: A 6-year study in the northern Mohave Desert: Journal of Arid Environments, v. 12, p. 141–149.

Brazel, A.J., and Nickling, W.G., 1986, The relationship of weather types to dust storm generation in Arizona (1965–1980): Journal of Climatology, v. 6, p. 255–275.

Brazel, A.J., Nickling, W.G., and Lee, J., 1986, Effect of antecedent moisture conditions on dust storm generation in Arizona, *in* Nickling, W.G., ed., Aeolian Geomorphology: Boston, Allen and Unwin Press, p. 261–271.

Chepil, W.S., 1945, Dynamics of wind erosion: II. Initiation of soil movement: Soil Science, v. 60, p. 397–411.

———1958, Soil conditions that influence wind erosion: U.S. Department of Agriculture Agricultural Research Service Technical Bulletin 1185, p. 1–40.

Chepil, W.S., Siddoway, F.H., and Armbrust, D.V., 1962, Climatic factor for estimating wind erodibility of farm fields: Journal of Soil and Water Conservation, v. 17, p. 162–165.

Crosswhite, F.S., and Crosswhite, C.D., 1982, The Sonoran Desert, *in* Bender, G.L., ed., Reference Handbook on the Deserts of North America: Westport, Conn., Greenwood Press.

Ezcurra, E., and Rodrigues, V., 1986, Rainfall patterns in the Gran Desierto, Sonora, Mexico: Journal of Arid Environments, v. 10, p. 13–28.

Folk, R.L., 1964, Petrology of sedimentary rocks: Austin, Texas, Hemphill, 170 p.

Food and Agriculture Organization, 1979, A provisional methodology for soil degradation assessment: Rome, Food and Agriculture Organization of the United Nations.

Fryberger, S.G., and Dean, Gary, 1979, Dune forms and wind regime, *in* McKee, E.D., ed., A Study of Global Sand Seas: U.S. Geological Survey Professional Paper 1052, p. 137–169.

Fryrear, D.W., Stout, J.E., Hagen, L.J., and Vories, E.D., 1991, Wind erosion: Field measurement and analysis: Transactions of the American Society of Agricultural Engineers, v. 34, no. 1, p. 155–160.

Gillette, D.A., Adams, John, Endo, Albert, Smith, Dudley, and Kihl, Rolf, 1980, Threshold velocities for input of soil particles into the air by desert soils: Journal of Geophysical Research, v. 85, no. C10, p. 5621–5630.

Gillette, D.A., Adams, John, Muhs, Daniel, and Kihl, Rolf, 1982, Threshold friction velocities and rupture moduli for crusted desert soils for the input of soil particles into the air: Journal of Geophysical Research, v. 87, no. C11, p. 9003–9015.

Henning, D., and Flohn, H., 1977, Climate aridity index map: United Nations Conference on Desertification, Nairobi, U.N. Environmental Programme.

Idso, S.B., Ingram, R.S., and Pritchard, J.M., 1972, An American haboob: Bulletin of the American Meteorological Society, v. 53, no. 10, p. 930–935.

Lettau, H.H., and Lettau, K., 1978, eds., Exploring the world's driest climate: Institute for Environmental Studies Report 101, University of Wisconsin–Madison, 265 p.

Lougeay, R., Brazel, A.J., and Miller, T.A., 1987, Monitoring changing desert biomass through video digitization of Landsat MSS data: An application to dust storm generation: Journal of Photogrammetric Engineering and Remote Sensing, v. 53, no. 9, p. 1251–1254.

MacKinnon, D.J., Elder, D.F., Helm, P.J., Tuesink, M.F., and Nist, C.A., 1990, A method of evaluating effects of antecedent precipitation on duststorms and its application to Yuma, Arizona, 1981–1988: Climatic Change, v. 17, p. 331–360.

Marshall, J.K., 1971, Drag measurements in roughness arrays of varying densities and distribution: Agricultural Meteorology, v. 8, p. 269–292.

McCauley, J.F., Breed, C.S., Grolier, M.J., and MacKinnon, D.A., 1981, The U.S. dust storm of February 1977, *in* Péwé, T.L., ed., Desert Dust: Origin, Characteristics, and Effect on Man: Geological Society of America Special Paper 186, p. 123–147.

McCauley, J.F., Breed, C.S., Helm. P.J., Billingsley, G.H., MacKinnon, D.J., Grolier, M.J., and McCauley, C.K., 1984, Remote monitoring of processes that shape desert surfaces: The Desert Winds Project: U.S. Geological Survey Bulletin 1634, 19 p.

Musick, H.B., and Gillette, D.A., 1990, Field evaluation of relationships between a vegetation structural parameter and sheltering against wind erosion: Land Degradation and Rehabilitation, v. 2, p. 87–94.

Nickling, W.G., 1988, The initiation of particle movement by wind: Sedimentology, v. 35, p. 499–511.

Skidmore, E.L., 1986, Wind erosion climatic erosivity: Climatic Change, v. 9, p. 195–208.

Stockton, P.H., and Gillette, D.A., 1990, Field measurement of the sheltering effect of vegetation on erodible land surfaces: Land Degradation and Rehabilitation, v. 2, p.77–85.

Thornthwaite, D.W., 1931, Climates of North America according to a new classification: Geographical Review, v. 25, p. 633–655.

Zingg, A.W., 1953, Wind tunnel studies of the movement of sedimentary material, *in* McNown, J.S., and Boyer, M.C., eds., Proceedings, Fifth Hydraulic Conference, Iowa Institute of Hydraulics: John Wiley and Sons, p. 111–135.

Zobeck, T.M., 1991, Abrasion of crusted soils: Influence of abrader flux and soil properties: Soil Science Society of America Journal, v. 55, no. 4, p. 1091–1097.

Wind Erosion Susceptibility Near Desert Wells, Arizona

By Stephen A. Wolfe *and* Paula J. Helm

DESERT WINDS: MONITORING WIND-RELATED SURFACE PROCESSES IN
ARIZONA, NEW MEXICO, AND CALIFORNIA

Carol S. Breed and Marith C. Reheis, *Editors*

U.S. GEOLOGICAL SURVEY PROFESSIONAL PAPER 1598–C

CONTENTS

FIGURES

TABLES

Wind Erosion Susceptibility Near Desert Wells, Arizona

By Stephen A. Wolfe[1] *and* Paula J. Helm[2]

ABSTRACT

The USGS Desert Winds Project established a Geomet station near Desert Wells, Arizona, in the arid northern part of the Sonoran Desert. Geometeorological data measured at this site have produced an 11-year record (1982–1992) upon which long-term means have been established. The area is hot and dry with a mean air temperature of 21°C and a mean annual precipitation of 128 mm. Most of the precipitation comes in monthly amounts of less than 13 mm, but downpours occur that can produce surface sheet flow or flash flooding in gullies and washes. Although the area has a relatively low wind-energy environment as compared to other world deserts, it is raked by severe dust storms (haboobs) that disrupt soil surfaces and deflate great quantities of material, causing erosion and property damage. Wind direction is variable with strong northwest/southeast prevailing winds and frequent winds of lesser influence from the southwest.

A 3-month experiment around the Desert Wells Geomet station using data from portable instruments, including a wind tunnel, quantified wind erosion susceptibility on various soil surfaces of the region. Study sites on three types of soil surfaces were investigated: (1) natural sandy loam soils that are loosely to poorly crusted and generally easily erodible (3 sites), (2) natural silty clay loam soils on which established crusts reduce the availability of surface-erodible material needed for saltation (2 sites), and (3) a silty loam soil on abandoned farmland that no longer bears the characteristics of a natural surface (1 site). Of the three sandy loam sites, only the dune site proved highly susceptible to wind erosion, having both a low threshold of erosion and a significant amount of loose erodible material. The other two sandy sites are partly protected, one by a gravel lag and the other by a mixed vegetation canopy with moderately high lateral cover, such that the wind erosion thresholds at both sites increase to nonerodible levels. The two sites with silty clay loam soils differ in wind erosion susceptibility. One site with vegetation and a hard algal crust is considered nonerodible because of its high wind erosion threshold and lack of loose material; but the other, a playa without vegetation, has a low wind erosion threshold but little loose available surface material. However, the playa becomes highly susceptible to wind erosion if the surface is disturbed. The silty loam of the abandoned farmland has the lowest wind erosion threshold but also has insufficient loose erodible material to be susceptible to deflation except when the surface is disturbed. If disturbed, this site would be the most susceptible to wind erosion.

INTRODUCTION

This paper documents a field study of wind erosion conducted between March and July of 1992 in collaboration with the Desert Winds Project at the Desert Wells Geomet site (Helm and Breed, chap. B, this volume; Tigges and others, chap. H, this volume), approximately 160 km west of Phoenix near Vicksburg, Ariz. (fig. 1). The study area, like much of western Arizona, consists of abandoned farmland, rangeland, and natural desert surfaces that are sparsely vegetated and have undergone varying degrees of disturbance; many such areas are known sources for dust emissions (Hyers and Marcus, 1981). As stated by Gillette (1986b), "the driving force for dust production is the motion of sand-sized particles." The purpose of this study is to assess wind erosion susceptibility in the Desert Wells region and to document near-surface atmospheric conditions under which wind erosion thresholds are exceeded. Field data to support this study were obtained from a portable, detailed instrument array and from the USGS Desert Wells Geomet station.

In this experiment, the approach to assessing susceptibility to wind erosion was to determine wind erosion thresholds of various types of surfaces in the Desert Wells area and to measure the amount of loose particles available for transport when that threshold is reached. This loose erodible sediment becomes an important factor in the production of dust storms during large wind erosion events (haboobs and

[1]Geological Survey of Canada, 601 Booth St., Ottawa, Ontario, K1A 0E8, Canada.
[2]U.S. Geological Survey, Building 3, 2255 North Gemini Dr., Flagstaff, AZ 86001.
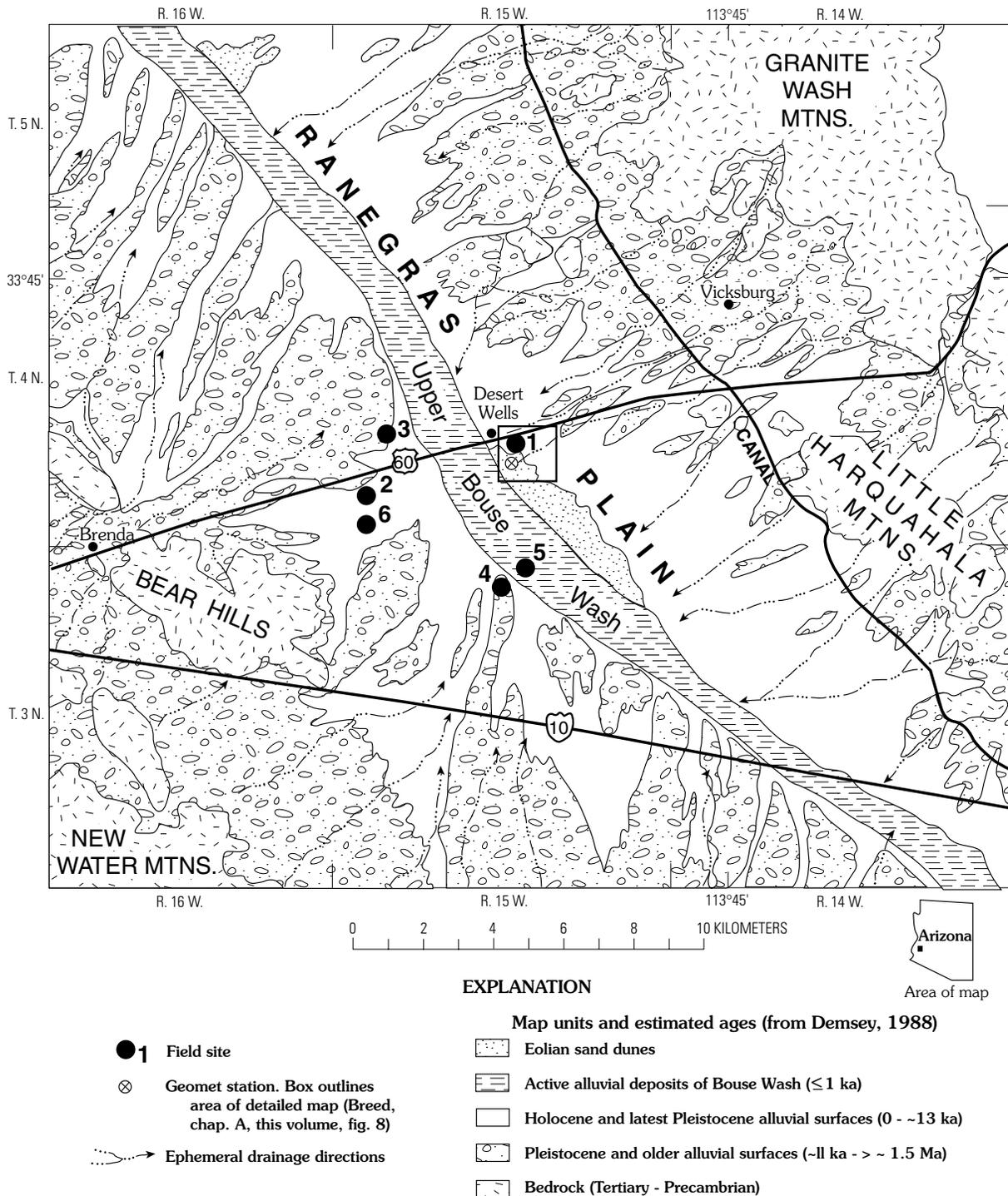
Figure 1. Index map of Desert Wells area showing field sites.

thunderstorms). Baseline wind erosion thresholds are defined by the shear stress needed to move loose, dry particles (Bagnold, 1941). Wind erosion thresholds are modified by vegetation, which affects the wind field at and near the surface. The availability of loose erodible sediment is further decreased by surface crusting; whereas surface disturbances such as grazing, farming, and offroad vehicle activity increase the amount of loose sediment available.

DESERT WELLS FIELD AREA

REGIONAL DESCRIPTION

The Desert Wells area (fig. 1 and fig. 6 of Breed, chap. A, this volume) occupies part of a broad alluvial valley, the Ranegras Plain, in the Sonoran Desert section of the Basin and Range physiographic province in western Arizona.

Desert Wells is named (informally) for an abandoned settlement that lies along Arizona State Route 60 about halfway between Salome and Quartzite. The Ranegras Plain is drained by Bouse Wash, an ephemeral tributary to the Colorado River (at Parker) that occupies a normally dry axial channel filled with clay, silt, and sand. Near Desert Wells, the Ranegras Plain is bounded by the Little Harquahala Mountains and Granite Wash Mountains to the east and by the Bear Hills and New Water Mountains to the west. Extensive pediments, mantled with broad alluvial fans that formed during the middle or late Pleistocene (Demsey, 1988), extend several kilometers from these ranges into the basin. The distal ends of the fans and the central part of the basin are surfaced by late Pleistocene to Holocene sediments, which include grussy sand, silt, and clay, with local gravels reworked from the debris mantles on the dissected piedmonts (Demsey, 1988). These latest Quaternary sediments fill the washes, cover the alluvial plains and playas, and form the sand dunes and sand sheets near the Geomet site (figs. 1, 2). Soils in these latest Quaternary sediments are only minimally developed. Soils in the region in general belong to the Torriorthent, Calciorthid, or Camborthid groups; the best developed profiles in the higher elevation areas contain cambic horizons over stage-I to -II calcic horizons (Demsey, 1988).

GEOMET SITE

A geometeorological (Geomet) station of basic type (Tigges and others, chap. H, this volume) was established by the USGS Desert Winds Project (McCauley and others, 1984) in January 1981 at a site on rangeland near Desert Wells (fig. 1). The station is at lat 33°42′08″N. and long 113°48′40″W., at an altitude of 344 m, on an alluvial plain surfaced by sediment of late Holocene age (Demsey, 1988). The surface of this broad intermontane basin slopes gently westward toward Bouse Wash and is slightly dissected by ephemeral gullies. Repeat photography from 1981 to the present documents occasional runoff at the site. Numerous small, barren playas dot the plain around the station. The Ranegras Plain marks the northeast margin of the Colorado River subdivision of the Sonoran Desert; hills that rise to elevations of 500 m or more to the east mark the southwest margin of the less arid Arizona Upland subdivision (Van Devender, 1990). On the Ranegras Plain, vegetation is sparse and consists mostly of creosotebush, bursage, mesquite, and occasional bunch grasses that are concentrated in areas of eolian sand drifts and dunes.

A small dune field and irregular eolian sand sheet deposits overlie the alluvial surface around the Geomet station (fig. 2; figs. 7, 8 of Breed, chap. A, this volume). The dunes are small barchanoid-type (transverse) ridges or mounds 0.3 to 1 m high. They lack slipfaces and are highly bioturbated by rodents. Both the dunes and sand sheets have some vegetation cover, unlike the surrounding hardpan and

Figure 2.   Dune site 1 near Geomet has bursage and creosotebush on loose sandy loam soil.

playa surfaces. The sand is mostly medium size, poorly sorted, and angular to subangular in shape. Though mostly quartz, it contains about 15 percent dark lithic fragments (including garnet schist), as well as abundant feldspar grains (G. Billingsley, oral commun., 1981). These characteristics indicate that the eolian sand is derived from sediment washed into the basin from sources in the nearby mountains. Although soil development in the eolian sand is minimal, soil type can be considered a sandy loam.

GENERAL CLIMATIC CONDITIONS

Geometeorological data have been recorded at the Desert Wells site intermittently in 1981 and continuously from January 1982 (Tigges and others, chap. H, this volume). Data from 1981 to 1986 are available on CD-ROM (Helm and others, 1998) and on the Internet at http://geochange.er.usgs.gov. An array of sensors is deployed on the Geomet station measuring meteorological parameters at 6-minute intervals. Wind speed, peak gust, and wind direction sensors are mounted on the mast at 6.1 m above the ground surface. Air-temperature, humidity, and precipitation sensors are mounted at a 2-m height, and a barometric-pressure sensor rests in the enclosure containing the data collection platform (DCP) at a height of 1.5 m. Soil temperature has been measured over the years at depths of 50 mm to 150 mm.

Threshold wind speed (u_t), the horizontal wind speed (measured at a 6.1-m height) that initiates sand movement on a bare, dry surface of mixed grain size (Bagnold, 1941; Helm and Breed, chap. B, this volume), is a sediment-transport parameter calculated from Bagnold equations and defines the standard wind speed used in Geomet site comparisons. Calculations for threshold wind speed depend on a single variable, mode of the surface grain sizes. The threshold shear velocity (u_{*t}) represents the minimum drag on the predominant surface grain size (mode) at which air can begin to

move those grains by direct fluid pressure. The shear velocity, in turn, provides the scaling factor needed to translate the minimum drag on the surface to the associated threshold wind speed value at the 6.1-m height of the anemometer at the Geomet sites.

Because the Geomet site is in an ephemeral wash on a hardpan surface and is adjacent to dunes and accumulated alluvium as well as desert pavement surfaces, the evaluation of a single modal grain size on which to base a calculation of site threshold wind speed is difficult. In 1981, moving sediment was trapped at the Geomet site in two sets of vertical PVC pipes with screened sections open to the wind. Two traps had open sections that extended from 0.06 m above ground level to a height of 0.30 m, and the other two had open sections between heights of 0.30 m to 0.60 m above the surface. Samples collected in these traps were analyzed for grain size distribution. By using a mean of the modal grain sizes captured in the lower level trap (0.06 to 0.30 m in height), a surface grain size can be established that represents the material moved by wind near the ground. This modal grain size is 0.30 mm, medium sand. The threshold wind speed calculated using this grain size is 8.4 m/s (at 6.1 m).

The drift potential, a measure of the potential capacity for sand movement based on the percentage of time that winds blow above threshold wind speed, is 43 VU (vector units). This value indicates that Desert Wells has a low wind-energy environment relative to that of major world deserts (Fryberger and Dean, 1979). However, samples of airborne sediment collected from the two upper level traps on August 6, 1981, included small pebbles (as large as 4.69 mm) and granules. The coarse grain sizes obtained from the samplers at these heights indicate airborne movement of particles in a saltation curtain well above the ground. Two days after these samples were collected, peak gust winds of nearly 144 km/h were recorded during passage of a storm through the Desert Wells area (McCauley and others, 1984). Severe wind abrasion destroyed the screens on the traps by late August, and the PVC pipe samplers were abandoned. The sampler results, though limited, suggest that high-speed winds in the area blow with great competence. Because sand-moving winds are infrequent, however, their annual capacity for sediment movement (drift potential) is relatively low.

The site sandrose, a circular histogram showing the direction and magnitude of the potential sand-moving winds (wind speeds greater than site threshold wind speed) using actual Geomet data (fig. 3), shows the variability of the wind field at Desert Wells. The resultant (arrow) shows the influence of strong northwesterly and southeasterly prevailing winds that blow through the area plus the lesser influence of winds from the southwest, which together produce a potential net sand-movement direction toward the east. The mean annual precipitation for the site, based on Geomet data for 1982–1992, is 128 mm. The precipitation frequency (fig. 4) verifies the arid nature of the site: 73 percent of the monthly rainfall occurs in amounts less than 13 mm, the minimum

DESERT WELLS
1982-1992
DP = 43
RDP = 6
RDP/DP = 0.14

N

scaling factor = 1
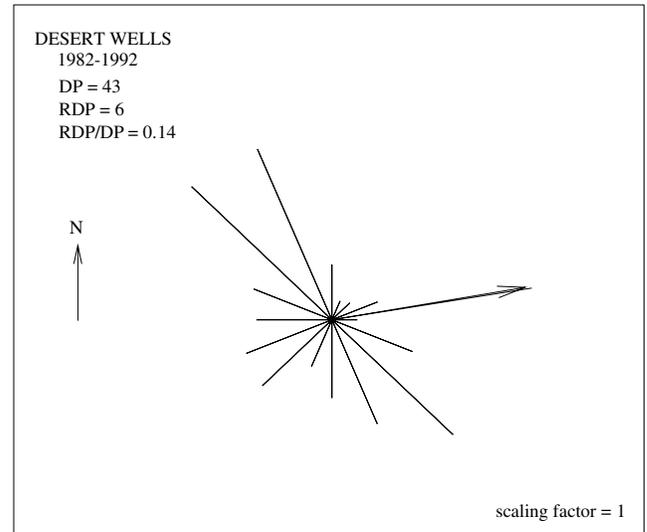
Figure 3. Desert Wells site sandrose. The sandrose is a circular histogram showing mean magnitude and upwind direction of the wind field for the period of record (Helm and Breed, chap. B, this volume). DP, drift potential (sand-moving capability of the wind from all directions); RDP, resultant drift potential (net sand-moving capability toward the resultant direction); RDP/DP, an index of directional variability of the wind field (1.00 = no variability). The scaling factor is a linear reduction value used to scale the sandrose to the plotting area.

Precipitation Frequency
Desert Wells, Arizona
1982-1992*

*1991 data not available
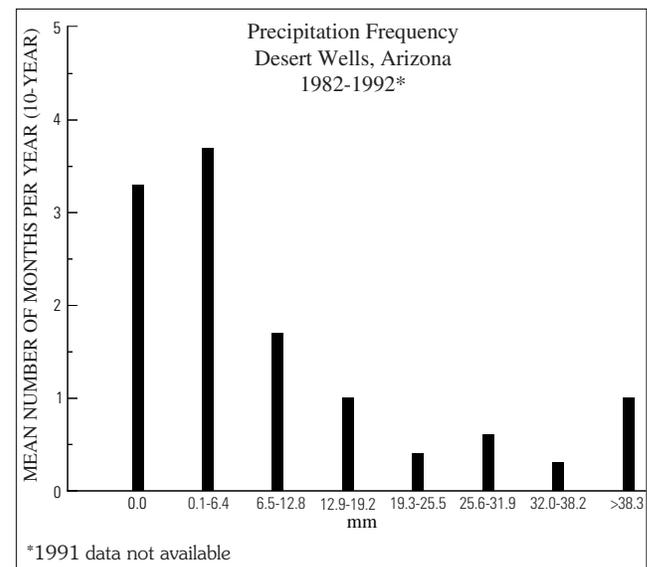
Figure 4. Monthly precipitation frequency distribution showing mean number of months per year with total rainfall in each precipitation range for the period of record at Desert Wells.

rainfall amount needed to produce a soil water content sufficient to reduce wind erosion (Chepil and others, 1962). In only one month during a year, on average, rain falls in

amounts greater than 38 mm, potentially wetting the ground sufficiently to produce runoff in the gullies and washes. The mean annual air temperature is 21°C.

To summarize, Desert Wells is an area of extremes: long dry periods punctuated by downpours and flash flooding; extended periods of time with low wind energy interrupted by convective storms with tornadic wind shears that produce huge, rolling dust clouds; varied ground surfaces that differ in texture, character, and vulnerability to wind erosion within a few meters of each other; and vegetation growth patterns that range from none to mixed vegetation types that partially protect the surfaces from wind erosion.

THE 1992 EXPERIMENT

PREVIOUS WORK

A wind erosion threshold is marked by the airborne transport of soil particles across a surface, primarily by saltation and suspension. Erosion thresholds have been measured effectively in field localities by placing open-floored wind tunnels over bare ground surfaces (Nickling and Gillies, 1989; Gillette, 1978). By using a series of Pitot tubes or other wind speed sensors, wind speed profiles near the ground surface may be determined. In general, it is possible to fit the mean wind speed (u) versus height (z) to the function for aerodynamically rough flow (Priestley, 1959):

$$u = \left(\frac{u_*}{k}\right)\ln\left(\frac{z}{z_0}\right) \qquad (1)$$

where

u_* is the shear velocity,
z_0 is the aerodynamic roughness length of the surface, and
k is von Karman's constant (0.4).

The threshold shear velocity of a bare surface (u_{*tS}) is determined from wind speed profiles at which continuous movement of sediment across a surface is first observed in the portable wind tunnel, marking the wind erosion threshold for that bare surface with resident surface grain size distribution. Erodibility (susceptibility) is a function of the wind erosion threshold.

Erodibility is also a function of the amount and distribution of loose erodible material on the soil surface. The susceptibility of a surface to wind erosion is highly sensitive to the grain size distribution of the loose soil, particularly to the percentage of dry soil particles with grain sizes less than 0.84 mm in diameter (Woodruff and Siddoway, 1965). In general, this value represents the fraction of surface soil material that is equivalent to coarse sand (0.25Φ) or finer and, therefore, transportable by wind in saltation and suspension. Larger soil particles and aggregates are considered nonerodible by most wind events. Recently, vacuum systems have been used to collect loose erodible material, and the weight of surface material with grain sizes less than 0.84 mm is evaluated on a mass per area basis as an indicator of the soil erodibility (Zobeck, 1989).

Finally, vegetation reduces the shear stress at ground level by extracting momentum from the atmosphere above the surface, thereby increasing the shear velocity needed to set surface material into motion (wind erosion threshold). The protection provided by vegetation may be considered a function of the vegetation height, width, spacing, porosity, and distribution. To date, the most useful parameter for characterizing vegetation cover in this context is the lateral cover (L_c), defined as the ratio of total frontal-silhouette area of roughness elements to the total surface area (Marshall, 1971; Musick and Gillette, 1990; Musick, chap. D, this volume):

$$L_c = DS \qquad (2)$$

where

D is the number of elements per unit area, and
S is the mean frontal-silhouette area per element.

The mean frontal-silhouette area is defined as:

$$S = \sum (h_i d_i)/N \qquad (3)$$

where

h_i is the element height,
d_i is the element diameter, and
N is the number of elements measured.

Following Musick and Gillette (1990) and Musick (chap. D, this volume), a solid cylinder shape was used as the model of element shape.

A vertical array of anemometers mounted above the vegetation canopy allows measurements of shear velocity (u_* and aerodynamic roughness length of the surface (z_0). In this way, the sheltering effects of vegetation can be assessed by the magnitude of the aerodynamic roughness length value and threshold shear velocity with vegetation (u_{*tR}). The ratio (R_t) of the threshold shear velocity of an erodible surface (u_{*tS}) to that of the same surface with nonerodible elements (vegetation) present (u_{*tR}) has been modeled by Raupach and others (1993) using the relation:

$$R_t = (1 - m\sigma L_c)^{-0.5}(1 + m\beta L_c)^{-0.5} \qquad (4)$$

where

m is a parameter accounting for the differences between average surface shear stress and maximum surface shear stress at any one point,

σ is the basal-to-frontal area ratio of the roughness elements, and

β is the ratio of the drag coefficient of an isolated roughness element on the surface to the drag coefficient of the surface itself.

Raupach and others (1993) suggest that, for potentially erodible shrub-vegetated surfaces, the coefficients β, σ, and m are approximately 90, 1, and 0.5, respectively.

FIELD METHODS

For this study, six field site locations (table 1) within a 5 km radius of the Geomet station (dune site 1; fig. 2) were selected in order to include the whole range of vegetation and soil cover in the Desert Wells area; they consist of rangeland (sites 3 and 5; figs. 5, 6), abandoned farmland (site 2; fig. 7), desert pavement (site 4; fig. 8), and a playa surface (site 6; fig. 9). A sample plot 40 m by 60 m was surveyed at each site, inside which wind profiles, surface sediment, and vegetation characteristics were determined. Because of the very sparse vegetation at the abandoned farmland site, a larger area of 300 m by 300 m was surveyed. The degree of sheltering afforded by vegetation at each site was determined through measurements of vegetation type, height, width, and distribution. All vegetation having heights greater than 0.15 m was surveyed within the 40 m by 60 m plots. In cases where the surface cover represented a mix of vegetation, the total lateral cover (L_c) was determined by summing the frontal-silhouette area per element of each vegetation type (Musick and Gillette, 1990; Musick, chap. D, this volume).

Near-surface atmospheric data, including wind speed, wind direction, and air temperature were recorded at 5-second intervals over 15-minute periods at the six sites. Seven anemometers, two wind-direction sensors, and five temperature sensors were attached to a 10-m tower and measured time-averaged velocity profiles at each site. Wind-profile data collected included the average wind speed at 1.5, 2.5, 3.5, 4.5, 5.5, 7.5, and 10.0 m above the surface, as well as maximum and minimum wind speeds and wind direction at 1.5 and 10.0 m. In all, more than 6,000 profiles were collected, comprising approximately 600 to 1,000 profiles at each site. Wind profile parameters, including shear velocity (u_*) and aerodynamic roughness length (z_0), were determined using only those wind profiles in which the minimum wind speed at a height of 1.5 m exceeded 1.5 m/s. This restriction eliminated periods in which winds may have stopped during the 15-minute period, and thereby removed unwanted calm periods and isolated gust events. The remaining profiles were fitted to equation 1, and profiles that met the condition of having a coefficient of determination (r squared) greater than 0.90 were used for computation of shear stress and aerodynamic roughness length. A total of 1,210 profiles met the preceding conditions (approximately 20 percent of the profiles collected), and the average r-squared fit to equation 1 was 0.97. Because the lower portion of the profiles was logarithmic for high wind-speed episodes, the remaining profiles were not corrected for atmospheric stability.

Baseline wind erosion thresholds (u_{*tS}) were determined using a portable wind tunnel similar to that described by Nickling and Gillies (1989). The wind tunnel is a noncirculating, sucking type that measures 1.0 m wide, 0.75 m high, and 12.0 m long. The working section is situated 10.0 m back from the intake to allow for development of a boundary layer of sufficient thickness. Six Pitot tubes ranging in height from 10 to 160 mm above the ground surface were used to determine near-surface wind-speed profiles. Threshold shear velocities were determined for the condition when surface soil sediment was first mobilized.

Soil surfaces were analyzed for soil texture, degree of surface crusting, aggregates, and amount of loose erodible material. A qualitative ranking procedure for evaluating

Table 1. Soil texture description.

[Abnd., Aabandoned; pvmnt, pavement]

Site number	Setting	Soil texture	Particle classification (percent)					Comments
			Gravel	Sand	Silt	Clay	<0.84 mm	
1	Dune (Geomet)	Sandy loam	4.7	59.0	26.0	10.3	84.2	Loose to very soft crust, 5.0 mm thick.
2	Abnd. farmland	Silty loam	0.9	12.8	62.9	23.4	97.5	Moderately hard crust, 10 mm thick.
3	Rangeland	Silty clay loam	0.0	7.3	64.7	28.0	99.7	Hard, curled algal/clay crust, 5.0 mm thick.
4	Desert pavement	Sandy loam	22.5	55.1	10.0	12.4	68.2	Loose desert pvmnt.
5	Rangeland	Sandy loam	5.3	66.5	1.3	16.9	87.2	Loose to soft crust, 5.0 mm thick.
6	Playa	Silty clay loam	0.0	8.2	52.9	38.9	100.0	Hard, curled algal/clay crust, 5.0 mm thick.

Figure 5. Rangeland site 3 has creosotebush on algal-crusted silty clay loam soil.

Figure 8. Desert pavement site 4 has creosotebush on sandy loam soil.

Figure 6. Rangeland site 5 has bursage and creosotebush on soft sandy loam soil.

Figure 9. Playa site 6 has algal-crusted silty clay loam soil and no vegetation.

Figure 7. Abandoned farmland site 2 has mesquite on crusted silty loam soil.

crustal hardness (pushing a finger into the surface crust) was used to evaluate the force of fracturing surface crusts. Crustal thickness was determined by sectioning the soil and measuring the crusted surface that separated from the underlying loose soil. Surface sediment samples were collected at each site from five plots, each 0.25 m by 0.25 m. Particle size analysis using sieve and pipette methods was performed on each sample to determine texture of the surficial sediment. Soil surfaces were inspected for the degree of surface crusting or development of protective gravel lags. The amount of loose erodible material was determined by vacuuming 0.10 m^2 plots of the surface soil; the mass of soil material collected in this way represents the amount of loose soil material. The amount of loose material susceptible to wind erosion was determined on the basis of percentage of dry soil with grain sizes less than 0.84 mm in diameter (Zobeck, 1989), obtained by hand-sieving soil samples through a 0.84-mm mesh.

EXPERIMENT SITE CHARACTERISTICS

SURFACE SOIL TEXTURE

Weak soils in the Desert Wells area have developed on late Pleistocene to Holocene fan or stream alluvium (Demsey, 1988) and are generally medium to moderately coarse textured loams (table 1). They vary with respect to the sedimentary characteristics of their alluvial or eolian parent material and their thickness over bedrock.

Much of the surface at the Geomet station (dune site 1, fig. 1) has been deflated to a hardpan overlain by a thin, patchy lag of very coarse, loose sand and granules; soil accumulations are limited to sandy loams in the dunes and drifts of eolian sand, which overlie the hardpan (fig. 2). Surface sediment both there and at rangeland site 5 (fig. 6) is sandy loam with loose surface particles and soft crusts. In contrast, the silty surfaces (sites 2, 3, and 6; figs. 7, 5, 9) generally have moderate to hard crusts. The surface crust on rangeland site 3 and on the playa (site 6) is hard, curled, polygonally shaped clay that is generally 5.0 mm thick. Crusting on these sites has been aided by algal growth induced by periodic surface flooding. Field observations indicate that fibrous strands of surface algae act to bind the crust, making it less susceptible to breakage and wind erosion.

The surface crust is weaker on the abandoned farmland (site 2), and there is no curling of the crust. Previous cultivation on the farmland had disturbed the soil, destroying any possible preexisting surface crust. Furthermore, although the site has not been cultivated in the last 10 years, no indication of regrowth of algae exists. The installation of ditches during cultivation has probably routed drainage around the abandoned farmland sufficiently to prevent annual surface flooding on the site. Consequently, though algal crusts occur on perennially flooded soils near the abandoned farmland, they are absent on the site itself. The surface sediment on desert pavement (site 4) is a coarse-textured sandy loam on alluvium in a dry wash; the surface material is not crusted, as much of the fine-textured sediment is protected by a gravel lag.

LOOSE ERODIBLE MATERIAL

Soil erodibility is largely a function of the amount and distribution of loose erodible surface material, which is readily transportable by wind and which typically acts as an abrader on crusted surfaces to initiate transport of additional particles into saltation and suspension (Gillette, 1986b). For each site, the total of loose surface material collected from vacuum samples, expressed in metric tons per hectare (t/ha), and the amount of loose erodible material, which is based on the proportion of loose surface material with grain size diameters less than 0.84 mm, are shown in table 2. A relatively

Table 2. Loose erodible material.

[t/ha, metric tons per hectare; Abnd., Abandoned; frmlnd, farmland; pvmnt., pavement]

Site	Loose surface material (t/ha)	Grain size <0.84 mm (%)	Loose erodible material (t/ha)
1 Dune	5.064	64.6	3.853
2 Abnd. frmlnd.	0.221	97.0	0.214
3 Rangeland	0.417	14.7	0.061
4 Desert pvmnt.	13.225	38.8	5.130
5 Rangeland	1.197	46.9	0.561
6 Playa	0.108	15.2	0.016

large amount of erodible material is available on the sandy loam surface at site 1, where the surface sediment (dune sand) is loose to softly crusted. In contrast, the crusted soils (sites 2, 3, and 6) have comparatively little loose erodible material, although the abandoned farmland contains considerably more than the other crusted sites. Site 4 (desert pavement) has the most loose erodible material, although much of this is protected by a gravel lag. A moderate amount of material is also available on rangeland site 5, which is similar in texture to the dune sand at site 1, but with a stronger crust. Thus, though the soils in the Desert Wells region typically contain a high proportion of sediment with grain sizes less than 0.84 mm in diameter, most of the fine-grained material is aggregated or crusted, thereby reducing the amount of loose erodible material. Lag gravels also shelter loose erodible material from being entrained.

A comparison of the percent of particles with diameters less than 0.84 mm (tables 1, 2) gives an indication of the amount of loose available material that would be present if the soil surfaces were disturbed. Disturbance of the soil surface generally breaks down soil aggregates and crust, thereby producing more loose erodible material. For example, most of the soil material at rangeland site 3 and playa site 6 is composed of potentially erodible material (particles less than 0.84 mm; table 1), but surface crusting allows only a small amount of this material to be readily available to erosion (table 2). Disturbance of surface crusts at these sites would result in most, if not all, of the surface material becoming erodible. Disturbance of the other sites would increase the soil erodibility to a lesser extent because of the greater percentage of nonerodible-sized particles (grain sizes > 0.84 mm). In all cases, however, the amount of material that is erodible would be increased by surface disturbance. Furthermore, surface disturbance at desert pavement site 4 would produce the least amount of additional erodible material, but the disturbance of the protective gravel lag at this site would likely result in considerably more deflation than at present.

VEGETATION COVER

Vegetation in the region is sparse with densities typically less than 30 percent (table 3). Within the study area, the

Table 3. Summary of vegetation description and aerodynamic roughness length.

[See text for definitions of L_c and z_0]

Site	Type	Vegetation Description				Aerodynamic roughness length, z_0, with vegetation (mm)
		Mean height (m)	Mean width (m)	Percent cover	Lateral cover (L_c)	
1 Dune	Bursage/ creosotebush	0.44	0.75	13.50	0.094	72
2 Abandoned farmland	Mesquite	1.20	1.32	0.04	0.000039*	4
3 Rangeland	Creosotebush	0.83	1.10	8.54	0.072	54
4 Desert pavement	Creosotebush	1.06	1.22	10.30	0.078	68
5 Rangeland	Creosotebush/ bursage	0.78	1.06	26.30	0.23	83
6 Playa	None	--	--	--	--	6

*Value does not include percent cover by grass.

vegetation is predominately creosotebush (*Larrea tridentata*), white bursage (*Ambrosia dumosa*), and velvet mesquite (*Prosopis juliflora var. velutina*). Several perennial bunch grasses and other herbaceous plants may also cover a significant proportion of the ground surface, especially where shrub vegetation is absent. Sites selected for study generally had an exposed soil surface dominated by shrub vegetation.

Mean height and width of vegetation cover at each site (table 3) were determined by averaging measurements taken on all plants more than 0.15 m tall. Two measurements of width, perpendicular to each other, were taken on each plant. The percent cover represents the ground area covered by vegetation as viewed from above and was determined from the sum of the plan view area of each plant, using the mean width of each plant as the plant diameter. The lateral cover (L_c) was calculated according to equation 2, using the mean frontal-silhouette area per element as calculated from equation 3. The total number of vegetation elements (> 0.15 m high) per plot area ranged from as few as 22 at the abandoned farmland site 2 to 595 at rangeland site 5.

Velvet mesquite shrubs were the largest elements surveyed in the area, averaging about 1.20 m tall (table 3); these plants tended to stand alone on the abandoned farmland site 2. Creosotebush and white bursage were mixed at the dune site 1 and rangeland site 5, with creosotebush elements dominating at site 5 and bursage dominating at site 1. Creosotebush averaged 0.83 m high at rangeland site 3 and 1.06 m at desert pavement site 4; white bursage generally averaged 0.32 m high. With the exception of the bare playa surface, the abandoned farmland was the most sparsely vegetated; mesquite elements there covered 0.04 percent of the 90,000 m^2 area surveyed. The percent vegetation cover at the

undisturbed sites was much greater than at the abandoned farmland site 2, ranging from 8.5 percent at rangeland site 3 to 26.3 percent at rangeland site 5. The sites with a mix of creosotebush and bursage (sites 1 and 5) also tended to have greater densities of vegetation cover because bursage partially fills the spaces between the creosotebush.

The lateral cover (L_c) at rangeland site 5 is similar to that of the Jornada, New Mexico, and Yuma, Arizona, Geomet sites (L_c equal to 0.28 and 0.17, respectively) examined in 1989 by Musick and Gillette (1990) and Musick (chap. D, this volume); lateral cover at dune site 1 is lower than these three sites. All four of these desert areas are characterized by a mix of vegetation types in which intervening spaces between larger elements are partly filled by smaller elements. Low lateral cover at abandoned farmland site 2, rangeland site 3, and desert pavement site 4 show expected densities for sites with single vegetation types. The lowest lateral cover value, on abandoned farmland site 2, verifies the sparse nature of the vegetation, although this locality contains the largest vegetation elements.

Aerodynamic roughness length (z_0) generally increases with lateral cover, indicating that a more abundant vegetation canopy increases momentum extraction from the atmosphere. The vegetation cover provides a momentum sink that increases aerodynamic drag and reduces surface shear stress. In this respect, sites with vegetation that effectively reduce surface shear stress are those with a mix of vegetation cover including creosotebush and bursage, such as dune site 1 and rangeland site 5. The abandoned farmland site 2, with sparse (creosotebush) vegetation, and the playa site 6, with no vegetation, have aerodynamic roughness length values less than 10 mm and consequently higher shear stress at the surface.

RESULTS

WIND EROSION THRESHOLDS FOR BARE SURFACES

Wind erosion thresholds of bare soil surfaces (u_{*tS}) at each site were determined using the open-floored portable wind tunnel. Tunnel sections were assembled without disturbing the test surface. At desert pavement site 4, the wind tunnel and trailer could not be transported onto the site because of soft ground. Problems with soft sediments were also encountered at dune site 1 and rangeland site 5. In these cases, the wind tunnel was set up on similar surfaces as close to the surveyed area as possible.

Threshold shear velocity of bare soil (u_{*tS}) was determined from the wind tunnel tests (table 4). Based on these thresholds, surfaces may be ranked by threshold values for wind erosion in the following manner: the abandoned farmland site 2, with a poorly developed silty loam crust, and dune site 1, with a loose sandy loam surface, have the lowest wind erosion thresholds (0.2 m/s); the algal-crusted, silty clay loam surfaces (sites 3 and 6) have intermediate thresholds of 0.4 to 0.5 m/s, as does the sandy loam surface with an undisturbed crust (site 5); the alluvial desert pavement site 4 has the highest wind erosion threshold, estimated as approximately 0.7 m/s.

WIND EROSION THRESHOLDS FOR VEGETATED SURFACES

By extracting wind momentum above the ground suface, vegetation cover increases the shear velocity required to initiate transport of soil particles at the surface. Threshold shear velocity ratios (R_t) were determined using equation 4 with suggested coefficients and lateral cover (L_c) values determined in table 3. As stated earlier, a cylindrical model was used in estimating L_c and was also used for approximating σ (basal-to-frontal area ratio) in equation 4. Using the cylindrical model, the range in σ values for creosotebush and mesquite shrubs is between 0.86 and 1.17 and is well approximated by 1.0. For mixed vegetation such as that encountered by Musick and Gillette (1990), Raupach and others (1993) show that R_t is well represented with values of 90, 1, and 0.5 for β, σ, and m, respectively, even though smaller elements such as bursage may be approximated as hemispheres with a σ value of 2. Threshold shear velocities for vegetated surfaces (u_{*tR}) were then determined in the following manner:

$$u_{*tR} = u_{*tS} / R_t \qquad (5)$$

Values of R_t and u_{*tR} are shown in table 4. Threshold shear velocities of vegetated surfaces (u_{*tR}) provide a basis for a new ranking of wind erosion thresholds. As a result of

Table 4. Threshold shear velocities for bare and vegetated surfaces.

[See text for definitions of u_{*tS}, R_t, and u_{*tR}]

Site	Threshold shear velocity (bare soil) u_{*tS} (m/s)	Threshold shear velocity ratio (R_t)	Threshold shear velocity (vegetation) u_{*tR} (m/s)
1 Dune	0.21	0.45	0.47
2 Abandoned farmland	0.20	0.99	0.20
3 Rangeland	0.52	0.49	1.06
4 Desert pavement	0.70*	0.48	1.46
5 Rangeland	0.50	0.32	1.56
6 Playa	0.44	1.00	0.44

*Estimate based on threshold velocities for gravel-covered surfaces by Gillette and others (1980).

the very sparse vegetation cover on the abandoned farmland, that site has the lowest wind erosion threshold with no significant change in the threshold due to vegetation. In contrast, the wind erosion threshold at dune site 1 increased by a factor of two as a result of vegetation and has a slightly higher threshold than the playa surface (site 6). All remaining surfaces (sites 3, 4, and 5) have high wind erosion thresholds, ranging from 1.0 to 1.5 m/s as a function of the vegetation cover.

DISCUSSION

WIND EROSION SUSCEPTIBILITY

Gillette (1986a) noted that surfaces with threshold shear velocities much greater than 1.0 m/s may be considered nonerodible, except possibly for the most powerful wind events. In all cases in the Desert Wells area, threshold shear velocities for bare soil surfaces (u_{*tS}) determined by portable wind tunnel measurements are well below this value, and therefore, wind erosion can potentially occur on any of them. Vegetation on a bare surface removes momentum from the wind, thus requiring larger threshold shear velocities to produce continuous sand movement on the surface below the vegetation canopy. Threshold shear velocities evaluated for vegetated surfaces (u_{*tR}) are greater than 1 m/s at three of the sites (3, 4, 5), thus transforming potentially erodible sites into nonerodible sites. Rangeland site 5, with the largest lateral cover consisting of mixed vegetation, needs a wind force of three times the bare-soil wind erosion threshold in order to initiate saltation on the surface. A threshold shear velocity of 1.56 m/s makes this site the least susceptible to wind erosion for the majority of wind events. A wind erosion threshold at rangeland site 3, with a creosotebush density of only 8.5 percent and low lateral cover of 0.072, increases from 0.5 m/s to 1.1 m/s, which shows that a relatively small amount of

vegetation cover can increase erosion thresholds by a factor of two or more. The dearth of loose erodible material caused by the algal/clay crusted surface further protects this natural site from wind erosion. Desert pavement site 4, with vegetation cover that doubles the threshold of erosion to 1.5 m/s and a gravel lag surface that prevents the large amount of loose erodible material from being entrained, ceases to be classified as susceptible.

Because of little or no vegetation cover on the abandoned farmland site 2 and playa site 6 surfaces, threshold shear velocities (u_{*tR}) are considerably below 1 m/s, and the two bare sites may be considered potentially susceptible to wind erosion. However, lack of loose erodible material on playa site 6 means that when the wind erosion threshold is reached, there is no loose material to move. The lack of loose erodible material on the abandoned farmland site 2, much of which is bound into the soft silty crust, also makes this site less susceptible to wind erosion. Large wind events at both sites could cause the breakup of protective crusts, thus releasing a significant amount of erodible material to the wind. Both sites are more susceptible to wind erosion following other surface disturbances that destroy soil aggregates and crusts, and thereby increase the amount of available loose material, most of which have diameters less than 0.84 mm.

The surface most susceptible to wind erosion is dune site 1, near the Geomet station, with a threshold shear velocity (u_{*tR}) of less than 0.5 m/s and a comparatively large amount of loose erodible material (dune sand) exposed at the surface. The mixed vegetation cover at this site (L_c=0.09) is sufficient to double the threshold of erosion; nevertheless, this doubling still produces a low wind erosion threshold. In addition, the availability of a relatively large amount of loose erodible material (3.9 t/ha) means that material is set into motion by most wind events. This surface is also likely to be resupplied with loose material from unconsolidated alluvium in Bouse Wash that is episodically blown into the area and added to the eolian deposits.

EVALUATION OF TWO WIND EVENTS AT DESERT WELLS

This section details atmospheric conditions under which soil erosion thresholds were exceeded. Two examples of high wind events produced by different storm systems, recorded by the Geomet station near dune site 1 and witnessed by the senior author, are described in detail. The first event was the passage of a squall line that mobilized the surface sand and thus produced an intense, haboob-type dust storm (Idso and others, 1972). The second event was a thunderstorm that, because of associated rainfall, did not result in significant eolian transport. However, strong wind shears associated with the thunderstorm resulted in considerable property damage in the area. Shear velocities were calculated from equation 1 using mean wind speed measurements (u) at the Geomet station and an aerodynamic roughness length of 72 mm (table 3) established earlier from the detailed anemometer array.

HABOOB (MAY 23, 1992)

The meteorological conditions for May 23, 1992 (fig. 10), when a haboob-type dust storm passed through the area from the southeast, show the local effects of a larger scale advancing squall line from the southeast. The passing of the storm was marked by an abrupt drop in air temperature of 7°C and simultaneous rise in relative humidity from 23 percent at 16:00 hours to 52 percent at 18:00 hours. The barometric pressure began to drop at 12:00 hours and to rise again at 18:15 hours, as the brunt of the storm hit the area.

As there was no precipitation associated with the passage of the May 1992 event, the soil surface remained dry. Figure 10 includes the calculated shear velocities at the Geomet station as well as the wind erosion threshold for the bare soil (u_{*tS}, determined from wind tunnel tests) and the threshold of the vegetated surface (u_{*tR}, calculated from equation 5). Vegetation cover near the Geomet site results in a doubling of threshold shear velocity from 0.21 m/s to 0.47 m/s (table 4). Consequently, the period in which winds were above the wind erosion threshold decreases from 73 percent of the time if the surface were bare to 19 percent with the vegetation cover.

The winds were generally from the west-northwest prior to the storm. Wind directions were variable between 16:00 and 18:00 hours and squalls that produced dust were seen moving across the site after 16:00 hours. These squalls were associated with unsettled weather, as evidenced by abrupt changes in air temperature and relative humidity at 18:00 hours. In general, the squalls mobilized sediment in open spaces where the vegetation cover was patchy. As shown in figure 11, the advancing haboob was marked by a dust cloud that extended several hundred feet into the air, forming a parabolic front in cross section. With the onset of the wind storm, the entire soil surface was mobilized. Visibility at eye level was reduced to less than 1 km at the haboob front but increased to more than 5 km thereafter. The winds shifted direction at 18:21 hours, blowing consistently from the east-southeast for more than an hour. During the event, mean wind speeds exceeded the site calculated threshold wind speed of 8.4 m/s, while peak gusts exceeded 19 m/s. Based on the shear velocities calculated from Geomet-recorded data during the main force of the storm, all but two sites (desert pavement site 4 and rangeland site 5) could have been active during this storm.

Figure 10. Atmospheric data for May 23, 1992, indicating haboob event.

Figure 11. Advance of dust cloud from haboob on May 23, 1992.

The storm was of short duration, as indicated by the slight increase in barometric pressure that accompanied the rainfall, but its intensity is obvious in the air temperature and humidity records. Air temperature reached a maximum of 37°C prior to the event but dropped rapidly to 23°C during the storm. The shear velocity at the Geomet station reached 1.5 m/s during the storm, and the peak gust reached 27 m/s. On the basis of the peak gust, the maximum shear velocity at the station likely exceeded 2.5 m/s.

The thunderstorm advanced over the Geomet station at approximately 12:30 hours on July 10 (fig. 13). The intense wind shear is indicated by the strongly concave profile of the storm cloud. During the storm, intense localized wind shears destroyed several structures within 3 km of the Geomet station. A mobile home (fig. 14) was dragged approximately 30 m from its initial position. Subsequently, the external structure of the home, together with all fixtures and furniture, was torn from the platform. Debris from the home was strewn across the ground for a distance of approximately 750 m. Accounts of the event suggest no associated funnel cloud. The location of greatest damage was confined to an area of about 1 km². Given these circumstances, the strong wind shear was most likely associated with down drafts from the convective cell. That such storms, with severe destructive wind shears but no funnel cloud, are repeated events at Desert Wells can be concluded from comparison of this storm with those reported on July 10, 1981, and on August 8, 1981, by former residents in the Desert Wells area and recorded by the Geomet station (McCauley and others, 1984, p. 14–18). Although these summer thunderstorms often are closely accompanied by precipitation, the threshold shear velocities were high enough to move material at all six sites before the rain fell.

THUNDERSTORM (JULY 10, 1992)

The meteorological conditions for July 10, 1992, when a thunderstorm passed through the Geomet area, are shown in figure 12. Unlike the event of May 23, this event was accompanied by 11.4 mm of rainfall in less than half an hour. The associated rainfall may have increased the threshold shear velocity to such a high value that the surface was never completely mobilized. As Belly (1964) and other researchers have shown, a relatively small amount of moisture on the soil surface can significantly increase the wind erosion threshold, although the condition tends to be temporary on sandy desert surfaces that dry out quickly (Helm and Breed, chap. B, this volume).

SUMMARY

The Desert Wells area is in an arid region with a relatively low wind-energy environment but a potentially
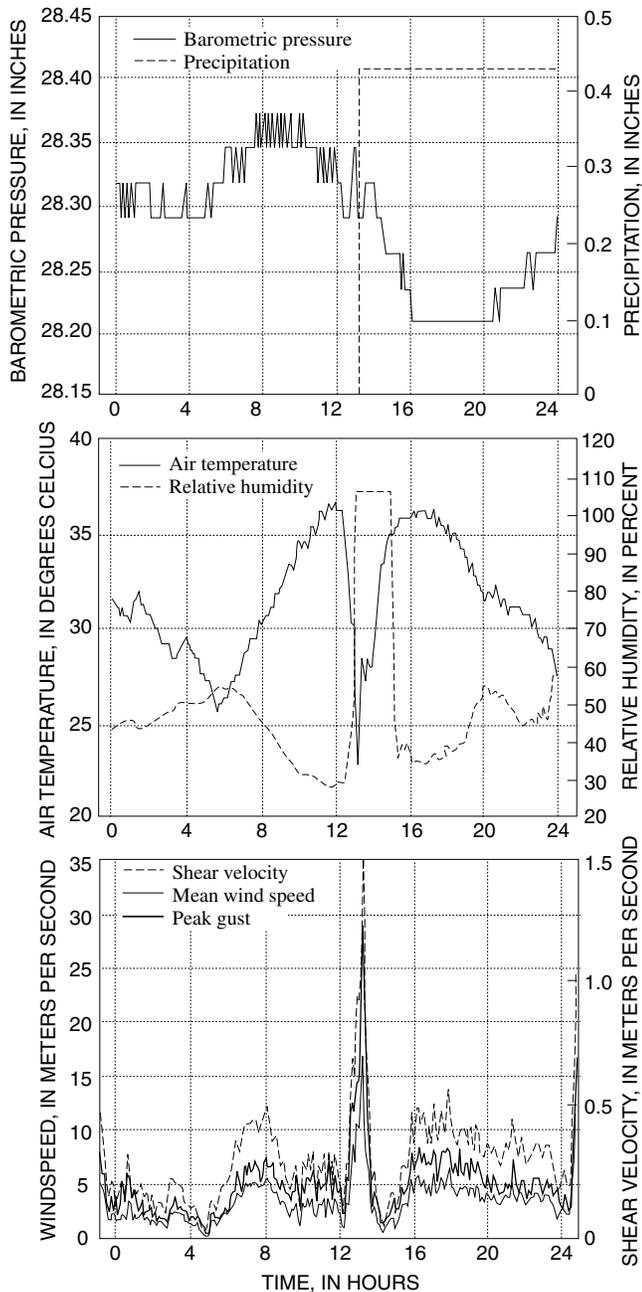
**Figure 12.** Atmospheric data for July 10, 1992, indicating thunderstorm.

Figure 13. Thunderstorm at 13:00 hours on July 10, 1992.

Figure 14. Destruction of mobile home.

high vulnerability to wind erosion. The area is known for its severe storms with mean shear velocities exceeding 1.5 m/s, velocities capable of mobilizing all the soil surfaces and producing large-scale dust storms. Wind erosion susceptibility is dependent upon bare-soil wind erosion thresholds, modifying effects of vegetation on thresholds, and the availability of erodible particles once threshold is exceeded. Soils in the region are weakly developed in alluvium and eolian sand, with most surficial material having grain sizes less than 0.84 mm. Soils with this texture are easily deflated by the wind, as shown by low

bare-soil wind erosion thresholds. Some vegetation, however, as demonstrated on a rangeland site, can increase wind erosion thresholds to levels such that surfaces are virtually nonerodible under most wind events. On the other hand, sparse vegetation on abandoned farmland may be inadequate to prevent deflation of soil. The natural dune surface at the Geomet site is highly susceptible to wind erosion, despite the vegetation cover, because of a low bare-soil wind erosion threshold and loose, erodible, sandy soil. In addition, the present vegetation, crusts, or gravel lag sufficiently protect the playa, desert pavement, and one rangeland area from wind erosion, except during extreme events. Nevertheless, where this natural protection is absent or is removed, erodibility is increased to those characteristic of bare surfaces, and these areas become extremely susceptible to wind erosion.

REFERENCES CITED

Bagnold, R.A., 1941, The physics of blown sand and desert dunes: London, Chapman and Hall, 265 p.

Belly, Pierre-Yves, 1964, Sand movement by wind, *with* Addendum 2, by Kadib, Abdel-Latif: U.S. Army Corps of Engineers, Vicksburg, Miss., Coastal Engineering Research Center Technical Memorandum 1, 85 p.

Chepil, W.S., Siddoway, F.H., and Armbrust, D.V., 1962, Climatic factor for estimating wind erodibility of farm fields: Journal of Soil and Water Conservation, v. 17, p. 162–165.

Demsey, K.A., 1988, Quaternary geologic map of the Salome 30×60 minute quadrangle, west-central Arizona: U.S. Geological Survey Cooperative Geologic Mapping (COGEOMAP) Program 14-08001-A0378, scale 1:100,000.

Fryberger, S.G., and Dean, Gary, 1979, Dune forms and wind regime, *in* McKee, E.D., ed., A Study of Global Sand Seas: U.S.Geological Survey Professional Paper 1052, p. 137–169.

Gillette, D.A., 1978, Tests with a portable wind tunnel for determining wind erosion threshold velocities: Atmospheric Environment, v. 12, p. 2309–2313.

———1986a, Wind erosion, *in* Soil Conservation: Assessing the National Resources Inventory, v. 2: National Research Council [U.S.], Committee on Conservation, Needs and Soil Conservation: Washington, D.C., National Academy Press, 314 p.

———1986b, Production of dust, *in* El Baz, F., and Hassan, M.H.A., eds., Physics of Desertification: Kluwer Academic Publishers, p. 251–260.

Gillette, D.A., Adams, J., Endo, A., Smith, D., and Kihl, R., 1980, Threshold velocity for input of soil particles into the air by desert soils: Journal of Geophysical Research, v. 85, no. C10, p. 5621–5630.

Helm, P.J., Breed, C.S., Tigges, Richard, and Creighton, Shawn, 1998, Geometeorological data collected by the USGS Desert Winds Project at Desert Wells, Sonoran Desert, central-west Arizona, 1981–1996: U.S. Geological Survey Open-File Report 98-361, CD-ROM.

Hyers, A.D., and Marcus, M.G., 1981, Land use and desert dust hazards in central Arizona: Geological Society of America, Special Paper 186, p. 267–280.

Idso, S.B., Ingram, R.S., and Pritchard, J.M., 1972, An American haboob: Bulletin of the American Meteorological Society, v. 53, no. 10, p. 930–935.

Marshall, J.K., 1971, Drag measurements in roughness arrays of varying densities and distribution: Agricultural Meteorology, v.8, p. 269–292.

McCauley, J.F., Breed, C.S., Helm, P.J., Billingsley, G.H., MacKinnon, D.J., Grolier, M.J., and McCauley, C.K., 1984, Remote monitoring of processes that shape desert surfaces: The Desert Winds Project: U.S. Geological Survey Bulletin 1634, 19 p.

Musick, H.B., and Gillette, D.A., 1990, Field evaluation of relationships between a vegetation structural parameter and sheltering against wind erosion: Land Degradation and Rehabilitation, v. 2, p. 87–94.

Nickling, W.G., and Gillies, J.A., 1989, Emission of fine-grained particulates from desert soils, *in* Leinen, M., and Sarthein, M., eds, Paleoclimatology and Paleometeorology: Modern and Past Patterns of Global Atmospheric Transport: New York, Kluwer Academic Publishers, p. 133–165.

Priestley, C.H.B., 1959, Turbulent Transfer in the Lower Atmosphere: Chicago, Ill., University of Chicago Press, 130 p.

Raupach, M.R., Gillette, D.A., and Leys, J.F., 1993, The effect of roughness elements on wind erosion threshold: Journal of Geophysical Research, v. 98D, p. 3023–3029.

Van Devender, T.R., 1990, Late Quaternary vegetation and climate of the Sonoran Desert, United States and Mexico: Chapter 8 *in* Betancourt, J.L., Van Devender, T.R., and Martin, P.S., eds., Packrat Middens: The Last 40,000 Years of Biotic Change: Tucson, University of Arizona Press, 467 p.

Woodruff, N.P., and Siddoway, F.H., 1965, A wind erosion equation: Soil Science Society of America, v. 29, p. 602–608.

Zobeck, T.M., 1989, Fast-vac—A vacuum system to rapidly sample loose granular material: Transactions of the ASAE, v. 32, no. 4, p. 1316–1318.

Field Monitoring of Vegetation Characteristics Related to Surface Changes in the Yuma Desert, Arizona, and at the Jornada Experimental Range in the Chihuahuan Desert, New Mexico

By H. Brad Musick

U.S. GEOLOGICAL SURVEY PROFESSIONAL PAPER 1598–D

CONTENTS

FIGURES

TABLE

Field Monitoring of Vegetation Characteristics Related to Surface Changes in the Yuma Desert, Arizona, and at the Jornada Experimental Range in the Chihuahuan Desert, New Mexico

By H. Brad Musick[1]

ABSTRACT

Vegetation is a potential influence on sediment transport by wind at the Geomet sites of the USGS Desert Winds Project. Vegetation at the Geomet sites is monitored by repeated measurement, at intervals of 1 to 2 years, of canopy structural variables along permanently marked transects. The variables measured are (1) vertically projected canopy cover, a conventional measure of vegetation amount, and (2) lateral cover, a variable identified by previous wind-tunnel experimentation as strongly related to the degree of vegetative sheltering against wind erosion. Lateral cover is defined for an array of plants as the ratio of canopy frontal-silhouette area to ground area occupied by the array. Line intersect sampling, in which selection probability is proportional to size, has proven to be an efficient sampling technique for field measurement of these variables.

Lateral and vertically projected cover have been monitored at the Jornada, New Mexico, and Yuma, Arizona, Geomet sites for periods of 6 years (1987–1992) and 5 years (1988–1992), respectively. The relative contribution of species to lateral cover and vertically projected cover was found to differ in some cases because tall, narrow canopies contribute more strongly to lateral than to vertically projected cover. Changes in lateral cover have resulted from changes in population density and (or) changes in plant size. At the Yuma site, total lateral cover decreased from 1988 to fall 1991 and then increased sharply in spring 1992 as herbaceous plants germinated and grew in response to abundant moisture in the winter of 1991–1992. Wind thresholds for eolian sediment transport, assuming dry soil conditions, are thus expected to have been lowest in summer and fall of 1991.

INTRODUCTION

On vegetated land surfaces, transport of sediment by wind is governed not only by wind strength and soil surface properties, such as particle-size distribution and moisture content, but also by the effects of vegetation. Soils that would otherwise be highly susceptible to wind erosion may be completely sheltered if a sufficient amount of vegetation is present. Lesser amounts of vegetation may provide partial protection by raising the wind threshold for particle movement and reducing the mass flux at given wind speeds.

The USGS Desert Winds Project has established sites for long-term continuous monitoring of sediment transport by wind and of the meteorological and land-surface variables influencing this transport (Breed, chap. A, this volume). The natural vegetation of these Geomet sites is monitored to identify and track changes that may account for some of the variation in susceptibility to wind erosion, both among sites and through time. This paper presents the methods used in monitoring vegetation and describes the changes observed and their potential effects on sediment transport.

The purposes of this paper are to (1) describe the canopy structural variables critical to determining susceptibility of desert surfaces to wind erosion, (2) describe the methods employed in measuring these variables at the Yuma and Jornada Geomet sites, and (3) present the results from monitoring of these variables over periods of 5 years at Yuma and 6 years at Jornada and discuss their significance.

Relations between observed sediment transport and the interactive effects of vegetation, wind, and other variables are examined elsewhere (Helm and Breed, chap. B, this volume).

[1]Air Quality Bureau, New Mexico Environment Department, P.O. Box 26110, Santa Fe, NM 87502.

71

CANOPY STRUCTURAL VARIABLES

AERODYNAMICALLY RELEVANT STRUCTURAL VARIABLES

The most direct influence of vegetation on wind erosion is to change the wind energy impinging on the soil surface. Plant canopies act as non-erodible roughness elements that absorb a portion of the total force of wind on the vegetated land surface, thereby reducing the amount of shear stress applied to the soil surface. Relative to a bare surface, greater wind strength above the canopy is required to achieve a given level of shear stress on the exposed soil surface, and the wind threshold for sediment transport is thus increased. Under a given natural wind regime, the frequency of sediment transport would decrease because exceeding the threshold would require stronger, less frequent winds. Absorption of a portion of the total shear stress by plants would also tend to reduce sediment mass flux at a given above-threshold wind strength.

The reduction in shear stress on the soil surface is dependent on the structural characteristics of the vegetation canopy. One approach for determining the relevant structural characteristics of vegetation and the relations between these variables and wind erosion is wind-tunnel experimentation using arrays of roughness elements as scale-model simulations of vegetation canopies. Relations derived from these simplified physical models under controlled conditions can then be tested at naturally vegetated field sites.

Simplified models of vegetation canopy structure are necessary to make wind-tunnel experimentation feasible and to derive generalized relations. Likewise, simplified conceptual models are inherent to the measurement of natural vegetation structure; even if not explicitly stated, a simplified model is implied when a limited number of measured variables is used to characterize the infinitely complex structure of natural vegetation. A model often applied to crops and forests describes vegetation as a horizontally homogeneous cloud of evenly dispersed leaves and stems (Thom, 1971). According to this model, variables that could be used to characterize canopy structure would include plant-area index (area of leaves and stems per unit ground area) and aerodynamic properties of individual leaves and stems. Measurements of vegetation in the Desert Winds Project and related studies are based on an alternative model describing vegetation as an array of discrete individual plant bodies (Marshall, 1971). Possible descriptive variables include the number, size, shape, and porosity of the individual plant bodies. For the widely dispersed shrubs and bunch grasses characteristic of naturally vegetated arid and semiarid sites, this structural model seems more appropriate than the cloud model.

Most wind-tunnel studies of the influence of roughness element arrays on shear stress partitioning and wind erosion have used solid objects of simple shape (e.g., cylinders, hemispheres) as roughness elements (Marshall, 1971; Lyles and others, 1974; Gillette and Stockton, 1989; van de Ven and others, 1989). The most important structural variable identified in these studies is lateral cover (L_c), also referred to as roughness density or frontal area index (FAI; Raupach and others, 1993). Lateral cover is defined as the ratio of frontal-silhouette area of roughness elements to ground area occupied by the array of elements (fig. 1). That is, if an area S is occupied by n elements each with frontal area F, then

$$L_C = \frac{nF}{S} \qquad (1)$$

Increasing lateral cover increases the wind threshold for sediment transport (Marshall, 1971; Lyles and others, 1974; Gillette and Stockton, 1989; Raupach and others, 1993) and decreases sediment transport at a given wind speed above the threshold (van de Ven and others, 1989; Hagen and Armbrust, 1994).

Another potentially important variable identified by wind-tunnel experiments is basal cover (fig. 1; the fraction of the soil surface covered by the bases of the roughness elements) or its complement, fractional area of exposed soil. The role of basal cover can be seen in the relation of shear stress on the exposed soil surface (S_s) to force on the exposed soil (F_s) and area of exposed soil (A_s):

$$S_s = \frac{F_s}{A_s} \qquad (2)$$

Increasing basal cover reduces A_s and thus tends to increase S_s (Raupach and others, 1993).

The statement that increasing basal cover tends to amplify shear stress on the surface might seem to be contradicted by observations that surface shear stress is decreased by adding roughness elements to a surface. The apparent contradiction can be explained by noting that adding roughness elements also increases L_c and thereby decreases F_s; adding roughness elements thus has two opposing effects on S_s: (1) drag exerted by the roughness elements (a function of lateral cover) reduces F_s, tending to decrease S_s, and (2) the covering of a portion of the soil surface (a function of basal area) confines this force to a smaller area of exposed soil A_s, tending to increase S_s.

The net effect on shear stress is determined by the relative strength of these opposing effects. In all but extreme cases, the reduction in force going to the soil strongly outweighs the effect of confining this force to a smaller area, and the net effect is thus a reduction in shear stress on the soil (Gillette and Stockton, 1989; Raupach and others, 1993; Musick and others, 1996).
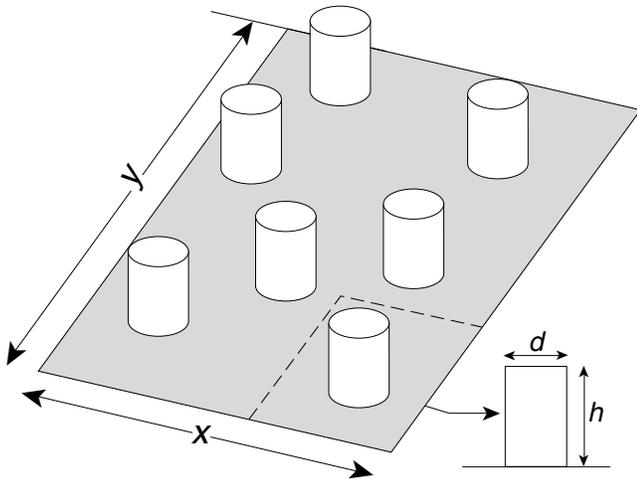
Figure 1. Schematic drawing of an array of roughness elements, illustrating dimensions used in calculation of lateral cover (adapted from Marshall, 1971). In this example, ground area $S = xy$ is occupied by $n = 7$ cylindrical roughness elements, each with frontal area $F = hd$. Lateral cover is given by equation 1.

Table 1. Properties of roughness element or plant body arrays likely to influence sheltering against wind erosion.

[Adapted from Marshall, 1971]

Property	Example or explanation
Roughness element or individual canopy properties	
Size	Height, diameter
Shape	Height/diameter ratio
Form	Hemisphere, cylinder
Porosity	Solid, porous; variation with height or across element
Orientation	Relation of long axis in *x-y* plane to wind direction
Flexibility	Effects of streamlining, fluttering on drag
Element roughness	Rough, smooth, protrusions, edges
Array properties	
Population density	Number per unit area
Composition	Heterogeneity in element properties
Distribution	Regular, random, aggregated
Orientation	Row direction relative to wind

The effects of lateral and basal cover described above are applicable only to sparse arrays. At very high roughness density, flow passes predominantly over rather than through the array. The aerodynamics of dense arrays characterized by this skimming flow are largely irrelevant to wind erosion because virtually complete protection of the surface is obtained at lower levels of roughness density, where L_c is on the order of 0.3–0.5 (Raupach, 1992; Raupach and others, 1993).

Table 1 lists a number of characteristics of roughness element arrays that are likely to influence shear stress partitioning and aerodynamic sheltering against wind eosion. Many of these characteristics are not accounted for by lateral and basal cover, and their quantitative influence is generally poorly known. Perhaps the most unrealistic aspect of current models is their use of solid objects to represent plant bodies that in nature are often highly porous. A recent study (Musick and others, 1996) found that porosity effects are potentially great (as much as 50 percent variation in wind threshold between different levels of porosity). Their results also indicated that effectiveness in increasing wind thresholds for erosion is greatest not for solid bodies, but at some intermediate level of porosity.

The complex structure of natural vegetation poses two difficulties in applying the results of wind-tunnel experiments that use structurally simple roughness element arrays to studies of wind erosion on natural land surfaces:

1. The simplified model of canopy structure may not include some aspects of structure that are important for wind erosion on natural land surfaces. The need to incorporate additional structural variables (table 1) can be evaluated by field validation studies, such as analysis of the Geomet data. Experimentation using more realistic structural models will likely identify additional structural variables important in determining eolian sediment transport.

2. Variables derived from a simple structural model may be difficult to define and measure when applied to complex natural structures. For example, the diameter of a circle is uniquely defined and measurable without ambiguity, but to determine the "diameter" of an irregular polygon, a shape typical of many plants, one must choose between alternative definitions and methods for measurement. Conventions adopted for measurement of lateral and basal cover in this study are given in the description of methods.

In summary, previous experiments have identified lateral and basal cover as canopy structural variables important in influencing eolian sediment transport and have determined a quantitative relation between these variables and wind thresholds for soil movement. To characterize natural canopy structure in terms of these two variables requires some simplifying assumptions and ignores plant-body porosity and other potentially important structural variables for which appropriate definitions and quantitative influences on sediment transport are unknown. However, a preliminary study indicates that these simplified methods of characterizing canopy structure can be combined with wind-tunnel results using solid roughness elements to obtain reasonably good predictions of wind thresholds for erosion on naturally vegetated surfaces (Musick and Gillette, 1990). Based on these methods, these authors estimate that the threshold vegetation, L_c, required for full sheltering of sandy soil from wind erosion is approximately 0.25.

CONVENTIONAL MEASURES OF
VEGETATION AMOUNT

As noted above, many difficulties arise if wind-tunnel studies of simple physical models are used to determine which vegetation variables should be measured. It might be asked whether it would be preferable to simply use conventional measures of vegetation amount, such as biomass or percent canopy cover (that is, percent area of canopies as viewed from above). Correlations between wind erosion and these conventional measures have been obtained (Ash and Wasson, 1983; Buckley, 1987), and predictive use of these correlations is appealing because the required vegetation data can be readily obtained by standard methods or may be retrieved from existing databases.

However, the complexity and variability of natural vegetation also poses difficulties when these conventional measures are applied to problems of wind erosion. These difficulties may be illustrated by considering a hypothetical experiment in which structural variability has been completely eliminated so that all the individual plant bodies are identical in every respect. Suppose that varying numbers of these replicate plants are arrayed on an erodible surface and the effect on wind threshold is measured. Wind threshold will then be found to correlate strongly with any measure of vegetation amount, including aerodynamically irrelevant quantities such as chlorophyll content per unit ground area. Functionally irrelevant variables would then serve as surrogate variables, related to wind threshold only through their fixed relation to the functionally relevant variables (such as L_c). If the relation between such a surrogate variable and wind threshold were then used to predict the results of future experiments, success would depend on the degree to which the original relation between the surrogate variable and functionally relevant variables was maintained. Similarly, field experiments at naturally vegetated sites may yield correlations between susceptibility to wind erosion and conventional measures of vegetation amount, but the predictive value of the relation will be unknown.

Relations between wind erosion and conventional measures of vegetation amount could, in theory, be generalized and given greater predictive power by incorporating coefficients dependent on plant-body structure. However, this raises the problem of how these structure-dependent coefficients would be determined. A purely empirical approach, in which the coefficients were empirically determined for each structurally different type of plant body, would be impractical in most cases. Alternatively, relations between the coefficients and functionally relevant canopy structure variables could be determined, but this would require knowledge of the relevant variables and their effects on wind erosion.

METHODS

During the course of the Desert Winds Project, different spatial patterns have been experimentally used for plant transects, and different techniques have evolved for characterizing canopy structural variables. These are described below.

VEGETATION AT THE GEOMET SITES

The Jornada Geomet site (lat 32°34′45″N., long 106°46′35″W.) is in the northern Chihuahuan Desert on the Jornada Experimental Range, a U.S. Department of Agriculture/Agricultural Research Service (USDA/ARS) rangeland research facility in south-central New Mexico (fig. 11 in Breed, chap. A, this volume). The Yuma Geomet site (lat 32°31′50″N., long 114°30′45″W.) is in the Yuma desert, a part of the Sonoran Desert, on the Barry M. Goldwater Air Force Range in southwestern Arizona (fig. 9 in Breed, chap. A, this volume). The Yuma site is much more arid, with a mean annual precipitation (1989–1992) of about 52 mm compared to about 233 mm for the Jornada site. Rainfall at both sites is bimodally distributed, falling in winter and summer, about half in summer at Jornada, and mostly in winter at Yuma. Detailed meteorological data for the Geomet sites at Yuma and Jornada are provided by Helm and Breed (chap. B, this volume); weather patterns associated with sand transport at the Yuma site are illustrated by Baudat and Breed (chap. E, this volume). Physiographic settings of the sites are described by Breed (chap. A, this volume).

The composition of the vegetation (species and growth form) played a role in determining the choice of sampling methods. At both the Jornada and Yuma Geomet sites, three species accounted for most of the perennial vegetation cover. The major perennial species at Jornada (fig. 2) are mesquite (*Prosopis glandulosa*), a winter-deciduous shrub; snakeweed (*Gutierrezia sarothrae*), a semi-woody subshrub; and dropseed (*Sporobolus* spp., mainly *S. flexuosus*), a warm-season bunch grass. The major species at Yuma (fig. 3) are creosotebush (*Larrea tridentata*), an evergreen shrub; white bursage (*Ambrosia dumosa*), a smaller drought-deciduous shrub; and big galleta (*Hilaria rigida*), a warm-season bunch grass with stiff, semi-woody stems and a shrub-like growth form. Vegetation structural variables were determined separately for each of the three major perennial species and for herbaceous plants when they were judged by visual observation to contribute significantly to the total amount (fig. 3*B*). These measurements were used to evaluate the relative contribution of each species (or ephemerals, as a group) to the total value of the measures and to understand how a change in species composition might influence protection of the soil surface against wind erosion.

Vegetation was sampled at Jornada in spring: February 1987, April 1988, April 1989, May 1990 (completed in July), and February 1992 (see table 2 in Breed, chap. A, this

Figure 2. Vegetation at Jornada Geomet site, May 1991. Arrows indicate three major species: mesquite (M), broom snakeweed (S), and dropseed (D).

volume, for definitions of seasons used in this project). This season was chosen because the seasonal distribution of high winds has a strong maximum during this period (Barchett, 1982). At Yuma, sampling was conducted in spring or early summer: May 1988, April 1989, June 1990, and March 1992. The sites were visited on a number of other occasions by the author and by other project personnel, and repeat photographs at a series of fixed stations were taken at irregular intervals.

Vegetation measurements at both sites were made along four permanently marked 200-m transects (fig. 4*A*). The transects at Jornada, established in 1987, were parallel and 50 m apart. The transects were located to the west-southwest from the Geomet tower because historical wind data for the nearby city of Las Cruces (Barchett, 1982) and sand streaks evident on Landsat images (fig. 11 in Breed, chap. A, this volume) indicated that erosive winds were predominantly from the west-southwest, and the transects were thus intended to characterize the area most likely to be upwind of the instruments during erosion events. At Yuma, high wind speeds were historically more variable in direction (MacKinnon and others, 1990), so the transects there were placed (in 1988) to extend radially from the Geomet station in the four cardinal directions (fig. 4*B*).

Several assumptions were made in the measurement of plant canopies. The solid cylinder was adopted as the model of plant-body shape for calculations of frontal area, which was thus calculated as the product of height and the mean of the longest and shortest diameters of a given individual. Height and diameter were taken as the limits of an imaginary

envelope encompassing the bulk of the plant body but excluding the occasional erratic branch. Adjacent plants were measured as a single individual plant body if their branches and foliage were substantially intermingled. Both dead and living individuals were sampled because standing dead plants contribute to sheltering against wind erosion. Living and dead individuals were usually not treated separately in our measurements because vitality could not always be reliably determined.

PERCENT VERTICALLY PROJECTED CANOPY COVER

Line intercept sampling was performed along the transect lines to obtain a conventional ecological measure of vegetation amount and species composition. In this method, the percentage of the total length of a line transect intercepted by a cover component (e.g., a plant species) gives a measure of the areal (vertically projected) cover fraction of that component (Grieg-Smith, 1964). This procedure provides a measure of basal area if one assumes that the envelope surrounding each plant body extends vertically to the soil surface.

LATERAL COVER

Two sampling schemes have been employed for measurement of lateral cover. In the original scheme, plant-body population density (plants/m^2 of ground area = n/S in eq. 1)

Figure 3.   Vegetation at Yuma Geomet site. *A*, March 13, 1991; *B* March 3, 1992. Arrows indicate three major species: creosotebush (C), white bursage (WB), and big galleta (BG).

and mean plant-body frontal area (m² of frontal area/plant = *F* in eq. 1) were each estimated independently, and lateral cover (m² of frontal area/m² of ground area) was calculated as the product of these two variables. Population density was obtained by counting plants in quadrats systematically arrayed along each transect line. Because species differed greatly in population density, each major species (as listed above for each site) usually required a different quadrat size. For each major species, a sample of plants for measurement

of canopy dimensions was obtained by selecting the individual of that species nearest to each of a series of fixed points along the transect.

A completed sample at each site consisted of four 200-m line intercept transects for percent canopy cover, as many as 40 quadrats per major species for population density, and 40 individuals of each major species for plant-body dimensions. Weather conditions and limitations on time and labor often required that sample sizes be reduced by half.
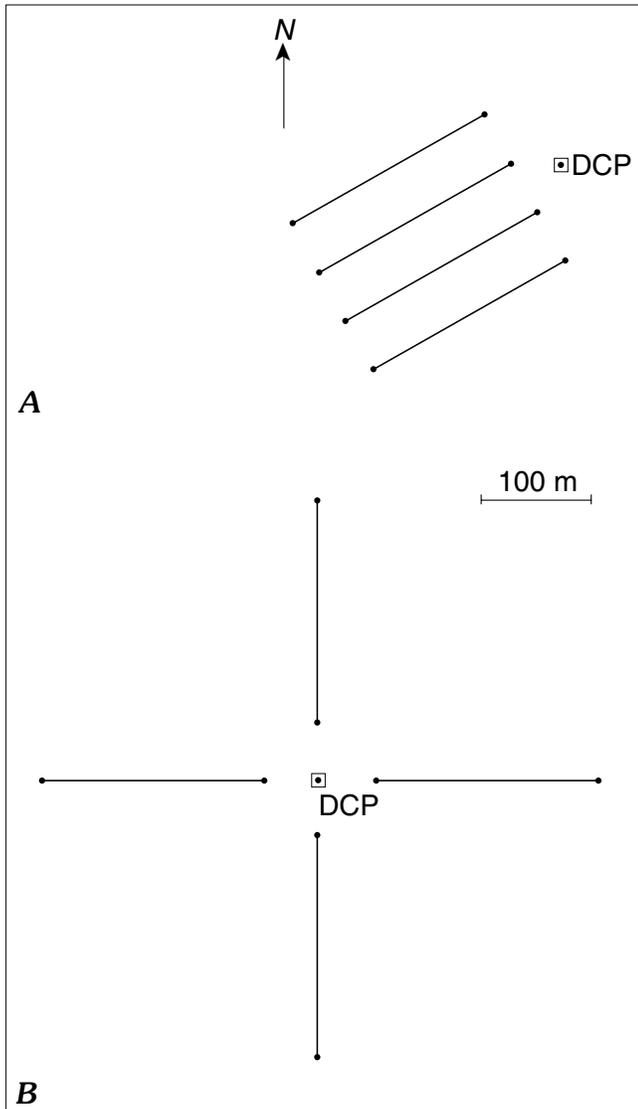
Figure 4. Orientation of permanent transects at (*A*) Jornada and (*B*) Yuma; DCP, Geomet data collection platform.

Although the scheme described above permits the calculation of lateral cover (eq. 1) in a straightforward way, several limitations became evident. Reliable estimates of the variance of the lateral cover estimate were difficult to obtain because lateral cover was calculated as the product of two independently sampled variables; the variance of the product thus depended on the covariance of the two directly measured variables. We could not assume that population density and plant-body dimensions varied independently because quadrats with high population density were observed to have a higher percentage of small individuals and thus a smaller mean plant-body size than low-density quadrats. Another related problem was that most of the labor was consumed in sampling the abundant smaller individuals in the population. The rarer large individuals that commonly accounted for much of a species' lateral cover were thus

severely undersampled, and the resulting lateral cover values were highly sensitive to the chance inclusion or exclusion of a few very large individuals.

These problems led to the adoption of line intersect sampling (LIS; de Vries, 1979), a technique in which the probability of an individual being selected for measurement is proportional to some measure of individual size. LIS is well suited for estimating per-unit-area values of variables closely related to size, such as frontal area or vertically projected area. The sample is biased to a known and correctable degree in favor of the larger individuals, and the measurement effort is thus automatically concentrated on those larger individuals that contribute the most to the area-wide sum or mean of the measured variable. Another advantage of the LIS method over the original sampling scheme is that variance of the lateral cover estimate can be obtained directly. Use of LIS also eliminates the labor required to lay out quadrats because it requires only the permanently marked transect lines already established at each site.

The theory underlying LIS sampling, given in detail by de Vries (1979), is summarized as follows. Each individual in the population is represented geometrically by a uniquely defined "needle" in the horizontal plane, and only those individuals whose "needle" is intersected by the transect line are included in the sample. For sampling of plant canopies, the "needle" is defined as the longest diameter of an imaginary envelope around the plant body in the horizontal plane (fig. 5). Assuming that the plant bodies are randomly oriented, the probability that a given individual's "needle" will be intersected (and the individual thus included in the sample) is directly proportional to the long diameter of the plant body and to the length of the transect line.

For any plant-body property, x_i, which can be measured (e.g., frontal area or vertically projected area), the total amount of x_i per unit ground area ($\hat{X}$) can be estimated without bias by:

$$\hat{X} = \frac{\pi}{2 \times L} \sum_{i=1}^{n} \left(\frac{x_i}{l_i} \right) \qquad (3)$$

where

    L is transect length,
    n is the number of individuals whose long diameters were intersected, and
    l_i is the long diameter of the *i*th plant body

A slightly different formula is required if the objects are circular. For this study, plant bodies with a ratio of long to short diameter of 1.1 or less were treated as circular; calculations indicated that the estimated quantities were not highly sensitive to the value of this ratio used as the criterion for circularity. LIS was also used in estimating population density (number of individuals per unit area). According to
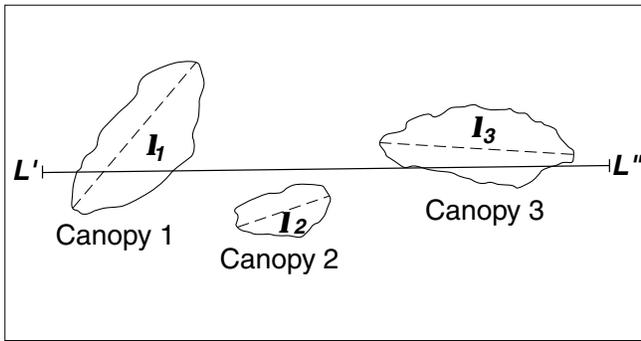
Figure 5. Schematic plan view of portion of line transect (L' to L'') illustrating criterion for inclusion of plant canopy in sample obtained by line intersect sampling (LIS). Each canopy has unique "needle," l_i, defined as long axis of imaginary envelope surrounding canopy. Canopy is included in sample if and only if "needle" is intersected by transect line; only canopy 1 meets this requirement in this example. (From de Vries, 1979.)

de Vries (1979), this is accomplished simply by defining the measured quantity as "presence" and setting all x_i equal to one. Formulae given by de Vries (1979) were also used to calculate the variance of the estimated per-unit-area quantities.

In preliminary tests, LIS was found to give results comparable to earlier methods for estimation of mesquite lateral cover at Jornada. LIS was first used as a replacement for previous sampling methods in spring 1992 at the Yuma Geomet site. Sampling of the three major perennial species was performed along eight 200-m transects, comprised of the four permanently marked transects (fig. 4B) plus a temporary transect parallel to each of the permanent transects. Herbaceous plants were very abundant at this site in spring 1992, and we found it not feasible to measure all herbaceous plants encountered along the full length of each transect. Therefore, a subsample of two 10-m segments along the first 100 m of each permanent transect was randomly selected for LIS sampling of the herbaceous plants.

RESULTS

JORNADA GEOMET SITE

During the period from 1987 to 1992, the three major species at Jornada (mesquite, snakeweed, and dropseed) usually accounted for more than 95 percent of the total vertically projected canopy cover. Herbaceous ephemerals were sometimes present but never contributed as much as 5 percent cover at any sampling time. Total cover varied from 33 percent to 42 percent and showed little net change from 1987 to 1992 (fig. 6). The most notable change was a shift in species composition, with mesquite increasing and
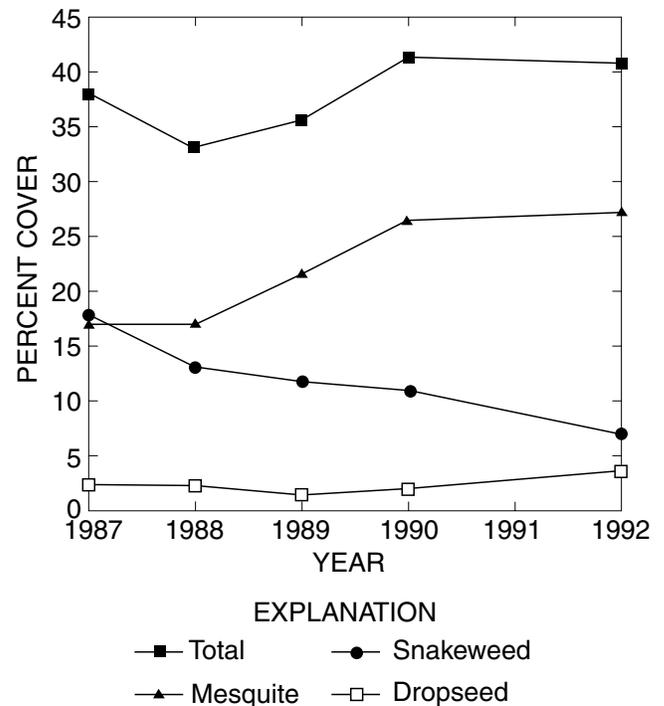

Figure 6. Vertically projected canopy cover at Jornada Geomet site in spring, 1987 to 1992 (two transects only).

snakeweed declining over this period. Dropseed cover increased slightly in 1992 relative to the previous sampling in 1990 and earlier years.

Comparison of a given species' relative contributions to vertically projected cover (fig. 6) and lateral cover (fig. 7) shows that these contributions are rarely the same and may be strikingly different. These differences result from differences in canopy shape. Canopies that are narrow relative to their height (or tall relative to their breadth), such as those of dropseed, contribute more strongly to lateral cover than to vertically projected cover.

Total lateral cover at Jornada was relatively constant from 1987 through 1990 and then increased sharply in 1992; most of the 1990–1992 increase was accounted for by a marked increase in dropseed lateral cover (fig. 7). The consistent trends of increasing mesquite and declining snakeweed noted for vertically projected cover are also evident in lateral cover.

Some understanding of the biological phenomena responsible for changes in lateral cover may be gained by examining separately the two quantities of which lateral cover is the product, population density and mean frontal area per individual. The nature of the changes in each species' lateral cover was examined by plotting population density, mean frontal area per plant, and lateral cover as a percentage of their respective values in 1987 (figs. 8–10). The increase in mesquite lateral cover is thus seen to have resulted from an increase in mean plant size (fig. 8).
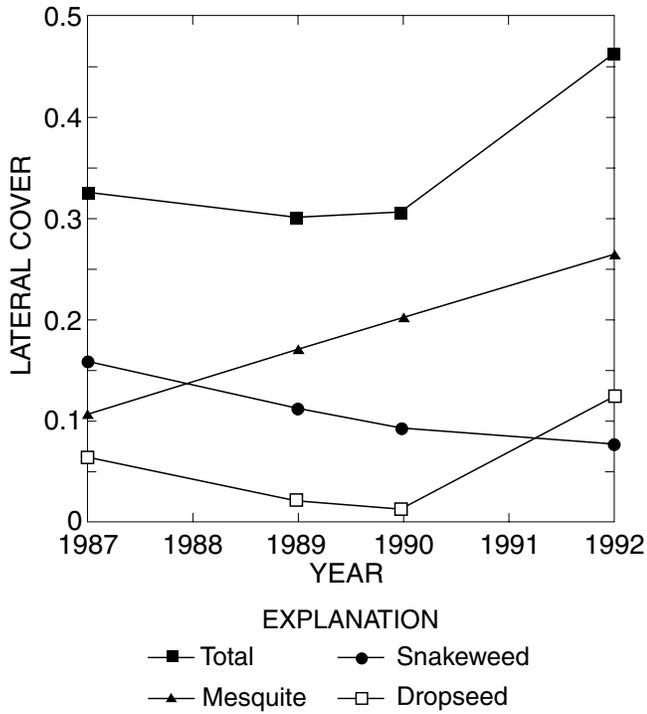
Figure 7. Lateral cover at Jornada Geomet site, 1987 to 1992 (two transects only).

Figure 8. Relative change from 1987 to 1992 in mesquite lateral cover and its components at Jornada Geomet site (spring season only).

**Figure 9.** Relative change from 1987 to 1992 in snakeweed lateral cover and its components at Jornada Geomet site (spring season only).
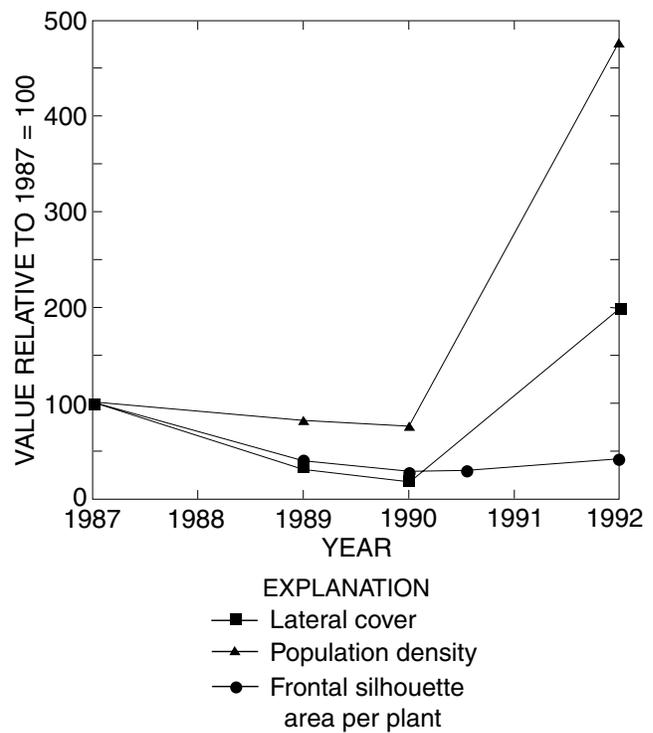

Figure 10. Relative change from 1987 to 1992 in dropseed lateral cover and its components at Jornada Geomet site (spring season only).

Snakeweed declined both in population density and in frontal area per plant, but the decrease in density was the more important factor in the decrease of snakeweed lateral cover (fig. 9). Rapid declines in local snakeweed populations are frequently observed but poorly understood; separating the effects of drought, insect-induced mortality, and natural senescence of even-aged stands has been difficult (Pieper and McDaniel, 1989). A widespread decline of snakeweed in New Mexico in 1989 has been attributed to exceptionally low early-summer rainfall in that year (McDaniel, 1989; Torell and others, 1989). The response of lateral cover to an episode of high snakeweed mortality is likely to be delayed and spread over subsequent years, because the semi-woody plant bodies persist as aerodynamic roughness elements after death. In 1989, the Jornada site was sampled in late spring (May), when living plants could be expected to show new growth and thereby be distinguishable from dead plants; approximately one-third of snakeweed individuals appeared to be dead at that time.

The decline in dropseed lateral cover from 1987 to 1990 can be attributed largely to a decrease in plant size, but the high lateral cover in 1992 resulted primarily from an increase in population density (fig. 10). The increase in density actually began earlier than shown in figure 10. In 1990 we observed many very small dropseed seedlings that were reported to have germinated after a heavy rain in July 1990 (R.P. Gibbens, USDA-ARS, oral commun., 1990). These seedlings were not sampled in 1990 because our primary goal was the determination of lateral cover, and these seedlings were so small that they were judged to make an insignificant contribution to dropseed lateral cover. The increase in dropseed population density recorded in 1992 probably reflects survival and growth of many of the seedlings which emerged in summer 1990.

YUMA GEOMET SITE

From 1988 through 1992, perennial vertically projected cover at the Yuma site was comprised of roughly equal amounts of creosotebush, white bursage, and big galleta (fig. 11). Creosotebush and white bursage cover were nearly constant, but big galleta cover decreased slightly from 1989 through 1992. Herbaceous cover was much more variable than at the Jornada site, varying from nearly absent in 1990 to approximately equaling the perennial cover in 1992. Visual observations and site photographs (see fig. 3) from 1990–1992 indicate that herbaceous cover was negligible throughout the summer and fall of 1991. The large amount of herbaceous cover present in spring 1992 resulted from the exceptionally wet late fall and winter of 1991–1992 (fig. 12), which was an El Niño phase of the El Niño–Southern Oscillation (ENSO) climatic cycle.

Total lateral cover decreased continuously through the dry years of 1988–1990 and then increased in 1992 to near
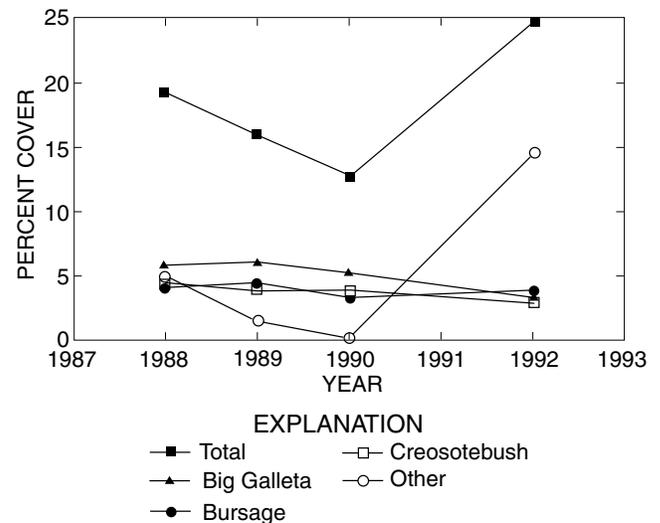

Figure 11. Changes in vertically projected cover at Yuma Geomet site, 1988–1992, as measured by line intercept. Category "Other" is primarily herbaceous plants.

the 1988 value, largely as a result of the growth of herbaceous plants beginning in winter of 1991–1992 (fig. 13). Because perennial lateral cover decreased continuously from 1988 to 1992, and herbaceous lateral cover was negligible until after the onset of cool-season rains in fall 1991, lateral cover would be expected to have fallen to its lowest level in late summer or early fall of 1991.

Most of the decrease in perennial lateral cover over the sampled period can be attributed to a marked decrease in big galleta, which had decreased in 1992 to only about one-fourth of its 1988 lateral cover value. Changes in lateral cover of creosotebush and bursage were smaller in both absolute amount and relative to their 1988 values. Since both dead and live tissues contribute to lateral cover, species differences in lateral-cover trends during the dry period of 1988 to 1991 may reflect not only differences in drought-induced mortality but also differences in the mechanical strength and thus the persistence of dead stems and individuals. Differences in persistence after death are difficult to measure in species such as big galleta and bursage where death is preceded by a period of drought-induced dormancy and the transition is not distinguishable by external appearance. Relative to bursage, big galleta appears to be more vulnerable to mechanical disaggregation after death because the primary stems arising from the root crown are long (often 1 m) and relatively flexible. In contrast, the bursage plant bodies are compact and stiff, comprised of a tangle of interlocking short branches.

Potential impacts of the vegetation changes on susceptibility of sediment to wind transport may be examined by predicting effects on wind thresholds for soil movement. Using a relation derived from results of wind-tunnel experiments (Raupach and others, 1993), the
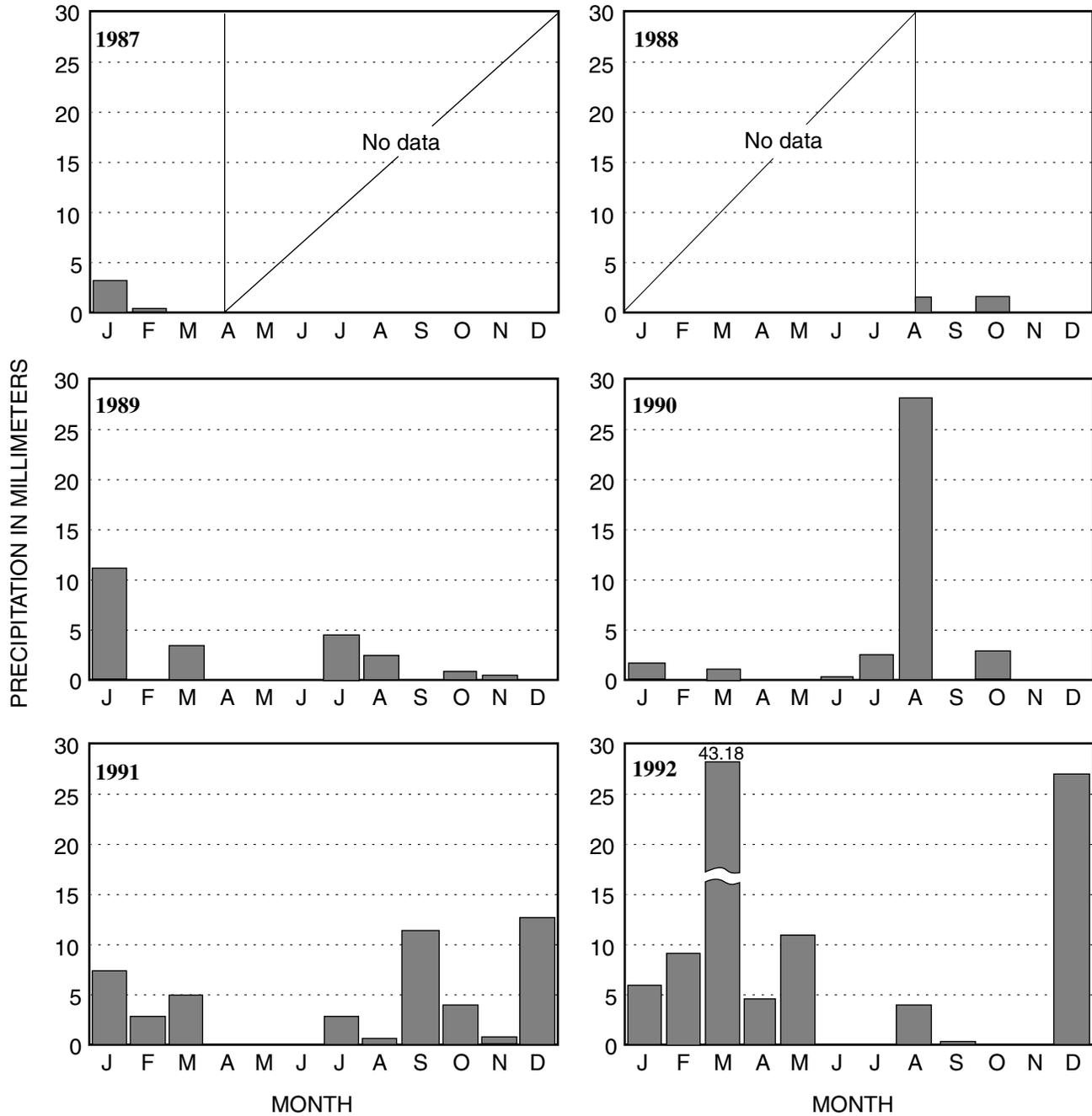
Figure 12. Monthly precipitation at Yuma Geomet site, 1987 to 1992.

measured values of lateral and vertically projected cover were first used to calculate the threshold friction velocity of the vegetated surface relative to the threshold the same soil surface would have if bare. Predicted vegetated-surface thresholds for the Yuma site (fig. 14) were then calculated assuming the soil surface was dry, with a bare-surface threshold friction velocity of 28 cm s^{-1} as determined for this site by Musick and Gillette (1990). The strong influence of lateral cover on wind threshold seen in wind-tunnel experiments and incorporated into the predictive relation

(Raupach and others, 1993) is evident in the similarity of trends in predicted threshold to those of lateral cover: decreasing from 1988 to 1990 (and presumably through summer 1991) and then markedly increasing in 1992. The predicted range in threshold friction velocities is substantial (about 30 cm s^{-1}), but potential effects on mass flux of sediment would depend on other variables, including the frequency of strong winds and of moist soil surface conditions. It should be noted that even when vegetative protection was at its predicted minimum in 1991, the
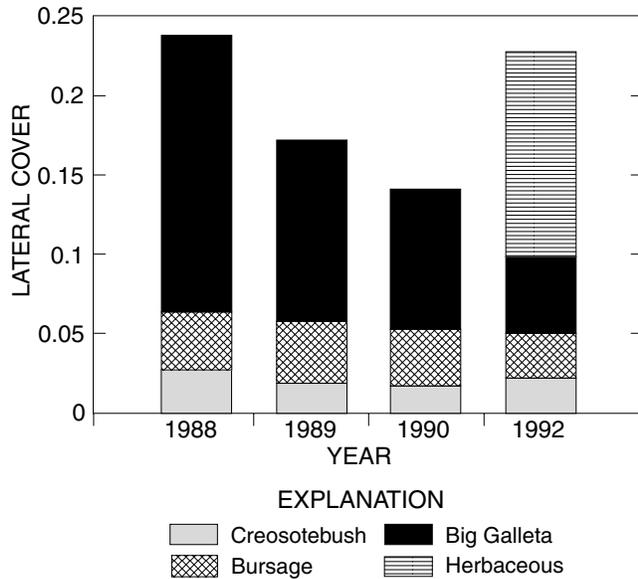
Figure 13. Changes in lateral cover at Yuma Geomet site, 1988–1990, and 1992. Herbaceous lateral cover was not sampled in 1988 and was negligible in 1989 and 1990. Vegetation was not sampled in 1991.

threshold friction velocity of 63 cm s^{-1} was substantially greater than for bare soil (28 cm s^{-1}). Measured wind and sand flux data for this site are examined by Helm and Breed (chap. B, this volume).

DISCUSSION

PATTERNS OF TEMPORAL VARIATION IN SHELTERING BY VEGETATION

The limited scope of the data set (annual sampling for 5–6 years at two sites) is insufficient for conclusive generalizations regarding temporal variation, but some tentative hypotheses may be advanced.

At both sites, total lateral cover was comprised of contributions by both slowly varying components and more rapidly varying components. Interannual variability tended to be related to growth form: least for woody shrubs, intermediate for perennial bunch grasses, and greatest for ephemeral herbaceous plants.

At the Yuma site, where all three growth forms made significant contributions to the total, the resulting patterns might be viewed as follows: The more stable components provide a slowly varying baseline level of protection; superimposed on this baseline level are occasional sharp increases in protection resulting from vigorous emergence and growth of ephemeral plants in wet years, perhaps followed by 1–2 years of declining protection as the dead ephemerals are removed by physical and biological processes. Variation in
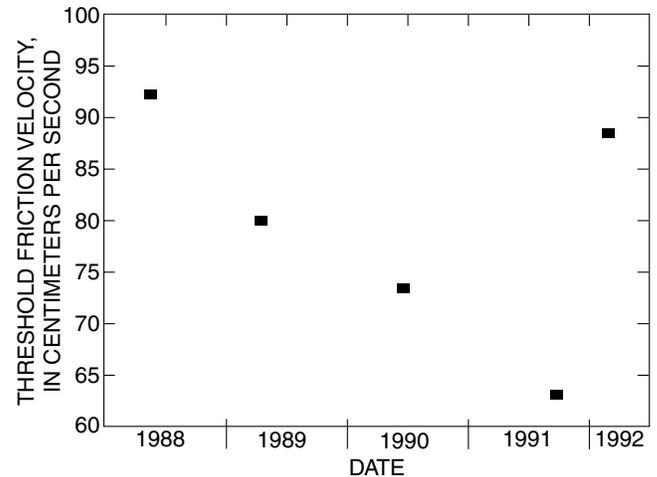

Figure 14. Predicted threshold friction velocities for movement of dry soil at Yuma Geomet site. Values were calculated using measured values of lateral cover and vertically projected cover from this study as input to a predictive equation proposed by Raupach and others (1993). Threshold friction velocity of dry soil if unvegetated was assumed to be 28 cm s^{-1}, as previously estimated for this site by Musick and Gillette (1990). Basal cover was assumed equal to measured value of vertically projected cover. Vegetation was not sampled in fall 1991; cover values for that time were estimated by subtracting from spring 1992 values the herbaceous vegetation that germinated and grew in late fall and winter of 1991–1992.

the ephemeral component might therefore account for much of the interannual variation in eolian sediment transport over periods of a decade or so. The more stable perennial components may be less important than ephemerals in accounting for interannual variability in wind erosion, but they may strongly influence long-term mean levels of wind erosion because they determine the level of vegetative sheltering during the often long periods when ephemerals are sparse or lacking.

Indirect methods for estimating or predicting vegetative sheltering are needed when detailed, in situ measurement is impossible, as in the problem of evaluating impacts of past and future climatic fluctuations. Climatic indices of eolian activity (e.g., dust storms, dune mobility) often include measures of moisture availability (e.g., precipitation-to-potential-evapotranspiration ratio, antecedent precipitation) that serve largely as surrogate measures of the protective influence of vegetation (Ash and Wasson, 1983; Lancaster, 1988; Brazel, 1989; MacKinnon and others, 1990; Muhs and Maat, 1993). Explicit consideration of the growth-form composition of vegetation and of the differences among growth forms may be useful in development of these indices. For example, accounting for all the variation in sheltering provided by a mixture of slowly and rapidly responding components might require a composite index including factors for both long-term (>1 yr) and short-term (<1 yr) antecedent moisture. Modeling of ephemeral responses could be made more detailed by accounting for effects of seasonal timing and

quantity of individual rainfall events, factors which have been shown to influence ephemeral response strongly (Beatley, 1974). In predicting effects of climatic change, it should be recognized that some or all of the more stable perennial components of vegetative sheltering could be eliminated from the system by extreme events or if a climatic threshold were crossed.

Remote sensing provides an indirect method for estimating vegetative protection over large areas. Explicit consideration of growth form composition might also be useful in selecting appropriate remote-sensing strategies. In a system where ephemerals are responsible for all the variation in sheltering, peak green biomass could be detected and measured by means of spectral indices such as visible/near-infrared contrast (Lougeay and others, 1987); a decay function would be necessary to estimate the decreasing protection provided by dead ephemerals. Green vegetation indices would be less successful in estimating protection by woody shrubs and perennial grasses, which often lack green leaves for extended periods. Promising new approaches include reflectance measures based on relations between shrub crown structure and shadowing of the surface (Franklin and Turner, 1992) and active microwave remote sensing (Musick and others, 1995, 1998).

The methods used for in situ measurement of vegetation structure in this study do not require special equipment, but are tedious and labor intensive. Development of methods for near-ground remote sensing of the relevant structural variables would greatly facilitate rapid and efficient field measurement of vegetative sheltering.

SUMMARY

On vegetated land surfaces, the structure and amount of vegetation may substantially influence sediment transport by wind. Wind-tunnel experiments are useful in determining the structural variables relevant to vegetative sheltering of erodible surfaces and in deriving predictive relations for the influence of vegetation. Monitoring of vegetation at the Geomet sites is designed, in part, to provide data for quantitative testing of the predictive relations derived from wind-tunnel studies. In addition, repeated quantitative measurements help in understanding how the natural variability in geomorphic processes such as wind erosion is affected by interannual variability in the vegetation.

Conventional measures of vegetation amount, such as vertically projected canopy cover, do not account for aspects of canopy structure relevant to aerodynamic sheltering of the soil surface. Vegetation sampling at the Jornada and Yuma Geomet sites has been designed primarily to measure lateral cover, a structural variable shown by wind-tunnel experiments to be strongly related to vegetative sheltering against wind erosion. Line intersect sampling provides an efficient sampling scheme for measurement of lateral cover.

Annual or biennial measurements of lateral cover over periods of 6 years (Jornada) and 5 years (Yuma) show changes in total lateral cover and in the relative contributions of different species to the total, which in some cases can be correlated with trends in rainfall. The changes in lateral cover, especially at Yuma, are likely to have resulted in significant changes in susceptibility of the surface to soil movement by wind.

The growth-form composition of vegetation may influence patterns of temporal variation in sheltering against wind erosion and has implications for development and interpretation of indirect measures of sheltering by vegetation.

REFERENCES CITED

Ash, J.E., and Wasson, R.J., 1983, Vegetation and sand mobility in the Australian desert dunefield: Zeitschrift für Geomorphologie Supplement, v. 45, p. 7–25.

Barchett, W.R., 1982, Wind energy resource information system: System operation: Technical Memorandum, U.S. Department of Energy contract DE-AC06-76RLO 1830, Richland, Wash., Battelle Pacific Northwest Laboratory.

Beatley, J.C., 1974, Phenological events and their environmental triggers in Mojave Desert ecosystems: Ecology, v. 55, p. 856–863.

Brazel, A.J., 1989, Dust and climate in the American Southwest, *in* Leinen, M., and Sarnthein, M., eds., Paleoclimatology and Paleometeorology: Modern and Past Patterns of Global Atmospheric Transport: Dordrecht, Kluwer Academic Publishers, p. 65–96.

Buckley, R., 1987, The effect of sparse vegetation on the transport of dune sand by wind: Science, v. 325, p. 426–428.

de Vries, P.G., 1979, Line intersect sampling—Statistical theory, applications, and suggestions for an extended use in an ecological inventory, *in* Cormack, R.M., Patil, G.P., and Robson, D.S., eds., Sampling Biological Populations: Fairland, Md., International Cooperative Publishing House, p. 1–70.

Franklin, J., and Turner, D.L., 1992, The application of a geometric optical canopy reflectance model to semiarid shrub vegetation: Institute of Electrical and Electronics Engineers (IEEE) Transactions on Geoscience and Remote Sensing, v. 30, p. 293–301.

Gillette, D.A., and Stockton, P.H., 1989, The effect of nonerodible particles on wind erosion of erodible surfaces: Journal of Geophysical Research, v. 94D, p. 12885–12893.

Grieg-Smith, P., 1964, Quantitative plant ecology (2nd ed.): New York, Plenum Press.

Hagen, L.J., and Armbrust, D.V., 1994, Plant canopy effects on wind erosion saltation: Transactions of the American Society of Agricultural Engineers, v. 37, p. 461–465.

Lancaster, N., 1988, Development of linear dunes in the southwestern Kalahari, southern Africa: Journal of Arid Environments, v. 14, p. 233–244.

Lougeay, R., Brazel, A.J., and Miller, T.A., 1987, Monitoring changing desert biomass through video digitization of Landsat MSS data: An application to dust storm generation:

Photogrammetric Engineering and Remote Sensing, v. 53, p. 1251–1254.

Lyles, L., Schrandt, R.L., and Schmeidler, N.F., 1974, How aerodynamic roughness elements control sand movement: Transactions of the American Society of Agricultural Engineers, v. 17, p. 134–139.

MacKinnon, D.J., Elder, D.F., Helm, P.J., Tuesink, M.F., and Nist, C.A., 1990, A method of evaluating effects of antecedent precipitation on duststorms and its application to Yuma, Arizona, 1981–1988: Climatic Change, v. 17, p. 331–360.

Marshall, J.K., 1971, Drag measurements in roughness arrays of varying density and distribution: Agricultural Meteorology, v. 8, p. 269–192.

McDaniel, K.C., 1989, Snakeweed populations in New Mexico, 1979–1989, in Huddleston, E.W., and Pieper, R. D., eds., Snakeweed: Problems and Perspectives: New Mexico State University Agricultural Experiment Station Bulletin 751, p. 13–25.

Muhs, D.R., and Maat, P.B., 1993, The potential response of eolian sands to greenhouse warming and precipitation reduction on the Great Plains of the U.S.A.: Journal of Arid Environments, v. 25, p. 351–361.

Musick, H.B., and Gillette, D.A., 1990, Field evaluation of relationships between a vegetation structural parameter and sheltering against wind erosion: Land Degradation and Rehabilitation, v. 2, p. 87–94.

Musick, H.B., Schaber, G.G., and Breed, C.S., 1995, Use of AIRSAR to identify woody shrub invasion and other indicators of desertification in the Jornada LTER: Summaries of the Fifth Annual JPL Airborne Earth Science Workshop, January 23–26, 1995: Jet Propulsion Laboratory Publication 95-1, v. 3, p. 31–34.

———1998, AIRSAR studies of woody shrub density in semiarid rangeland: Jornada del Muerto, New Mexico: Remote Sensing of Environment, v. 66, p. 29-40.

Musick, H.B., Trujillo, S.M., and Truman, C.R., 1996, Wind-tunnel modeling of the influence of vegetation structure on saltation threshold: Earth Surface Processes and Landforms, v. 21, p. 589–605.

Pieper, R.D., and McDaniel, K.C., 1989, Ecology and management of broom snakeweed, in Huddleston, E.W., and Pieper, R.D., eds., Snakeweed: Problems and Perspectives: New Mexico State University Agricultural Experiment Station Bulletin 751, p. 1–12.

Raupach, M.R., 1992, Drag and drag partition on rough surfaces: Boundary-Layer Meteorology, v. 60, p. 375–395.

Raupach, M.R., Gillette, D.A., and Leys, J.F., 1993, The effect of roughness elements on wind erosion threshold: Journal of Geophysical Research, v. 98D, p. 3023–3029.

Thom, A.S., 1971, Momentum absorption by vegetation: Quarterly Journal of the Royal Meteorological Society, v. 97, p. 414–428.

Torell, L.A., Williams, K., and McDaniel, K.C, 1989, Probability of snakeweed die-off and invasion on rangeland, in Huddleston, E.W., and Pieper, R.D., eds., Snakeweed: Problems and Perspectives: New Mexico State University Agricultural Experiment Station Bulletin 751, p. 71–83.

van de Ven, T.A.M., Fryrear, D.W., and Spaan, W.P., 1989, Vegetation characteristics and soil loss by wind: Journal of Soil and Water Conservation, v. 44, p. 347–349.

Meteorological Influences on
Eolian Activity at the Yuma Desert
Geomet Site, Arizona, 1988–1993

By Michael R. Baudat *and* Carol S. Breed

DESERT WINDS: MONITORING WIND-RELATED SURFACE PROCESSES IN
ARIZONA, NEW MEXICO, AND CALIFORNIA

Carol S. Breed and Marith C. Reheis, *Editors*

U.S. GEOLOGICAL SURVEY PROFESSIONAL PAPER 1598–E

CONTENTS

FIGURES

TABLES

Meteorological Influences on Eolian Activity at the Yuma Desert Geomet Site, Arizona, 1988–1993

By Michael R. Baudat[1] *and* Carol S. Breed[2]

ABSTRACT

Field monitoring of wind erosion at the Yuma desert Geomet site produced a record of 201 sand-flux events and concurrent wind speeds and directions over a $5^{1}/_{2}$-year period. Sources of sand-moving winds associated with these events are identified with types of synoptic-scale and mesoscale weather systems. Local visibility data, from the Marine Corps Air Station in Yuma, Ariz. (about 9.5 mi northwest of the desert site), indicate that dust was airborne (though from uncertain sources) during several periods when sand-moving winds were recorded at the Geomet site.

Analysis of the data provides preliminary estimates of the frequency of dust-generating sand-flux events associated with specific types of weather patterns on a seasonal and yearly basis.

INTRODUCTION

Sediment-moving (effective) winds that accompany various types of synoptic-scale (large-scale) and mesoscale weather systems are monitored in the Yuma desert, southwest Arizona, by automated wind and sand-flux sensors at the Yuma Geomet station (Breed, chap. A, this volume). Helm and Breed (chap. B, this volume) document many episodes of local sediment transport associated with winds of measured speed, direction, and duration at the Yuma locality.

This chapter reports the results of a preliminary meteorological analysis of winds monitored from mid-1988 through 1993 by examining them in the regional context provided by the daily weather maps of the National Oceanic and Atmospheric Administration (NOAA). The purpose of this analysis is to relate the locally monitored sand-flux activity over the period of Geomet station record to the regional wind climatology in this most arid part of the Southwestern United States.

[1]5701 E. Villa Circle, No. 8104, Flagstaff, AZ 86004.
[2]U.S. Geological Survey (retired), 189 Wilson Canyon Rd., Sedona, AZ 86336.

PROCEDURES

SOURCES OF DATA

Information used in this analysis includes (1) a $5^{1}/_{2}$-year set of digital data recorded by the geometeorological sensors on the Yuma desert Geomet station, including the SENSIT, an automated piezoelectric sand-flux sensor described by Tigges and others (chap. H, this volume); (2) regional weather patterns interpreted from daily weather maps from the National Oceanic and Atmospheric Administration (NOAA); and (3) hourly ground observations of visibility and cloud cover from the Marine Corps Air Station (MCAS) at Yuma.

METHODS

Daily data logs for the Yuma Geomet station were examined for completeness of the record, for anomalies such as broadcast errors or sensor malfunctions, for winds above the calculated threshold speed for sand transport, and for sand-flux events recorded by the SENSIT. Records for all days, including non-eventful periods, were tracked in the data logs, and from these records a list of sand-flux events was compiled that covers the time from SENSIT installation (in May 1988) to January 1, 1994.

Certain basic criteria were applied to the SENSIT data before any set of values was considered a valid record of a sand-flux event. A sand-flux event is considered to begin when sand-flux values rise above the inactivity baseline (or background noise constant) and when the recorded wind speeds at that time are high enough to support transport, based on the calculated threshold of about 8 m/s (17.9 mi/h) for sediment movement there (Helm and Breed, chap. B, this volume). An event is considered to end when the sand-flux values return to their respective base figures. Some SENSIT signals are obviously spurious: for example, when the values for peak and average sand-flux rise above the inactivity baseline, but the independently recorded wind-speed profile for that period of time shows wind speeds well below threshold.

Spurious events are also recorded when rain strikes the SEN-SIT, but because precipitation is independently and concurrently recorded by a rain gauge, ambiguous SENSIT signals produced by raindrops can be disregarded. Elimination of such questionable events leaves an annual list of unambiguous eolian sand-flux events that forms the basis for this study.

Regional information was examined to identify synoptic weather systems that might have produced sand-moving winds in the Yuma area. Major weather features that occurred in the Southwest during each day when a sand-flux event was recorded were identified using daily weather maps from NOAA, which include surface analysis and 500-millibar winds-aloft charts. Symbology on the charts includes barometric pressure isobars, precipitation isohyets, high and low temperature data, and individual reports from primary weather stations. Weather maps based on these sources are shown in figures 1–5; each corresponds to a set of Geomet data (tables 1–5).

Types of weather systems associated with recorded eolian activity were coded (table 6), based on the first author's subjective analysis of the NOAA weather maps under the guidance of local National Weather Service meteorologists (B. Peterson, oral commun., 1992). Main sources of winds common to the Southwest were tabulated; they range from large-scale gradient winds through possible mesoscale convective processes.

These categories largely correspond to those used by Brazel and Nickling (1986) to relate dust events to weather types in southern Arizona. Differences reflect our attempt to identify as many large-scale, wind-producing systems on the charts as possible rather than including only the weather patterns responsible for dust-storm activity in a given period or area.

Additional weather information, intermediate in scale between the weather maps' regional conditions and the local conditions at the Geomet station, was obtained from the hourly observations by MCAS meteorologists in the nearby city of Yuma, Ariz.; they include cloud type, percentage of sky cover, and obstructions to visibility (blowing sand and dust). These additional data were searched for indications of mesoscale convective processes that might have affected the Yuma desert site but are not generally discernible from the large-scale data.

The growth or decline of vegetation, which corresponds to the seasonal weather conditions in the Yuma desert, is a key factor that affects the capacity of wind to move sediment (Musick, chap. D, this volume). For this reason, we have categorized the regional weather conditions by seasons designated according to the vegetation growth cycle as follows: spring, Feb. 1–May 31; Summer, June 1–Sept. 30; and fall/winter, Oct.1–Jan. 31. As a consequence, for this report, a year of data begins February 1 and ends January 31. Data on dust-producing winds, classified according to different definitions of winter and summer by different authors as

shown by Breed (chap. A, this volume, table 2), may therefore be difficult to compare.

INTERPRETATION

WEATHER PATTERNS ASSOCIATED WITH EFFECTIVE WINDS

SYNOPTIC-SCALE GRADIENT WINDS

Three synoptic-scale sources of strong winds were identified as associated with the recorded eolian activity. Any one of these large-scale patterns of weather alone can provide winds capable of sand and dust transport, but some can also set the meteorological stage for further dynamic mesoscale events. Types of large-scale weather systems associated with recorded sand-flux events in the Yuma desert are described below and illustrated with figures and recorded Geomet station data showing sand-flux activity for each weather condition.

Type 1A: multiple-pressure-center systems—(fig. 1, table 1) These are the dominant weather patterns that produce effective winds in the late winter and spring. Low-pressure centers associated with the prevailing westerlies typically migrate southeastward from the Pacific Northwest and affect the entire western region of the United States. When these lows encounter domes of high pressure, commonly resident over the Midwest and the West Coast, strong winds are generated between the pressure centers.

Type 1B: single-pressure-center systems—(type 3 of Brazel and Nickling, 1986) These are tropical disturbances, including hurricanes. Isolated high- and low-pressure centers are the most common causes of winds in the summer, fall, and winter months in the study area (fig. 2, table 2). High-pressure centers are often the dominant feature in the winter and early spring and influence the western region from the Pacific Ocean. Non-thermal low-pressure centers are influential in the fall and winter. These lows migrate in from the west and northwest and are often accompanied by strong winds and heavy precipitation.

Of particular importance are the thermal low-pressure-center systems that occur in the Southwest during the summer and early fall months (fig. 3, table 3). During these months, the higher, more direct angle of solar insolation causes intense surface heating in the Sonoran and Chihuahuan Deserts. Surface heating creates a zone of low pressure, commonly centered directly over Yuma and extending to the northwest through the San Joaquin and Sacramento Valleys of California. This thermal low may be accompanied by unseasonably high temperatures in the Great Valley as hot air is pushed along the western slope of the Sierras.

Surface heating over the desert Southwest contributes to the Arizona monsoon, as moist tropical air masses move into the southern part of the State from both the Gulf of Mexico and the Gulf of California (Bryson and Lowry, 1955; Hales, 1972; Brenner, 1974; Carleton, 1986). The mesoscale convective processes associated with this thermal activity play a major role in eolian transport in deserts of Arizona and are described in type 3, under the heading "Mesoscale Processes."

Studies of the distribution and the effectiveness of various types of storm winds in Arizona are complicated by the influence of the El Niño–Southern Oscillation (ENSO), a vast area of warm sea-surface temperatures that periodically extends from Australia to South America. This phenomenon greatly affects tropical storm generation in the Pacific and enhances the flow of moist air up the western coasts of South America, Mexico, and the United States. In the Southwest, the unusually wet winter of 1991–1992 (fig. 6) was associated with an El Niño, whose influence persisted into the summer 1992 monsoon season, with unusually heavy rains (Redmond, 1993). Webb and Betancourt (1990) suggest that the presence of an earlier El Niño also resulted in the incursion of more tropical depressions than usual, thus doubling the frequency of spring floods in southern Arizona.

Occasionally, hurricanes that occur in the late summer and early fall in the Pacific Ocean migrate up the Gulf of California and bring strong winds and substantial amounts of subtropical moisture into Arizona. The unusually heavy rains that brought severe flooding to Arizona in October 1983 during an El Niño accompanied the end stage of Octavio, a Pacific hurricane, which moved inland into Arizona toward a low-pressure center (Webb and Betancourt, 1990). Such unusually heavy rainfalls can affect vegetation growth that will tend to inhibit eolian activity during the next year's windy season, as recognized by Brazel and Nickling (1987) and MacKinnon and others (1990).

Type 1C: pressure-trough systems—(type 4 of Brazel and Nickling, 1986) These also induce winds associated with a few sand-flux events. The troughs are occasionally found associated with deep, surface low-pressure centers either preceding or following a frontal passage and are upper-level (cut-off) lows (fig. 4, table 4). They affect wind speed and direction in much the same manner as gradient winds of established circular pressure systems.

Type 2A: single pressure centers associated with frontal activity—(types 1A and 1B of Brazel and Nickling, 1986) These are common in the fall, winter, and spring (fig. 5, table 5). Although these systems often come in contact with single-pressure systems without fronts (type 1B, this paper) during the fall and winter, in the spring they share dominance with multiple-pressure systems. Associated fronts most often originate in the cold-polar-maritime and continental-air-mass source regions, located off the western coast of and in the interior of Canada, respectively. When these fronts and single-pressure centers join, the resulting systems

commonly bring increased cloud cover, higher winds, and precipitation to the Yuma desert region.

Frontal passages that move in from the north and northwest unaccompanied by single-pressure systems also influence wind speed, direction, and temperature but are relatively rare. Such systems were associated with two sand-moving events in the Yuma desert in the spring of 1992.

MESOSCALE PROCESSES

Type 3: convective processes—(type 2 of Brazel and Nickling, 1986) These occur when increased amounts of moisture and atmospheric instability from intense thermal activity cause build-ups of cumulus clouds. Synoptic conditions such as the thermal low mentioned above (fig. 3) promote development of towering cumulus clouds. Within the cumulus cells, particularly the high-base dry cells, the evaporation and condensation processes that take place as the cell matures typically produce significant downdrafts. Downdrafts occur not only from within mature cumulonimbus cells, but within cumulus of only moderate upward development as well. These bursts of cold, dry air can last from a few minutes to several hours. When the outflow of the downburst reaches the ground, it spreads laterally, causing a local cold front commonly called a gust front or pseudo-cold front. The gust front can be tracked across an area by rapid changes in wind direction and speed and by rapid cooling and rising pressure at the surface. It is at the outflow boundary of the advancing gust front that eolian transport begins, as saltating sand there typically generates an advancing wall of dust known in the Southwest (as in parts of North African deserts) as a "haboob" (Idso and others, 1972).

> Individual cell downbursts will usually last only minutes, but with numerous cells and cell regeneration, the events may seem to last for hours although oscillating in intensity. Such effects would typically happen in embedded or heavy cloud activity. With fewer clouds the oscillation would be greater, with longer periods of light wind between significant winds (B. Peterson, National Weather Service, written. commun., 1994).

In addition to examining weather maps for certain regional conditions likely to favor convection (fig. 3), local observations were reviewed for evidence of cumulus cloud formation, which indicates mesoscale convective activity. For each sand-flux event recorded at the Geomet site, the corresponding hourly observation from the Marine Corps Air Station was examined to determine the types and amounts of cloud cover reported within a 20-minute period or less surrounding the event. The presence of moderate or towering cumulus or cumulonimbus clouds, particularly to the southeast of MCAS where the Geomet station is located, indicated that conditions there were conducive to sand-flux events of convective origin. Visibility of less than 11.3 km (less than 7 mi) was also examined as evidence of blowing dust, which we considered an indicator of convective
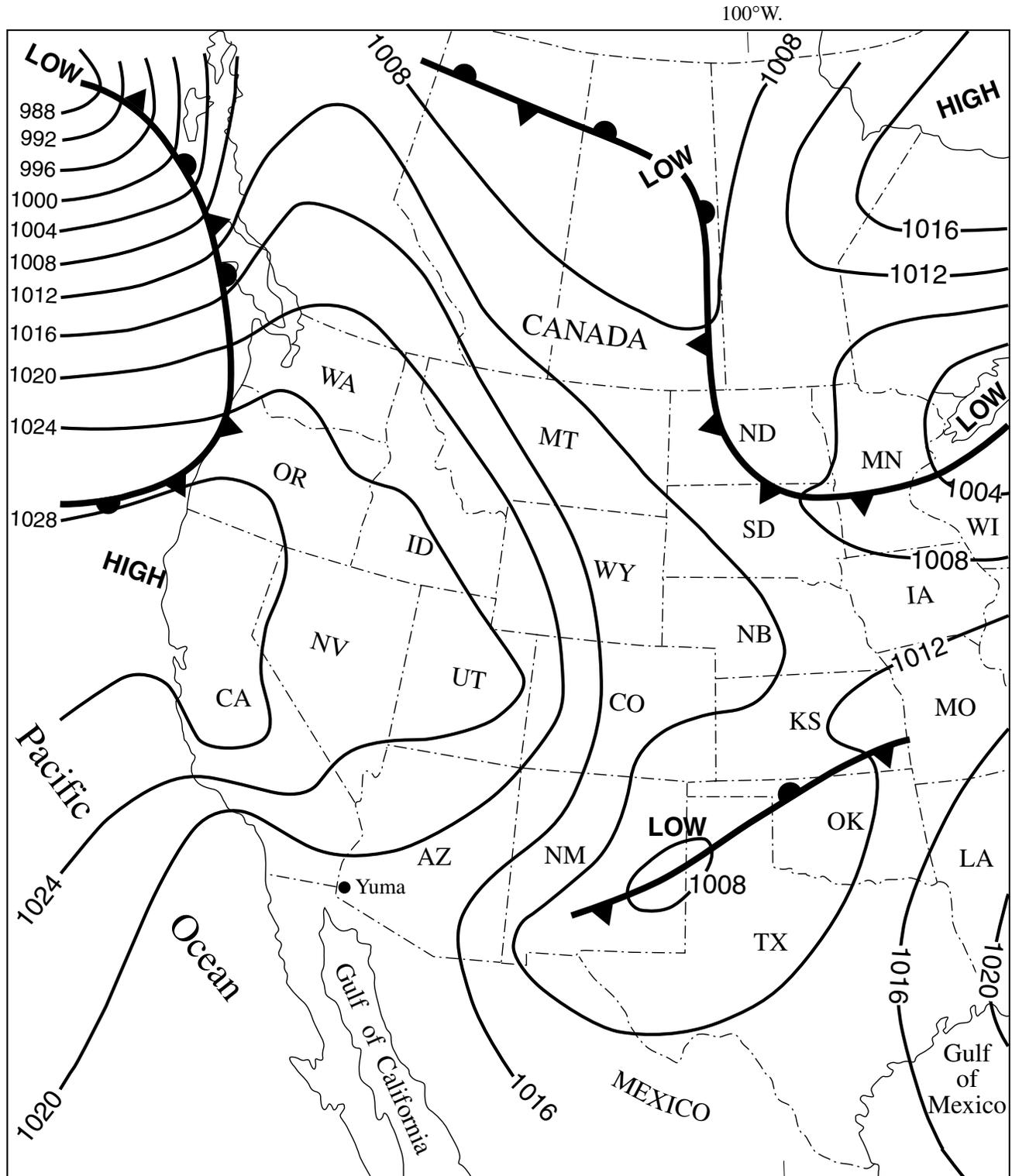
Figure 1. Weather map for January 14, 1991, showing multiple-pressure-center system (type 1A), associated with the sand-flux event shown by the Geomet data in table 1. Barometric pressure shown in millibars.

activity, although the sources of the dust could not be identified. On many of the days and even at the same times that sand-flux events were recorded at the Geomet site, visibility at Yuma MCAS was reduced by blowing sand and dust, sometimes to as low as 0.1 km (1/16 mi). Based on these

local cloud and dust observations, a total of 13 possible convective events were identified; all but one (in spring 1990) occurred in summer.

Of the seven sand-flux events identified in the summer of 1988, one event was thought to be of convective origin. In

Table 1.   Yuma Geomet station 6-minute data for January 14, 1991, from 12:03 to 15:57 m.s.t.

[During this time, winds caused by a multiple-pressure-center system (type 1A, cf. fig. 1) caused the sand-flux event recorded between 13:51 and 14:51 during the 4-hour period shown below. A strong Pacific high was in place over the Western United States, as well as a low-pressure center over New Mexico and Texas. This multiple-pressure-center system caused strong winds in most of Arizona, which was in the area between the two pressure centers, where stronger winds were generated. Time shown in hours and minutes past midnight (hhmm); Wind dir., Wind direction in degrees; h, height above ground at which measurements were made; "Wind speed" and "Peak gust" shown in miles per hour; Avg., Average]

| Time | Wind dir. | h = 6 m | | h = 2.64 m | h = 1.2 m | | Sand-flux | | Comments |
		Wind speed	Peak gust	Wind speed	Wind speed	Peak gust	Peak	Avg.	
1203	352.7	16.5	21.7	14.0	11.9	16.4	0.00	0.00	
1209	357.4	14.4	19.6	12.3	10.4	15.7	0.00	0.00	
1215	347.4	15.9	20.5	13.7	11.7	16.2	0.00	0.00	
1221	343.9	13.7	19.3	11.8	10.2	16.5	0.00	0.00	
1227	339.2	13.6	17.5	11.4	9.7	13.6	0.00	0.00	
1233	348.6	12.3	17.1	10.6	9.2	14.3	0.00	0.00	
1239	342.4	13.2	18.0	11.3	9.9	14.5	0.00	0.00	
1245	344.8	13.3	18.2	11.7	10.0	15.0	0.00	0.00	
1251	342.8	12.2	17.1	10.3	8.9	13.4	0.00	0.00	
1257	344.6	14.1	18.6	12.0	10.2	14.9	0.00	0.00	
1303	344.6	12.1	18.4	10.5	8.9	13.2	0.00	0.00	
1309	337.0	15.0	21.9	12.4	10.6	15.8	0.00	0.00	
1315	359.2	16.3	24.3	13.7	11.5	17.6	0.00	0.00	
1321	345.0	15.7	24.1	13.3	11.2	20.0	0.24	0.01	
1327	347.1	17.2	25.3	14.6	12.2	18.1	0.00	0.00	
1333	347.2	17.2	24.7	14.7	12.6	20.2	0.00	0.00	
1339	349.3	17.5	23.9	15.2	12.9	18.6	0.00	0.00	
1345	358.5	17.7	24.5	15.0	12.8	21.4	0.00	0.00	
1351	344.9	20.3	27.5	17.3	14.8	24.1	0.13	0.01	Sand-flux event.
1357	345.8	19.0	28.4	16.1	13.7	20.5	0.12	0.01	
1403	348.8	20.7	27.6	17.4	14.7	20.5	0.00	0.00	
1409	350.1	22.4	30.7	18.8	15.8	23.3	1.94	0.08	
1415	355.6	20.9	29.5	18.0	15.4	23.6	1.94	0.05	
1421	356.1	22.8	30.0	19.3	16.4	26.7	2.31	0.26	
1427	344.9	23.9	33.7	20.1	17.2	26.0	12.83	0.60	
1433	344.3	23.8	31.0	20.3	17.3	26.4	3.27	0.31	
1439	351.9	23.0	30.4	19.2	16.2	23.9	0.93	0.10	
1445	356.6	23.3	32.1	19.6	16.5	24.8	3.56	0.35	
1451	0.0	21.0	28.5	17.9	15.3	22.2	0.14	0.01	
1457	3.6	21.1	26.4	17.6	14.7	20.6	0.00	0.00	
1503	0.2	18.9	26.3	16.2	13.6	19.0	0.00	0.00	
1509	7.9	18.5	25.5	15.6	13.2	18.6	0.00	0.00	
1515	10.1	19.6	28.9	16.2	13.7	20.9	0.00	0.00	
1521	356.4	18.9	27.6	16.0	13.6	20.6	0.00	0.00	
1527	5.9	16.8	24.6	14.4	12.3	20.2	0.00	0.00	
1533	352.5	16.6	22.3	14.4	12.2	20.1	0.00	0.00	
1539	1.4	16.3	22.7	13.5	11.2	18.4	0.00	0.00	
1545	1.2	15.7	21.8	13.3	11.1	17.5	0.00	0.00	
1551	354.7	15.5	22.4	13.3	11.4	18.4	0.00	0.00	
1557	347.7	15.1	21.3	12.7	10.8	16.1	0.00	0.00	
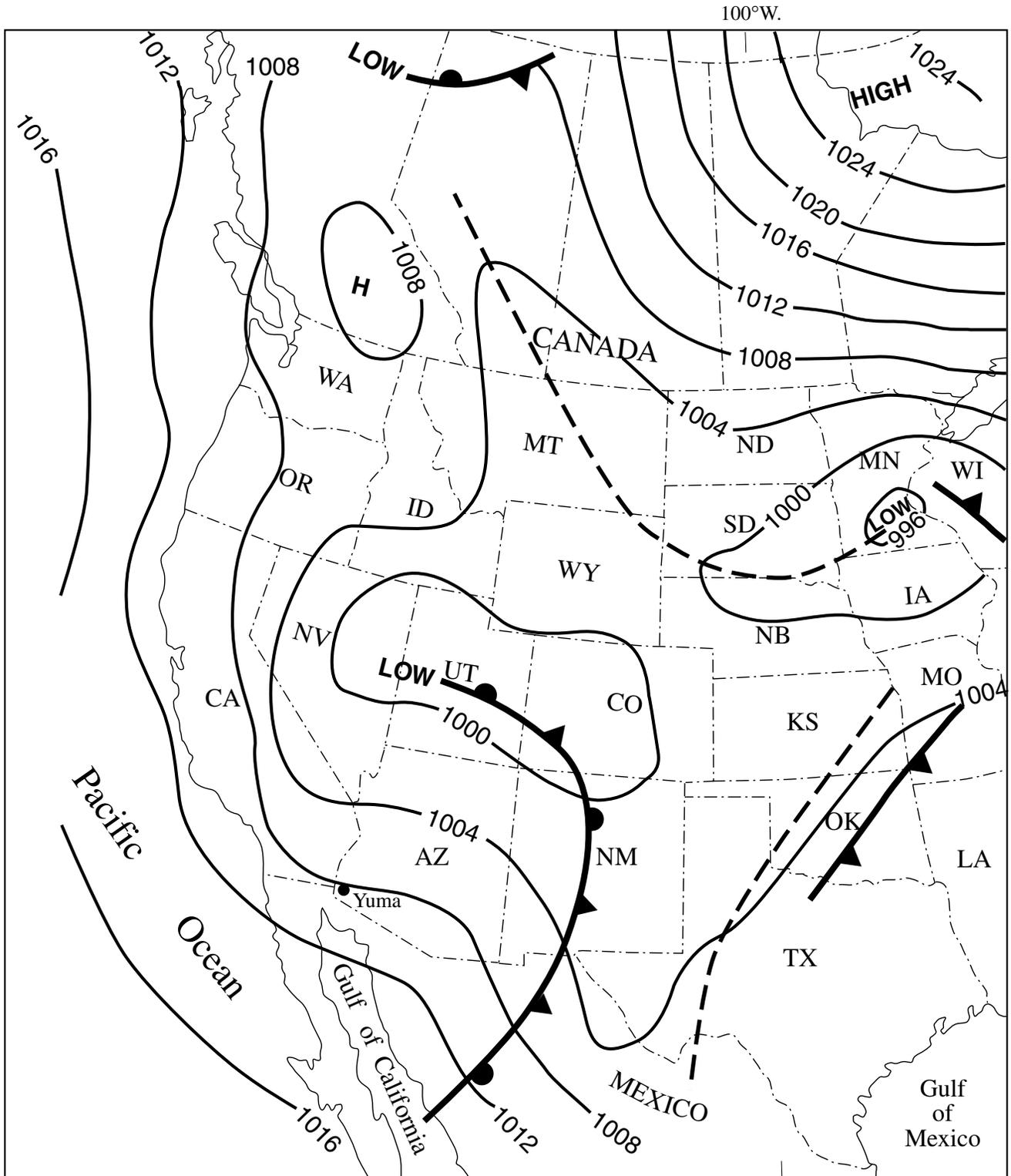
Figure 2.   Weather map for March 21, 1991, showing single-pressure-center system (type 1B, other than thermal low), associated with the sand-flux event shown by the Geomet data in table 2. Barometric pressure shown in millibars.

1989, no events were suspected to be of convective origin. In 1990, one event of 19 in the spring and four of the 18 summer events may have been convective. In 1991, five events of the 21 summer events were thought to be convective, while in 1992, none were suspect. In 1993, two events of 17 in the summer may have been of convective origin.

Table 2.   Yuma Geomet station 6-minute data for March 21, 1991, from 10:51 to 14:39 m.s.t.

[During this time, a single low-pressure center (other than thermal) of moderate strength was centered over Utah and Colorado (type 1B, cf. fig. 2). Even though an occluded front was associated with this low, its influence on the Yuma area was minimal by the time the sand-flux event shown below was recorded between 12:33 and 12:39. The winds were westerly, and speeds were erratic. Time shown in hours and minutes past midnight (hhmm); Wind dir., Wind direction in degrees; h, height above ground at which measurements were made; "Wind speed" and "Peak gust" shown in miles per hour; Avg., Average]

Time	Wind dir.	h = 6 m		h = 2.64 m	h = 1.2 m		Sand-flux		Comments
		Wind speed	Peak gust	Wind speed	Wind speed	Peak gust	Peak	Avg.	
1051	252.2	9.8	13.8	7.6	6.0	9.3	0.00	0.00	
1057	254.8	9.5	14.6	7.7	6.4	12.3	0.00	0.00	
1103	260.7	10.4	15.1	8.6	7.0	12.0	0.00	0.00	
1109	266.3	9.7	15.5	7.4	6.1	10.8	0.00	0.00	
1115	277.6	10.8	16.8	9.5	8.1	13.2	0.00	0.00	
1121	277.5	14.6	20.2	12.4	10.4	16.9	0.00	0.00	
1127	289.4	13.3	20.8	11.4	9.8	15.7	0.00	0.00	
1133	288.7	9.3	17.3	8.1	7.0	12.3	0.00	0.00	
1139	269.9	11.6	20.1	9.8	8.2	15.6	0.00	0.00	
1145	251.9	8.4	13.7	6.7	5.6	11.1	0.00	0.00	
1151	260.7	8.8	13.5	7.7	6.5	10.9	0.00	0.00	
1157	241.2	10.5	16.1	9.1	7.5	11.8	0.00	0.00	
1203	256.4	6.7	14.4	5.6	4.8	10.7	0.00	0.00	
1209	256.3	9.2	18.1	7.8	6.3	16.4	0.00	0.00	
1215	265.2	11.2	16.7	9.4	7.9	12.5	0.00	0.00	
1221	260.9	9.7	16.6	7.9	6.5	11.6	0.00	0.00	
1227	261.1	12.2	19.5	10.0	8.1	15.9	0.00	0.00	
1233	251.0	10.9	19.5	8.9	7.4	15.6	0.00	0.00	
1239	257.4	11.5	23.7	9.0	7.5	14.7	0.57	0.03	Sand-flux event.
1245	260.1	9.8	20.2	8.0	6.5	15.7	0.00	0.00	
1251	259.7	12.7	18.6	11.1	9.2	15.1	0.00	0.00	
1257	274.2	8.7	13.5	7.7	6.5	10.2	0.00	0.00	
1303	248.3	8.3	14.5	6.3	5.2	11.2	0.00	0.00	
1309	266.2	10.8	15.7	9.0	7.6	14.2	0.00	0.00	
1315	276.1	8.7	16.9	7.5	6.5	13.1	0.00	0.00	
1321	265.3	12.6	22.4	10.8	9.1	18.0	0.00	0.00	
1327	269.9	8.6	15.3	7.3	6.4	14.1	0.00	0.00	
1333	257.7	5.9	12.8	4.8	4.1	9.9	0.00	0.00	
1339	299.1	7.1	16.1	6.1	5.2	10.9	0.00	0.00	
1345	256.8	9.5	15.9	7.8	6.4	12.2	0.00	0.00	
1351	278.6	10.2	17.9	8.8	7.3	13.0	0.00	0.00	
1357	288.9	10.7	17.9	9.3	8.0	15.0	0.00	0.00	
1403	285.3	9.0	15.1	7.7	6.6	11.7	0.00	0.00	
1409	281.9	13.7	20.6	12.0	10.1	17.0	0.00	0.00	
1415	271.1	14.3	29.7	11.4	9.4	28.9	0.00	0.00	
1421	284.6	12.2	18.5	10.5	9.0	15.3	0.00	0.00	
1427	294.8	12.5	18.3	10.6	8.8	15.1	0.00	0.00	
1433	279.9	15.3	19.0	12.9	11.0	15.6	0.00	0.00	
1439	276.4	11.9	16.4	10.2	8.5	13.1	0.00	0.00	
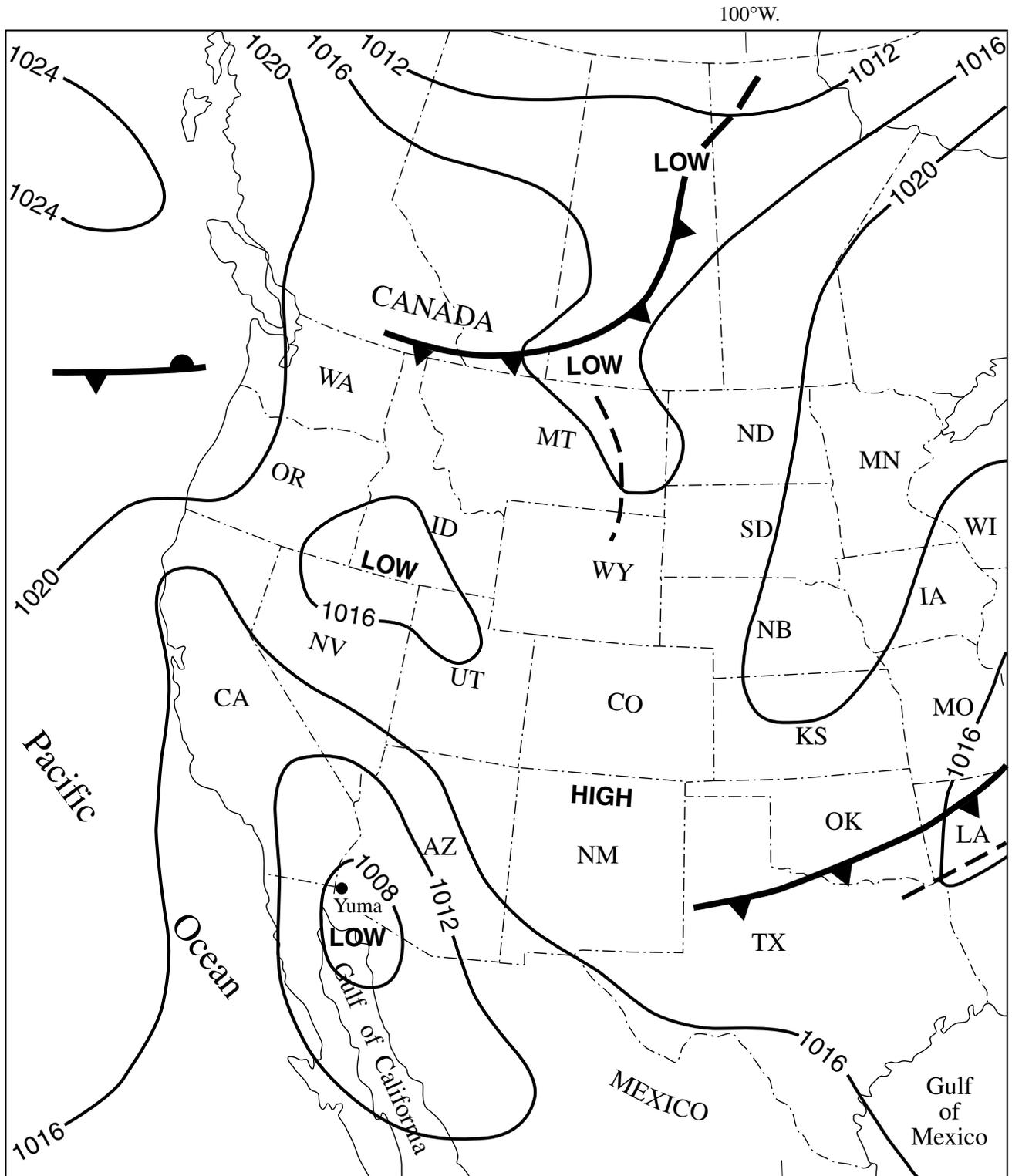
**Figure 3.**   Weather map for July 29, 1991, showing single-pressure-center system (type 1B, thermal low), associated with the sand-flux event shown by the Geomet data in table 3. Barometric pressure shown in millibars.

DETAILED ANALYSIS OF
SAND-FLUX EVENTS

The main goal of this study is to identify the sources of winds that are temporally associated with specific, recorded

sand-flux events; to track variations in wind effectiveness from season to season and year to year; and to identify apparent trends and relations between episodes of eolian activity and recorded land-surface climatological conditions. After four major types of wind-producing weather systems

Table 3. Yuma Geomet station 6-minute data for July 29, 1991, from 16:57 to 20:51 m.s.t.

[These winds were caused by the influence of a thermal low centered over the Yuma area (type 1B, cf. fig. 3) and were accompanied by recorded sand-flux activity from 18:45 to 19:09. Further wind producing/affecting mesoscale processes can occur under this synoptic condition if suitable moisture is present in the lower atmosphere (e.g., monsoonal flow). Note the variability of wind direction and speed during the 4-hour period shown below. Time shown in hours and minutes past midnight (hhmm); Wind dir., Wind direction in degrees; h, height above ground at which measurements were made; "Wind speed" and "Peak gust" shown in miles per hour; Avg., Average]

Time	Wind dir.	h = 6 m		h = 2.64 m	h = 1.2 m		Sand-flux		Comments
		Wind speed	Peak gust	Wind speed	Wind speed	Peak gust	Peak	Avg.	
1657	251.0	7.6	13.0	6.1	5.0	9.9	0.00	0.00	
1703	237.4	6.5	9.2	5.2	4.5	7.7	0.00	0.00	
1709	252.0	6.3	11.6	5.1	4.3	8.7	0.00	0.00	
1715	213.6	9.0	12.4	7.6	6.3	9.2	0.00	0.00	
1721	208.2	7.1	10.9	6.0	5.0	8.3	0.00	0.00	
1727	229.0	6.2	10.4	4.7	4.0	7.7	0.00	0.00	
1733	225.3	7.9	13.5	6.2	5.2	10.9	0.00	0.00	
1739	231.9	8.3	12.0	6.1	4.8	8.3	0.00	0.00	
1745	223.1	8.2	11.5	6.9	5.7	9.2	0.00	0.00	
1751	192.4	8.3	11.5	7.2	6.1	9.5	0.00	0.00	
1757	199.1	9.7	13.7	8.5	7.1	9.8	0.00	0.00	
1803	202.2	8.6	14.3	7.6	6.3	11.0	0.00	0.00	
1809	186.6	9.0	12.5	7.8	6.4	9.4	0.00	0.00	
1815	178.7	11.7	20.8	9.9	8.3	15.0	0.00	0.00	
1821	184.1	13.0	19.6	11.4	9.4	14.5	0.00	0.00	
1827	168.7	12.2	18.3	10.6	8.8	12.7	0.00	0.00	
1833	164.6	12.3	17.4	10.8	9.2	15.1	0.00	0.00	
1839	175.9	15.4	20.9	13.2	11.0	18.5	0.00	0.00	
1845	162.1	15.7	35.9	13.6	11.6	27.6	0.84	0.05	Sand-flux event.
1851	130.1	20.6	28.5	17.9	15.1	22.2	0.47	0.01	
1857	138.4	22.4	29.2	19.1	16.1	24.5	1.26	0.18	
1903	134.8	20.3	27.9	17.4	14.5	22.7	1.49	0.08	
1909	138.5	20.1	28.4	17.6	14.9	22.6	0.20	0.02	
1915	142.8	18.9	25.9	16.2	13.6	18.5	0.00	0.00	
1921	140.1	18.7	27.1	16.1	13.6	21.1	0.00	0.00	
1927	149.8	16.2	24.7	13.6	11.7	18.5	0.00	0.00	
1933	158.2	14.6	20.7	12.5	10.7	16.4	0.00	0.00	
1939	164.4	13.3	18.5	11.4	9.5	14.1	0.00	0.00	
1945	168.3	12.2	15.9	10.4	8.9	12.9	0.00	0.00	
1951	180.0	9.8	13.2	8.4	7.0	10.6	0.00	0.00	
1957	179.9	6.6	8.9	5.5	4.6	6.6	0.00	0.00	
2003	174.1	6.8	10.1	5.5	4.5	7.1	0.00	0.00	
2009	170.6	7.0	10.3	5.7	4.8	7.7	0.00	0.00	
2015	150.3	9.0	12.7	7.4	6.3	8.8	0.00	0.00	
2021	123.6	12.5	22.1	10.7	9.1	16.0	0.00	0.00	
2027	121.0	22.7	31.8	19.5	16.3	23.0	0.00	0.00	
2033	119.4	20.7	29.4	17.7	14.7	23.7	0.00	0.00	
2039	122.3	19.7	27.9	17.3	14.3	21.0	0.00	0.00	
2045	124.5	17.3	24.4	14.9	12.6	18.7	0.00	0.00	
2051	128.0	18.2	24.8	15.6	13.2	19.1	0.00	0.00	
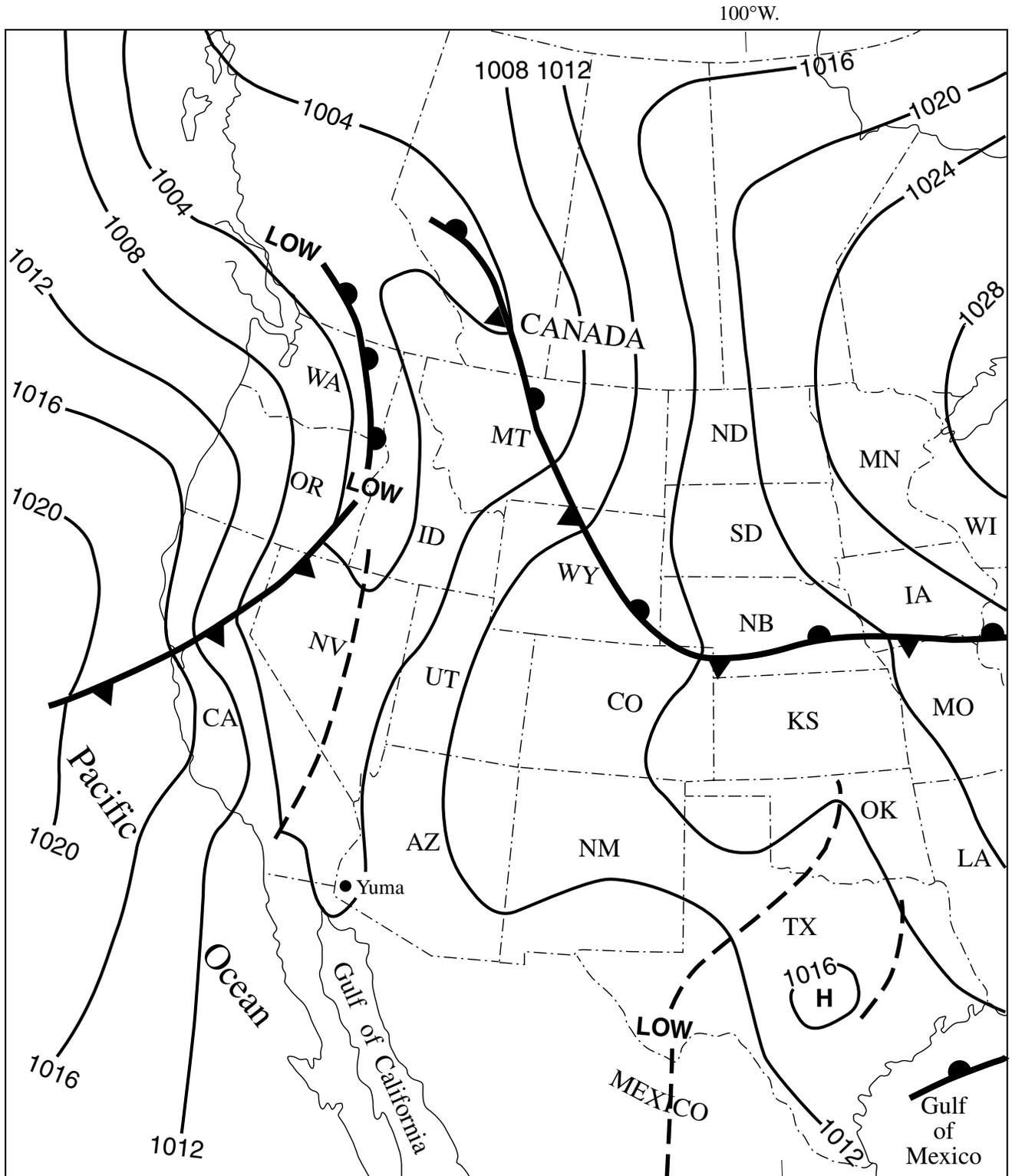
Figure 4.   Weather map for May 8, 1991, showing pressure-trough system (type 1C), associated with sand-flux event shown by Geomet data in table 4. Barometric pressure shown in millibars.

associated with sand-flux events (table 6) were identified based on analysis of the regional data, the local Geomet data were examined for seasonal and yearly trends and relations. A total of 201 unambiguous sand-flux events were recorded by the SENSIT (Tigges and others, chap. H, this volume) during the $5^1/_2$-year period (fig. 7). Comparison of the frequency of events shows a wide variation from year to year. Numbers of events for 1988–1992 should not be compared

Table 4. Yuma Geomet station 6-minute data for May 8, 1991, from 12:27 to 16:21 m.s.t.

[The winds on this day were caused by a passage of a pressure trough through the Yuma area during mid-morning (type 1C, cf. fig. 4). Even though the sand-flux event this day was short (from 14:15 to 14:27), strong winds were present throughout most of the day. Time shown in hours and minutes past midnight (hhmm); Wind dir., Wind direction in degrees; h, height above ground at which measurements were made; "Wind speed" and "Peak gust" shown in miles per hour; Avg., Average]

| Time | Wind dir. | h = 6 m | | h = 2.64 m | h = 1.2 m | | Sand-flux | | Comments |
		Wind speed	Peak gust	Wind speed	Wind speed	Peak gust	Peak	Avg.	
1227	168.9	16.7	25.2	14.9	12.5	19.6	0.00	0.00	
1233	160.6	16.1	25.0	13.9	11.9	18.6	0.00	0.00	
1239	172.3	18.0	26.2	15.5	13.1	19.9	0.00	0.00	
1245	162.1	15.9	22.8	14.0	11.8	17.4	0.00	0.00	
1251	164.6	15.1	21.2	12.8	11.0	16.2	0.00	0.00	
1257	170.7	16.5	25.0	14.4	12.1	20.7	0.00	0.00	
1303	164.7	17.8	22.6	15.3	12.8	18.3	0.00	0.00	
1309	160.1	16.2	23.9	14.2	12.2	18.7	0.00	0.00	
1315	164.2	18.6	27.5	16.1	13.5	20.3	0.00	0.00	
1321	166.7	17.0	25.3	14.7	12.3	19.9	0.00	0.00	
1327	174.2	17.1	23.7	14.9	12.5	19.9	0.00	0.00	
1333	167.9	15.8	25.4	13.3	11.2	20.4	0.00	0.00	
1339	168.0	16.7	23.5	14.7	12.5	19.6	0.00	0.00	
1345	172.7	16.2	25.1	14.2	12.0	17.6	0.00	0.00	
1351	162.6	19.4	27.4	17.0	14.4	21.1	0.00	0.00	
1357	170.8	17.7	28.1	15.1	12.6	20.4	0.00	0.00	
1403	161.7	17.9	24.2	15.5	13.3	19.5	0.00	0.00	
1409	169.5	18.1	26.1	15.7	13.2	21.4	0.00	0.00	
1415	161.6	19.0	29.8	16.6	14.2	23.4	2.83	0.16	Sand-flux event.
1421	170.9	16.6	25.1	14.5	12.3	19.9	0.00	0.00	
1427	165.8	18.7	28.7	16.2	13.8	23.1	0.78	0.05	
1433	166.0	17.1	25.3	14.9	12.5	18.6	0.00	0.00	
1439	177.5	17.6	23.5	15.2	12.8	19.9	0.00	0.00	
1445	171.8	17.5	26.9	15.2	12.7	20.3	0.00	0.00	
1451	179.2	19.0	28.5	16.6	14.0	24.4	0.00	0.00	
1457	167.8	18.2	27.7	15.8	13.3	24.4	0.00	0.00	
1503	165.0	19.2	27.6	16.5	13.9	21.3	0.00	0.00	
1509	168.4	19.9	28.8	17.1	14.4	21.1	0.00	0.00	
1515	165.5	17.3	24.4	15.0	12.6	18.0	0.00	0.00	
1521	161.3	18.3	24.4	15.7	13.3	18.0	0.00	0.00	
1527	162.5	17.4	27.0	15.2	12.9	23.5	0.00	0.00	
1533	161.4	18.0	27.5	15.6	13.2	19.4	0.00	0.00	
1539	172.3	17.8	26.1	15.5	12.9	20.3	0.00	0.00	
1545	163.1	18.5	26.1	16.0	13.4	20.7	0.00	0.00	
1551	162.5	16.7	24.1	14.3	12.1	18.1	0.00	0.00	
1557	166.2	20.2	26.1	17.5	14.8	19.6	0.00	0.00	
1603	173.6	16.5	23.1	14.2	11.9	16.7	0.00	0.00	
1609	165.0	16.9	24.0	14.8	12.3	20.4	0.00	0.00	
1615	168.9	17.5	24.7	15.0	12.8	19.8	0.00	0.00	
1621	168.4	19.8	25.6	17.2	14.5	20.7	0.00	0.00	
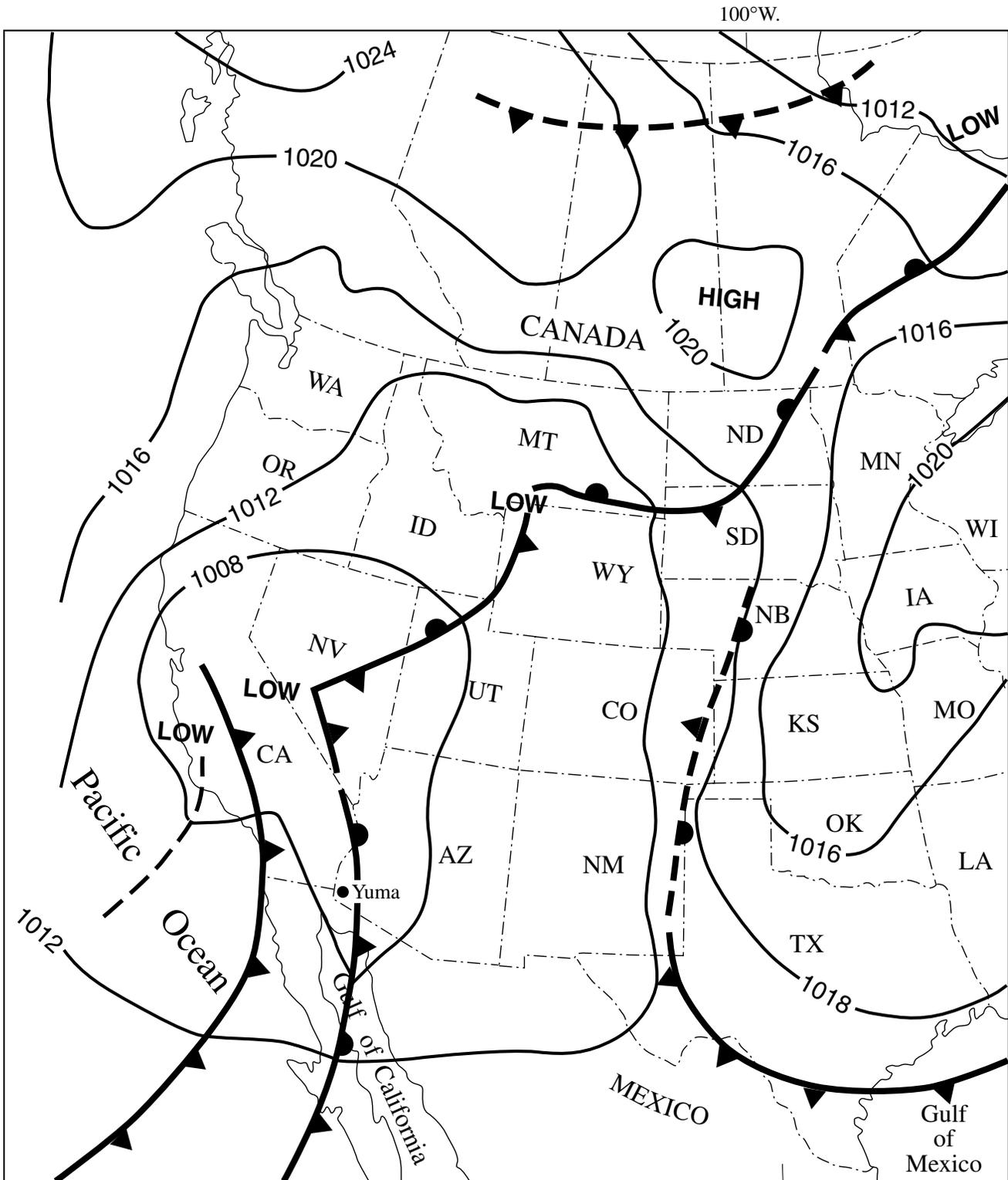
Figure 5. Weather map for March 26, 1993, showing pressure-center system with frontal activity (type 2A), associated with sand-flux event shown in Geomet data in table 5. Barometric pressure shown in millibars.

directly or uncritically with the number of events recorded in 1993, when a SENSIT of much greater sensitivity replaced the original SENSIT. However, when the frequency of sand-flux events each year is examined by seasons (fig. 8), the numbers remain surprisingly constant from season to season.

Table 5. Yuma Geomet station 6-minute data for March 26, 1993, from 06:51 to 10:45 m.s.t.

[On this day, winds were caused by a weak low-pressure center with two cold fronts that was in place over the southwestern portion of the country (type 2A, cf. fig. 5). The second frontal passage began around 08:45 with the sand-flux event beginning just prior to the front moving through and sporadically continuing into the next hour. The frontal passage was evident by substantial changes in wind direction and wind speeds (see data below) as well as a drop in air temperature (not shown). Time shown in hours and minutes past midnight (hhmm); Wind dir., Wind direction in degrees; h, height above ground at which measurements were made; "Wind speed" and "Peak gust" shown in miles per hour; Avg., Average]

Time	Wind dir.	h = 6 m		h = 2.64 m	h = 1.2 m		Sand-flux		Comments
		Wind speed	Peak gust	Wind speed	Wind speed	Peak gust	Peak	Avg.	
0651	135.6	10.2	14.4	8.8	7.0	11.9	0.65	0.64	
0657	131.6	9.1	13.3	7.7	6.1	9.2	0.65	0.65	
0703	128.1	8.5	12.2	7.2	5.8	8.1	0.65	0.65	
0709	129.2	8.9	12.8	7.4	6.1	9.8	0.65	0.65	
0715	129.9	8.8	12.2	7.3	5.9	7.9	0.65	0.65	
0721	127.6	9.3	12.5	7.7	6.2	9.1	0.65	0.64	
0727	130.8	9.4	12.9	8.1	6.4	9.7	0.65	0.64	
0733	136.4	9.2	12.4	7.6	6.0	9.5	0.65	0.65	
0739	136.5	9.5	13.2	7.9	6.4	10.4	0.65	0.64	
0745	136.2	11.0	15.2	9.5	7.7	12.3	0.65	0.64	
0751	139.5	10.7	14.6	9.1	7.5	10.6	0.65	0.64	
0757	139.9	10.1	14.6	8.7	7.0	10.7	0.66	0.64	
0803	138.1	11.3	19.1	9.5	7.4	13.7	0.66	0.63	
0809	139.9	11.3	16.5	9.8	8.0	12.7	0.66	0.63	
0815	143.7	12.7	16.1	10.7	8.8	13.8	0.67	0.65	
0821	151.1	11.5	16.4	9.8	8.0	12.4	0.68	0.65	
0827	148.7	12.1	16.6	10.3	8.5	13.2	0.67	0.65	
0833	154.3	11.1	14.5	9.8	8.1	11.7	0.67	0.65	
0839	151.3	11.4	15.9	9.6	7.9	11.4	0.71	0.64	Sand-flux event.
0845	157.3	11.2	15.7	9.7	8.0	12.7	0.69	0.67	
0851	266.8	8.9	15.9	7.6	6.2	11.7	0.75	0.68	
0857	297.7	19.8	27.7	16.9	13.8	22.4	0.74	0.69	
0903	304.7	18.3	25.6	15.3	12.2	21.1	0.69	0.66	
0909	303.2	17.4	24.1	14.9	12.0	17.8	0.67	0.66	
0915	309.7	18.6	24.8	15.4	12.2	16.4	0.67	0.66	
0921	312.4	16.8	23.4	14.2	11.3	17.2	0.71	0.68	
0927	314.7	16.4	24.1	13.5	10.7	18.3	0.68	0.66	
0933	319.8	16.8	23.3	13.9	11.3	18.0	0.67	0.66	
0939	314.5	15.2	24.0	12.7	10.1	19.0	0.67	0.66	
0945	307.3	14.4	19.3	11.9	9.2	14.5	0.66	0.65	
0951	314.8	13.2	20.1	11.0	8.8	15.6	0.67	0.65	
0957	304.9	15.0	22.6	12.5	9.9	18.7	0.67	0.65	
1003	311.7	19.4	28.2	16.1	12.7	21.5	0.68	0.66	
1009	316.8	17.5	25.2	14.6	11.8	18.2	0.67	0.65	
1015	316.0	13.4	19.2	11.1	9.2	14.0	0.66	0.65	
1021	315.2	16.9	23.0	14.3	11.1	18.3	0.68	0.66	
1027	308.6	16.7	24.9	14.4	11.6	18.8	0.67	0.65	
1033	311.8	15.8	22.0	13.2	10.3	17.4	0.67	0.65	
1039	312.6	14.6	21.0	12.1	9.6	14.1	0.67	0.66	
1045	307.6	12.7	17.9	10.9	8.8	14.0	0.67	0.65	

Table 6. Synoptic coding of sand-flux events.

SYNOPTIC-SCALE GRADIENT WINDS	
A.	Multiple pressure systems (common in spring) (fig. 1).
B.	Singular pressure center (including tropical storms and cyclones) other than thermal (fig. 2), and thermal lows (fig. 3).
C.	Pressure trough(s) (fig. 4).
FRONTAL ACTIVITY	
A.	Front(s) associated with pressure center(s) (fig. 5).
B.	Isolated front(s) (any season).
MESOSCALE CONVECTIVE PROCESSES (INCLUDING ARIZONA MONSOONS)	
	Air-mass thunderstorms (increased activity in summer and fall) and high-base, dry thunderstorms where downbursts may occur (fig. 3).

In this analysis, no one time of year stands out dramatically for blowing sand and dust in the Yuma desert. This result contrasts with the findings of Brazel and others (1986). Their monthly data, when tabulated according to the seasons defined in this report, indicate much higher percentages of time that dust blew in spring and summer months than in fall/winter months (as recorded by the National Weather Service station at the Yuma International Airport, next to MCAS). Their frequencies (number of storms) are, however, listed not monthly but by seasons (Nickling and Brazel, 1984) that differ from ours (their

mean winter is October–May, although their summer is the same (June–September); numbers of storms per "season" are thus not directly comparable). Some differences may be explained by the visibility criteria chosen to define dust-producing events: Nickling and Brazel (1984), for example, show a greater number of events in their winter (1992) than in summer when the 11.3-km visibility criterion is used, but a greater number in summer than in winter when the more restrictive 1.6-km or 1.0-km visibility criterion is used. Using the 11.3-km visibility criterion from MCAS to identify dust-producing events that affected Yuma during the $5\frac{1}{2}$-year period of this report, 55 events occurred in all of the spring months combined, compared with 64 in the summer months, and 84 in the fall/winter months. These data suggest that dust production in the
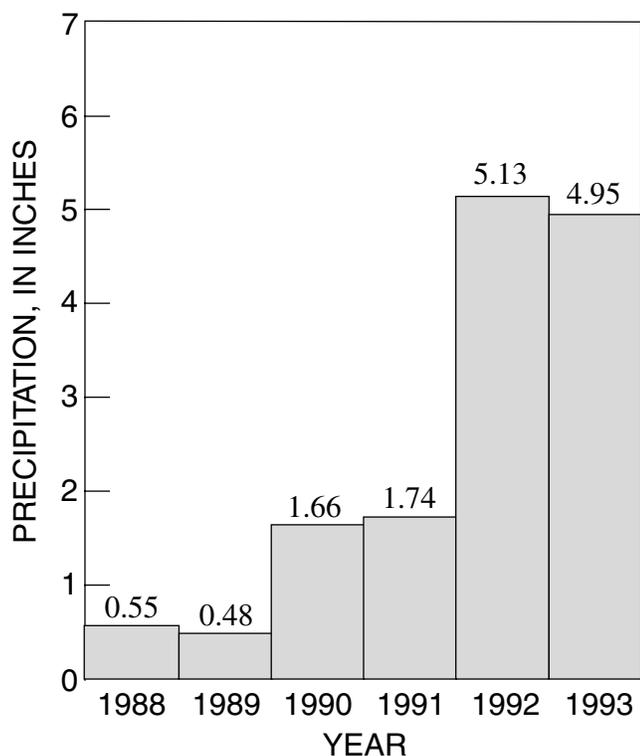

Figure 6. Yuma Geomet station annual precipitation May 1988–December 1993. 1988 records only a partial year of precipitation.
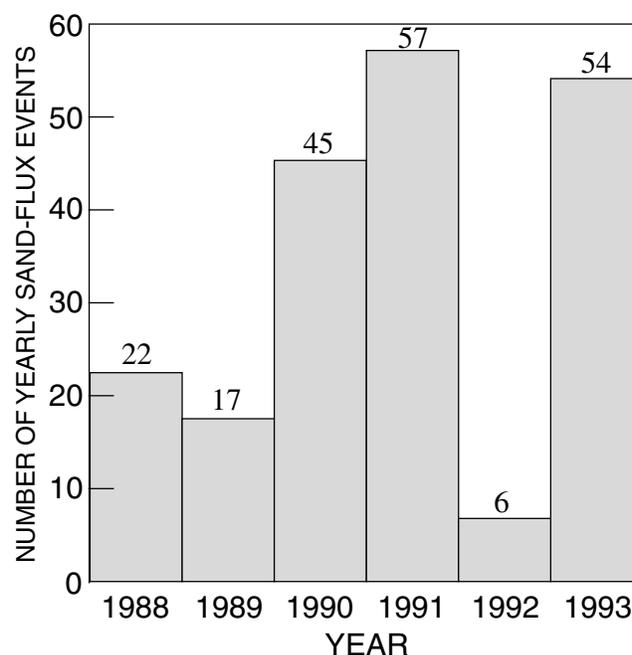

Figure 7. Number of yearly sand-flux events, Yuma Geomet station (201 total). (Data for 1988 are for May through January).
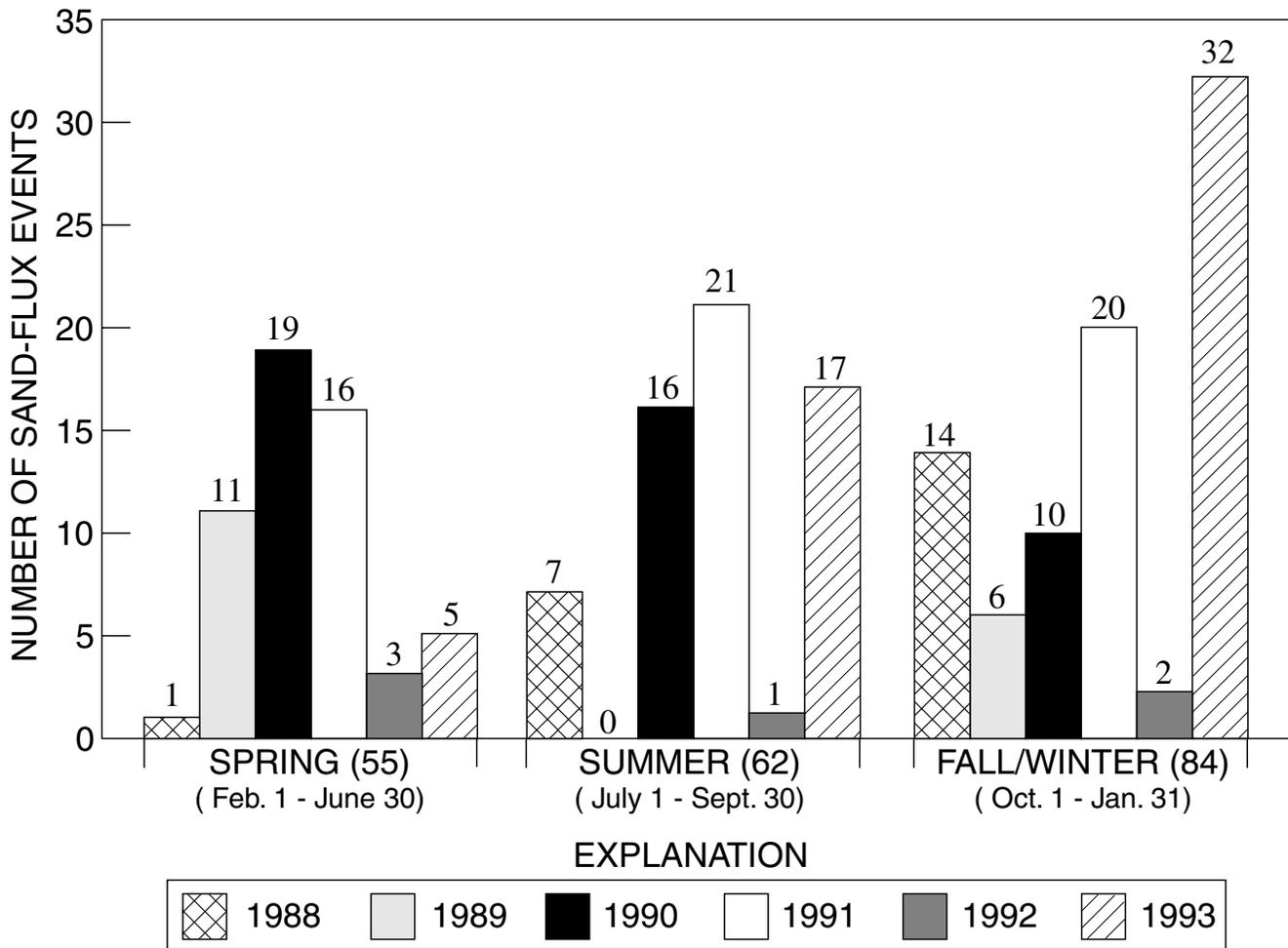
Figure 8.   Number of sand-flux events per season per year, Yuma Geomet station. (Data for 1988 are for May through January.)

Yuma area, in the extreme southwest corner of the Sonoran Desert (figs. 1, 9, Breed, chap. A, this volume), is more influenced by winter storms, which dominate the weather patterns of the Mojave Desert, than by winds associated with summer thunderstorms, which dominate weather patterns in more easterly parts of the Sonoran Desert.

RECORDED EOLIAN EVENT FREQUENCIES CATEGORIZED BY WEATHER-SYSTEM TYPES

In the year-by-year analysis of sand-flux events and their probable source winds, the numbers of events per year (event frequencies) have been sorted according to the different types of weather systems associated with them (figs. 9–11). Only cautious yearly comparisons can be made because various equipment breakdowns and satellite-relay failures caused occasional losses of Geomet data (Tigges and others, chap. H, this volume).

Beginning in May 1988, the sand-flux events in the remaining months of that year were associated with three of

the four types of dominant synoptic-scale systems. Multiple-pressure-center systems accompanied five events: one in the summer and four in the fall and winter. Single-pressure-center systems were associated with 12 events: six in the summer and six in the fall and winter. Single-center systems with fronts accompanied five events: one in the spring and four in the fall and winter.

In 1989 the SENSIT was down during the summer months, but for the rest of the year, recorded events were accompanied by winds associated with the same types of synoptic-scale weather systems as in 1988. Multiple-pressure-center systems were associated with six events: two in the spring and four in the fall and winter. Single-pressure-center systems were associated with four events: three in the spring and one in the fall and winter. Single-center systems with fronts accompanied seven events: six in the spring and one in the fall and winter.

Two years of high-frequency eolian activity occurred in 1990 and 1991. In 1990, 45 events were recorded. Multiple-pressure systems were associated with nine events: four in spring, one in summer, and four in the fall and winter. Single

Figure 9. Association of weather types with sand-flux events recorded during spring (Feb. 1–May 31) 1989–1993 (no data for 1988).


Figure 10. Association of weather types with sand-flux events recorded during summer (June 1–Sept. 30), 1988–1993.

Figure 11. Association of weather types with sand-flux events recorded during fall/winter (Oct. 1–Jan. 31), 1988–1993.

and 10 in the fall and winter. Pressure troughs accompanied two events in the spring.

In sharp contrast to 1990 and 1991, in 1992 (fig. 7) the SENSIT recorded far fewer (six) sand-flux events. Multiple-pressure-center systems were associated with only one event in the fall and winter. Single-pressure centers accompanied two events: one in spring and one in the summer. A single-pressure center with a front was associated with one event in the fall and winter, and isolated fronts accompanied two events in the spring.

Numbers of sand-flux events recorded in 1993 suggest a surprisingly high frequency of eolian activity, but are undoubtedly biased by the replacement of an older SENSIT with a new model with greater sensitivity. Multiple-pressure-center systems were associated with four events, all in the fall and winter seasons that are characteristically associated with this weather pattern. Single-pressure-center systems were by far the most numerous, with 43 occurrences: two in the spring, 17 in the summer (most of which were thermal lows), and 24 in the fall and winter. A pressure trough was associated with one event in the spring. Pressure centers with fronts accompanied six events: two in the spring and four in the fall and winter.

EFFECTS OF RAINFALL

When the annual frequency of eolian events is compared with annual rainfall (figs. 6, 7), the effects of precipitation are evident. Sand-flux activity was highest during drier years. Precipitation records and repeat photography, which show the changes in vegetation at the site (fig. 3, in Musick, chap. D, this volume), strongly suggest inhibition of the effectiveness of winds during a

centers were associated with a very high frequency, totaling 24 events: five in spring, 16 in summer, and three in the fall and winter. Single centers with fronts accompanied 12 events: nine in spring and three in the fall and winter.

A second year of high-frequency eolian activity (57 events) followed in 1991. Multiple-pressure-center systems were associated with eight events: two in spring, one in summer, and five in the fall and winter. Single-pressure-center systems again were associated with a very high frequency of 26 events: two in spring, 19 in summer, and five in the fall and winter. Single-pressure centers with fronts accompanied 21 events: 10 in spring, one in summer,

period that began in late 1991 and continued throughout 1992 and into 1993. Precipitation for the years 1988 through 1991 was below the 63.5 mm (2.5 inch) mean annual amount, but in the El Niño year of 1992 the Yuma Geomet site received 103.63 mm (4.08 in)—nearly twice the mean annual amount, and an even greater amount in 1993 (fig. 6). Following the return of rains in the fall of 1991, a marked increase in the vegetation density at the site was documented (Musick, chap. D, this volume). As a probable result of the protective effect of the vegetation cover, eolian activity was greatly diminished in 1992 and 1993. Field data from the Geomet site thus supports the conclusions of Brazel and Nickling (1986) and Brazel and others (1986) regarding the inhibiting effect of long-term (past winters') antecedent moisture on dust generation in southern Arizona.

SUMMARY AND CONCLUSIONS

Previous work (Nickling and Brazel, 1984; Brazel and others, 1986; Brazel and Nickling, 1987) related dust storms in Arizona to certain types of weather, based on analysis of meteorological data from NOAA weather maps and standard weather stations. This report provides additional evidence of these relations by incorporating the results of a field monitoring experiment at the Yuma desert Geomet site. There, episodes of eolian sand transport (sand-flux events) were recorded concurrently with wind speeds and directions over a period of more than 5 years. In this report, sources of the winds associated with the sand-flux events are identified with several types of synoptic-scale and mesoscale weather systems by inspection of daily weather maps from NOAA and by inference from hourly observations of visibility and cloud data recorded at the nearby MCAS station in Yuma. Some of the MCAS observations suggest that several recorded sand-flux events at the Geomet site were accompanied by blowing dust in the area, although the sources of dust are not known.

Analyses of these data provide preliminary estimates of the frequency of dust-generating sand-flux events associated with specific types of wind sources (weather patterns) on a seasonal and yearly basis. Sand-flux events and associated blowing dust are produced year-round by winds associated with several different types of weather systems that occur in a fairly regular pattern. However, numbers of events, by season, and relative effectiveness of different weather systems show wide variations from year to year. We attribute the large interannual variations in event frequency to the effects of vegetation growth enhanced by the previous year's precipitation (long-term antecedent precipitation as recognized by Brazel and others, 1986; MacKinnon and others, 1990; discussed by Wolfe and Helm, chap. C, this volume; Musick, chap. D, this volume). Assessments of normal variability are complicated, however, by the occurrence of a major ENSO, beginning in the winter of 1991–1992 and continuing

through 1993, which brought unusually heavy rainfall to the Yuma desert. In 1992, and continuing through the spring of 1993, sand-flux events at the Yuma site became markedly less frequent (although following a change in the monitoring equipment in 1993 sand-flux event frequency is apparently much higher than in earlier years). We consider the non-ENSO years of 1988–1991 to be representative of the rainfall amounts normally expected in this area, which is classified according to the Budyko aridity index (Henning and Flohn, 1977) as the most arid in the United States. Continued monitoring of sand-flux events beyond the 1992–1993 El Niño will document the lag time that occurs before reestablishment of an active eolian regime under normal meteorological conditions in the Yuma desert.

REFERENCES CITED

Brazel, A.J., and Nickling, W.G., 1986, The relation of weather types to dust storm generation in Arizona (1965–1980): Journal of Climatology, v. 6, p. 255–275.

———1987, Dust storms and their relation to moisture in the Sonoran-Mojave Desert region of the Southwestern United States: Journal of Environmental Management, v. 24, no. 3, p. 279–291.

Brazel, A.J., Nickling, W.G., and Lee, Jeffery, 1986, Effect of anecedent moisture conditions on dust storm generation in Arizona, *in* Nickling, W.G., ed., Aeolian Geomorphology: Boston, Allen and Unwin, p. 261–271.

Brenner, I.S., 1974, A surge of maritime tropical air—Gulf of California to the Southwest United States: Monthly Weather Review, v. 102, no. 5, p. 375–389.

Bryson, R.A., and Lowry, W.P., 1955, The synoptic climatology of the Arizona summer precipitation singularity: Bulletin of the American Meteorological Society, v. 36, p. 329–339.

Carleton, A.M., 1986, Synoptic-dynamic character of "bursts" and "breaks" in the Southwest U.S. summer precipitation singularity: Journal of Climatology, v. 6, p. 605–623.

Hales, J.E., Jr., 1972, Surges of maritime tropical air northward over the Gulf of California: Monthly Weather Review, v. 100, p. 298–306.

Henning, D., and Flohn, H., 1977, Climate aridity index map: United Nations Conference on Desertification. [Nairobi, Kenya, U.N. Environment Programme].

Idso, S.B., Ingram, R.S., and Pritchard, J.M., 1972, An American haboob: Bulletin American Meteorological Society, v. 53, p. 930–935.

MacKinnon, D.J., Elder, D.F., Helm, P.J., Tuesink, M.F., and Nist, C.A., 1990, A method of evaluating effects of antecedent precipitation on duststorms and its application to Yuma, Arizona, 1981–1988: Climatic Change, v. 17, p. 331–360.

Nickling, W.G., and Brazel, A.J., 1984, Temporal and spatial characteristics of Arizona dust storms (1965–1980): Journal of Climatology, v. 4, p. 645–660.

Redmond, K.T., 1993, Climatic impacts of the 1991–92 western winter, *in* Redmond, K. T., and Tharp, V. L., eds., Proceedings of the Ninth Annual Pacific Climate (PACLIM) Workshop, April 21–22, 1992: California Department of Water Resources,

Interagency Ecological Studies Program, Technical Report 34, p. 123–132.

Webb, R.H., and Betancourt, J.L., 1990, Climatic effects on flood frequency: An example from southern Arizona, *in* Betancourt, J.L., and MacKay, A.M., eds., Proceedings of the Sixth Annual Pacific Climate (PACLIM) Workshop, March 5–8, 1989: California Department Water Resources, Interagency Ecological Studies Program Technical Report 23, p. 61–66.

Remote-Sensing (Landsat MSS) Record of Vegetation Changes in the Yuma Desert, Arizona, 1980–1988

By J.K. Crowley *and* T.L. Bowers

DESERT WINDS: MONITORING WIND-RELATED SURFACE PROCESSES IN
ARIZONA, NEW MEXICO, AND CALIFORNIA

Carol S. Breed and Marith C. Reheis, *Editors*

U.S. GEOLOGICAL SURVEY PROFESSIONAL PAPER 1598–F

CONTENTS

FIGURES

TABLES

Remote-Sensing (Landsat MSS) Record of Vegetation Changes in the Yuma Desert, Arizona, 1980–1988

By J.K. Crowley[1] *and* T.L. Bowers[2]

ABSTRACT

Sixteen Landsat multispectral scanner (MSS) scenes acquired from 1980–1988 were used to study Sonoran Desert vegetation in the vicinity of an automated Geomet (geological and meteorological) monitoring station near Yuma, Ariz. The MSS data were coregistered and calibrated to reflectance using ground targets and then used to construct a time-series of normalized difference vegetation index (NDVI) images. Both spatial and temporal variations in NDVI values were observed in the study area, including unexpected spatial patterns associated with differences in the timing of NDVI maxima. NDVI variations at the Geomet site were examined in conjunction with the available station precipitation, temperature, and wind-speed measurements. The results indicate that, taken individually, climatic variables show only weak correlations with NDVI variations. This points to more complex interactions as important determinants of plant growth, including coupled temperature, wind, and surficial geologic effects on soil moisture. Modeling studies are needed to examine such interactions and to better define the role of other biologic factors, such as seed-germination inhibitors, in controlling Sonoran vegetation response to climatic stimuli.

INTRODUCTION

The sensitivity of desert soils and vegetation cover to human disturbance and to changing climatic conditions is an important global change research issue. Every continent contains stabilized eolian sand and (or) dust deposits, many of which are vulnerable to reactivation by climatic changes or adverse land management practices. In view of this potential problem, it is desirable to understand the climatic factors and surficial processes that control desert soil and vegetation stability. Also needed are ways to monitor changes over large areas and to evaluate whether observed changes in surficial materials exceed the normal limits of natural variation.

As part of a program to study the stability of present-day eolian deposits under monitored climatic conditions, an array of Geomet (geological and meteorological) automated data-collection stations is currently operating in five desert areas of the Southwestern United States. The stations record long-term measurements of surface wind speeds, rainfall, temperature, sand movement, and other environmental parameters (McCauley and others, 1984; McCauley and Rinker, 1987; Breed, chap. A, this volume). Although the Geomet stations are providing valuable data for characterizing desert conditions and for process studies, the Geomet data are single-point measurements and, thus, have limited utility for regional monitoring. Such monitoring needs can perhaps be met by analyzing satellite remote-sensing imagery; however, to use satellite data effectively, it is first necessary to learn how local ground measurements are related, either directly or indirectly, to concurrent remote-sensing observations. To explore this question, Landsat multispectral scanner (MSS) images acquired from 1980–1988 have been processed for an area of Sonoran Desert surrounding the Yuma, Arizona, Geomet station. The purpose of the study is to characterize vegetation and other surface changes in the Yuma area from a remote-sensing perspective and to examine correlations between the Geomet measurements and the remote-sensing data. The period of study includes the El Niño–Southern Oscillation (ENSO) rainfall of 1982–1984, which was accompanied by large, temporary, vegetation cover increases in the Yuma region (MacKinnon and others, 1990).

STUDY AREA

The Yuma desert study area is centered approximately 20 km east-southeast of the city of Yuma in the southwestern corner of Arizona. The focus of this report is a 40×25-km area of an intermontane basin, bounded to the west by the irrigated Colorado River floodplain near Yuma, and to the east by the Gila Mountain range (fig. 1). This area includes several types of terrain developed on basin-filling sediments of Quaternary

[1]U.S. Geological Survey, Mail Stop 954, 12201 Sunrise Valley Dr., Reston, VA 20192.

[2]Earth Satellite Corporation, 6011 Executive Blvd., Suite 400, Rockville, MD 20852.
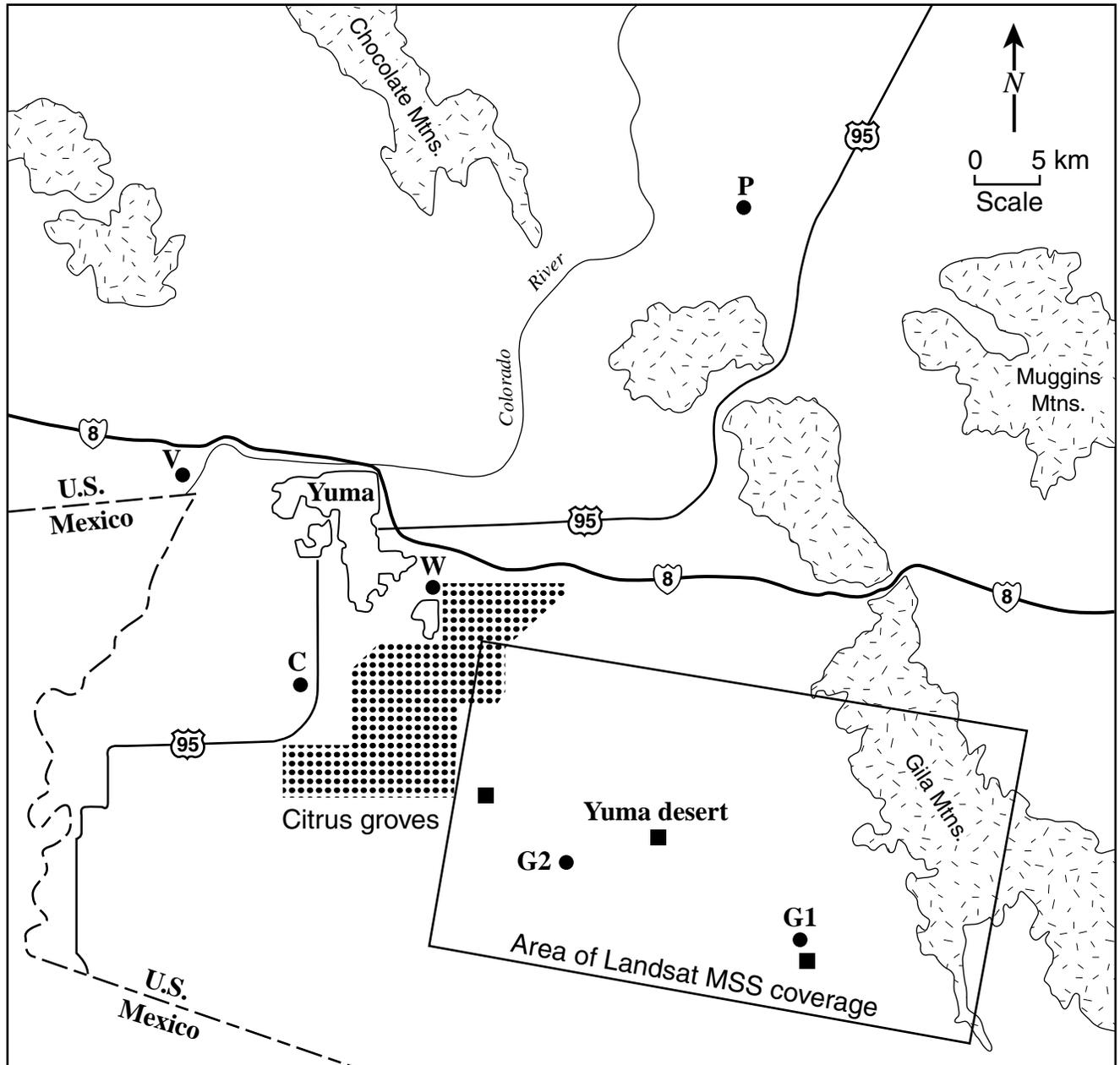
Figure 1. Location map showing area of Landsat MSS coverage near Yuma, Ariz. Points G1 and G2 within the MSS coverage area indicate the Geomet station location at two different times. Other weather stations in the general area are shown by solid circles: C, citrus station; P, proving grounds station; V, Yuma Valley station; W, Weather Service office. Solid squares within the image area mark the locations of NDVI response curves for the western, central, and southeast image areas (left to right).

age (fig. 9 in Breed, chap. A, this volume). The southern portion of the study area has low topographic relief (< 5 m) and, in the southwest quadrant, consists of a partly vegetated sand sheet, generally less than 2 m in thickness; the southeast quadrant, in contrast, lacks eolian sand cover and is surfaced by unconsolidated alluvial outwash. These mobile surface materials overlie a semi-consolidated substrate consisting of alluvial fan sediments derived from the Gila Mountains, fluvial deposits of the nearby Colorado and Gila Rivers, and intercalated eolian sand. The northwest and north-central

parts of the study area exhibit greater topographic relief (10–20 m) in the form of dissected river terrace deposits of Pleistocene age (Morrison, 1983), which are surfaced by well-developed desert pavements and discontinuous mantles of "blow sand" a few centimeters to 0.5 m thick. A calcic soil horizon (probably stage III of Machette, 1985) is encountered in the basin-fill sediments about 1 m below the surface in localities throughout the study area (Schaber and Breed, 1993). Perennial but sparse vegetation covers approximately 5–20 percent of the study area, with the greater amounts

occurring along intermittent stream drainages, particularly in the north-central part. Creosotebush (*Larrea tridentata*), white bursage (*Ambrosia dumosa*), and big galleta (*Hilaria rigida*) grass are the predominant perennial plant species over the sand plains and terraces comprising most of the study area (Crosswhite and Crosswhite, 1982). Major drainages support palo verde (*Cercidium microphyllum*), mesquite (*Prosopis velutina*) and a few other tree species. On the northeast side of the study area, igneous and metamorphic crystalline rocks are exposed in the Gila Mountains, which locally reach elevations of 1,000 m. Vegetation is practically absent on the varnished, closely packed pavement surfaces of alluvial fans adjacent to the mountain range. Additional discussion of the geology and hydrology of the Yuma study area is given by Olmsted and others (1973).

The location of the Yuma Geomet station for nearly all of the period of study (February 1982 to May 1986) is designated by "G1" on figure 1. The station was relocated 2.5 km to the north of G1 in late May 1986, where it operated until April 1987. To accommodate changes in military practice bombing and aerial strafing (the Geomet station is on the Luke Air Force Range, administered by the Marine Corps Air Station in Yuma), the Geomet was moved again in May 1988 to a third location approximately 13 km to the west-northwest where it continues to operate today (fig. 1, G2). Several conventional weather stations in the Yuma area have long-term precipitation records, and their locations are also indicated on figure 1.

DATA-ANALYSIS METHODS

The data set used for this report was constructed from 16 different MSS scenes acquired from 1980–1988. Except for single scenes in 1980 and 1981, there are two scenes for each year—one scene collected in mid-winter, and one scene collected in late spring or early summer (table 1). These data were coregistered to a common base image, and a 512-pixel by 306-line subset covering the study area was extracted. To aid in the location of control points for the coregistration, linear contrast stretches were applied to each of the original images. Although the stretches were slightly different for each image, scene-to-scene variations in digital number values related to stretching differences, scanner characteristics, and solar illumination effects were removed in the subsequent calibration process, outlined below.

The coregistered MSS data were processed to construct images of the normalized difference vegetation index (NDVI) as discussed by Sabins (1987) and Tucker and others (1985). This index makes use of the large spectral contrast between near-infrared and visible reflectance levels that is characteristic of green vegetation. To calculate an NDVI image, MSS band 5 (red) is subtracted from MSS band 7 (near-infrared), and the result is divided by the sum of the same two bands. Such NDVI images are a useful estimator

Table 1. Landsat MSS data for Yuma, Arizona, study area.

	Date	Abbreviation	Scene I.D.	Platform
1.	Jan. 16, 1980	W80	30682-17292	Landsat 3
2.	May 25, 1981	S81	22315-17301	Landsat 2
3.	Feb. 1, 1982	W82	22567-17315	Landsat 2
4.	July 4, 1982	S82	31582-17361	Landsat 3
5.	Jan. 6, 1983	W83	40174-17385	Landsat 4
6.	May 30, 1983	S83	40318-17394	Landsat 4
7.	Feb. 26, 1984	W84	40590-17380	Landsat 4
8.	May 24, 1984	S84	50084-17380	Landsat 5
9.	Jan. 19, 1985	W85	50324-17403	Landsat 5
10.	June 8, 1985	S85	50484-17401	Landsat 5
11.	Feb. 7, 1986	W86	50708-17370	Landsat 5
12.	June 15, 1986	S86	50836-17335	Landsat 5
13.	Jan. 25, 1987	W87	51060-17301	Landsat 5
14.	July 4, 1987	S87	51220-17350	Landsat 5
15.	Feb. 13, 1988	W88	51444-17394	Landsat 5
16.	Aug. 7, 1988	S88	51620-17405	Landsat 5

of green biomass, and also provide a first-order correction for the scene-to-scene effects of solar illumination differences (Tucker and others, 1985). However, to analyze multitemporal NDVI data quantitatively, it is necessary to further calibrate the digital imagery to provide consistent measurement units. This is especially true of Landsat MSS data, which in this case were acquired from four different Landsat satellites over a period of 9 years. The calibration method applied in this study utilized laboratory hemispherical reflectance measurements of samples representing bright and dark target areas within the MSS scenes. The bright target, a 5×5-pixel area of bare sand in the southern portion of the image, was represented spectrally by a sand sample collected 7 km away at the present Geomet site (fig. 1, G2). The dark target, a 5×5-pixel area of desert pavement in the east-central part of the image, was represented by the average spectrum of nine varnished mafic (amphibolite) rock fragments collected from the pavement surface. This dark target area was remarkable for its low albedo and virtually complete absence of soil and vegetation cover. Knowing the laboratory reflectance values in each MSS bandpass (fig. 2), as well as the digital number values of the calibration targets in each MSS image, a scalar (slope) and offset (intercept) term were calculated for each band to linearly transform the MSS digital numbers to percent reflectance (Roberts and others, 1985) (fig. 3). Data that have been stretched previously can be calibrated by this method as long as any earlier transformations were also linear. Probably the most important source of calibration uncertainty is the need to identify field targets that have not changed in spectral composition through time, a criterion that is difficult to evaluate. To
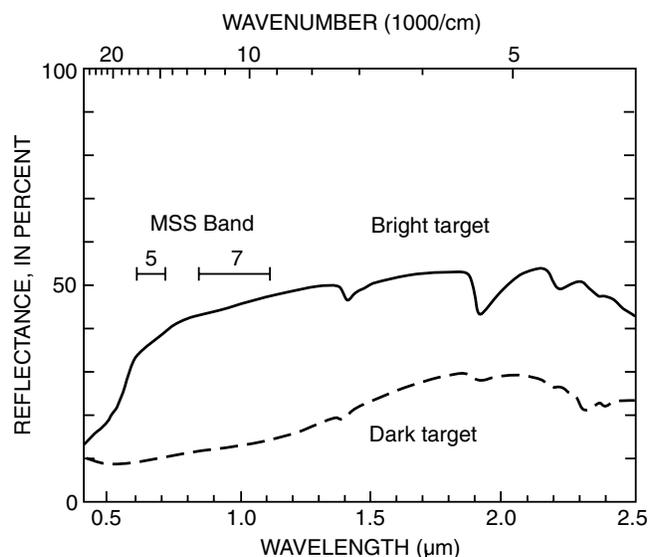
Figure 2. Laboratory reflectance spectra of field samples used to characterize ground targets for data-calibration purposes. The bright target, a relatively barren sandy area near the southern edge of the area of Landsat MSS coverage (see fig. 1), is represented by a spectrum of sand collected near the present Geomet site. The dark target, an alluvial fan surface consisting mainly of mafic igneous rocks, is represented by an average of 9 spectra for samples collected on the fan. Wavelength ranges of the MSS bands used in the NDVI calculation are also shown.
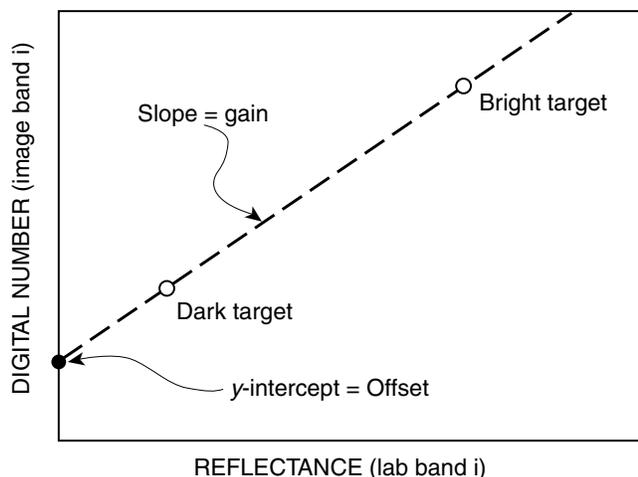

Figure 3. Schematic diagram depicting the use of bright and dark ground targets to determine the equation of a line (e.g., slope and offset terms) that will calibrate satellite digital numbers to percent reflectance. The digital number values for the ground targets are obtained from the uncalibrated image data; the reflectance values for the ground targets are obtained from laboratory (or field) spectral measurements. The diagram is a modification of a similar diagram in Farrand and others (1994).

choose suitable ground targets for this study, preliminary NDVI images (i.e., constructed before calibration) were examined to identify prospective calibration sites having minimal vegetation influence. After the final calibration

targets were selected, and the calibration applied, the NDVI images were recalculated. Further discussion of the MSS data calibration is given in Appendix 1.

The calibrated NDVI images were assembled into a single data "cube" (dimensions 512×306×16 pixels), from which curves for 5×5-pixel areas were extracted depicting how NDVI values changed through time at different ground locations. A curve-matching program was then used to classify image areas having similar NDVI response curves. The curve-matching algorithm has been described by Mazer and others (1988) and is part of the SPAM (spectral analysis manager) software package formerly distributed by the Jet Propulsion Laboratory for analyzing imaging spectrometer data. Two additional data cubes containing the calibrated MSS band-5 images, and the MSS band-7 images also were constructed to aid in assessing surface reflectivity changes related to changing vegetation cover in the study area.

Correlations between Geomet precipitation, temperature, and wind-speed data and the Landsat NDVI variations were explored using mathematical analysis software. The choices of input data for the correlation analyses are explained below.

RESULTS

NDVI CURVES AND "CLASSIFIED" IMAGE

Figure 4 shows three plots illustrating changes in NDVI through time for different 5×5-pixel areas in the Yuma desert. The approximate image locations where the curves were extracted from the data cube are marked by small squares on figures 1 and 5. The curves reveal that there have been important NDVI response differences within the study area. For example, the upper curve in figure 4, representing the southeast image area near the original Geomet site, shows a pronounced NDVI maximum during the winter of 1984. This contrasts with the earlier NDVI maximum observed in the central part of the image during the winter of 1983 (fig. 4, middle curve). A third curve extracted from the western part of the image (fig. 4, bottom curve) shows relatively constant, high NDVI values throughout the period of study.

The curve-matching program permits other areas having similar NDVI response curves to those shown in figure 4 to be identified in the image data. Examination of the curve-matching output (fig. 5) indicates that a major portion of the study area can be classified using only the three NDVI curves described above. Pixels characterized by a strong NDVI maximum in the winter of 1984, shown in blue on figure 5, appear to be limited to a rather small area of the image near the first Geomet site. The desert floor in this area is surfaced by granule to pebble lag (reworked alluvium), and a blow sand cover is intermittently present (Breed, chap. A, this volume). The alluvial surface is dissected by small runoff
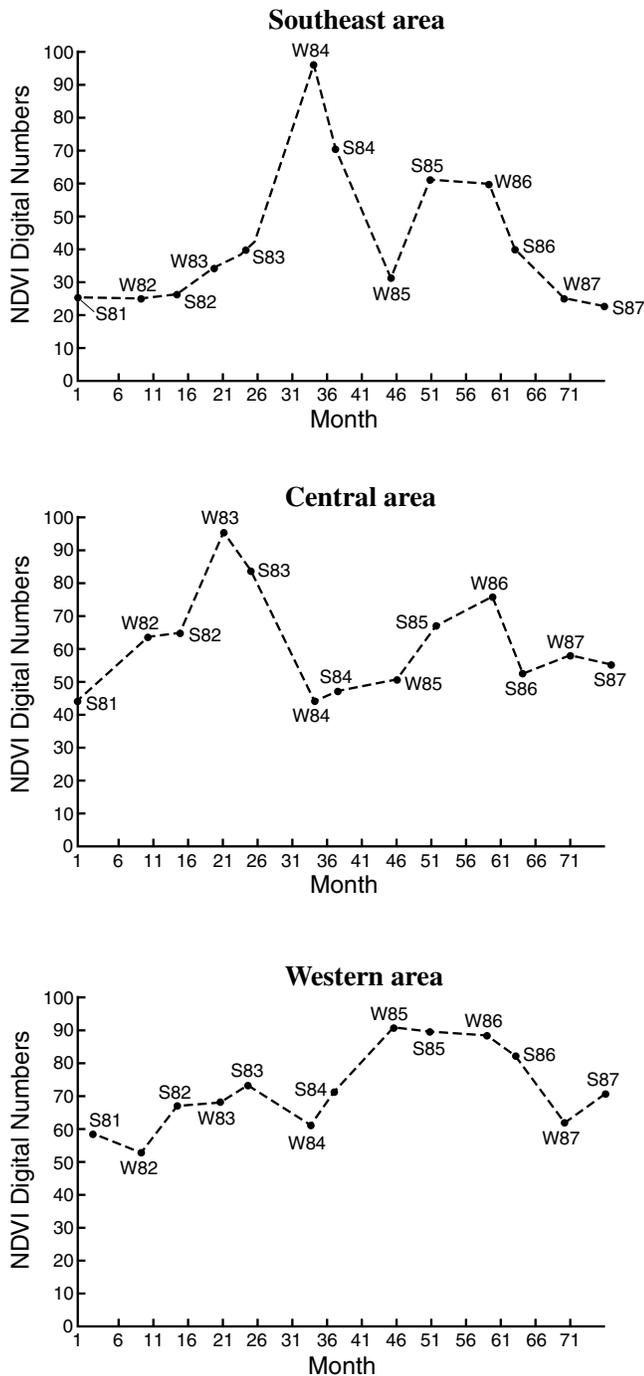
Figure 4. Curves showing NDVI variations for three 5×5-pixel areas (shown on area of Landsat MSS coverage—see fig. 1) during the period May 1981 to July 1987. Higher NDVI values indicate increased green vegetation cover. Raw NDVI values were rescaled by 300× for image-display purposes. The upper curve (southeast area) shows variations near the original Geomet site. The middle curve (central area) shows variations typical of the central portion of the MSS study area. The bottom curve (western area) shows variations in the western portion of the study area. Note the different timing of NDVI maxima in the southeast and central area curves.

channels from the piedmont fans to the east, suggesting that runoff reaching this part of the desert from the adjacent highlands may be an important factor in NDVI variations. Pixels characterized by an NDVI peak in the winter of 1983, shown in yellow on figure 5, are widely distributed, with some concentration evident in the central portion of the image. The yellow pixels coincide with the presence of eolian sand sheets, which in this region commonly act as a "mulch" to conserve water above less-permeable substrates. Such areas are relatively favored sites for vegetation growth compared with sites lacking suitable sand cover and (or) substrate conditions (Breed and others, 1984). Red pixels, representing the least variable NDVI response (fig. 4, lower curve), mainly occur in areas adjacent to the citrus groves and in the large intermittent drainage located in the north-central part of the image. These are localities where denser vegetation is supported by irrigation and generally more accessible ground water. Henceforth, the blue, yellow, and red areas of the "classified" image (fig. 5) will be referred to as the southeast, central, and western image areas, respectively. Areas in figure 5 that remain unclassified include the mountainous northeastern quadrant, which is severely affected by scene-to-scene shadowing differences, and the citrus groves on the northwestern margin of the image, which exhibit NDVI changes influenced mainly by canopy development and short-term irrigation practices.

COMPARISONS BETWEEN NDVI, PRECIPITATION, TEMPERATURE, AND WIND

Figure 6 shows precipitation data from the Yuma Geomet station and from four other weather stations in the surrounding area. As illustrated by these data, and recognized by other workers (MacKinnon and others, 1990; Ezcurra and Rodrigues, 1986), rainfall patterns in the Lower Colorado Valley portion of the Sonoran Desert are inhomogeneous (e.g., spatially variable). The variation from station to station in the Yuma area presents a problem if attempts are made to combine precipitation data collected from different sites. At location G1, the Geomet data are available from February 1982 to April 1987 (fig. 6, months 10–72), although there are several gaps within this period (see fig. 7). Because the Geomet is the only natural desert site with a precipitation record, it is the only location where direct comparisons can be made between precipitation measurements and NDVI response. Therefore, to ensure the validity of such comparisons, the G1 data have not been augmented with measurements from other sites. The plots in figure 6 all show the same time interval from May 1981 to July 1987, spanning the Geomet record at site G1 as well as the period of MSS images 2–14 (table 1).

Examination of the precipitation data (fig. 6) indicates that the Geomet site was slightly more arid than the other

0   5 KILOMETERS   N
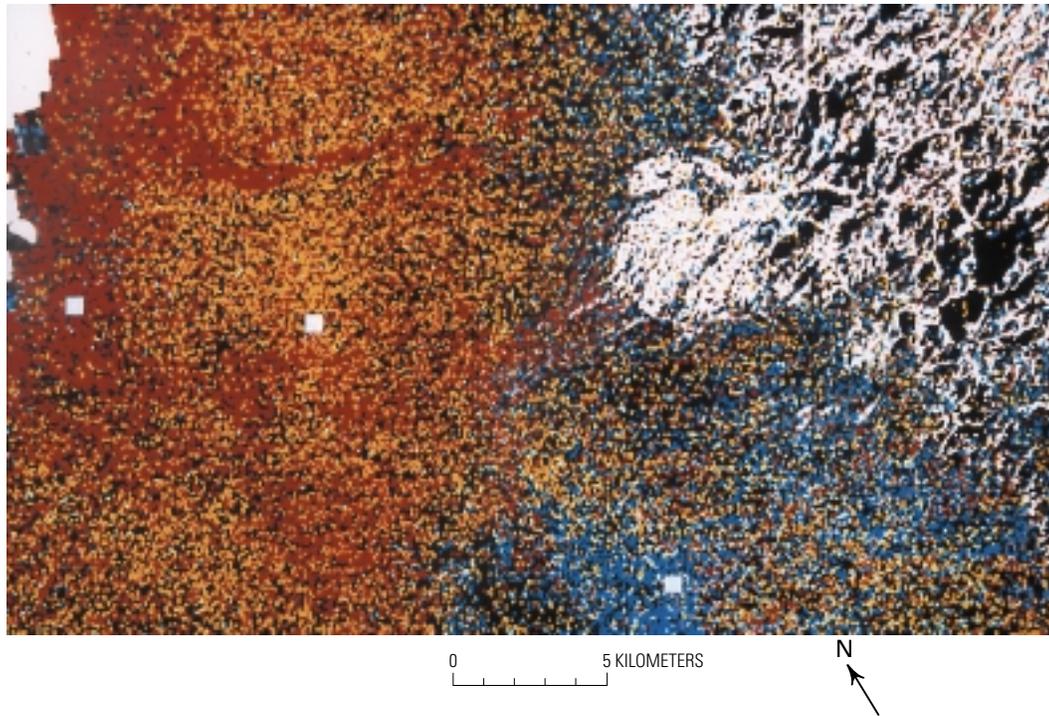
Figure 5. Image of Yuma study area (area of Landsat MSS coverage—see fig. 1) classified by principal components showing spatial patterns of NDVI response variations. Solid squares mark locations of NDVI response curves used to classify the image. Areas in the southeast part of the image (blue pixels) exhibit NDVI response curves similar to the upper curve in figure 4. Areas in the central part of the image (yellow pixels) exhibit NDVI response curves similar to the middle curve in figure 4. Areas in the western part of the image (red pixels) exhibit NDVI response curves similar to the lower curve in figure 4. White and black areas of the image were not classified (see text).

sites during the early part of the study period. Note that four of the five sites, including the Geomet, show a large spike in precipitation in month 28 (August 1983), whereas only three sites, the Weather Service office (WSO), citrus area station, and Yuma Valley station, show an earlier spike in month 20 (December 1982). This type of precipitation disparity probably is an effect of Arizona's summer monsoonal rains, which commonly bring precipitation to the entire southwestern corner of the State. In contrast, rains associated with winter storms from the northwest often do not extend to the Geomet site, even when rain falls in the city of Yuma. The variable distribution of winter rainfall appears to be reflected in NDVI response curves for different portions of the study area, as discussed below; however, the relationship between NDVI and precipitation is by no means simple.

Figure 7A shows the NDVI curve for the southeastern Yuma desert superimposed on the Geomet station precipitation data. The figure indicates that the NDVI maximum followed heavy rains associated with the El Niño phenomenon in August 1983 (month 28), October 1983 (month 30), and December 1983 (month 32). However, the contribution of the August 1983 precipitation spike to the development of the winter 1984 NDVI maximum is questionable. Other

workers have reported that summer precipitation mainly stimulates the growth of short-lived summer annual plant species (Beatley, 1974a; Crosswhite and Crosswhite, 1982), which ordinarily would complete their life cycle prior to the mid-winter MSS observations. It can be noted that three of the four other weather stations also reported high precipitation in August 1983, but the NDVI curves for the central and western parts of the study area do not show an increased vegetation response in the winter of 1984. Furthermore, low NDVI responses for the Geomet site following the July 1984 (month 39) and August 1986 (month 64) precipitation spikes also may indicate the poor sensitivity of winter and spring MSS observations for discerning summer annual plant development.

For the reasons just outlined, high winter and spring NDVI values primarily reflect the amount of precipitation received during the preceding fall-winter period (henceforth termed "antecedent precipitation"). There was significant antecedent precipitation in the fall-winter seasons prior to the observed NDVI maxima in February 1984 and June 1985, in distinct contrast to the low amount of such precipitation in other years of the study (fig. 7A). Precipitation was sparse in the latter part of 1985, and thus, the rather high NDVI value seen for the January 1986 MSS data seems
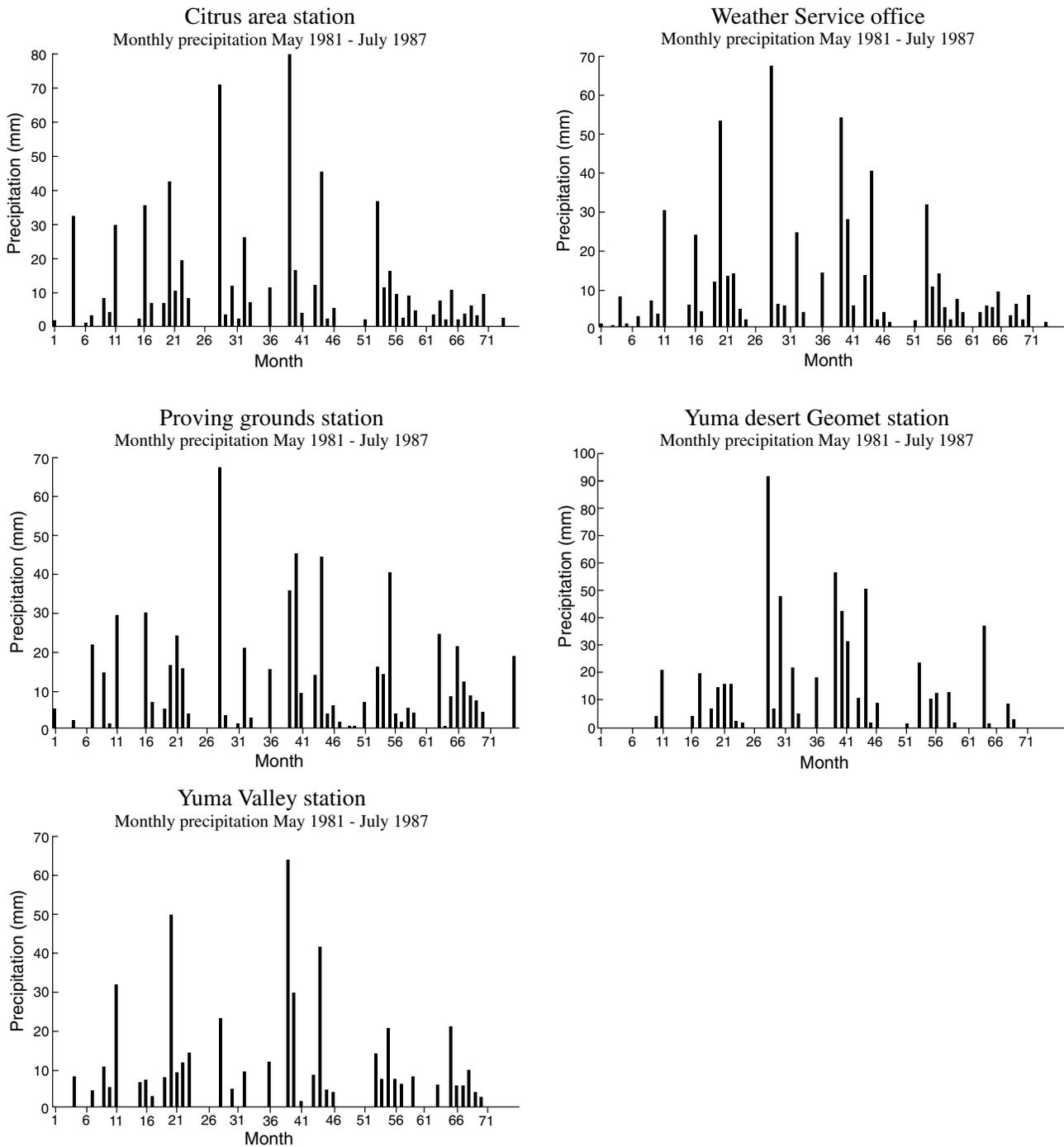
Figure 6. Precipitation records of weather stations in the Yuma region, including the Geomet station. Station locations are shown on figure 1.

inconsistent—until it is realized that the fall 1985 Geomet data are incomplete (fig. 7A). One of the other regional weather stations (fig. 6, proving grounds station) does show significant precipitation in November 1985 (month 55), indicating that some rainfall may be missing in the Geomet station record prior to the elevated NDVI values in January 1986.

The NDVI curve for the central (yellow) area on the "classified" image (fig. 5) can be compared with precipitation data from the WSO site located several kilometers west of the study area (fig. 7B). As seen in the WSO data, there was rainfall in the city of Yuma in December 1982 (fig. 7B, month 20), which, as usual, was much heavier than that recorded at the Geomet station (fig. 7A). This rainfall
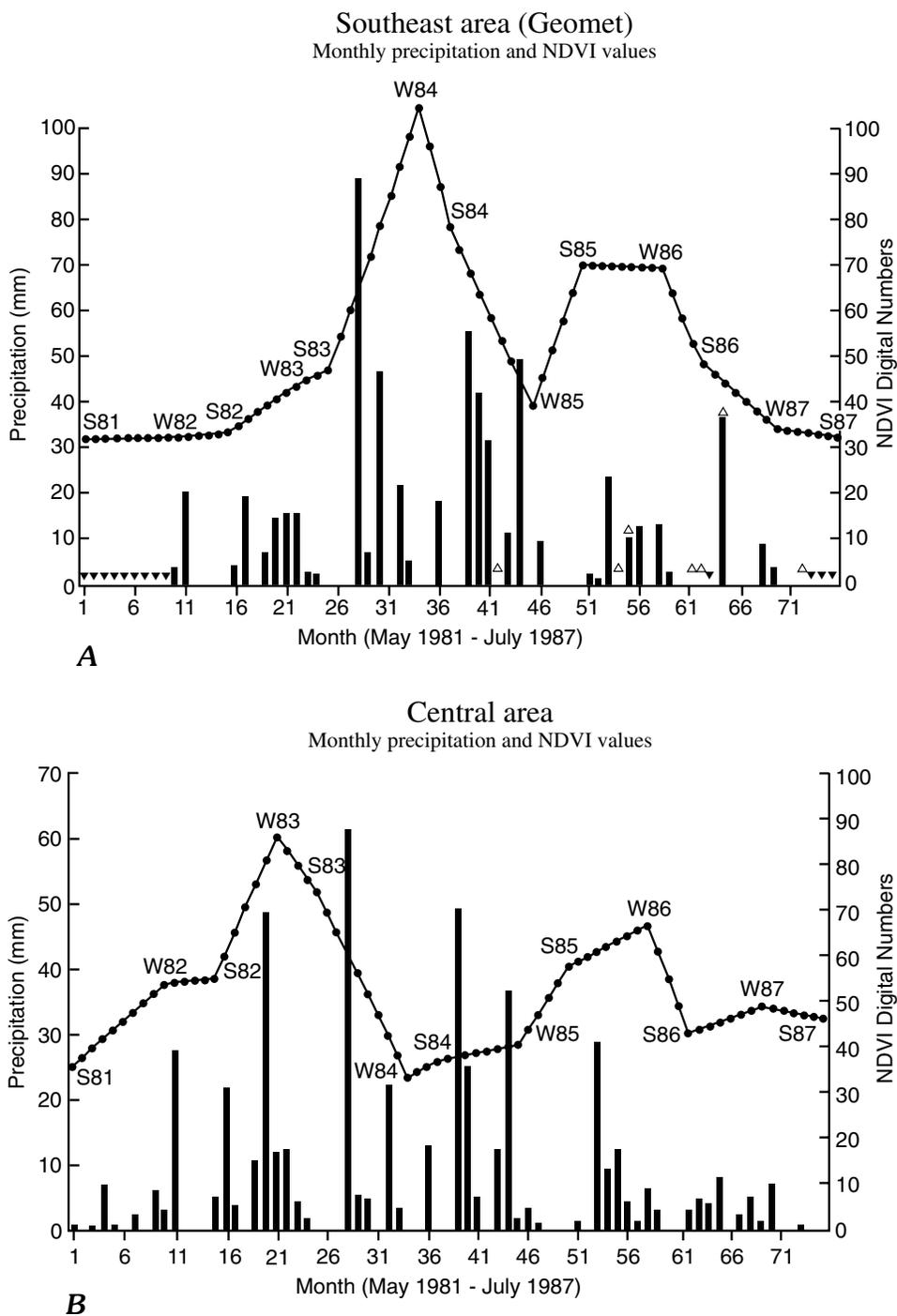
Figure 7. *A*, Comparison of NDVI response curve for the southeast image area (cf. fig. 4) with monthly precipitation data from the Geomet station. Solid triangles show months for which no Geomet data are available. Open triangles mark months for which the Geomet data are incomplete. Absence of bar indicates zero precipitation for that month. The NDVI response curve is defined by 13 alternating winter and spring/summer MSS observations. *B*, Comparison of the NDVI response curve for the central image area (cf. fig. 4) with monthly precipitation data from the Weather Service office located several kilometers west of the study area (fig.1).

presumably accounts for the NDVI maximum seen immediately following in the January 1983 MSS data for many parts of the study area (fig. 5, yellow pixels). This strong vegetation increase was very rapid, evidently requiring no more than 4 weeks to develop. However, if such a rapid NDVI response is possible following heavy rains, why

Table 2.   Data set used in correlation analyses.

[NDVI, normalized difference vegetation index; 7-mo. precip., 7-month running precipitation total (in milli-meters); 4-mo. precip., 4-month running precipitation total (in millimeters); 2-mo. wind, 2-month running average wind speed (in kilometers per hour); 2-mo. temp., 2-month running average departures from normal. Leaders (--) indicate no data]

Month/year	NDVI	7-mo. precip.	4-mo. precip.	2-mo. wind	2-mo. temp.
7/82	26	23.9	--	15.6	-2.0
1/83	35	--	39.9	13.1	+0.6
5/83	39	54.6	--	14.1	-1.6
2/84	96	--	73.7	12.3	+0.7
5/84	70	91.7	--	12.5	+1.4
1/85	31	--	92.7	10.7	-0.4
6/85	61	71.4	--	12.8	+0.9
6/86	39	37.6	--	13.6	0.0
1/87	25	--	11.4	11.0	+0.6

did a similar response not occur in the central study area during the winters of 1984 and 1985? One possiblity is that other, as yet undetermined, climatic factors produced less favorable growing conditions at these times. Unfortunately, the WSO climatic data are not well-suited for addressing this question because the station in the city does not represent the same ground location as the NDVI curve. To examine how other climatic variables, such as temperature and wind conditions, may affect vegetation development, it is necessary again to focus on the Geomet site.

Correlations were examined between the Geomet data and NDVI values from the southeast image area in nine MSS scenes spanning the February 1982 to April 1987 period. A 10th MSS scene (February 1986) was excluded from the correlation analysis because the Geomet data for the preceding several months were substantially incomplete. To allow for a time delay between precipitation and NDVI response, 4-month and 7-month running precipitation totals were calculated from the monthly Geomet data. NDVI values for the winter MSS scenes were then associated with precipitation values for the preceding 4-month periods; NDVI values for the spring/summer MSS scenes were associated with precipitation totals for the preceding 7-month periods (table 2). Temperature and wind were hypothesized to produce more immediate effects on vegetation, and therefore a slightly different procedure was followed with the Geomet temperature and wind-speed data. The temperature data in table 2 are 2-month running-average departures from normal, and the wind speeds are 2-month running averages. The temperature departures from normal were calculated using the Yuma Weather Service office record as a base and then applying a correction of +2.07°C to account for site and instrument differences at the Geomet station. The accuracy of this correction value, which was determined by taking the average of 30

uncorrected Geomet monthly departure values, is not critical to the analysis. The effect of an error would be to shift the temperature departures either up or down, without changing the magnitude of the temperature excursions. No time-offset was applied to the temperature and wind-speed values associated with the NDVI values in table 2. In other words, the wind-speed value for each MSS date equals the average wind speed for that month and the preceding month. Table 3 shows cross correlations between the NDVI, precipitation, temperature, and wind-speed values listed in table 2.

Surprisingly, only a weak correlation is indicated between antecedent precipitation and NDVI response in the vicinity of the Yuma Geomet site (r = 0.6). Notwithstanding the small number of data points, the limited correspondence between precipitation amounts and the vegetation index indicates that other factors are involved in determining the NDVI response to rainfall events.

Table 3.   Cross-correlation matrix for NDVI, precipitation, temperature, and wind data from the Yuma, Arizona, Geomet site.

[Data are listed in table 2. NDVI, normalized difference vegetation index; 7-mo. precip., 7-month running precipitation total (in millimeters); 4-mo. precip., 4-month running precipitation total (in millimeters); 2-mo. wind, 2-month running average wind speed (in kilometers per hour); 2-mo. temp., 2-month running average departures from normal. Leaders (--) indicate no data]

	4- and 7-mo. precip.	2-mo. temp.	2-mo. wind
NDVI	0.60	0.56	–0.13
4- and 7-mo. precip.	--	0.36	–0.37
2-mo. temp.	--	--	–0.61

One factor that might influence the NDVI response is temperature. Unseasonably warm or cold temperatures can inhibit the ability of desert plant species to take advantage of favorable rainfall conditions (Beatley, 1974a). A relatively high r value (r = 0.56) was found for the correlation between NDVI variations and the 2-month running average of temperature departures from normal (table 3). We note that the minimum in NDVI for January 1985 corresponds with below-normal temperature values. Similarly, the maximum in NDVI in February 1984 corresponds with slightly elevated temperatures. Did the below-normal temperatures in the fall and early winter of 1984 delay the January 1985 response of vegetation to otherwise favorable precipitation conditions (fig. 7A)? It seems clear that temperature effects on NDVI, like precipitation effects, cannot easily be studied in isolation from other variables.

Wind-speed relations with NDVI values at the Geomet station were also studied. The correlation between the NDVI and wind-speed values is not significant at r = –0.13 (table 3). Despite the low correlation value between NDVI and wind speed, it may be important that the rainfall that preceded the February 1984 NDVI maximum occurred at a time of relatively low average wind speeds. Low wind speeds might have aided in the retention of both soil and plant moisture and, thus, contributed to the unusually strong vegetation response.

CHANGES IN SURFACE REFLECTIVITY RELATED TO VEGETATION CHANGES

To assess reflectivity variations associated with vegetation changes, reflectivity curves were extracted from data cubes composed of the calibrated MSS band-5 and MSS band-7 images (fig. 8). These curves indicate that transient vegetation cover changes can cause important changes in surface reflectivity. The largest change in reflectivity was observed near the Geomet site during the winter 1984, where increased vegetation cover locally reduced the MSS band-5 reflectivity from about 33 to 17 percent reflectance. Other parts of the study area generally showed smaller reflectivity variations on the order of +5 percent reflectance. Reflectivity variations in MSS band 7 were smaller than those seen in MSS band 5, the most extreme change being a decrease of 11 percent reflectance. Note that the reflectivity minimum for the band-7 data in the southeast image area lags the minimum in band 5 by one MSS observation (in this case an interval of 3 months). A possible explanation for this unexpected result is discussed below.

DISCUSSION

Spatial variations in NDVI response are the result of many factors, including differences in vegetation communities, soil properties, antecedent precipitation, and other local physiographic and climatic influences. Some of these factors are relatively unimportant in the study area. For example, site orientation and elevation variations are minimal, excluding the Gila Mountains, which were not studied because of shadowing and illumination problems. Similarly, air temperature and wind conditions should be fairly uniform over the study area at any given time and, thus, should not directly cause spatial (as opposed to temporal) differences in NDVI response. The major remaining variables are precipitation and soil properties, and the spatial NDVI response differences seen in figure 5 probably reflect uneven distributions of rainfall and subsequent runoff, compounded by differences in soil moisture-holding capacity.

Precipitation has been shown by many workers to be a primary factor controlling the species composition and density of vegetation in desert regions (Beatley, 1974a, 1974b; Crosswhite and Crosswhite, 1982). But, if precipitation is so important, why is the correlation between the NDVI values and associated Geomet precipitation data so poor? The correlation results might be explained by (1) surficial processes and biologic adaptations that control vegetation growth cycles, and (2) difficulties in discerning short-term (1–3 month) vegetation changes remotely. Surficial processes reflect the interaction of climatic and geologic variables and, thus, are not directly linked to any single climatic measurement. For example, one process that is likely to be important is soil desiccation, which involves the interaction between wind, temperature, rainfall, and soil properties (Koller, 1972). Even after a heavy rainfall, strongly desiccating conditions (e.g., high winds and high temperatures) might produce low-soil-moisture conditions and relatively limited vegetation growth. Conversely, a minor rainfall might significantly enhance soil moisture under favorable conditions of low winds and moderate temperatures. To better understand the effects of climatic variables on soil moisture, concurrent soil-moisture measurements are needed. Another important surficial process in the Yuma region is sand movement, which occurs when threshold wind-shear conditions are exceeded. Episodes of sand movement might disrupt the growth of recently germinated seedings, ultimately reducing the NDVI response. Sand-flux sensors operating at several Geomet sites, including Yuma, will eventually provide additional data about how substrate stability affects vegetation growth, and vice versa.

Certain environmental adaptations of desert plants may also modify the precipitation-NDVI responses. In particular, seed germination of many desert annuals is inhibited by chemicals in the seed coat until the chemicals are removed by rainfall leaching. Moreover, germination is necessarily temperature dependent to ensure that summer and winter annuals time their appearance to exploit the conditions to which they are specifically adapted (Koller,

Reflectivity changes in MSS band 5
Yuma AZ, southeast image area

Reflectivity changes in MSS band 7
Yuma AZ, southeast image area
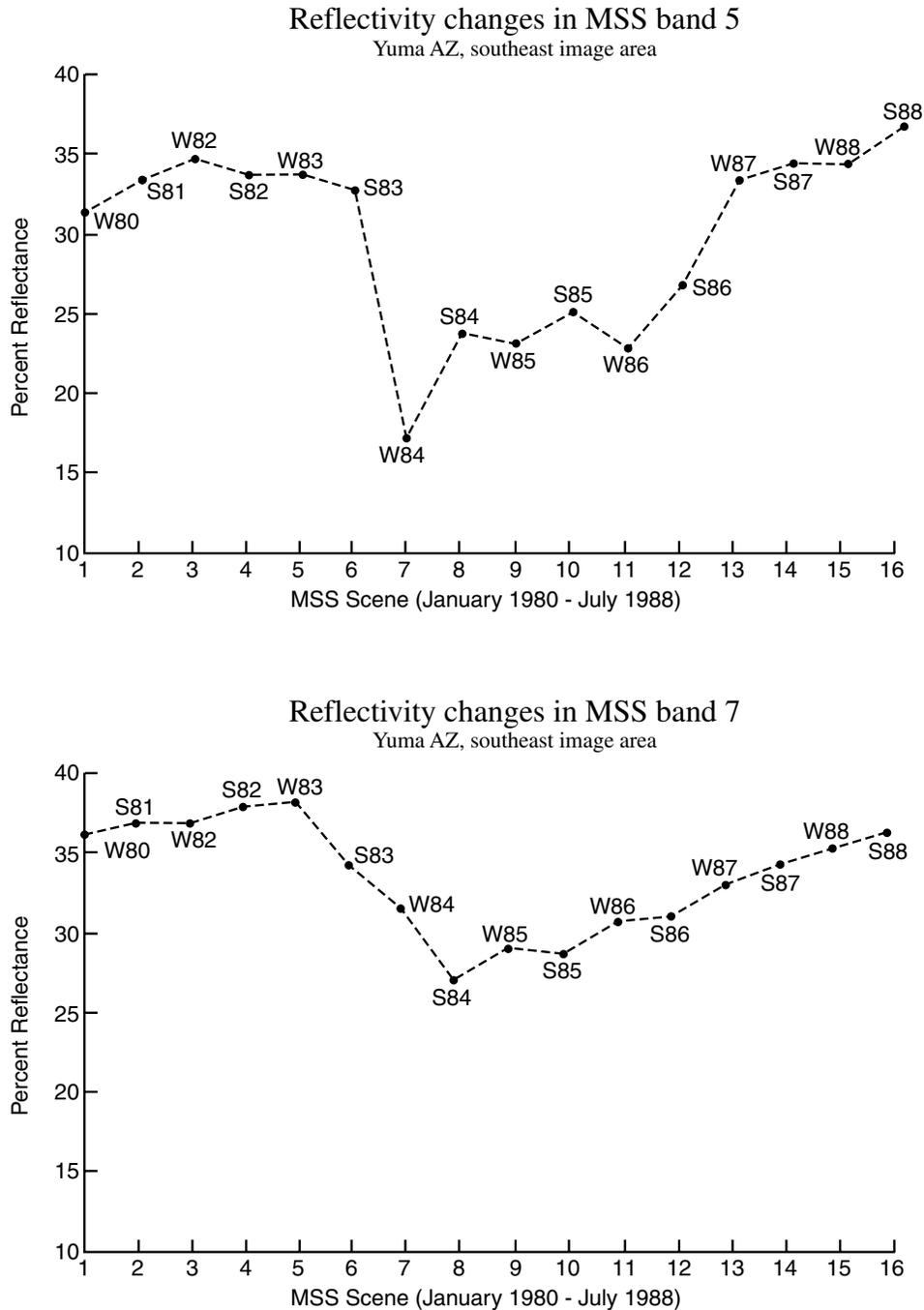
Figure 8. Reflectivity changes in the area of the Yuma Geomet station. Changes in MSS band-5 reflectivity were more pronounced than in MSS band 7. This is a result of the strong absorbing effect of chlorophyll at the band-5 wavelength. The displacement of the minimum reflectivity in band 7 relative to band 5 may be due to abundant dry (non-green) vegetation cover following the NDVI maximum.

1972; Went, 1949). Retarded germination of newly formed seeds due to chemical germination inhibitors might produce lower than expected NDVI values in years immediately following major "blooms." This, in fact, is the pattern observed in the MSS data: the NDVI curve for the southeast image area (fig. 7*A*), exhibits low values in the winter 1985, whereas the central image area (fig. 7*B*), shows low NDVI values for the winter 1984. Even though these NDVI patterns point to possible effects of germination inhibitors, it should be noted that other causes, particularly variable precipitation and soil moisture-retention differences, cannot presently be ruled out.

Another key question concerns the timing and frequency of the MSS observations. It is possible that the effect of germination inhibitors or other factors is to delay vegetation growth only slightly, but enough nonetheless to reduce the NDVI response in the mid-winter MSS data. This points to a more general problem, namely that if vegetation changes occur on a 3- or 4-month growth cycle with variable onset times (Beatley, 1974a), then a 6-month sampling interval with remote-sensing data cannot track the associated NDVI changes accurately. To understand complex seasonal relations between soil moisture, vegetation development, and remote-sensing observations, higher temporal resolution remote-sensing data and detailed ground studies of the vegetation are needed.

During the time covered by the present study, reflectivity variations associated with vegetation changes were relatively minor for most parts of the study area. However, decreases in reflectivity were locally significant in some places and might indicate the regional potential for reflectivity changes during periods of high rainfall. Interestingly, the reflectivity minimum for the MSS band-7 data occurred several months later than the minimum in band 5. This may be a result of the reflectivity contribution of senescent vegetation that has lost much of its chlorophyll but still covers a large fraction of the ground surface. If true, this reflectance behavior introduces yet another variable to be accounted for when attempting to model relations between remote-sensing indices of biomass and ground meteorological and geological measurements.

The results of this study do point to the utility of remote-sensing data for helping to place Geomet and other ground measurements within a larger regional context. The "classified" color image (fig. 5) showed important variations in NDVI response over the study area that could not have been anticipated from the ground weather station data. This added information can be very useful in helping to constrain research results based on ground data alone. For example, in a study of antecedent precipitation effects on dust emissions, MacKinnon and others (1990) developed a model to predict "potential" dust loads based on wind conditions in upwind dust-source areas. They were able to evaluate the effects of antecedent precipitation on potential dust levels by using wind and precipitation data from the Yuma Geomet station in combination with visibility data (e.g., a proxy for actual dust emissions) from the Yuma Marine Corps Air Station. MacKinnon and others (1990) found that antecedent precipitation and dust loadings showed a moderately strong negative correlation, presumably reflecting the important stabilizing effects of rainfall-enhanced vegetation cover. Unusually low dust loads under strong wind conditions in the spring of 1983 were ascribed to high regional vegetation cover, although photographs taken at the Geomet station in March 1983 show vegetation to be at a less developed stage than seen the following year at the February 1984 NDVI peak. The NDVI response pattern seen in figure 5 confirms that the timing, if not the degree,

of vegetation growth at the Geomet site during 1983–1984 was somewhat different from other parts of the study area. Indeed, by the time of the January 1983 MSS observation (low NDVI at the Geomet site), other places in the region do appear to have above-average green vegetation cover that might help to explain the low airborne dust levels (fig. 5, yellow pixels; fig. 7*B*, month 21).

CONCLUSIONS

The Landsat MSS-based NDVI data examined in this study are sensitive to changes in vegetation abundance and are very useful for recognizing regional differences in vegetation response that are not easily discernible from single-point ground measurements. On the other hand, multitemporal NDVI data acquired only twice a year do not appear to provide a simple proxy measurement for estimating precipitation or other important environmental parameters in the Sonoran Desert. During the period of study, there were aspects of the NDVI response that could not be directly explained by precipitation, temperature, wind, or other climatic observations. A better understanding of the NDVI variations, and especially their utility for environmental studies, will require remote-sensing data with higher temporal resolution, as well as modeling efforts to clarify relations between surficial geology, soil moisture, evapotranspiration, rainfall-temperature-wind variations, and plant-germination mechanisms. Even though the situation is complex, the dynamic response of Sonoran Desert vegetation to climatic and geologic variables presents an opportunity for regional monitoring if we can learn to model the interactions and to exploit remote-sensing spectral signatures more completely.

REFERENCES CITED

Beatley, J.C., 1974a, Phenological events and their environmental triggers in Mohave Desert ecosystems: Ecology, v. 55, p. 856–863.

———1974b, Effects of rainfall and temperature on the distribution and behavior of *Larrea tridentata* (creosote-bush) in the Mohave Desert of Nevada: Ecology, v. 55, p. 245–261.

Breed, C.S., McCauley, J.F., Breed, W.J., McCauley, C.K., and Cotera, A.S., Jr., 1984, Eolian (wind-formed) landscapes, *in* Smiley, T.L., Nations, J.D., Peive, T.L., and Schafer, J.P., eds., Landscapes of Arizona, The Geological Story: Lanham, Md., University Press of America, p. 359–413.

Crosswhite, F.S., and Crosswhite, C.D., 1982, The Sonoran Desert, *in* Bender, G.L., ed., Reference Handbook on the Deserts of North America: Westport, Conn., Greenwood Press, p. 163–319.

Ezcurra, E., and Rodrigues, V., 1986, Rainfall patterns in the Gran Desierto, Sonora, Mexico: Journal of Arid Environments, v. 10, p. 13–28.

Farrand, W.H., Singer, R.B., and Merenyi, E., 1994, Retrieval of apparent surface reflectance from AVIRIS data: A comparison

of empirical line, radiative transfer, and spectral mixture methods: Remote Sensing of Environment, v. 47, p. 311–321.

Koller, D., 1972, Environmental control of seed germination, *in* Kozlowski, T.T., ed., Seed Biology, Volume II: New York, Academic Press, p. 1–101.

Machette, M.N., 1985, Calcic soils of the Southwestern United States, *in* Weide, D.L., ed., Soils and Quaternary Geology of the Southwestern United States: Geological Society of America Special Paper 203, p. 1–21.

MacKinnon, D.J., Elder, D.F., Helm, P.J., Tuesink, M.F., and Nist, C.A., 1990, A method of evaluating effects of antecedent precipitation on duststorms and its application to Yuma, Arizona, 1981–1988: Climatic Change, v. 17, p. 331–360.

Markham, B.L., and Barker, J.L., 1983, Spectral characterization of the Landsat-4 MSS sensors: Photogrammetric Engineering and Remote Sensing, v. 49, p. 811–833.

Mazer, A.S., Martin, M., Lee, M., and Solomon, J.E., 1988, Image processing software for imaging spectrometer data analysis: Remote Sensing of Environment, v. 24, p. 201–210.

McCauley, J.F., Breed, C.S., Helm, P.J., Billingsley, G.H., MacKinnon, D.J., Grolier, M.J., McCauley, C.K., 1984, Remote monitoring of processes that shape desert surfaces: The Desert Winds Project: U.S. Geological Survey Bulletin 1634, p. 1–19.

McCauley, J.F., and Rinker, J.N., eds., 1987, A workshop on desert processes, September 24–28, 1984—Report on the conference: U.S. Geological Survey Circular 989, 21 p.

Morrison, R.B., 1983, Late Pliocene and Quaternary geology, El Centro quadrangle: Tucson, Ariz., Arizona Bureau of Geology and Mineral Technology, 6 p., scale 1:250,000.

Olmsted, F.H., Loeltz, O.J., and Irelan, B., 1973, Geohydrology of the Yuma area, Arizona and California: U.S. Geological Survey Professional Paper 486-H, 227 p.

Roberts, D.A., Yamaguchi, Y., and Lyon, R.J.P., 1985, Calibration of airborne imaging spectrometer data to percent reflectance using field spectral measurements: Ann Arbor, Mich., Proceedings of the Nineteenth International Symposium on Remote Sensing of Environment, October 21–25, 1985.

Sabins, F.F., 1987, Remote Sensing, Principles and Interpretation: New York, W.H. Freeman, 449 p.

Schaber, G.G., and Breed, C.S., 1993, Subsurface mapping with imaging radar in deserts of Africa and Arizona, *in* Geoscientific Research in Northeastern Africa: Technical University of Berlin, Germany, June 1993, 5 p.

Tucker, C.J., Townshend, J.R.G., and Goff, T.E., 1985, African land-cover classification using satellite data: Science, v. 227, p. 369–375.

Went, F.W., 1949, Ecology of desert plants. II. The effect of rain and temperature on germination and growth: Ecology, v. 30, p. 1–13.

APPENDIX 1. CALIBRATION OF THE MSS DATA

Diffuse reflectance spectra representing the bright and dark calibration targets were measured in the laboratory by using a Beckman model 5240 spectrophotometer equipped with an integration sphere. Nine varnished rock chips collected from the dark target area were measured and the resulting (very similar) spectra were averaged. A sample of unconsolidated sand collected at the present Geomet site (fig. 1; G2) was used to characterize the bright target area, located approximately 7 km to the southeast. The sand was poured into a 3-cm-diameter sample cup and measured several times, each time with a slightly different part of the sample in the spectrometer field of view. These virtually identical spectra were also averaged. Because the eolian sand deposits in the study area are continuously reworked by wind action, only minor spatial variations in sand composition are expected. Calibration errors resulting from such variations, or from other errors in the laboratory spectral measurements, can potentially affect the magnitude of derived NDVI values but not the relative pattern of NDVI changes through time.

The next step in the calibration procedure was to determine average MSS bandpass reflectance values for the calibration targets by convolving appropriate MSS band-5 and band-7 filter functions with the two calibration spectra. Although the MSS sensors do exhibit minor response differences, a single set of square-wave filter functions was used. The filter function for band 5 was centered at 650 nm and had a bandwidth of 100 nm; the function for band 7 was centered at 910 nm and had a bandwidth of 200 nm. Note that most of the MSS data compared to the Geomet data (e.g., fig. 7*A*) were acquired from Landsats 4 and 5, which have practically identical MSS sensor characteristics (Markham and Barker, 1983).

The MSS digital number values of the calibration targets within each scene were linearly transformed to match the reflectance values calculated from the laboratory calibration spectra. Because the relationship between the digital numbers and the reflectance values is determined by the transformation, reexamining the calibration targets after the transformation does not provide a meaningful check on calibration accuracy (other than to rule out potential computational errors). There is no way to prove that the calibration of any retrospective MSS data set is absolutely correct without a program of concurrent field measurements.

The principal source of uncertainty in this calibration method is spectral variability in the calibration targets, which are assumed to be unchanging with time. If undetected, such variability can cause errors in the derived reflectance and NDVI values. Vegetation-cover changes are the most likely cause of spectral variability in the Yuma region, and although an effort was made to select calibration targets having minimal vegetation, some minor cover changes are possible. Significant calibration errors would obscure the spectral content of the MSS data, suppressing both within-scene and scene-to-scene NDVI variations. Such whole-scene calibration errors appear to be relatively small insofar as different parts of the study area do show independently varying NDVI response curves.

Dust Deposition and Its Effect on Soils—
A Progress Report

By Marith C. Reheis

DESERT WINDS: MONITORING WIND-RELATED SURFACE PROCESSES IN
ARIZONA, NEW MEXICO, AND CALIFORNIA

Carol S. Breed and Marith C. Reheis, *Editors*

U.S. GEOLOGICAL SURVEY PROFESSIONAL PAPER 1598–G

CONTENTS

FIGURES

Dust Deposition and Its Effect on Soils— A Progress Report

By Marith C. Reheis[1]

ABSTRACT

A dust-deposition project established in the U.S. Geological Survey in 1984 monitors the rate of dust influx to soils in southern Nevada and California. Dust-trap sites were initially chosen to provide data on dust influx at soil-study sites and to provide input to a computer model that relates soil carbonate to paleoclimate by comparing modern dust influx to source lithology, distance from source, and climate. In 1991, additional sites were established to help monitor deflation from the artificially drained Owens Lake, California, and to analyze dust deposition at high-altitude meteorological stations in the Great Basin.

Analysis of data collected from 1984 to 1995 from sites distant from direct human influence indicates that deposition rates of silt plus clay are substantially higher (mean of 11.3 ± 4.6 g/m^2/yr) south of lat 36°N. than to the north (mean of 6.4 ± 1.8 g/m^2/yr). Extensive alluvial plains appear to be more important sources of dust than undisturbed dry lake beds and playas in the modern climatic regime. The mineralogy of the dust varies with grain size and source lithology: clay mineralogy is similar among most of the samples, whereas sand mineralogy mainly reflects the lithology of the substrate around the sample site. Comparisons of dust data with soil data show that the upper horizons of soils can consist mainly of eolian dust.

Initial results from samples collected in 1991–1994 in Owens Valley indicate that sites near and south of the dry bed of Owens Lake have abnormally high dust-deposition rates. The rates progressively decrease downwind (south) of the lake bed and are highest in winter. Winter rates decrease from about 1,500 mg/m^2/day on the lake bed to 40 mg/m^2/day at Little Lake, 50 km to the south; summer rates decrease from 290 to 30 mg/m^2/day. In contrast, sites north of the lake bed receive about the same amount of dust in summer and in winter, ranging from about 15 to 25 mg/m^2/day. The soluble salt content of dust deposited around Owens Lake commonly exceeds 25 percent, about twice that of dust deposited in relatively undisturbed areas of the southern Basin and Range. Dust deposition rates at the south end of Owens Lake are one to two orders of magnitude greater than regional average rates.

INTRODUCTION

The source, entrainment, transportation, and deposition of eolian dust are topics of increasing interest in the scientific community, and the effects of eolian processes are of increasing importance to the global community. Among the most important reasons for this interest are: (1) On a global scale, analysis of ice cores from Antarctica and sediment cores from ocean basins shows that glacial episodes coincide with episodes of increased dust in the atmosphere (e.g., Petit and others, 1990); the dust can reflect incoming radiation and thus increase ice cover. (2) Globally, eolian dust has been shown to be a major component of soils forming under a wide range of climates (Syers and others, 1969; Yaalon and Ganor, 1973). Dust is important to soil fertility and can control the chemistry of atmospheric precipitation (e.g., Lindberg and others, 1986). (3) In arid and semiarid regions, eolian dust plays a significant role in soil formation and geomorphic process. For example, desert pavements, ubiquitous features in arid regions, form when eolian dust infiltrates and accumulates beneath a surface layer of stones (McFadden and others, 1987); this process acts to smooth initially rough surfaces. Once formed, however, soil horizons that are formed both by the infiltration of dust and by other processes decrease the porosity of the soil and promote runoff. The erosion caused by runoff acts to increase surface roughness. (4) Detailed studies of dust influx can permit better estimations of paleoclimate from soil properties (Mayer and others, 1988). The dust deposition project within the U.S. Geological Survey addresses aspects of the latter two topics: soil formation, geomorphic process, and paleoclimate.

This chapter presents a brief review of results from southern Nevada and California and discusses work in progress in Owens Valley, California. For more details and

---

discussion, readers are referred to published papers on dust-influx rates and composition (Reheis and Kihl, 1995; Reheis, 1997), on modern dust and soils (Reheis and others, 1995), and to data available to the public at the follwing Web site: http://geochange.er.usgs.gov/pub/dust/.

ACKNOWLEDGMENTS

My greatest appreciation goes to Rolf Kihl (Institute of Arctic and Alpine Research, University of Colorado), who performed most of the chemical and sedimentological analyses and worked closely with me to develop techniques of analyzing very small samples. Without his patience, attention to detail, and humor in the face of quality-assurance interrogation, this project could never have achieved its goals. I am grateful to the numerous field assistants and colleagues who gave help and advice.

HISTORY OF THE PROJECT

A project to study modern dust in southern Nevada and California was initiated in 1984 under the auspices of the Yucca Mountain Site Characterization project (Interagency Agreement DE-AI08-78ET44802). The primary purpose of the dust-deposition project was to provide data on modern dust composition and influx rates, which were incorporated in a computer model relating soil carbonate to paleoclimate. A secondary purpose was to provide data on dust-influx rates at specific sites (fig. 1) where soil chronosequences (soils of different ages formed under similar conditions of climate, parent material, relief, and vegetation; Jenny, 1941) were studied in support of tectonic and stratigraphic investigations for the Yucca Mountain project (vicinity of Fortymile Wash, fig. 1); sites were also examined that had been previously studied for other reasons. Some sites were also selected to provide dust data to soil studies by other investigators along the Elsinore fault and in the Transverse Ranges (fig. 1).

The dust-deposition project has evolved since termination of its funding by the Yucca Mountain project in 1991. The project now operates under the auspices of the Global Change and Climate History Program and is part of a multi-project effort to monitor climatic controls on eolian processes in deserts of the Southwestern United States. In support of that effort, dust traps were established in Owens Valley (fig. 1) in order to help monitor deflation from the dry bed of Owens Lake. In addition, some dust traps were established in the central and northern Great Basin at high-altitude meteorological stations (not shown on fig. 1) where the geochemistry of rain and snow is being studied by Meyer Rubin and G.I. Smith of the U.S. Geological Survey.

DESIGN OF THE DUST-DEPOSITION STUDY

DISTRIBUTION OF SITES

Previous studies of dust deposition in relation to soil genesis have generally been restricted geographically and (or) temporally; most studies focused on a small area (for example, the Channel Islands, California; Muhs, 1983) or at most a small region (such as the Edwards Plateau, Texas; Rabenhorst and others, 1984), and samples were collected only for 1 year. Exceptions include a regional, 2-year study by Smith and others (1970) on the Great Plains and a local, 10-year study by Gile and others (1981) in southern New Mexico. To my knowledge, the dust-deposition project begun in 1984 is the first such survey to be both regional in extent and long term.

The sampling design for this study was not statistically based; rather, sites were chosen to provide data on dust influx at soil-study sites and to answer specific questions about the relations of dust to source, distance from source, and climate (fig. 1). Dust-trap sites that coincide with soil-study sites include, from north to south, Trail Canyon, Fortymile Wash, and Kyle Canyon, Nevada, and Silver Lake, Cima, Cajon Pass, Vidal Junction, and the southern part of the Elsinore fault, California. Some sites were chosen for their proximity to potential dust sources of different lithologic composition (e.g., playas and alluvium derived from granitic, calcareous, and mafic rocks). Other sites were selected along transects downwind from a dust source; these transects generally cross topographic barriers and include sites east of Tonopah (43–46) crossing rhyolitic rocks of the Kawich Range, sites downwind of northern (40, 36, 35) and central Death Valley (38, 39, 11–14) across lithologically diverse mountain ranges, and sites downwind of Desert Dry Lake crossing calcareous rocks of the Sheep Range (47–50) north of Kyle Canyon (fig. 1). In addition, some sites were chosen for their proximity to weather stations.

Specific locations for dust traps were chosen on the basis of the above criteria plus accessibility, absence of dirt roads or other artificially disturbed areas upwind, and inconspicuousness. The last factor is important because the sites are not protected or monitored except at the time of sample collection; hence, most sites are at least 0.5 mi from a road. Despite these precautions, some of the dust traps were tampered with, often violently. This is a particular problem in areas close to population centers, and most of these sites (52–54, near Los Angeles, and 17–19 and 22, near Las Vegas, fig. 1) were eventually abandoned. A few other sites, including those that appeared to be greatly influenced by nearby cultivation (20, 21, and 41) or vehicular dust (6, 8, 24, and 32), were also eliminated in 1989.

The 59 dust traps that were built in 1984 and 1985 were sampled annually through 1989 to establish an adequate
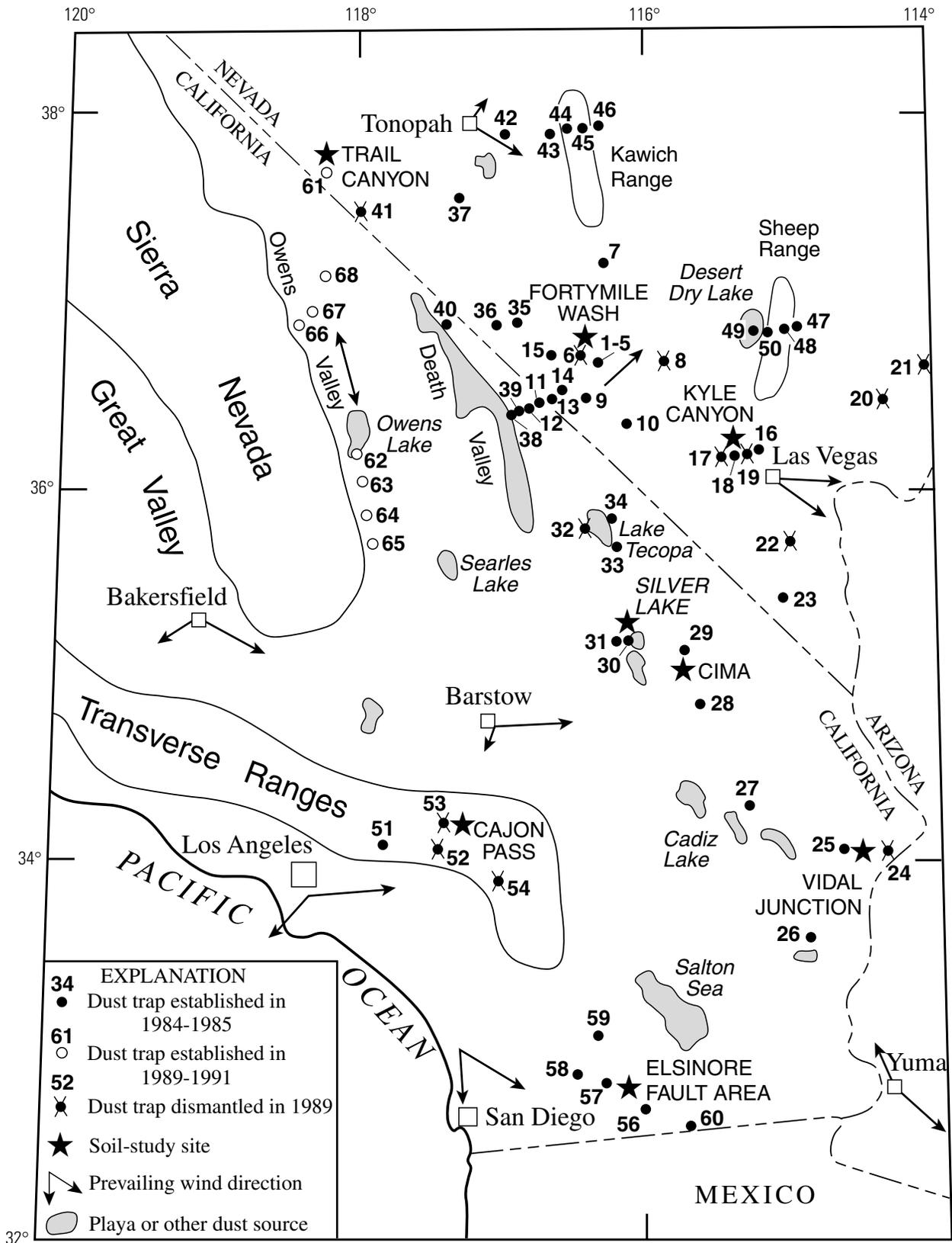
Figure 1. Map showing locations of dust traps, soil-study sites, prevailing winds, and principal geographic features in southern Nevada and California. Wind data are compiled from the National Climatic Center (1981), from Duell (1990; Owens Valley), from unpublished data of the Nevada Test Site climatology office, and from informal records of small airports; arrows represent annual wind directions and relative strengths.

statistical basis to calculate annual dust flux. Sampling continues at 46 of these sites every 2 years as opportunity and funding permit. New dust traps that were emplaced in 1991 in and near Owens Valley (62–68) are sampled as often as twice a year.

DESIGN OF DUST TRAPS

There are as many different designs of dust traps as there are published studies of modern dust. The designs vary depending on the purpose of the study (such as measuring total deposition or amount added to soils), the sampling interval (days or years), protection of equipment (expensive equipment is not expendable), amount of funding, and personal preference. In this study, the most important factors that influenced dust-trap design were: (1) measuring the amount of dust added to soils, (2) sampling on an annual basis, (3) no protection other than being difficult to find, and (4) the cost and ready availability of components that could be replaced from sources in small towns.

The original design consisted of a Teflon-coated, angel-food cake pan painted flat black on the outside to maximize water evaporation and mounted on a steel fence post about 2 m above the ground (fig. 2A). A circular piece of $^1/_4$-inch-mesh, galvanized hardware cloth was fitted into the pan so that the cloth rests 3–4 cm below the rim, and the part of the pan above the hardware cloth was filled with glass marbles (fig. 2B). The Teflon coating is non-reactive and adds no mineral contamination to the dust sample should it flake. The 2-m height mostly eliminates entrapment of sand-sized particles that travel by saltation rather than suspension; sand grains are not generally relevant to soil genesis because they are too large to be translocated downward and they weather very slowly owing to their low ratio of surface area to mass. The marbles imitate the effect of a gravelly surface and prevent the infiltrated dust from being blown away. The empty space below the hardware cloth provides a reservoir that helps prevent water from overflowing the pan during large rainstorms.

This basic design was modified in 1986 in two ways. In many areas, the traps became favored perching sites for a wide variety of birds. As a result, significant amounts of non-eolian sediment were locally added to the samples (as much as five times the normal amount of dust at some sites). All dust traps were fitted with two metal straps looped in the shape of an inverted basket over the top of the pan (fig. 2B) and the top surfaces of the straps were coated with Tanglefoot. This sticky material never dries and effectively discourages birds from roosting. In addition, extra dust traps surrounded by alter-type wind baffles (fig. 2A) were constructed at four sites characterized by different types of vegetation. The wind baffles simulate the effect of ground-level wind speed at the 2-m height of the dust trap and permit comparison of the amount of dust caught by an unshielded

trap with the amount that should be caught at ground level where vegetation reduces wind velocity. In 1989, extra dust traps were constructed at many sites in order to increase the total sample collected at each site.

SAMPLING AND ANALYSIS

Samples are obtained from the dust traps by carefully washing sediment from the marbles, screen, and pan with distilled water into plastic liter bottles. Laboratory analyses are performed using standard laboratory techniques for soil samples (see Black and others, 1965; Singer and Janitzky, 1986) that have been adapted for use on very small samples (the nonorganic content of a dust sample collected for this study typically weighs less than one gram). These adaptations generally result in larger standard errors than normal for the various techniques because the amount of sample used is smaller than the recommended amount. In addition, a sample is commonly used in more than one analysis if the preceding analytical procedures are nondestructive.

Analyses on dust samples collected from 1984 through 1995 included, in the order they were performed: (1) moisture, (2) organic matter, (3) soluble salts and gypsum, (4) calcium carbonate ($CaCO_3$), (5) grain size, (6) major-oxide chemistry, and (7) mineralogy of the sand, silt, and clay fractions. The database for any given site commonly contains gaps depending on how far the sample for a particular year could be stretched through the analytical cascade. In some cases, samples from different years at the same site or adjacent sites were combined to obtain enough material for measuring grain size, major-oxide composition, or mineralogy.

SUMMARY OF RESULTS FROM 1984 TO 1995

DUST COMPOSITION AND INFLUX RATES

The sand content (mostly fine and very fine sand) of most of the dust samples from this study is less than 30 percent, but the amount varies greatly among the sites and from year to year. At site 40, for example, the sand content has consistently been less than 10 percent, whereas samples from sites 14, 25, and 60 commonly have a sand content greater than 50 percent. These three sites are in large, open, sparsely vegetated alluvial plains and may be subject to more intense and (or) frequent windstorms capable of lofting sand to a height of 2 m or more. At site 1, the percentage sand from samples taken in 1985 to 1989 was 21.1, 44.4, 18.2, 20.8, and 32.7, respectively. Many of the 1986 samples from other sites in southern Nevada were anomalously sandy compared to samples from other years.
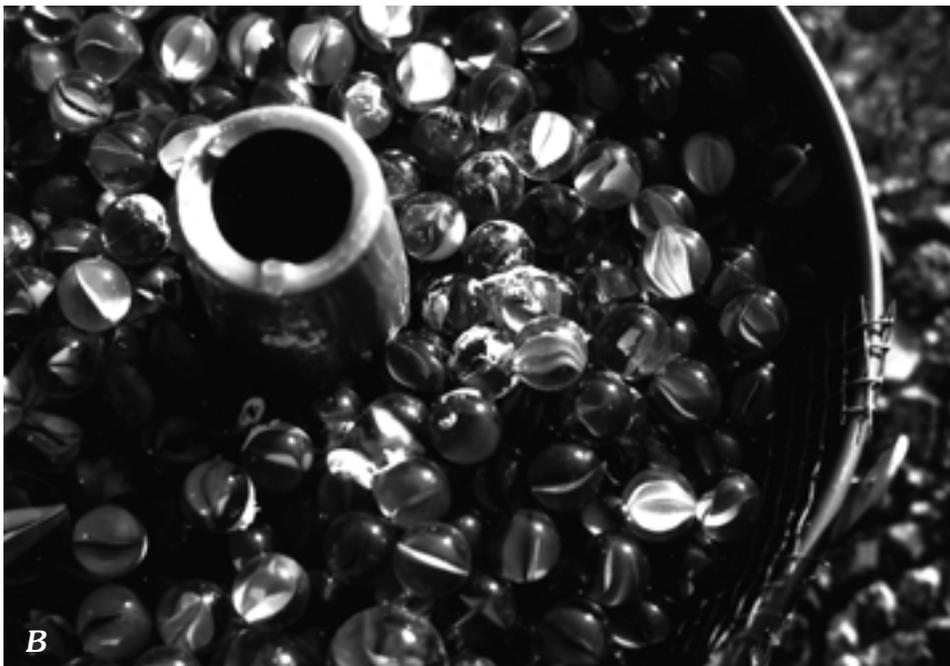
Figure 2. Photographs of dust-trap equipment. *A*, dust trap consisting of angel-food cake pan mounted on steel fence post 2 m above ground. Bird defenses (crossed metal straps coated with Tanglefoot) arch above the pan. Four sites in the network also have duplicate dust traps enclosed within a wind baffle, shown here with access gate open. *B*, closeup of marbles in pan resting on galvanized hardware cloth; white splotches are bird feces.

The average annual influx rate of silt and clay ranges from about 4 to 20 g/m^2/yr; these rates are similar to those estimated by Gillette and Hanson (1989) using a computer model based on simulated dust production from agricultural soils. With few exceptions, the influx rates are geographically distributed such that sites north of about the latitude of Las Vegas (fig. 1) receive 8 g/m^2/yr or less, whereas sites to the south receive more. The mean influx rate in the northern area is 6.4±1.8 g/m^2/yr and ranges from 3.8 to 11.7. The mean rate in the southern area is 11.3±4.6 g/m^2/yr and ranges from 6.0 to 20.7; both the largest and the smallest influx rates in this area are south of the Salton Sea. There is no obvious correlation of high dust-influx rates with proximity to playas or dry lake beds; in fact, most sites near such potential dust sources have relatively low influx rates. This finding suggests that most playas and dry lake beds have stabilized surfaces that do not deflate much in the current climatic regime except when disturbed, as suggested by Gillette and others (1982).

All samples contain significant amounts of CaCO$_3$; average percentages for 1985–1995 range from 8 to 30 and average rates range from 0.7 to 6.4 g/m^2/yr. At the beginning of this study, it was hypothesized that the proportion of CaCO$_3$ should be highest both in areas underlain by calcareous alluvium and in areas downwind from playas. This hypothesis appears to be generally true, except that percentage CaCO$_3$ is relatively low downwind from some playas and dry lake beds such as Cadiz Lake (site 27, fig. 1), probably due to low CaCO$_3$ content of the alluvium, and Lake Tecopa (sites 32–34, fig. 1), possibly because the dissected, calcareous lake sediments at this site are mostly older than middle Pleistocene and hence are moderately indurated. When influx rates of CaCO$_3$ are considered, however, the results are quite different than expected. Influx rates remain high in most areas of carbonate rocks and downwind from some playas. However, influx rates of CaCO$_3$ are influenced by the total dust influx; hence, areas of high dust influx, such as the Transverse Ranges and near the Mexican border, have high rates of CaCO$_3$ influx even though the percentage of CaCO$_3$ in the dust is low.

All samples also contain significant amounts of soluble salts; average percentages for 1985–1995 range from 5 to 24, and average rates range from 0.7 to 3.8 g/m^2/yr. It was thought that the proportion of soluble salts should be highest downwind from playas and dry lake beds. Although this is generally true, salt content is also relatively high in unexpected places, such as in the Kawich Range east of Tonopah, along the Arizona-California border, and locally in the Transverse Ranges and west of the Salton Sea (fig. 1). Influx rates of soluble salts are strongly related to the rate of total dust influx; the only areas with high influx rates of salt are in southern California and they are not downwind of playas.

In summary, it appears that playas and dry lake beds act as local sources of CaCO$_3$ and soluble salts, but the total amount of dust contributed by these sources is relatively minor. Extensive, sparsely vegetated alluvial plains and bajadas seem to be the major sources of eolian dust in the study area (Reheis and Kihl, 1995).

MINERALOGY OF DUST AND RELATION TO SOURCE AREAS

Analysis of X-ray diffraction data indicates that the different size fractions of a sample have different mineralogy. The clay (<2 μm) fraction of all samples is dominated by smectite and mica (illite, biotite, or muscovite) in varying proportions. The clay fraction of all samples also contains small to large amounts of quartz and trace to small amounts of kaolinite and mixed-layer illite-smectite; most samples also contain small amounts of chlorite. Palygorskite is present in a few samples from site 26 (fig. 1).

The silt (2–50 μm) fraction of all samples contains moderate to large amounts of quartz and feldspar and trace amounts of mica. The feldspar varieties vary in their relative proportions among the sites, although nearly all samples contain at least some anorthoclase and (or) orthoclase. High-temperature feldspars are most abundant in samples from areas with rhyolitic rocks, whereas low-temperature feldspars are most abundant in samples from areas with other rock types such as basalt, limestone, or granite. Trace amounts of hornblende (tremolite and actinolite), pyroxene, chlorite, and dolomite are also common in the silt fraction. Calcite is present in only a few samples because it was mostly removed from the silt and clay fractions by pretreatment.

The sand fraction (0.05–2.0 mm) of most of the samples also contains abundant quartz; however, much less quartz is found in samples from areas where the substrate is mainly volcanic or carbonate rock than in those from granitic or mixed-lithology substrates. The proportions of different feldspar varieties vary in the sand fraction more than those in the silt fraction. For example, high-temperature sanidine and albite in the sand fraction are present only in samples from areas with rhyolitic rocks, whereas such feldspars in the silt fraction are present in some samples from areas dominated by other lithologies. The sand fraction of some samples, especially those from areas underlain by carbonate rocks, contains trace to moderate amounts of calcite (not removed from the sand fraction) and dolomite.

The variation in mineralogy with grain size and lithology of the substrate appears to be largely related to the proximity of the source or sources (Reheis and Kihl, 1995). Sand mineralogy differs strongly among samples from areas with different lithologic substrates because sand grains are not likely to travel far from their source due to their weight and their ratio of surface area to mass. Silt mineralogy apparently reflects a mix of local and long-range sources, based on the presence of minerals in dust samples that are not found or occur in very different proportions in the local substrate

rocks. Clay mineralogy is similar among most of the samples; this suggests either that clay particles can travel far from their source and become mixed with clays from other sources and (or) that the clay mineralogy of surface sediments is similar over most of southern Nevada and California.

PRELIMINARY RESULTS FROM OWENS VALLEY

Dust-trap sites 62–68 in Owens Valley (fig. 1; also see fig. 14 in Breed, chap. A, this volume) were established to assess the deposition rate and composition of dust derived from the dry bed of Owens Lake. This lake was artificially desiccated beginning in the 1910's when the Owens River was diverted by the Los Angeles Department of Water and Power. Sites 62 to 65 are on a transect within a narrow valley that extends from the south end of the dry lake bed southward about 50 km to where the valley broadens. Sites 66 and 67 are on opposite sides of Owens Valley about 50 km north of Owens Lake and are located near natural dust traps in collapsed lava tubes. These natural dust traps are being investigated by researchers at Humboldt State University (La Farge and Burke, 1993); data from their study will permit comparison of long-term dust-influx rates with the short-term rates measured by this project. Site 68 is high in the White Mountains and is expected to receive little or no dust from the dry bed of Owens Lake.

Data from seasonal samples taken from November 1991 to September 1994 indicate that dust deposition is strongly influenced both by location with respect to Owens Lake and by season (Reheis, 1997). From Owens Lake south, dust-influx rates are one to two orders of magnitude greater than those at similar latitudes elsewhere in eastern California and southern Nevada (mostly 5–10 $g/m^2/yr$). North of Owens Lake, the dust-influx rates are similar to those elsewhere and are slightly higher on the east side of the valley than on the west side. Winter rates decrease from about 1,500 $mg/m^2/day$ on the lake bed to 40 $mg/m^2/day$ at Little Lake, 50 km to the south; summer rates decrease from 290 to 30 $mg/m^2/day$. In contrast, sites north of the lake bed receive about the same amount of dust in summer and in winter, ranging from about 15 to 25 $mg/m^2/day$. Annually, dust-deposition rates have varied by nearly an order of magnitude.

The soluble salt content of dust deposited around Owens Lake commonly exceeds 25 percent, about twice that of dust deposited elsewhere in the southern Basin and Range, but $CaCO_3$ contents are similar. Deposition rates of $CaCO_3$, salt and <50-μm particles (minerals plus $CaCO_3$) are, respectively, about 70, 100, and 190 $g/m^2/yr$ at the south end of Owens Lake; these rates are one to two orders of magnitude greater than regional average rates. The rates decrease rapidly south of the lake bed but remain significantly higher than regional rates to a distance of about 35 km.

Conclusions from the Owens Valley study are at present speculative because they are based on only 3 years of data (Reheis, 1997). Nevertheless, the very high dust-influx rates at the south end of Owens Lake and the progressive decrease in influx rates southward from Owens Lake clearly show that the lake bed is the major source of dust in this area and that the prevailing winds are northerly. It appears that the influence of the lake bed does not extend much past Searles Lake (fig. 1) because the measured amount of dust approaches natural background levels at site 65. However, the distant sites (including those to the north) may still receive significant amounts of dust from Owens Lake because deposition rates prior to the desiccation of the lake are unknown.

IMPLICATIONS FOR SOIL GENESIS

Many studies have suggested or shown that eolian dust is progressively incorporated into soils of semiarid and arid regions. Data from this project permits the eolian component of the fine fraction (silt plus clay) of some soils to be differentiated from the fine fraction of the soil parent material and from in-situ weathering products. For example, a recent study of soils and eolian dust on the Kyle Canyon fan (sites 16–19, fig. 1) proved, on the basis of thin sections and major-oxide chemistry, that most of the silt and clay in the A and upper B horizons consisted of eolian dust (Reheis and others, 1992). Comparison of the clay mineralogy of soils and modern dust at the same site suggests that very young soils (late Holocene) may have a different mineralogy than the dust (Reheis and others, 1995). With time, however, the clay mineralogy of A horizons becomes similar to that of the dust because the A horizons consist primarily of dust accumulated beneath desert pavement (McFadden and others, 1987). In contrast, the mineralogy of deeper horizons is distinct from that of both the dust and the underlying parent material, suggesting authigenesis of some of the clay minerals. For example, palygorskite commonly is found in subsurface horizons of aridic Pleistocene soils near sites 1–5 (Taylor, 1986), 16–19 (Reheis and others, 1992), 20 (Gardner, 1972), 24 (McFadden, 1982), and 30 (author's unpub. data), but palygorskite is not found in the parent materials of these soils nor in the dust samples from these sites. Therefore, palygorskite in the soils at these sites formed in place.

Modern dust-deposition rates are more than large enough to account for middle and late Holocene rates of accumulation of silt, clay, and $CaCO_3$ at many sites in southern Nevada and California (Reheis and others, 1995). However, the early Holocene soil-accumulation rates in areas near late Pleistocene pluvial lakes are much higher than modern rates and clearly indicate a dust-deflation and

dust-deposition event that caused rapid formation of fine-grained, shallow soil horizons on uppermost Pleistocene and lower Holocene deposits.

FUTURE RESEARCH DIRECTIONS

The sources and pathways of eolian dust are important because the composition of dust can control the chemistry of precipitation and enhance soil fertility. For example, Schlesinger and Peterjohn (1988) have suggested that the $CaCO_3$ content of dust derived from the arid Southwestern United States neutralizes airborne sulfate pollutants and increases the pH of precipitation, and Swap and others (1992) concluded that productivity of the Amazon rain forest depends on trace elements in dust derived from Africa. Soils formed on loess are among the most fertile soils in the world, and it is possible that the fertility of soils formed on many other types of deposits might be affected by long-term additions of small amounts of dust.

Results to date from the dust-deposition project provide general information on the source and composition of dust and on modern rates of deposition in southern Nevada and California. Based on these results, it seems likely that, under the present climatic conditions, playas and dry lake beds that were desiccated naturally in the Pleistocene or early Holocene (unlike Owens Lake) are not principal sources; rather, most dust seems to be generated from large, sparsely vegetated alluvial plains and bajadas. Future work should focus on these source areas to understand how they will behave under different climatic conditions; future work should also focus on whether significant changes in source areas and their rate of dust production will occur if the climate changes. In addition, the pathways of dust derived from different source areas should be traced. Trace-element and isotopic studies of modern dust, mostly likely of the silt fraction, at the source are needed to characterize the composition of dust in enough detail to trace former and present pathways and identify the contributions of different sources to soils and sediment sinks such as loess.

REFERENCES CITED

Black, C.A., Evans, D.D., White, J.L., Ensminger, L.E., and Clarke, F.E., eds., 1965, Methods of soil analysis: Madison, Wis., American Society of Agronomy, Inc., no. 9, part 1, p. 1–770; part 2, p. 771–1572.

Duell, L.F.W., Jr., 1990, Estimates of evapotranspiration in alkaline scrub and meadow communities of Owens Valley, California, using the Bowen-ratio, eddy-correlation, and Penman-combination methods: U.S. Geological Survey Water-Supply Paper 2370-E, 39 p.

Gardner, L.R., 1972, Origin of the Mormon Mesa caliche, Clark County, Nevada: Geological Society of America Bulletin, v. 83, p. 143–156.

Gile, L.H., Hawley, J.W., and Grossman, R.B., 1981, Soils and geomorphology in the Basin and Range area of southern New Mexico—Guidebook to the Desert Project: New Mexico Bureau of Mines and Mineral Resources Memoir 39, 222 p.

Gillette, D.A., Adams, John, Muhs, Daniel, and Kihl, Rolf, 1982, Threshold friction velocities and rupture moduli for crusted desert soils for the input of soil particles into the air: Journal of Geophysical Research, v. 87, no. C11, p. 9003–9015.

Gillette, D.A., and Hanson, K.J., 1989, Spatial and temporal variability of dust production caused by wind erosion in the United States: Journal of Geophysical Research, v. 94, no. D2, p. 2197–2206.

Jenny, Hans, 1941, Factors of Soil Formation: New York, McGraw-Hill, 281 p.

La Farge, D.W., and Burke, R.M., 1993, In situ weathering vs. eolian additions to soils: A proposed solution from lava tubes and cumulic soils, Owens Valley, Calif.: Geological Society of America Abstracts with Programs, v. 25, no. 5, p. 65.

Lindberg, S.E., Lovett, G.M., Richter, D.D., and Johnson, D.W., 1986, Atmospheric deposition and canopy interactions of major ions in a forest: Science, v. 231, p. 141–145.

Mayer, Larry, McFadden, L.D., and Harden, J.W., 1988, Distribution of calcium carbonate in desert soils—A model: Geology, v. 16, p. 303–306.

McFadden, L.D., 1982, The impacts of temporal and spatial climatic changes on alluvial soils genesis in southern California: Tucson, University of Arizona, Ph.D. thesis, 430 p.

McFadden, L.D., Wells, S.G., and Jercinovich, M.J., 1987, Influences of eolian and pedogenic processes on the origin and evolution of desert pavements: Geology, v. 15, p. 504–508.

Muhs, D.R., 1983, Airborne dust fall on the California Channel Islands, U.S.A.: Journal of Arid Environments, v. 6, p. 223–228.

Petit, J.R., Mounier, L., Jouzel, J., Korotkevich, Y.S., Kotlyakov, V.I., and Lorius, C., 1990, Palaeoclimatological and chronological implications of the Vostok core dust record: Nature, v. 343, p. 56–58.

Rabenhorst, M.C., Wilding, L.P., and Gardner, C.L., 1984, Airborne dusts in the Edwards Plateau region of Texas: Soil Science Society of America Journal, v. 48, p. 621–627.

Reheis, M.C., 1997, Dust deposition downwind of Owens (Dry) Lake, 1991–1994: Preliminary findings: Journal of Geophysical Research, v. 102, no. D22, p. 25999–26008.

Reheis, M.C., Goodmacher, J.C., Harden, J.W., McFadden, L.D., Rockwell, T.K., Shroba, R.R., Sowers, J.M., and Taylor, E.M., 1995, Quaternary soils and dust deposition in southern Nevada and California: Geological Society of America Bulletin, v. 107, p. 1003–1022.

Reheis, M.C., and Kihl, Rolf, 1995, Dust deposition in southern Nevada and California, 1989–1989: Relations to climate, source area, and source lithology: Journal of Geophysical Research, v. 100, no. D5, p. 8893–8918.

Reheis, M.C., Sowers, J.M., Taylor, E.M., McFadden, L.D., and Harden, J.W., 1992, Morphology and genesis of carbonate soils on the Kyle Canyon fan, Nevada, U.S.A.: Geoderma, v. 52, p. 303–342.

Schlesinger, W.H., and Peterjohn, W.T., 1988, Ion and sulfate-isotope ratios in arid soils subject to wind erosion in the southwestern USA: Soil Science Society of America Journal, v. 52, p. 54–58.

Singer, M.J., and Janitzky, Peter, 1986, eds., Field and laboratory procedures used in a soil chronosequence study: U.S. Geological Survey Bulletin 1648, 49 p.

Smith, R.M., Twiss, P.C., Krauss, R.K., and Brown, M.J., 1970, Dust deposition in relation to site, season, and climatic variables: Soil Science Society of America Proceedings, v. 34, p. 112–117.

Swap, R., Garstang, M., Greco, S., Talbot, R., and Kållberg, P., 1992, Saharan dust in the Amazon basin: Tellus, v. 44B, p. 133–149.

Syers, J.K., Jackson, M.L., Berkheiser, V.E., Clayton, R.N., and Rex, R.W., 1969, Eolian sediment influence on pedogenesis during the Quaternary: Soil Science, v. 107, p. 421–427.

Taylor, E.M., 1986, Impact of time and climate on Quaternary soils in the Yucca Mountain area of the Nevada Test Site: Boulder, University of Colorado, M.S. thesis, 217 p.

Yaalon, D.H., and Ganor, E., 1973, The influence of dust on soils during the Quaternary: Soil Science, v. 116, p. 146–155.

Design and Operations of Geomet Stations of the Desert Winds Project

By Richard Tigges, Carol S. Breed, *and* Paula J. Helm

DESERT WINDS: MONITORING WIND-RELATED SURFACE PROCESSES IN ARIZONA, NEW MEXICO, AND CALIFORNIA

Carol S. Breed and Marith C. Reheis, *Editors*

U.S. GEOLOGICAL SURVEY PROFESSIONAL PAPER 1598–H

CONTENTS

FIGURES

TABLES

Design and Operations of Geomet Stations of the Desert Winds Project

By Richard Tigges,[1] Carol S. Breed,[2] *and* Paula J. Helm[3]

ABSTRACT

This chapter describes the design of the Desert Winds automated data-collection Geomet stations and the procedures for operating them in the field. In addition to station design, emphasis is on instrumentation; calibration and maintenance; collection, storage, and retrieval of data; and problem-solving.

INTRODUCTION

The stations are designed to provide field-based physical data of sufficient resolution to support scientific studies of surface (mostly eolian) processes under monitored climatic conditions. Because they collect both *geo*logical and *met*eorological data, we refer to them as Geomet stations (fig. 1, table 1). Located in remote areas, the stations are automated and solar powered. They are unattended on a daily basis, but they do require scheduled servicing and repair: weekly cleaning and checking by a custodian and periodic servicing (including calibration) and repair, generally at 6-month intervals, by a skilled technician (table 2). At 1- or 2-hour intervals, each station transmits digital data from its array of sensors to the geostationary operational environmental satellite (GOES). From GOES, the data are relayed to (and stored at) the receiving station of the National Environmental Satellite Data Information Service (NESDIS) at Wallops Island, Va.; NESDIS is operated by the National Oceanic and Atmospheric Administration. From Wallops Island, the data were transmitted via land lines to the U.S. Geological Survey computers at project headquarters in Flagstaff, Ariz. (fig. 2). In 1998, data receipt and storage was transferred to the Desert Research Institute in Reno, Nev.

A Geomet station is located in each of the five main subdivisions of the North American Desert (see Breed, chap. A,

this volume), thus forming a transect across the Southwest's major climatic zones. This network provides the capability for long-term, high-resolution monitoring of climatic conditions and surface geologic processes in areas considered representative of each zone. Supplemental data for short-term studies can be provided by much smaller, portable stations ("ministations") that carry a minimal array of sensors and that can be deployed temporarily, either in conjunction with the fixed stations or independently.

DESIGN OF THE GEOMET STATIONS

The original stations, all in Arizona, were installed in 1979 at Gold Spring, in 1981 at Desert Wells, and in 1982 at Yuma. All were basic stations (fig. 3A), equipped with standard sensors to record observations of a set of near-surface phenomena: average and peak-gust wind speeds, wind direction, precipitation, relative humidity, barometric pressure, air temperature, and soil temperature (McCauley and others, 1984). After an evaluation of the basic system in 1984 (McCauley and Rinker, 1987), two superstations (fig. 1) of far more advanced design were added—one in the Jornada del Muerto grasslands of southern New Mexico in 1986 and the other at Owens Lake, California, in 1992. The Yuma and Gold Spring sites were retrofitted to superstation status in 1988 and 1990, respectively. For security reasons, the Desert Wells station was not retrofitted; it lies halfway between a State highway and an Interstate highway and is visible from the former. The four superstations have a much larger and more varied complement of sensors than those of the basic design. The Geomet sensor arrays, measurement types, and sample intervals are summarized in tables 1 and 3.

The framework for all fixed Geomet stations consists of one or more free-standing towers, a solar power system, a data-collection platform (DCP) with a radio transmitter, and eight or more sensors.

The DCP tower (fig. 3A) is a tripod 1.8 m on a side and 1.6 m tall, constructed of high-quality aluminum pipe. A wide base makes this tower very stable, even in peak-gust winds of nearly 80 knots (McCauley and others, 1984). Three adjust-

---

[1]U.S. Geological Survey, Box 25046, Mail Stop 980, Denver Federal Center, Denver, CO 80225.
[3]U.S. Geological Survey, Building 3, 2255 North Gemini Dr., Flagstaff, AZ 86001.

Figure 1. Geomet superstation on sandy alluvial plain in the Yuma desert. Data-collection platform (DCP) tower (A) is similar to basic station shown in figure 3*A*, but modifications include additional solar panels and soil-temperature sensors. Wind tower (B) holds sensors for wind speed, air temperature, and a combined air-temperature and humidity sensor (A, fig. 3*B*). Radiation tower (C) holds four Eppley sensors (A, fig. 5*A*) for incoming and outgoing long- and short-wave solar radiation. Two of the four Everest radiometers (fig. 5*D*) are in view, attached to white posts at D. Sand-flux sensor (SENSIT) and windblown-particle catcher (fig. 6) are at ground level near wind tower but not in view.

able footpads enable the tower to be leveled, and rebar stakes driven through holes in the footpads increase its stability. A 6-m mast is mounted on one corner of the tower; a lightning rod on the top of the mast is connected with a ground rod at the base of the tower. A hinge arrangement at the bottom of the mast allows it to be lowered for servicing of instruments. Several sensors mounted on the tower are connected with a DCP attached to one side of the tower. A cross-arm at the top of the mast provides a mounting surface for the wind-direction sensor. The basic station has a single wind-speed sensor also mounted on the cross-arm, whereas the superstations have three wind-speed sensors mounted on a separate wind tower (described below). A precipitation gauge is fastened to the DCP tower on top of the tripod. The barometric-pressure sensor is mounted to the base 1.2 m above the ground. The soil-temperature probe is buried 4 cm beneath the ground surface, outside the perimeter of the DCP tower. The basic station has one relative-humidity and one air-temperature sensor mounted to the DCP tower base at the 1.6-m level. Superstations have one relative-humidity and two air-temperature sensors mounted on the wind tower (described below).

All of the four superstations have, in addition to the DCP tower, a wind tower (fig. 3*B*). This structure is a 6-m tall, three-sided (31.75 cm on a side) communication tower. A lightning rod attached to the top connects with a ground rod at the base of the tower. Three guy wires provide stability: two are attached to earth anchors, the third to a winch that allows the tower to be lowered. Lowering, easily accomplished by one person, allows servicing of tower instruments from the ground. Wind-speed sensors mounted on cross-arms at 1.2, 2.64, and 6 m above the ground provide profiles of average and peak-gust wind speeds, from which key parameters are calculated for studies of wind erosion (Helm and Breed, chap. B, this volume). At the superstations, air-temperature sensors are mounted on the cross-arms of the wind tower at 1.2 and 6 m above the ground; the lower sensor is coupled with a relative-humidity sensor. Two buried soil-temperature probes have been added to the basic 4-cm probe to provide profiles of additional soil temperatures at 10- and 20-cm depths. At Jornada, experimental soil-heat-flux sensors, at the same depths as soil-temperature sensors, provide ground heat-flow data (fig. 4*B*). Various types of experimental soil-moisture sensors have been tested at the Geomet stations but none have performed satisfactorily, and none are presently in place.

A radiation tower (C, fig. 1; fig. 5*A*) presently is deployed at each of the Yuma and Jornada superstations.
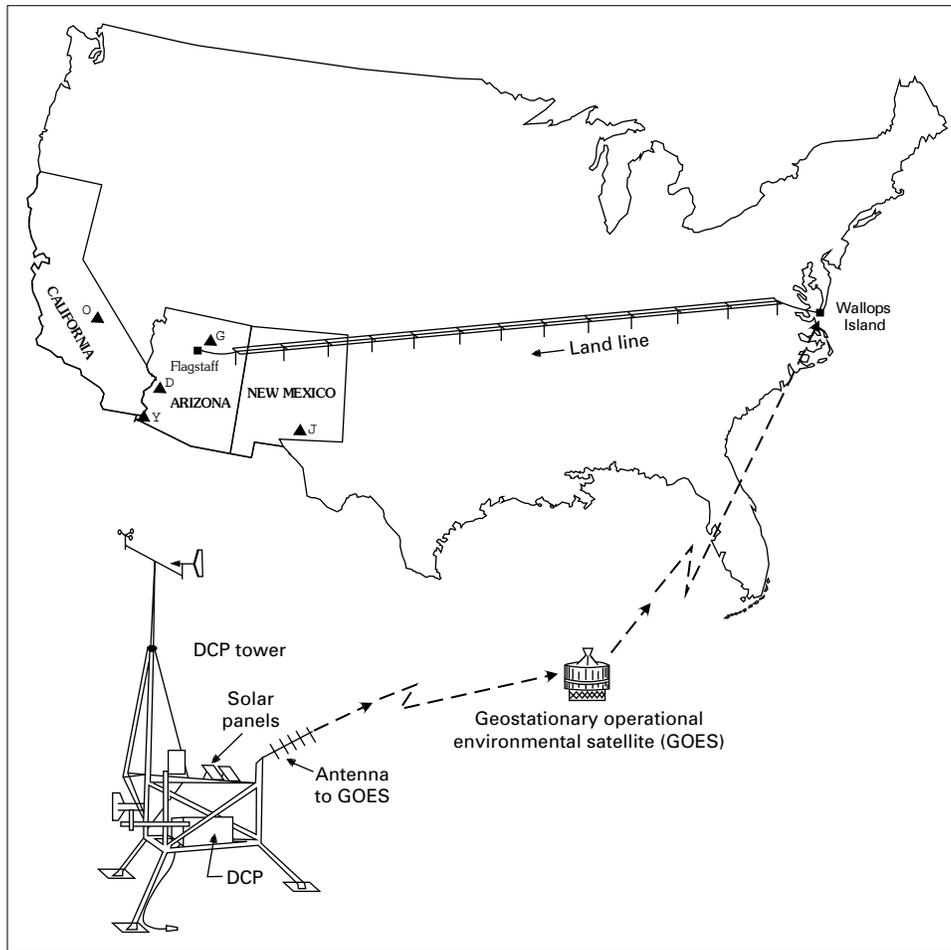
Figure 2. Data-transmission links between Geomet stations (triangles), GOES satellite, NESDIS receiving site at Wallops Island, Va., and Desert Winds Project headquarters at Flagstaff, Ariz. Data are transmitted from each Geomet station and archived daily at Flagstaff. Geomet stations: G, Gold Spring; J, Jornada; D, Desert Wells; Y, Yuma; O, Owens Lake (after McCauley and others, 1984).

Each tower supports four Eppley solar-radiation sensors. These towers are large levers mounted on pivots (like off-center teeter-totters). The base of the tower also rotates horizontally. Instruments on the long end of the lever (A, fig. 5A) are suspended 4.2 m above the ground. Two of these instruments look up at the sky and two look down at the ground. This tower design is necessary to allow the downward-looking radiometers a wide field-of-view. A counterbalance on the short end (Yuma) or a hydraulic lift (Jornada) allows one person to maneuver the boom vertically. Guy wires keep the tower stable when it is upright. To service the radiometers, the tower is lowered, then rotated horizontally. The radiometers can thus be serviced without disturbing the ground surface directly below their 4.2-m monitoring position.

The Geomet radiation towers (fig. 5A) were designed by the Desert Winds Project and constructed to meet project specifications peculiar to each site. Several experimental designs were used to provide easy access for maintenance, a wide downward field-of-view, and protection from damage by animals or blowing dust (see Appendix 1). Scaffolding was used at Owens Lake.

At all superstations, an automated sensor (SENSIT), which detects sand flux, and a manually operated wind-blown-particle catcher (Fryrear, 1986) monitor saltation of surface sediment moved by the recorded winds (fig. 6). These instruments are deployed on the ground surface a few meters from the towers to avoid effects of these obstacles on wind speeds and directions at the ground surface.

The Geomet stations have three power requirements: power for the DCP electronics and GOES transmitter; power for the basic sensors; and, at the superstations, power for additional sensors. The stations are in remote locations away from commercial power, and planned maintenance visits to these sites are at 6-month intervals (table 2). Their power systems must, therefore, be self sufficient, and they cannot require constant attention.

Table 1. Geomet stations and their equipment/sensor complement.

[All are superstations except Desert Wells, which is basic. Leaders (--) indicate that equipment/sensor is not present]

Equipment/ sensor	Site locations				
	Gold Spring	Desert Wells	Yuma	Owens Lake	Jornada
Data-collection platform tower	1	1	1	1	11
Wind tower	1	--	1	1	1
Wind direction	1	1	1	1	1
Wind speed	3	1	3	3	3
Peak gust[1]	2	1	2	2	2
Air temperature	2	1	2	2	2
Precipitation	1	1	1	1	1
Barometric pressure	1	1	1	--	1
Relative humidity	1	1	1	1	1
Soil temperature	3	1	3	1	3
Heat flux	--	--	--	--	3
Windblown-particle catcher	2	--	1	1	1
Sand flux	1	--	1	1	1
Radiation tower	--	--	1	--	1
Radiation stand	1	--	--	--	1
Radiation scaffold	--	--	--	1	--
Shadow-band stand	--	--	--	1	1
Eppley radiometers	2	--	4	2	14
Everest infrared thermometer	4	--	4	1	4

[1]Recorded at 1.2- and 6-m levels.

The stations use battery power (gel-cell type) and solar panels, both of which require little maintenance. Solar panels supply daytime power and charge the batteries. The choice of this system imposes power restrictions on the DCP, and all sensors must have low power requirements.

At Desert Wells, the two batteries and external solar panel perform well, supplying enough power for the DCP and the basic sensors. The superstation DCP's contain one battery charged through an internal regulator by an external solar panel. An additional input allows use of external power. Internal circuitry and program control allow the sensor power to be turned on just prior to and during a sampling period. Power to the basic sensor is turned off at all other times. Such a switched power provision is important where power is limited. Although the superstations receive ample sunlight to support most sensors, these stations require additional power to operate the Everest radiometers and the SENSIT sand-flux sensors, which require constant power.

The necessary power is supplied by additional batteries charged by two 40-watt solar panels (see Appendix 1).

The DCP (A, fig. 4A) is the heart of the station. The DCP is a specially designed Handar 540A-1 or Handar 570. The instrument's box is 40 cm wide, 30 cm high, and 23.75 cm deep. Each box contains a programmable microprocessor, memory for program and data storage, as many as six sensor interface cards, and a GOES radio transmitter. All sensors are interfaced to the 540A-1 DCP through a junction box, also mounted on the DCP tower. Sensors are wired directly to a terminal strip on the 570 DCP, which requires a special enclosure (B, fig. 4A).

The solar-powered battery system, coupled with radio transmission via Earth-orbiting satellite, allows operation of Geomet stations in remote areas, and it obviates the need to visit the stations frequently to collect data recorded on paper rolls or digital tapes. (Local custodians do visit the sites weekly to collect sediment from the windblown-particle catcher and to remove dust from solar panels and radiation sensors, as described later in this chapter.) Automated DCP's generally work very well—the Geomet station at Gold Spring has operated almost continuously, without major problems, since August 1979 (fig. 7). Problems with sensor performance, station operations, or satellite transmission are usually immediately apparent as gaps or errors in the electronic data stream received in Flagstaff. Troubleshooting, preventive maintenance, and security procedures are discussed below and in Appendix 1.

INSTRUMENTATION

Following are detailed descriptions of the instruments deployed at the Geomet stations and their requirements for calibration and maintenance (table 2).

DATA-COLLECTION PLATFORM (DCP)

Description.—The DCP (figs. 3A, 3B) processes and stores the signals from the sensors until the data are transmitted via the GOES satellite. The transmitting antenna to the satellite is a cross-element yagi attached to one corner of the DCP tower (E, fig. 3B). The GOES satellite radio assembly (mounted on the inner lid of the DCP enclosure box at each site) consists of a fully certified 10-watt synthesized radio transmitter referenced to a 1-Mhz temperature-compensated crystal oscillator. The transmitter may be set to any of the 266 allowable GOES frequencies assigned by NESDIS and to the international frequencies assigned by the World Meteorological Organization.

Calibration.—All DCP circuits are checked on each maintenance visit to the Geomet sites. The visits, at 6-month intervals (table 2), are made by a qualified electronics technician. The circuit checks require insertion of the proper

Table 2. Scheduled maintenance at Geomet stations.

Operation	Frequency	Performed by
Reset data-collection platform clock	6 months	Technician.
Replace long-wave radiometer battery	6 months	Technician or custodian.
Calibrate Eppley radiometers	1 year	Technician.
Calibrate Everest infrared thermometers	6 months	Technician.
Rebuild/calibrate anemometers	As necessary	Technician.
Rebuild/calibrate wind-direction sensor	As necessary	Technician.
Clean air-temperature/ relative-humidity filters	6 months	Technician.
Clean Eppley radiometer domes	Weekly	Custodian.
Clean solar panels	Weekly	Custodian.
Clean Everest lens	Weekly	Custodian.
Clean precipitation gauge	As necessary	Technician or custodian.
Check radio and data-collection platform	6 months	Technician.
Collect samples from windblown-particle catcher	Weekly	Custodian.
Check power systems	6 months	Technician.
Replace power-system batteries	2 years	Technician.
Check all temperature sensors for accuracy	6 months	Technician.
Check relative humidity against psychrometer	6 months	Technician.

stimulus and measurement of the result for each circuit. The DCP manufacturer markets a pluggable card for this purpose, which is useful in the laboratory. In the field, however, we have found that hand-held simulators (hand-made in our laboratory) are more useful because they allow introduction of electronic stimuli so that cables and connectors can be checked as well.

A simple switch provides the necessary stimulus to check the precipitation interface circuit. A precision resistance simulates a given temperature and is used to check each of the temperature interface circuits. A hand-held voltage source provides the stimulus to calibrate the relative-humidity circuitry. Another hand-held device generates a pulse to check wind-speed circuits. The technician also measures output power from the GOES radio at both the radio and the antenna and reflected power at the antenna.

Maintenance.—Maintenance includes examination of all cables and connectors for proper connections, cleanliness, and damage. A desiccant (moisture-absorbing crystals) inside the DCP enclosure box effectively removes moisture from the box, thus preventing damage to the electronics. The desiccant is replaced each time the DCP is opened; used desiccant is baked for 12 to 24 hours, stored in an airtight container, and reused.

AIR-TEMPERATURE SENSOR

Description.—This instrument is a solid-state, precision, linear thermistor placed in a compact cylindrical assembly. The resistance of the thermistor is inversely proportional to the temperature. The resistance is measured by a voltage divider circuit, and the result is linearized by a look-up-table routine. A convection-aspirated shield around the thermistor reduces the effect of solar radiation on air temperature and protects the thermistor from precipitation. This instrument is mounted either to the DCP tower at the 1.8-m level (E, fig. 3*A*, basic station), or to the wind tower at the 1.2- and 6-m levels (A and A1, fig. 3*B*, superstation). It is simple, rugged, and reliable.
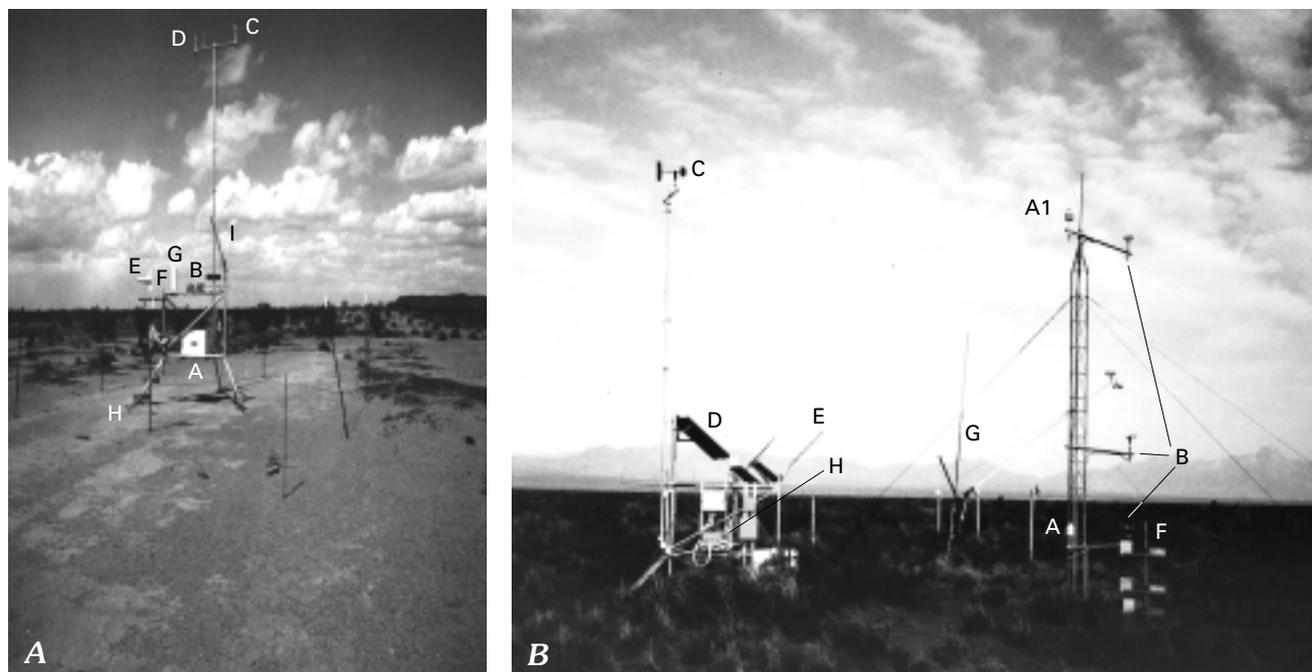
Figure 3.   Two Geomet stations of contrasting complexity: *A*, A lone data-collection platform (DCP) tower is the basic Geomet station at Desert Wells, west of Vicksburg, Ariz. A, Box housing DCP, barometric-pressure sensor, and batteries; B, Solar panels; C, Anemometer; D, Wind-direction sensor; E, Air-temperature sensor; F, Humidity sensor; G, Precipitation sensor; H, Soil-temperature sensor (buried 4 cm below ground surface); I, Antenna for transmission of data from DCP to GOES satellite (see fig. 2). Top of mast on tripod base is 6 m above ground. *B*, Wind tower (at right) next to modified DCP tower at Geomet superstation at Jornada, N. Mex. In addition to basic equipment shown in figure 3*A*, this and other superstations in network (fig. 2) contain wind and radiation towers or scaffolding and many more sensors, including sand-flux devices. A, Combined air-temperature and humidity sensor; A1, Air-temperature sensor; B, Three-cup anemometer; C, Wind-direction vane; D, Extra solar panels; E, Antenna to GOES; F, Sand catcher; G, Radiation sensors; H, Barometric-pressure sensor.

Calibration.—Calibration requires taking a temperature reading near the thermistor with a hand-held thermometer. A chart provides a value for the resistance, which must agree with the resistance of the instrument, taken with an ohmmeter. Cross-checking the temperature readings from the two sensors (1.2- and 6-m) at the superstations provides a daily indication of their performance.

Maintenance.—Periodic maintenance consists of removing the shield and cleaning a filter that protects the thermistor.

RELATIVE-HUMIDITY/AIR-TEMPERATURE SENSOR

Description.—The temperature-sensor part of this combined instrument (A, fig. 3*B*) is the same as the air-temperature sensor described above. The humidity sensor is a capacitor consisting of a metallic grid deposited on a glass plate and covered by a hygroscopic polymer film. The dielectric constant of the polymer material increases with the amount of water absorbed, such that capacitance depends on the relative humidity. The basic response to changes in humidity is rapid (approximately 1 s to reach 90 percent of the final value). However, a filter that protects the sensor from dust and physical damage slows the response to 20 to 30 s. The humidity-recording part of this sensor is mounted next to the air-temperature thermistor, so that both are sampling the same volume of air. The instrument is mounted on the base of the DCP tower (basic station) or at the 1.2-m level of the wind tower (superstation).

Calibration.—Calibration of the humidity sensor requires a strictly controlled laboratory environment. Therefore, when calibration is necessary, the instrument is returned to the manufacturer's facility. The manufacturer suggests calibration every 24 months. At 6-month intervals, the instrument's accuracy is checked by comparing its readings with those taken by a psychrometer. The psychrometer consists of two thermometers that are identical except that the bulb of one is wrapped with a wet wick. Evaporation from the wet bulb causes it to register a lower temperature than that of the dry bulb. The difference between the two temperatures constitutes the relative humidity.

Maintenance.—Periodic servicing consists of removing the shield and cleaning a filter that protects the capacitor.

Table 3. Specifications of sensors at Geomet stations.

[RH, relative humidity]

Sensor type	Measurement type	Unit	Accuracy
Sampled at 6-minute intervals			
Wind direction	Mean	degrees	±5°
Wind speed	Mean	mph	±5%
Peak gust	Maximum	mph	±5%
SENSIT sand flux	Mean and maximum	kinetic energy	Experimental
Sampled at 12-minute intervals			
Precipitation	Count	0.25 mm	±0.25 mm
Solar radiation (Eppleys)	Mean	watts/meter^2	±1% temperature dependence ±0.5% linearity
Air temperature	Instant	°C	±0.2°C, 0°–60°C ±0.6°C, –50°–0°C
Thermal radiation (Everests)	Mean	°C	±0.5°C
Sampled at 1-hour intervals			
Humidity	Instant	percent	±2%, 0 to 80% RH ±5%, 80 to 100% RH
Soil temperature	Instant	°C	±0.1°C, –20°–50°C ±0.3°C,–50° to –20°C
Barometric pressure	Instant	inches of mercury	±0.3% of range
Battery voltage	Instant	volts	±5%
Heat flux	Mean	Btu/hr	to 1%

SOIL-TEMPERATURE SENSOR

Description.—This sensor is a precision, linear thermistor housed in a waterproof, stainless steel enclosure. The resistance of the thermistor is inversely proportional to the soil temperature. Resistance is measured by a voltage divider circuit, and the result is linearized by a look-up-table routine. The probes lie in the soil at depths of 4, 10, and 20 cm, and they are connected to the DCP by weather- and animal-proof cables.

Calibration.—A hand-held thermometer is used to check the soil temperature near the probes. This reading is cross-referenced to a resistance chart. If calibration is correct, the resistance value of the chart will match the resistance of the instrument as measured with an ohmmeter. Faulty instruments are replaced and then repaired in the laboratory.

Daily monitoring and cross-checking of data transmitted from each of the three probes generally indicates their condition and accuracy. When working properly, the three probes normally follow the same basic pattern of response, with increasing lag and decreasing extremes as depth increases.

Maintenance.—These sensors are reliable, and they require little maintenance other than checking their depth. When installing them, we insert a surveyors' flag at the 4-cm depth and mark the flagstaff's position at the ground surface. This mark is checked during each visit to a site; if it is unchanged, we know that the instruments have remained at the required depth. To mark the flagstaff's position, we have found that a wheel collar used to hold wheels on model airplanes works well—it does not erode away as pen marks do or move as tape does. Some time is needed for the ground to stabilize after sensor installation, and we therefore try not to cause any unnecessary disturbance once the instruments have settled in.

HEAT-FLUX SENSOR

Description.—Each heat-flux sensor (fig. 4*B*) consists of a set of two transducers separated by a ceramic, paper, and glass pad. Heat flowing through soil causes a slight temperature difference across the sensor. This difference is directly proportional to the heat flux and is expressed as a plus or minus analog voltage.
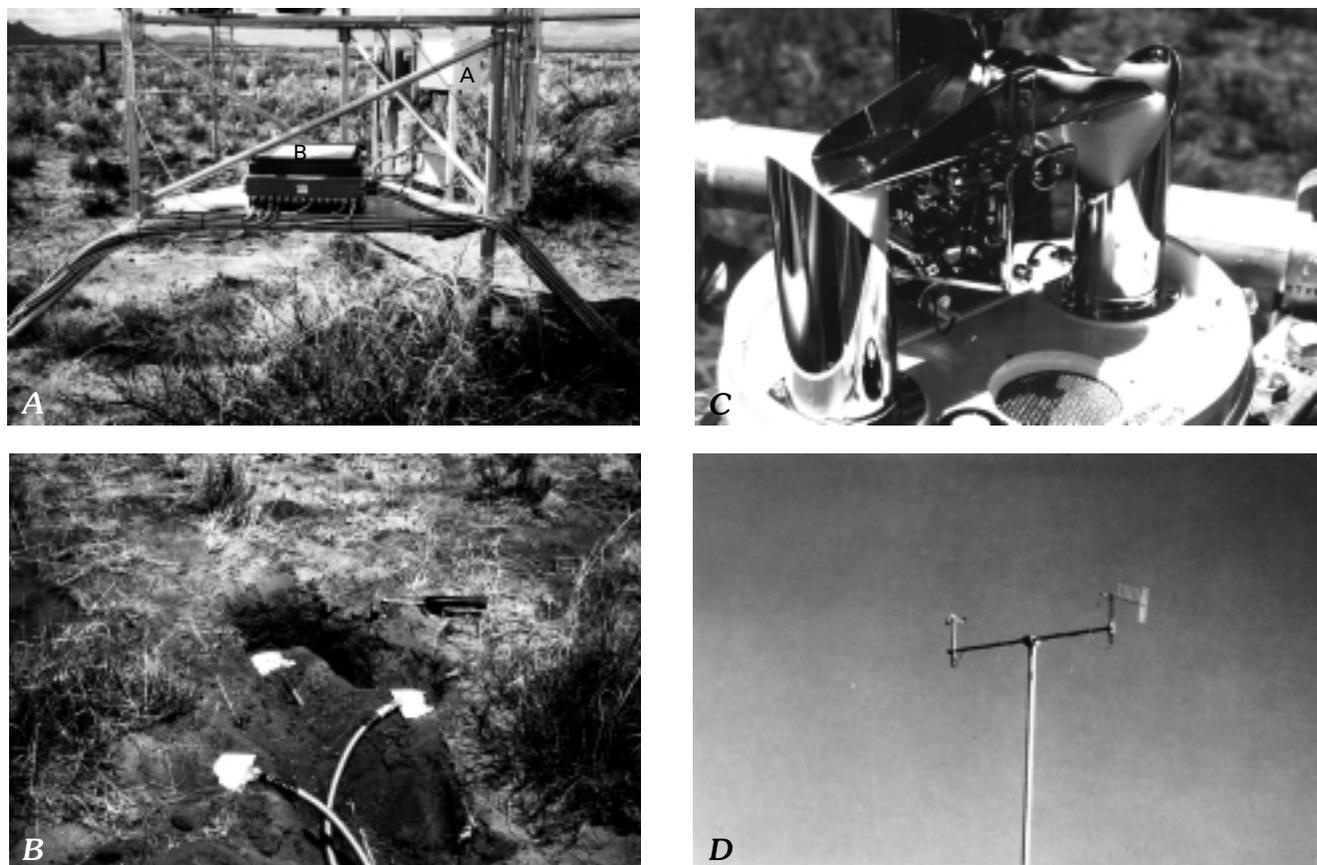
Figure 4. Close-up views of some components of Geomet stations. *A*, A close-up view of DCP tower at Jornada showing two different DCP's: shown at A is Model 540 Handar DCP; shown at B is environmentally sealed enclosure box for model 570 Handar DCP, which requires special protection from elements. *B*, Heat-flux sensors with buried cables; *C*, Open precipitation gauge showing tipping bucket; *D*, Wind-direction vane with needles.

Calibration.—Computer programs use a calibration constant, supplied by the manufacturer, to convert these small voltages to amount and direction of heat flow.

Maintenance.—These experimental instruments, presently deployed only at the Jornada station, lie buried near the soil-temperature probes. They are reliable, and they require little upkeep other than maintaining the proper depth.

BAROMETRIC-PRESSURE SENSOR

Description.—The barometric-pressure sensor is an aneroid barometer that utilizes an evacuated bellows sensitive to changes in absolute pressure. As pressure changes, motion of the bellows moves a contact across a precision potentiometer, producing an output resistance proportional to the barometric pressure.

Housed in a weatherproof container, the barometer is mounted on the DCP tower (H, fig. 3*B*). The container is typically a length of polyvinyl chloride (PVC) pipe capped on both ends. A small hole on the side allows air to enter, and a small drain hole in the bottom lets moisture escape.

Calibration.—New calibration is required if the barometer is moved to another site with an elevation outside the sensor's range. Comparing data with that obtained at another local site indicates proper operation of the instrument. It is sent to the manufacturer for calibration if it has failed or if it records spurious readings. Barometric pressure is recorded at all sites but Owens Lake.

Maintenance.—Insuring that the holes are clean and that the instrument remains upright are the only maintenance requirements.

PRECIPITATION SENSOR

Description.—The precipitation sensor is a funnel with a 20-cm-diameter orifice to collect and direct rain to a tipping bucket mechanism (fig. 4*C*). The funnel and mechanism are housed in a metal cylinder that is secured to a corner of the DCP tower, 1.8 m above the ground (G, fig. 3*A*). Coupled to the tipping bucket is a magnetically activated reed switch, which momentarily closes each time the bucket tips; a depth of 0.25 mm of collected water causes the bucket to tip. The
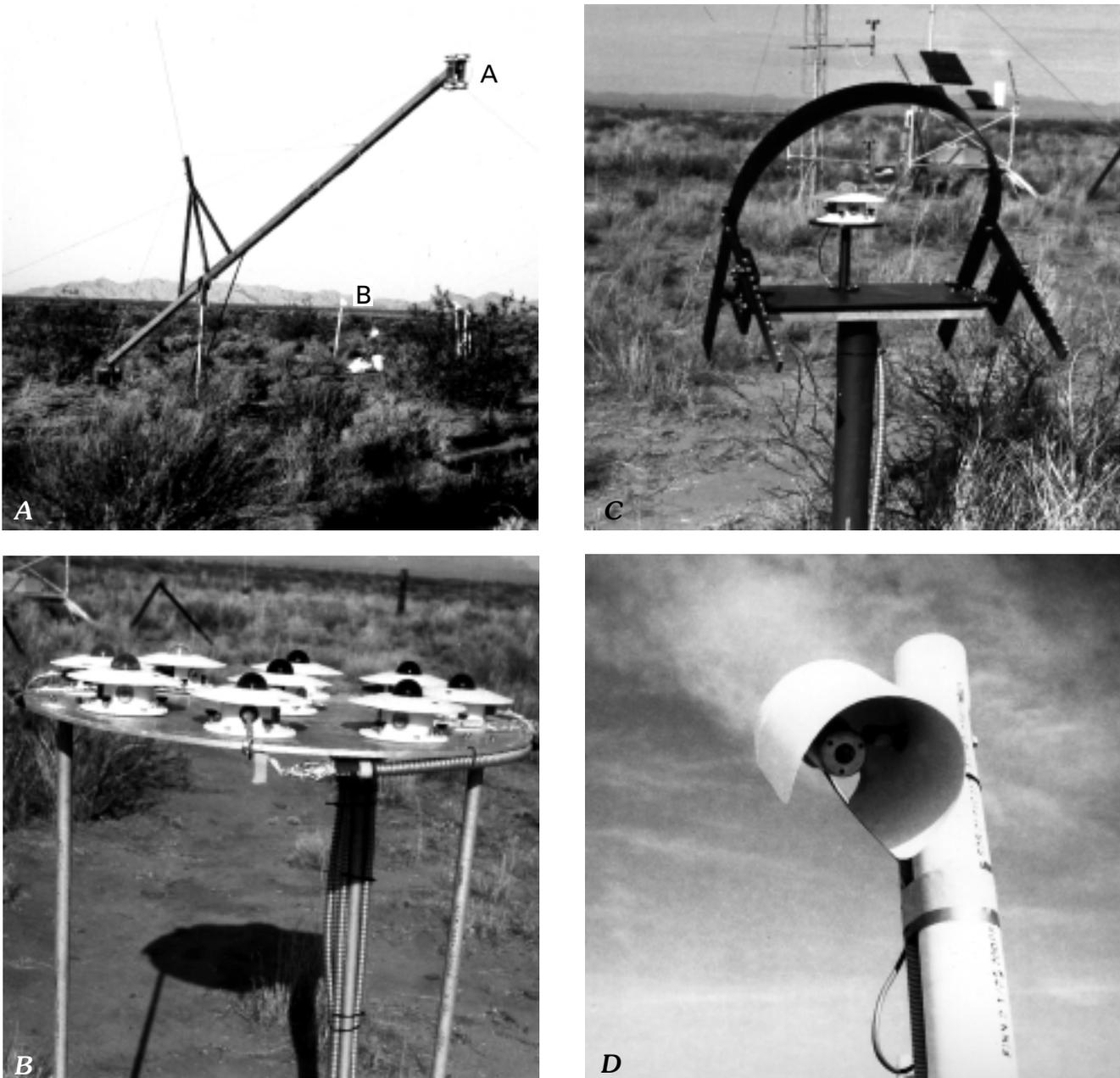
Figure 5.   Radiation sensors that automatically record incoming and outgoing solar energy in relation to monitored meteorological and ground-surface conditions. *A*, Four Eppley sensors mounted on arm of radiation tower at A record incoming and outgoing (reflected) solar energy in range of 0.2 to 2.8 μm (visible and near-infrared). Sensors mounted on posts below tower at B are Everest radiometers (see *D*). *B*, A "pie" of Eppleys records incoming solar radiation in discrete wavebands that correspond to parts of spectrum imaged by certain space-borne and airborne remote-sensing systems. *C*, A shadow-band Eppley sensor provides reference data necessary for determining atmospheric transmission of solar energy, particularly for studying the effects of airborne particulates (dust). *D*, Experimental Everest radiometers record variations in surface-soil and vegetation characteristics under recorded meteorological conditions such as precipitation and temperature. These data are useful for determining range of spectral variability of natural materials and for discriminating artifacts or camouflaged materials against natural background (Krusinger, 1988). Photograph *A* taken at Yuma; *B*, *C*, and *D* taken at Jornada.

water drains out the bottom of the gauge and a second bucket moves into position to collect more water; the procedure is repeated until no more is available for collection. Switch closures are counted by an interface circuit in the DCP. This hardware count is periodically added to a running count maintained by DCP software.

Calibration.—Slowly pouring measured amounts of water through a clean, level instrument will verify
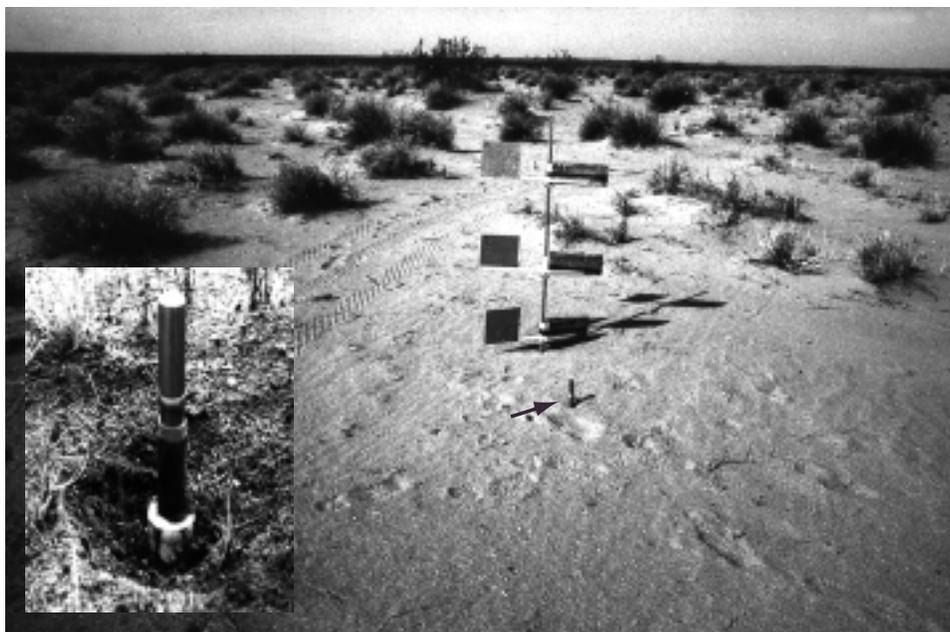
Figure 6. The SENSIT (arrow), a device that detects windblown-particle movement by recorded winds in near-real time, is shown here at Geomet site at Yuma, Ariz. This device is an automated sand-flux sensor with no moving parts (see text). Inset shows circular piezoelectric crystal near top of sensor and buried housing that protects electronic components, which are connected by cable with the DCP. Sediment moved during each wind storm is sampled at three levels above ground by windblown-particle catcher behind SENSIT (Fryrear, 1986). Wind vanes keep open ends of sample pans oriented into wind. This device is used with SENSIT to monitor sediment movement by Geomet-recorded winds. After each sediment-moving event, samples must be collected and weighed to provide basis for calculating mass transport.

calibration. Enough liquid is poured through the instrument to cause 10 tips. This measured amount is then divided by 10 to produce an average amount per tip. Mechanical adjustments, if necessary, are then made.

Maintenance.—Maintenance consists of cleaning debris from inlet and outlet screens and from the tipping mechanism and keeping the instrument level.

WIND-DIRECTION SENSOR

Description.—This instrument is a heavy-duty aluminum and stainless steel wind vane that is coupled to a precision micro-torque potentiometer, which has low rotational torque. The wire-wound potentiometer produces an output resistance that varies in proportion to the wind direction. The wind direction vane is mounted on the DCP tower at the top of the 6-m mast (C, fig. 3*B*; fig. 4*D*).

Calibration.—Calibration is accomplished by inserting a locating pin into the body of the instrument to orient the wind vane with an internal potentiometer. Pointing the vane exactly to the south and locking the instrument in place completes the calibration.

Maintenance.—Maintenance requires observation of the instrument for signs of damage and verification that

readings (in degrees) agree with vane direction. This sensor is very reliable and normally requires little maintenance except for protection from birds (see Appendix 1).

WIND-SPEED SENSOR (ANEMOMETER)

Description.—The anemometer consists of three cups mounted on a rotor shaft that rotates on instrument-quality stainless steel bearings. A magnet on the rotor shaft moves near a Hall-effect transducer, which detects the field of the rotating magnet. This detected field produces a pulse rate in proportion to the wind velocity. A single anemometer is mounted to the top of the DCP tower mast at the basic station (C, fig. 3*A*). Three anemometers are mounted on the wind tower at each superstation, at 1.2, 2.64, and 6 m above the ground (B, fig. 3*B*).

Calibration.—Operations of the anemometers are checked each time they are rebuilt. In 1993 we began calibration in a wind tunnel, which produces a calibration constant for each instrument. This constant is entered into the DCP program upon installation of the instrument. When placed on a tower in the field, anemometers are considered to be working properly if the daily average of anemometer readings at each of three heights plots as a straight line on a log-height,
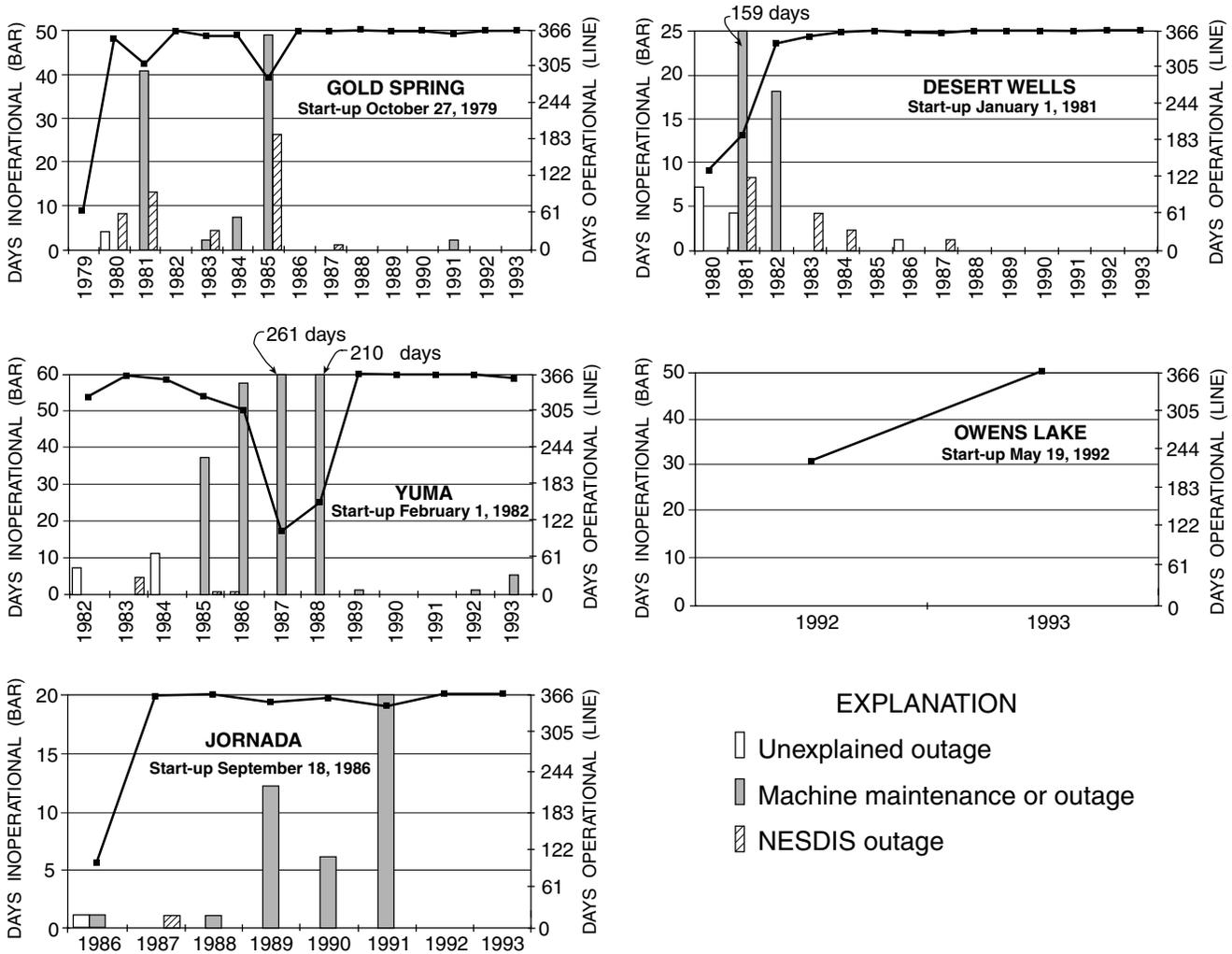
Figure 7. Graphs showing operational history of each Geomet station. Line graphs show total numbers of days per year when station was operational. Bar graphs show total numbers of days per year when operations were interrupted for 24 hours or more by (1) unexplained or miscellaneous external causes, including vandalism or lightning; (2) maintenance requirements or malfunction of machines; or (3) NESDIS problems with satellite transmission or computer systems. (Note that values differ along *y* axes at left and right sides of graphs.) Outages during early years were due to problems with new equipment or to power failure or to lack of back-up equipment. Large outages for Yuma in 1987 and 1988 were due to (1) repositioning of the station to avoid bombing and strafing on the military range, and (2) upgrading to superstation status.

linear, average-wind-speed graph. This field method, however, only insures consistent operations between anemometers and is not a true calibration against a known standard. At present, anomalies in the wind-speed data are common, and it is difficult to distinguish signal from noise.

Maintenance.—The anemometers require periodic cleaning and bearing replacement. The period between their rebuilding depends on the frequency of storms and the type of airborne contaminants (such as dust and salt) that get into the bearings. Daily checks, made by cross-referencing the three wind speeds transmitted from each station, provide a good indication of the condition of the anemometers.

WINDBLOWN-PARTICLE CATCHER

Description.—A field dust sampler, designed for U.S. Department of Agriculture (USDA) research (Fryrear, 1986), collects samples of sand and dust particles moving at three levels above the ground (fig. 6). The USDA standard heights for sample pans are 15, 50, and 100 cm, but the lowest sampler pans at Desert Winds sites are set as closely as possible at the height of the sand-flux sensor (see Helm and Breed, chap. B, this volume). A wind vane on each sampler pan keeps it pointed into the wind. Particle-laden air passes through each sampler opening; once inside,

it reduces speed and particles settle in the sampler pan. (For an analysis of sampler performance, see Stout and Fryrear, 1989.)

Calibration.—Calibration consists of checking and adjusting the heights of the three catchers.

Maintenance.—Maintenance of this mechanical device requires cleaning of plugged screens, insuring free rotational movement of the catchers, tightening screws, and replacing worn parts.

SAND-FLUX SENSOR

Description.—The sand-flux sensor (trade name SENSIT, fig. 6) is an experimental device that automatically detects particles moving in saltation (bouncing along the ground). The sensor has no moving parts and is invariant to wind direction (which is recorded independently by the Geomet wind-direction sensor). The upper part of the SENSIT contains an exposed, ring-shaped, piezoelectric crystal, which is mounted on a post connected to a buried electronics housing. Windborne grains (in the diameter range of about 50 μm to 1 mm) impact the sensor, deform the piezoelectric crystal, and produce a charge proportional to the impact. The resultant signals represent particle movement; each pulse represents one count. At present, a hardware limitation enables us to record only one of these signals, as a frequency. This deficiency limits our use of the SENSIT to the detection, but not yet to the measurement, of particle movement.

Monitoring SENSIT performance in the laboratory allows us to determine the background signal produced by a free-running source within the instrument. After deployment in the field, this background signal provides an indication that the sensor is working. We monitor this constant background signal in the same way as signals from other constantly active instruments (such as temperature sensors). A signal change during a normally inactive period (such as a time of low wind speeds) alerts us to a change in the instrument's condition that would otherwise go undetected. When sediment movement does occur, the resultant signal is integrated with the background signal. The background signal is later subtracted in the laboratory, leaving only the signal produced by particle movement.

Calibration.—The SENSIT is adjacent to the wind-blown-particle catcher (fig. 6). The mass of sediment caught by the sampler pan at the lowest level of the catcher provides a value with which to calibrate the SENSIT (Helm and Breed, chap. B, this volume).

Maintenance.—Periodic maintenance consists of ensuring that the piezoelectric crystal is at a constant height above the surface and checking for damage from weather, animals, and man.

RADIATION SENSORS

Description.—Eppley radiation sensors, mounted above the ground at the superstations (A, fig. 5A), include one or more short-wave, precision spectral pyranometers (PSP's) that record energy (in W/m^2) in the visible and in the reflected (near-visible) infrared part of the spectrum (0.2–2.8 μm), and one or two long-wave precision infrared radiometers (PIR's) that record energy in the thermal infrared (3–50 μm). One PSP at each superstation looks upward to measure incoming short-wave solar and sky radiation; at Yuma and Jornada, one PSP looks downward to measure outgoing (reflected) ground-surface radiation.

One PIR at each superstation measures incoming long-wave radiation; at Yuma and Jornada, a second PIR measures reflected and emitted ground-surface thermal radiation.

Jornada also has nine upward-looking PSP's that measure incoming short-wave solar and sky radiation in narrow, defined wavelength bands in the visible to near-visible infrared parts of the spectrum (at 0.385, 0.485, 0.529, 0.562, 0.603, 0.623, 0.686, 0.707, and 0.780 μm). These sensors are mounted on a round metal platform or "pie," positioned approximately 1.5 m above the ground (fig. 5B). A single PSP mounted in a shadow-band stand (to screen direct sunlight) at Jornada and Owens Lake records just the diffuse-sky component of solar radiation (fig. 5C).

In addition to the Eppleys, four downward-looking Everest radiometers (infrared thermometers: D, fig. 1; fig. 5D) measure thermal radiation from the ground surface (recorded as surface brightness temperature) in the spectral range of 8–14 μm at Gold Spring, Yuma, and Jornada. Each radiometer has a 15° field-of-view and is mounted on a 1.83-m-tall PVC pipe. These instruments are pointed at selected ground targets, such as bare soil or vegetation (Krusinger, 1988). Graphs of some of the radiation data from the Jornada site are shown in figure 8.

Calibration.—Annual calibration is required for the Eppley instruments. They are delivered to a calibration facility at the U.S. Army Topographic Engineering Center at Fort Belvoir, Va. When the instruments are reinstalled, we enter the new calibration constants into the DCP program and record serial numbers and instrument locations.

Figure 8 (following page). Graphs showing data from radiation sensors at Jornada Geomet station. *A*, Two days' data on incoming solar and sky radiation measured by upward-looking Eppley precision infrared radiometer (PIR) (Lwi) and precision spectral pyranometer (PSP) (Swi) on radiation tower (see A, fig. 5A), by PSP (Swid) on shadow-band fixture (see fig. 5C), and by nine PSP instruments (Swi) on "pie" (see fig. 5B). Lwi is long-wave incoming radiation. Swi is short-wave incoming radiation; number following Swi is measured wavelength in nanometers. Swid is diffuse radiation. *B*, One day's data from Everest infrared thermometers (B, fig. 5A; fig. 5D). (Courtesy of A.E. Krusinger, U.S. Army Topographic Engineering Center, Ft. Belvoir, Va.)

A

B
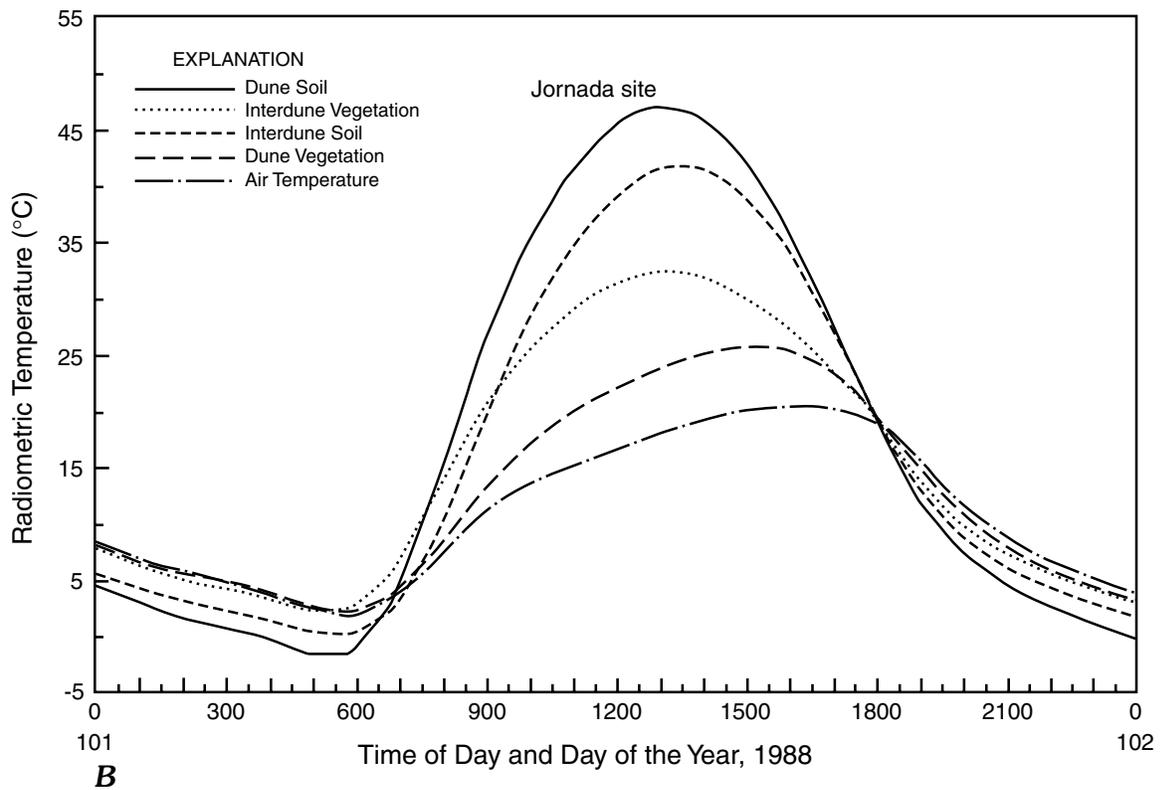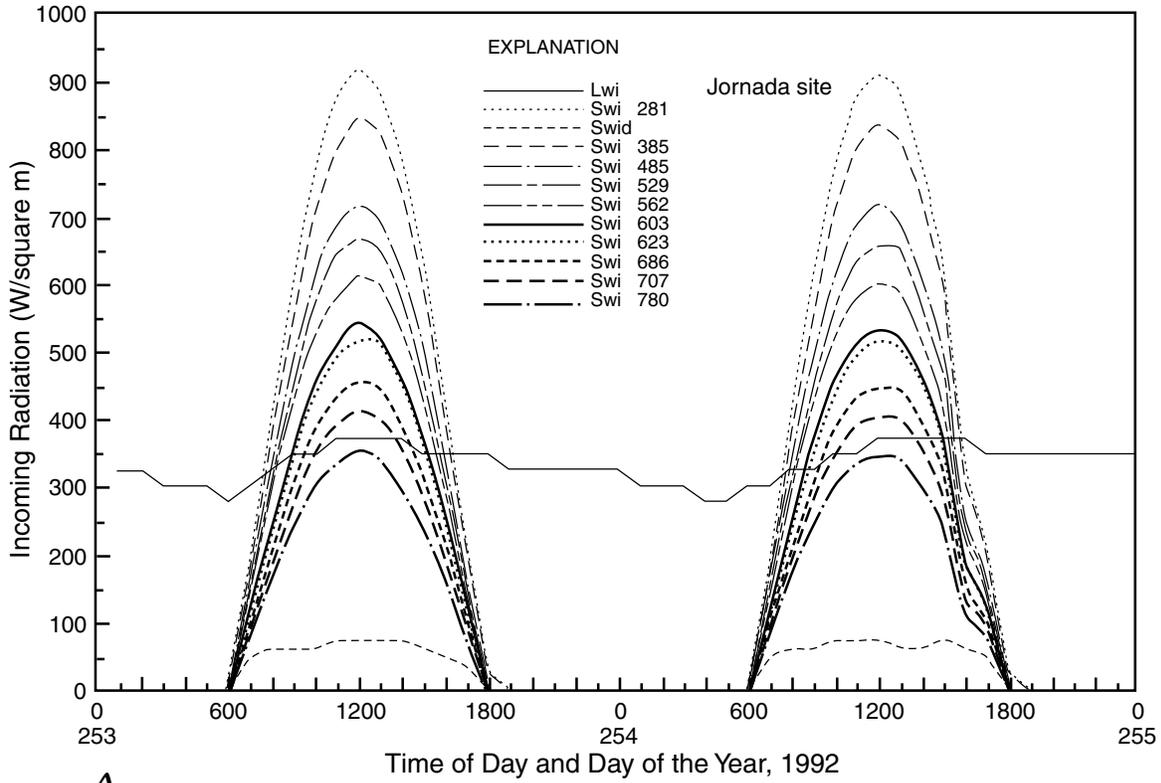
The Everest instruments are replaced by newly calibrated ones every 6 months. The removed instruments are calibrated at the U.S. Army Topographic Engineering Center at Fort Belvoir, Va., and rotated to the next station. A record of instrument serial numbers and locations provides a history of instrument performance and also contains calibration constants used by software at the laboratories at Flagstaff and Fort Belvoir.

Maintenance.—Weekly servicing of the Eppley instruments includes careful cleaning of the glass hemisphere of each instrument. Leveling of the instruments is critical and is also checked. The diffuse-radiation instruments at Jornada and Owens Lake (now dismantled) require adjustment of their shadow bands to maintain the shadow on each instrument's dome (fig. 5*C*). Semi-yearly servicing requires replacement of the batteries in long-wave Eppley instruments.

Everest instruments are checked weekly. Maintenance includes cleaning the lens and insuring that each sensor is properly positioned such that the selected target remains in the instrument's view. Repeat photography of each Everest target was begun in 1992 to help interpret surface-temperature data.

DATA COLLECTION, STORAGE, AND RETRIEVAL

Data collected from the automated sensors at each Geomet site must be directed through a series of steps within the DCP before becoming recognizable and usable for scientific research. These steps are directed by a software program within the DCP. Generally, one software "channel" for each sensor controls the program actions required to monitor it. However, for the wind-speed sensors, two software channels are needed for each hardware sensor; one channel monitors average wind speed while the other monitors peak gusts. The user programs each channel by specifying the monitoring schedule, the data-processing algorithms, the location of the hardware sensor to be monitored, and the format in which the data are to be transmitted. Once programmed, the DCP continuously samples data from each sensor on the programmed schedule. The original data signals are produced by the sensors in various forms: some sensors produce analog voltages, others vary a resistance, and still others produce electrical pulses. Each signal is converted in real time into digital form by interface circuit cards. Each channel's data-processing algorithm then converts this digital data into its final form (average, peak, temperature, count). Lastly, the data are stored in the DCP memory, where they remain until transmitted on the GOES radio.

The GOES satellites are in geostationary orbit above the Earth and are nominally stationed 22,240 miles (35,790 km) above the equator. The two available for our use are GOES East (also known as GOES-8), at approximately long 75°W., and GOES West (or GOES-9), at approximately long 135°W. At present, all Geomet stations are assigned channels and time slots on GOES West. Periodically (once every 2 hours for one DCP at Jornada, once an hour for all others), the DCP program collects Geomet data from memory and formats them so that they can be transmitted in pseudo-binary form, a compression code that enables transmission within the time frame allotted by NESDIS. Transmission to

GOES is in the 401.7- to 402.0-Mhz band. GOES-8 (West) receives this signal and retransmits it to a receiving station at Wallops Island, Va. At Wallops Island, the "data collection system automatic processing subsystem" sorts and stores the data in user files. High-speed dedicated or low-speed dial-up lines transfer the data to project headquarters in Flagstaff, Ariz., where sophisticated software performs a series of checks and balances to document missing or erroneous data. Finally, software converts the pseudo-binary code to ASCII, separates it by station and time, formats, and stores the data on disks and tapes for analysis by scientists. These latter two steps were transferred to the Desert Research Institute in Reno, Nev., in 1998. The tabulated data for part of one day at the Gold Spring site are shown in figure 9. Detailed coding of the data for quality, changes in sensors, and gaps due to NESDIS or Geomet station malfunctions (fig. 7) is currently in progress, in preparation for the planned open-file release of the data on CD-ROM.

PORTABLE MINISTATIONS

These small stations (fig. 10) are equipped with a minimum array of sensors to provide supplementary monitoring of wind erosion, either in a "stand-alone" environment or as a temporary enhancement to a fixed station. The single tower is a 3-m-high tripod arrangement. It is designed for quick installation and easy portability. A DCP and solar panel are mounted on the tower. Sensors monitor air temperature, precipitation, soil moisture, DCP internal air temperature, battery voltage, wind speed, and sand flux.

The DCP can record 32 channels of data: 16 have 24-bit counter inputs, and 16 have analog inputs. A palm-top computer contains the program that samples sensor outputs and stores the data in static RAM (SRAM), a credit-card size, removable, memory module containing as much as two megabytes. Data must be manually retrieved from the DCP periodically; frequency depends on the number of channels recorded, the length of the sample period, and the mode of operation (continuously or only during specified events). The

---

Figure 9 (following page). Data collected and transmitted by Geomet station at Gold Spring on August 9, 1990, between 1 minute after midnight and 5:31 a.m. Gold Spring was then a basic station. Asterisks are place-holders to accommodate additional data, within this format, as they were recorded by an upgraded superstation array of sensors in later years. The entire archival Gold Spring data set for 1980–1993 was released in this format on CD-ROM. Date is in format yyddd. Latitude (Lat) and longitude (Long) shown to four decimal places (decimal point omitted). Time in hours and minutes since midnight (hhmm). Humidity in percent. Ppt., precipitation in inches. Bar., barometric pressure in inches of mercury (or inches Hg). Wind direction specified in degrees east from north. Wind speed in miles per hour. Meter values indicate height above ground surface; centimeter values indicate depth below ground surface. temp., temperature in degrees Celsius.

Date	Lat (°N.)	Long (°W.)	Time	Humidity	Ppt.	Bar.	Wind direction	6 m Wind speed	6 m Peak gust	2.64 m Wind speed	1.2 m Wind speed	1.2 m Peak gust	6 m Air temp.	1.2 m Air temp.	4 cm Soil temp.	10 cm Soil temp.	20 cm Soil temp.
90221	351200	1113700	0001				126.54	15.73	19.66	*****	*****	*****	*****	19.81			
90221	351200	1113700	0007		1.46		126.54	15.34	19.27	*****	*****	*****	*****	19.42			
90221	351200	1113700	0013		1.46		128.65	14.55	16.91	*****	*****	*****	*****	19.42			
90221	351200	1113700	0019		1.46		118.10	14.95	19.66	*****	*****	*****	*****	19.02			
90221	351200	1113700	0025	49.42	1.46	24.629	120.21	14.55	16.91	*****	*****	*****	*****	19.42	26.48	*****	*****
90221	351200	1113700	0031		1.46		120.21	14.95	18.09	*****	*****	*****	*****	19.42			
90221	351200	1113700	0037		1.46		120.21	14.55	18.49	*****	*****	*****	*****	19.02			
90221	351200	1113700	0043		1.46		111.78	14.55	17.31	*****	*****	*****	*****	19.02			
90221	351200	1113700	0049		1.46		113.89	14.95	17.70	*****	*****	*****	*****	18.63			
90221	351200	1113700	0055		1.46		118.10	16.13	19.66	*****	*****	*****	*****	19.02			
90221	351200	1113700	0101		1.46		124.43	15.73	20.84	*****	*****	*****	*****	19.02			
90221	351200	1113700	0107		1.46		122.32	15.34	18.88	*****	*****	*****	*****	18.63			
90221	351200	1113700	0113		1.46		118.10	16.91	21.24	*****	*****	*****	*****	18.63			
90221	351200	1113700	0119		1.46		113.89	17.31	22.02	*****	*****	*****	*****	18.63			
90221	351200	1113700	0125	61.18	1.46	24.629	118.10	18.09	22.42	*****	*****	*****	*****	19.02	26.08	*****	*****
90221	351200	1113700	0131		1.46		113.89	17.31	22.42	*****	*****	*****	*****	18.63			
90221	351200	1113700	0137		1.46		115.99	18.49	24.38	*****	*****	*****	*****	19.02			
90221	351200	1113700	0143		1.46		118.10	15.34	19.27	*****	*****	*****	*****	18.63			
90221	351200	1113700	0149		1.46		118.10	14.16	17.31	*****	*****	*****	*****	18.24			
90221	351200	1113700	0155		1.46		120.21	14.95	18.09	*****	*****	*****	*****	18.24			
90221	351200	1113700	0201		1.46		118.10	14.55	19.66	*****	*****	*****	*****	18.24			
90221	351200	1113700	0207		1.46		128.65	12.19	16.52	*****	*****	*****	*****	17.85			
90221	351200	1113700	0213		1.46		122.32	12.98	16.91	*****	*****	*****	*****	17.85			
90221	351200	1113700	0219		1.46		120.21	12.98	16.91	*****	*****	*****	*****	17.46			
90221	351200	1113700	0225	63.14	1.46	24.629	111.78	11.80	14.95	*****	*****	*****	*****	17.46	25.69	*****	*****
90221	351200	1113700	0231		1.46		115.99	12.19	14.55	*****	*****	*****	*****	17.06			
90221	351200	1113700	0237		1.46		109.67	10.23	12.98	*****	*****	*****	*****	17.06			
90221	351200	1113700	0243		1.46		103.34	8.65	10.62	*****	*****	*****	*****	16.67			
90221	351200	1113700	0249		1.46		103.34	8.65	9.44	*****	*****	*****	*****	16.67			
90221	351200	1113700	0255		1.46		99.12	9.05	11.41	*****	*****	*****	*****	16.28			
90221	351200	1113700	0301		1.46		90.69	8.65	10.23	*****	*****	*****	*****	15.89			
90221	351200	1113700	0307		1.46		99.12	9.05	10.23	*****	*****	*****	*****	15.89			
90221	351200	1113700	0313		1.46		107.56	10.23	11.41	*****	*****	*****	*****	15.89			
90221	351200	1113700	0319		1.46		105.45	10.23	12.59	*****	*****	*****	*****	15.89			
90221	351200	1113700	0325	70.77	1.46	24.629	103.34	9.83	11.41	*****	*****	*****	*****	15.89	24.91	*****	*****
90221	351200	1113700	0331		1.46		103.34	9.83	10.62	*****	*****	*****	*****	15.89			
90221	351200	1113700	0337		1.46		99.12	9.44	11.41	*****	*****	*****	*****	15.50			
90221	351200	1113700	0343		1.46		90.69	9.83	11.41	*****	*****	*****	*****	15.50			
90221	351200	1113700	0349		1.46		80.14	9.44	11.01	*****	*****	*****	*****	14.71			
90221	351200	1113700	0355		1.46		82.25	9.05	9.44	*****	*****	*****	*****	14.32			
90221	351200	1113700	0401		1.46		97.01	9.05	10.62	*****	*****	*****	*****	14.71			
90221	351200	1113700	0407		1.46		90.69	9.44	10.62	*****	*****	*****	*****	15.10			
90221	351200	1113700	0413		1.46		84.36	9.05	11.01	*****	*****	*****	*****	15.10			
90221	351200	1113700	0419		1.46		86.47	9.83	11.01	*****	*****	*****	*****	15.10			
90221	351200	1113700	0425	75.69	1.46	24.629	88.58	9.83	11.41	*****	*****	*****	*****	15.10	24.52	*****	*****
90221	351200	1113700	0431		1.46		86.47	9.05	11.80	*****	*****	*****	*****	15.50			
90221	351200	1113700	0437		1.46		90.69	9.44	11.01	*****	*****	*****	*****	15.50			
90221	351200	1113700	0443		1.46		101.23	9.83	11.80	*****	*****	*****	*****	15.50			
90221	351200	1113700	0449		1.46		103.34	10.23	13.37	*****	*****	*****	*****	15.50			
90221	351200	1113700	0455		1.46		105.45	11.41	16.13	*****	*****	*****	*****	15.50			
90221	351200	1113700	0501		1.46		109.67	11.01	14.95	*****	*****	*****	*****	15.50			
90221	351200	1113700	0507		1.46		105.45	11.01	14.55	*****	*****	*****	*****	15.50			
90221	351200	1113700	0513		1.46		109.67	9.83	12.59	*****	*****	*****	*****	15.50			
90221	351200	1113700	0519		1.46		105.45	9.05	11.41	*****	*****	*****	*****	15.50			
90221	351200	1113700	0525	74.13	1.46	24.629	97.01	8.65	11.01	*****	*****	*****	*****	15.50	23.73	*****	*****
90221	351200	1113700	0531		1.46		90.69	7.08	9.83	*****	*****	*****	*****	15.10			

Figure 10. Automated DCP ministation (left) and windblown-particle catcher (right) monitoring wind erosion on field near village of Kyokotsmovi (New Oraibi) on Hopi Indian Reservation, northeastern Arizona (Helm and Breed, chap. B, this volume).

Desert Winds Project can deploy two of these stations to provide experimental data, to supplement a fixed Geomet station, or to operate where placement of a fully instrumented, fixed Geomet station is unnecessary or impractical.

SUMMARY

The Desert Winds Project's experience during more than a decade indicates that Geomet stations containing automated data-collection platforms provide a practical means for continuous monitoring of near-surface ground and atmospheric conditions in harsh desert environments. Such stations can be left unattended by technicians for periods of weeks or even months except when dust, corrosion, or breakdowns of the sensor system cause problems. Most of these problems can be avoided by weekly basic custodial inspections and cleaning and by twice-yearly checks and repairs by skilled technicians. Operations of the present Desert Winds Project network consist of the maintenance of five fixed stations and two supplemental ministations and the computer management of data arriving daily from all of the automated sensors. These operations require the attention of one full-time staff member trained in electronics engineering, who is assisted by local custodians and other project personnel as needed.

REFERENCES CITED

Fryrear, D.W., 1986, A field dust sampler: Journal of Soil and Water Conservation, v. 41, no. 2, p. 117–120.

Krusinger, A.E., 1988, An empirical surface temperature model: Ft. Belvoir, Va., U.S. Army Engineering Topographic Laboratory, Corps of Engineers, Report ETL-0503, 126 p.

McCauley, J.F., Breed, C.S., Helm, P.J., Billingsley, G.H., MacKinnon, D.J., Grolier, M.J., and McCauley, C.K., 1984, Remote monitoring of processes that shape desert surfaces: The Desert Winds Project: U.S. Geological Survey Bulletin 1634, 19 p.

McCauley, J.F., and Rinker, J.N., eds., 1987, A workshop on desert processes, Flagstaff, Arizona, September 24–28, 1984—Report on the conference: U.S. Geological Survey Circular 989, 21 p.

Stout, J.E., and Fryrear, D.W., 1989, Performance of a wind-blown particle sampler: American Society of Agricultural Engineers, Transactions, v. 32, no. 6, p. 2041–2045.

APPENDIX 1.—PROBLEMS UNIQUE TO GEOMET STATION OPERATIONS AND THEIR SOLUTIONS

POWER REQUIREMENTS AND PROBLEMS

The Geomet stations used wet-cell car and bus batteries in the past, but maintenance requirements were high, and boil-over and discharge of corrosive gasses damaged containers and electrical circuits. Better wet-cell batteries designed for long-term solar-system use are now available. Suppliers recommend the use of wet-cell batteries in hot environments, but these batteries require service at 40- to 60-day intervals. Because of the remote placement of the Geomet stations, and the schedule for service at 6-month intervals, gel-cell batteries are our best choice at present.

The Everest thermometers and SENSIT sand-flux sensors require additional and constant power. The original approach to this problem was to seal four gel-cell batteries in an ammo box (a metal military-surplus ammunition box) and bury it underground. The idea was to keep the batteries cool and dry. A solar panel provided daytime power to the sensors and power to charge the batteries. This arrangement worked well at some sites, but at Yuma, soil temperatures (as high as 130°F day time, 104°F nighttime) never allowed nighttime cooling, and the batteries cooked until they burst (in a few months). At the Owens Lake site (a playa), salts in the ground severely damaged the metal ammo box. We moved the batteries at these two sites to the DCP tower, where we placed them in a white reflective container and added a temperature-compensated regulator. This regulator stops charging when battery voltage reaches 14.3 volts and resumes charge at 13.2 volts. The temperature compensation adjusts charging thresholds according to battery temperature. A modular design easily allows the use of one to four batteries without the requirement of a new wiring harness. Connections are by keyed and pluggable harnesses, allowing system expansion or reduction as needed. Changing a battery takes only a few minutes, which enables servicing when speed is essential. We also added a power sensor and a software channel so that we can remotely monitor battery condition. The redesigned system has allowed battery replacement at 2-year intervals, and old batteries removed from the system have shown no sign of swelling or bursting.

Where possible, power systems once located underground have been placed above ground.

PROTECTION FROM RANGE ANIMALS, WILDLIFE, PEOPLE, AND THE SUN

Geomet stations at the Jornada Experimental Range, Gold Spring, and Desert Wells have barbed-wire fences around their perimeters to protect the equipment from range cattle.

Wind-direction sensors are an attraction to roosting birds. Large birds, such as the ravens and crows common to the semiarid range country, can bend the vane as well as cause extreme stress to bearings and potentiometer windings, resulting in premature failure. Attachment of vertical rods (e.g., sharp, flexible darning needles) to the horizontal vane provides a deterrent (fig. 4D). This modification extends the life and improves the reliability of the instrument.

Sensors buried in the soil sometimes attract curious critters who dig around them. Some have a habit of chewing on cables (both buried and within reach above the ground). One such sensor came equipped with a blinking light intended to indicate proper functioning. The light attracted an abnormal amount of attention (a good idea that proved to be not so good).

Ultraviolet (UV) rays cause damage to cable jackets. When exposed to the sun, an outer jacket that is UV protected will last much longer. Alternatives for UV protection are to run cable in conduit, or to wrap it with aluminum plumber's tape. We use both. The aluminum tape is useful for protecting above-ground cable from UV, especially if the cable has connectors on both ends and thus cannot be easily run through conduit.

Excrement from birds sometimes plugs the screens on the precipitation sensor. Bees, insects, and bird nests can also cause problems. The only solution is periodic cleaning. People digging with shovels can cause severe damage to buried cables that are not protected by conduit. Vandalism or unintended damage by people are dangers from which we have little protection, except for that afforded by difficult access and low visibility. At each Geomet site, a local custodian inspects the station and cleans equipment weekly (table 2).

CORROSION

Corrosion damage from airborne and surface materials must be considered. Most Geomet sites experience little problem as we use non-rusting materials including aluminum, stainless steel, and fiberglass. The station at Owens Lake was an unfortunate exception. The salts in the playa sediment on which the station sat corroded and destroyed the metal conduit used to house sensor cables. A solution to this problem may be to use a PVC conduit. PVC performs well underground, but it deteriorates rapidly when exposed to ultraviolet rays. Possibly a combination of the two, PVC underground and metal above ground, will be a better solution.

Metal cable connectors also corrode. Fine salts can infiltrate, causing damage to the connectors themselves and internal damage to electrical connections. Our experience shows that screw-on connectors have had no salt infiltration.

Snap-on plastic connectors with rubber or soft plastic boots also have performed well, at least in the short term. These connectors are on the bottom portion of the DCP, shaded from direct sunlight. UV probably would not be a problem there, but we do not know what heat will do in the long term. Bayonet connectors allow salt penetration, causing internal damage. Wrapping these connectors with aluminum tape is somewhat helpful, but salt infiltration still occurs. Sealing the connectors with silicone works well, but wind-borne materials eventually wear the coating away. A silicone seal covered by aluminum tape will stand up to the elements for a longer period.

In corrosive environments, extra care must be taken to seal cable entrances and doors to junction boxes and electronics housings. Salt infiltration will cause corrosion on such components as terminal strips and circuit boards, resulting in intermittent or shorted connections. Circuits can begin to "grow," causing unexplainable and ever-changing problems. Sealing the cable entrances with silicone rubber works well but is messy work. Replacing a sensor or sensor cable requires cutting away of the silicone, which can be tedious. Door seals are less of a problem. A silicone paste is normally applied to the rubber door seal. In dust-prone environments such as the Geomet sites we tend to use the paste sparingly, as it collects dust and sand. We use aluminum tape around the doors as well for additional protection.

Another solution to protecting the electronic components entails placing the DCP and other vulnerable parts in an environmentally sealed container (B, fig. 4A). We have protected a DCP at the Jornada site in this way because this particular DCP has exposed terminal strips for sensor connections. The interior of this fiberglass enclosure and the equipment it houses have remained clean, which suggests that this precaution could be a solution to the corrosion problem. However, the harsh chemicals found at Owens Lake are not present at Jornada, which therefore may not provide an adequate test.

Nuts and bolts should be aluminum, stainless steel, heavily galvanized steel, or plastic. All these materials work well, but stainless steel is the best. At Owens Lake, after a year of exposure, some of the aluminum nuts and bolts became very corroded, and nickel-plated U-bolts rusted and were difficult to deal with. Galvanized nuts and bolts that were in contact with the surface did not do well. However, the heavily galvanized wind tower, as well as the stainless-steel hardware, held up well. To our surprise, aluminum nuts and bolts were seldom a problem to remove. In some applications were strength is not a factor, plastic or nylon bolts and nuts work well. Some of our precipitation gauges use these materials.

Salt, like desert dust, collects in every small orifice imaginable. It collects in the anemometer cups and inside the ice shield, affecting the instruments' balance. It collects also in machined holes containing Allen screws, corroding the screw threads and making the screws so difficult to remove

that they must be drilled out. Salt also collects on the filters protecting the air-temperature and relative-humidity instruments and inside the precipitation gauge.

To prevent salt buildup in the anemometers, we cover the Allen screw holes with aluminum tape. We now apply anti-seize compound to the screws when rebuilding the instruments. Clean water works well to remove salt buildups on filters and anemometer cups. Distilled water can be used to clean electronics, but finding really clean mineral-free water is difficult, particularly in field localities. Distilling a local supply would be the best procedure, if the necessary equipment were available. After cleaning, the electronic components should be thoroughly dried in a low-temperature oven.

We are trying some protective coatings to see if they will prevent corrosion of nuts and bolts. We have successfully used anti-seize compound on steel screws that held the cover on the Owens Lake precipitation gauge. These screws had rusted badly and took considerable time and patience to remove. We applied a coating of anti-seize compound, and, 6 months later, removal was easy.

As an experiment, we attached common drywall screws to a 2.5-m-long board, applied protective coatings from the local hardware store to some of the screws, and left the board on the ground at the Owens Lake site. After 6 months, the following results were obtained:

Although the silicon lubricant was the most effective anti-corrosion agent, it collected salt and sand, which may be a problem. Neither the Teflon lubricant nor the rust inhibitor prevented rust. The Goop was a failure because, after the sun had hardened it, it was impossible to remove.

Another way to avoid corrosive effects may be to place all instruments well above the saltation layer, as far as possible from suspended fine particles such as dust. At Owens Lake we erected a 6-m-high aluminum scaffold and mounted radiometers at the top. Although the heaviest concentrations of airborne material were below the instruments, corrosion still occurred on instruments and connections.

ELECTROSTATIC DISCHARGE

Electrostatic discharge comes from a variety of sources. The most commonly thought-of source (but not the most common) is atmospheric (lightning). Lightning is also the one most difficult to deal with. Nonetheless, it is best to protect a site in every practical way. The simplest approach is to hold the entire system at the same potential. This approach entails using connectors that provide alternate paths to earth ground and shielded cables whose shields are connected to earth ground. The shields may provide a less resistive path to earth ground than the signal wire. The longer the sensor cable, the more likely a problem will occur. Lightning rods can also provide a low-resistance path to earth ground. The use of varistors, or spark gaps, on all input signals is recommended by many manufacturers. The ground side of these devices is connected to earth ground. In summary, no procedure will provide absolute protection from lightning, but one should apply at least basic precautions. Most equipment manufacturers provide specific recommendations.

The most common source of electrostatic discharge, which probably has the most likelihood of damaging a Geomet system, is the human body. When a person touches an electrical component, if that person is at a different potential than the component, an electrostatic discharge occurs. (The phenomenon is like rubbing one's feet on a carpet and then touching someone to produce a shock.) It most often occurs when the humidity is low. The voltage transferred in such encounters is in the thousands of volts, and it can severely damage today's miniaturized electrical components. The most common protection from such electrostatic discharge is a wrist strap with a long, flexible wire lead that is attached to the equipment ground. The strap neutralizes any potential difference between a person and the instrument.